Treating Metastatic Disease through Manipulation of Regulatory T cells

Ellyn Louise Hughes

Cardiff University

Doctor of Philosophy (Ph. D.)

2017

Declaration

STATEMENT 1

This work has not previously been accepted in substance for any degree and is not currently submitted in candidature for any degree.

Signed……(candidate) Date…….

STATEMENT 2

This thesis is being submitted in partial fulfillment of the requirements for the degree of Ph.D.

Signed……(candidate) Date…….

STATEMENT 3

This thesis is the result of my own independent work / investigation, except where otherwise stated. Other sources are acknowledged by explicit reference.

Signed……(candidate) Date…….

STATEMENT 4

I hereby give consent for my thesis, if accepted, to be available for photocopying and for inter-library loan, and for the title and summary to be made available to outside organisations.

Signed……(candidate) Date…….

STATEMENT 5

I hereby give consent for my thesis, if accepted, to be available for photocopying and for inter-library loan after expiry of a bar on access previously approved by the Graduate Development committee.

Signed……(candidate) Date…….

Acknowledgements

Firstly, I would like to acknowledge Tenovus for funding this PhD as well as providing support in developing other skills in public engagement. The work that Tenovus do for people affected by cancer in Wales is inspiring, and I am honored to have been a part of this charity.

Secondly, I would like to thank my supervisors, Professor Awen Gallimore and Dr. Ann Ager. Though this PhD has had its ups and downs, your continued support has guided me through to completion. My confidence as a scientist has grown, along with my ability to problem-solve and overcome obstacles throughout this PhD thanks to your supervision.

Next I would like to acknowledge Dr. Stephen Paisey and the rest of the team at PETIC for their help with getting the PET/CT scanner up and running for this project, as well as providing the radioactivity even when the cyclotron was in maintenance!

I would also like to thank everyone in the Gallimore/Godkin lab, particularly office 3F04, not only for the advice and support given during lab meetings and presentations, but also for the good times outside of work!

Two fellow scientists, and wonderful friends, have also been incredibly supportive throughout my PhD. Amanda and Diana, thank you for always being there during my stresses and for providing endless cups of tea and Starbucks visits!

I would also like to thank my parents, Jayne and Nigel, for their unfaltering support both throughout my education and at home. From a young age, my parents inspired my scientific curiosity and encouraged me to take any opportunities to further my interest and understanding. They have always been there to support and help me through my stresses and celebrated with me in my achievements.

Finally, I would like to thank my partner Jonathan for his unwavering patience and support throughout each stage of my PhD. Thank you for putting up with my changing moods, for listening to my complaints and worries, and for believing in me even when my own belief faltered.

Summary

$CD4^+Foxp3^+$ regulatory T cells (Tregs) are the main regulators of peripheral tolerance and prevent the development of fatal autoimmune disease in humans and mice. Furthermore, Tregs have also been implicated in suppressing anti-tumour immune responses and are often enriched at sites of primary and metastatic tumours. While studies have shown the effect of Treg ablation on the control of primary tumours, few studies have examined their contribution to metastasis progression.

In this thesis I hypothesised that the depletion of Tregs could promote control over metastasis. To address this, a highly metastatic murine mammary carcinoma cell line 4T1 was injected into transgenic mice expressing the diphtheria toxin receptor in Foxp3+ cells. Foxp3+ cells were depleted by administration of diphtheria toxin and the impact of this on growth of primary tumours and metastases was assessed and measured in *in vitro* clonogenic assays. Results of these experiments indicated that Treg-depletion led to control of primary tumour growth and in some mice to control of metastases. Control of metastases was linked to control of primary tumour growth.

In order to measure metastasis *in vivo,* a PET/CT imaging technique was optimized. Primary tumours and large metastatic nodules were successfully imaged in mice using F^{18} FDG as a radiotracer. However, the studies described herein revealed that micrometastases in mouse lungs were too small to be reliably identified using PET data parameters. CT imaging did however enable detection of increases in tissue density within the lungs, which was suggestive of micrometastases. Data obtained in this way also indicated that Treg-depletion promotes control of metastasis in some mice.

Collectively, the findings described in this thesis indicate that Treg-depletion can contribute to control of metastatic disease and should therefore represent an important component of novel immunotherapies.

Table of Contents

List of Abbreviations

ACT, Adoptive Cell Therapy
ADP, Adenosine Di-Phosphate
AMP, Adenosine Mono-Phosphate
APC, Antigen Presenting Cell
ATP, Adenosine Tri-Phosphate
bFGF, basic fibroblastic growth factor
BAC, Bacterial Artificial Chromosome
BMDCs, Bone Marrow Derived Cells
CARs, Chimeric Antigen Receptors
CCL, C-C motif Chemokine Ligand
CCR, C-C motif Chemokine Receptor
CCRCC, Clear Cell Renal Cell Carcinoma
CD, Cluster Differentiation
CNS, Conserved Non-coding Sequence
COX, Cyclooxygenase
CRC, Colo-Rectal Cancer
CSF-1, Colony Stimulating Factor 1
CT, Computed Tomography
CTLA4, Cytotoxic T Lymphocyte-associated Antigen 4
CTLs, Cytotoxic T Lymphocytes
CXCL, C-X-C motif Chemokine Ligand
CXCR, C-X-C motif Chemokine Receptor
CY, Cyclophosphamide
DCs, Dendritic Cells
DCIS, Ductal Carcinoma *in situ*
DEREG, DEpletion of REGulatory T cells
DN, Double Negative
DNA, Dexoyribo-Nucleic Acid
DP, Double Positive
DTR, Diphtheria Toxin Receptor
DTx, Diphtheria Toxin
EAE, Experimental Autoimmune Encephalomyelitis
ECM, ExtraCellular Matrix
EGF, Epidermal Growth Factor
EMT, Epithelial to Mesenchymal Transition
FAK, Focal Adhesion Kinase
FDA, US Food and Drug Administration
FDG, Fluoro-deoxyglucose
FLT, Fluoro-Thymidine
FOV, Field Of View
Foxp3, Forkhead Box Protein 3
FSPG, Fluoropropyl-L-Glutamate
GATA-3, GATA protein 3
G-CSF, Granulocyte Colony Stimulating Factor
GFP, Green Fluorescent Protein
GITR, Glucocorticoid-Induced TNFR-Related protein
GM-CSF, Granulocyte Macrophage Colony Stimulating Factor
GR1, Granulocyte 1

Gy, Gray
HGF, Hepatocyte Growth Factor
HPA, Hot Pixel Average
HPFOV, High Power Field Of View
HPRT, Hypoxanthine-guanine Phosphoribosyltransferase
HU, Hounsfield Units
IBD, Inflammatory Bowel Disease
IDC, Invasive Ductal Carcinoma
IDO, Indoleamine 2,3-dioxygenase
IFN, Interferon
IGF, Insulin-like Growth Factor
IL, Interleukin
IPEX, Immunodysregulation, Polyendocrinopathy, Enteropathy, X-linked disease
i.p, Intraperitoneal
irAE, Immune Related Adverse Events
ITAM, Immunoreceptor Tyrosine-based Activation Motif
i.v, Intravenous
JAK-STAT,
LAG-3, Lymphocyte Activation Gene 3
LN, Lymph Node
LOX, Lysyl Oxidase
mAbs, Monoclonal Antibodies
MALT, Mucosal Associated Lymphoid Tissue
MAPK, Mitogen Activated Protein Kinases
MBq, Mega-Becquerel
MCA, Methylcholanthrene
mCRPC, metastatic Castration Resistant Prostate Cancer
MDSCs, Myeloid Derived Suppressor Cells
MHC, Major Histocompatibility Complex
MMP, Matrix Metalloproteinase
NBFS, Neutral Buffered Formalin Solution
Nf-κB, Nuclear Factor Kappa-light-chain-enhancer of activated B cells
NHL, Non-Hodgkin's Lymphoma
NK, Natural Killer
Nrp1, Neuropilin 1
NSCLC, Non-Small Cell Lung Carcinoma
OCT, Optimum Cutting Temperature compound
PBMCs, Peripheral Blood Mononuclear Cells
PBS, Phosphate Buffered Saline
PD-1, Programmed Death receptor 1
PDGF, Platelet Derived Growth Factor
PD-L1, Programmed Death Ligand 1
PET, Positron Emission Tomography
PGE2, Prostaglandin E2
pMHC, Peptide MHC
PTC, Papillary Thyroid Cancer
PTEN, Phosphatase and tensin homologue
RAG, Recombination Activating Gene
RNI, Reactive Nitrogen Intermediate

ROIs, Regions Of Interest
ROS, Reactive Oxygen Species
s.c, Subcutaneous
SPECT, Single Photon Emission Computed Tomography
SSTR, Somatostatin Receptor
STAT3, Signal Transducer and Activator of Transcription
SUV, Standardised Uptake Value
TAAs, Tumour Associated Antigens
TAMs, Tumour Associated Macrophages
Tconv, Conventional T cell
TCRs, T Cell Receptors
TGF, Transforming Growth Factor
Th, T helper cell
TLG, Total Lesion Glycolysis
TNF, Tumour Necrosis Factor
Tregs, Regulatory T cells
VEGF, Vascular Endothelial Factor
VEGFR, Vascular Endothelial Factor Receptor
WT, Wild Type
6-TG, 6-Thioguanine

Chapter One

1. Introduction

1.1 Cancer

Cancer is a leading cause of mortality in humans with the number of people developing cancer increasing to every one in two (World Health Organization: Cancer Research UK). There are over 200 types of cancer that may affect each tissue within the body.

1.1.1 Development of cancer

Accumulation of genetic mutations through spontaneous DNA damage during proliferation of healthy cells or through inheritance of a genetic disorder leads to the uncontrolled proliferation of cells and the development of malignant tumours (Vogelstein et al. 2013). Further growth and invasion of malignant cells leads to distant-site metastasis, which is the main cause of fatality amongst cancer patients.

In 2000 Hanahan and Weinberg described the hallmarks of cancer detailing the traits obtained by neoplastic cells during the formation of a malignant tumour in a review which was later updated (Hanahan and Weinberg 2000; Hanahan and Weinberg 2011). Cancer cells must acquire the characteristic of chronic proliferation and resistance to anti-growth factors. Along with resistance to programmed cell death and acquisition of replicative immortality, this promotes healthy cells to create a large mass

(Hanahan and Weinberg 2000). The next important characteristic is the process of angiogenesis. In order for rapidly growing tumours to obtain all the nutrients and oxygen required for tissue growth, tumours must have an adequate blood supply (Hanahan and Weinberg 2000). Due the rapid growth of a tumour and unusual angiogenic structures, the developing vasculature often displays excessive branching and undifferentiated blood vessels leading to erratic blood flow, leakiness and hypoxia (Ten Hagen et al. 2008). Another hallmark is the invasion of the surrounding healthy stroma by cancer cells, which ultimately culminates in the dissemination of cancer cells and metastasis to distant sites (discussed further in Section 1.2). In 2011, Hanahan and Weinberg described a further two hallmarks of cancer, which are often seen as the most important traits of cancer cells. Firstly, the ability of cancer cells to deregulate cellular energetics allows chronic proliferation, survival and therefore tumour growth. The final hallmark acquired by cancer cells is the ability to evade the immune system and avoid destruction allowing propagation of tumours (Hanahan and Weinberg 2011).

1.1.2 Immune surveillance and immune evasion

1.1.2.1 History of immune surveillance

Immune surveillance refers to the continuous monitoring of host tissues by the immune system (Burnet 1957). This mechanism allows the detection of nascent cancer cells and initiates their destruction before development of a tumour. Therefore, cancer cells that have progressed into developing tumours have somehow evaded immune destruction. Paul

Ehrlich first postulated this idea in the early 1900s, hypothesizing that the frequency of genetic mutations occurring during DNA replication would naturally lead to an “overwhelming frequency” of tumour development without the presence of immune surveillance (Dunn et al. 2002; Ehrlich 1909).

Interestingly, immunocompromised patients have an increased frequency of certain cancers, however this observation has been made with mainly virus- induced carcinomas (Vajdic and van Leeuwen 2009). The development of transgenic mice propelled the investigation of immune evasion, and gave further strength to the hypothesis of anti-tumour immune responses. Mice deficient for IFN-γ or perforin, therefore lacking the function of CTLs, NK cells or Th1 helper cells, displayed increased tumour incidence (Smyth et al. 2000a; Street et al. 2001; Street et al. 2002; van den Broek et al. 1996). Further more, transplantable tumours from immunodeficient mice were unable to initiate secondary tumour growth in syngeneic immunocompetent equivalents, whereas tumours developed in immunocompetent mice and subsequently transplanted were able to grow in a secondary immunocompetent host (Smyth et al. 2000b). These studies sprouted the hypothesis of immune editing whereby highly immunogenic cancer cells are detected and destroyed by the surveying immune system and remaining weakly immunogenic cancer cells fail to elicit an immune response and are allowed to propagate. Conversely, in immunodeficient hosts there is no selective depletion of highly immunogenic cancer cells therefore when transplanted into an immunocompetent host these cells are recognised and destroyed (Smyth et al. 2006a).

Clinical epidemiology supports the hypothesis of immune surveillance and immune editing in humans (Bindea et al. 2010; Ferrone and Dranoff 2010; Nelson 2008). In cancer such as colorectal and ovarian, patients with a higher tumour infiltration of NK cells and CTLs have a better overall prognosis and survival (Nelson 2008; Pages et al. 2009). Interestingly, immunodeficient transplant recipients have an increased incidence of donor-derived cancers, suggesting that dormant tumours in donor patients kept in check by immune surveillance are able to grow in recipients due to a lack of anti-tumour immune response (Birkeland et al. 1995; Morath et al. 2004; Myron Kauffman et al. 2002; Pham et al. 1995).

1.1.2.2 Immune editing in cancer

The process of cancer immune editing is 3-fold: firstly, highly immunogenic tumour cells are eliminated by the immune system during immune surveillance. Secondly, tumour cells that avoid immune destruction undergo editing by the adaptive immune response in the process of equilibrium. Finally, tumour cells are able to escape the immune system and propagate to form solid tumours (Mittal et al. 2014; Schreiber et al. 2011).

In the phase of equilibrium tumour cells are kept in a state of dormancy, validated by Koebel in 2007 where a role for the adaptive immune system was demonstrated in dormancy in a methylcholanthrene (MCA)-induced tumour and further corroborated by other preclinical models (Eyles et al. 2010; Koebel et al. 2007; Loeser et al. 2007). In humans, this phase has also been demonstrated as described above whereby recipients of transplants develop tumours arising from donor organs (Strauss and

Thomas 2010). The state of dormancy requires a balance of cytokines, such as interleukin (IL)-23 involved in tumour promotion and IL-2 involved in tumour clearance, and regulatory (Treg and MDSCs) and effector immune cells (CTLs and NK cells) (Teng et al. 2012; Wu et al. 2013). The transition from equilibrium to escape involves the shifting of the balance in favour of immune escape rather than elimination. Many immunotherapies are designed to target this phase of immune editing, with the aim of tipping the balance in favour of tumour cell destruction (Quezada et al. 2011).

In the final escape phase of cancer immune editing, loss of Tumour Associated Antigens (TAAs), an establishment of an immunosuppressive microenvironment, and resistance to cytotoxic destruction are some of the key mechanisms that allow escape from immune-mediated tumour cell clearance (Mittal et al. 2014; Schreiber et al. 2011). Further mutations arising within an immune suppressive tumour microenvironment can result in the development of neoantigens (Schumacher and Schreiber 2015). The recognition of these neoantigens by T cells can be unleashed through checkpoint blockade as discussed in section 1.1.4 (Figure 1.1).

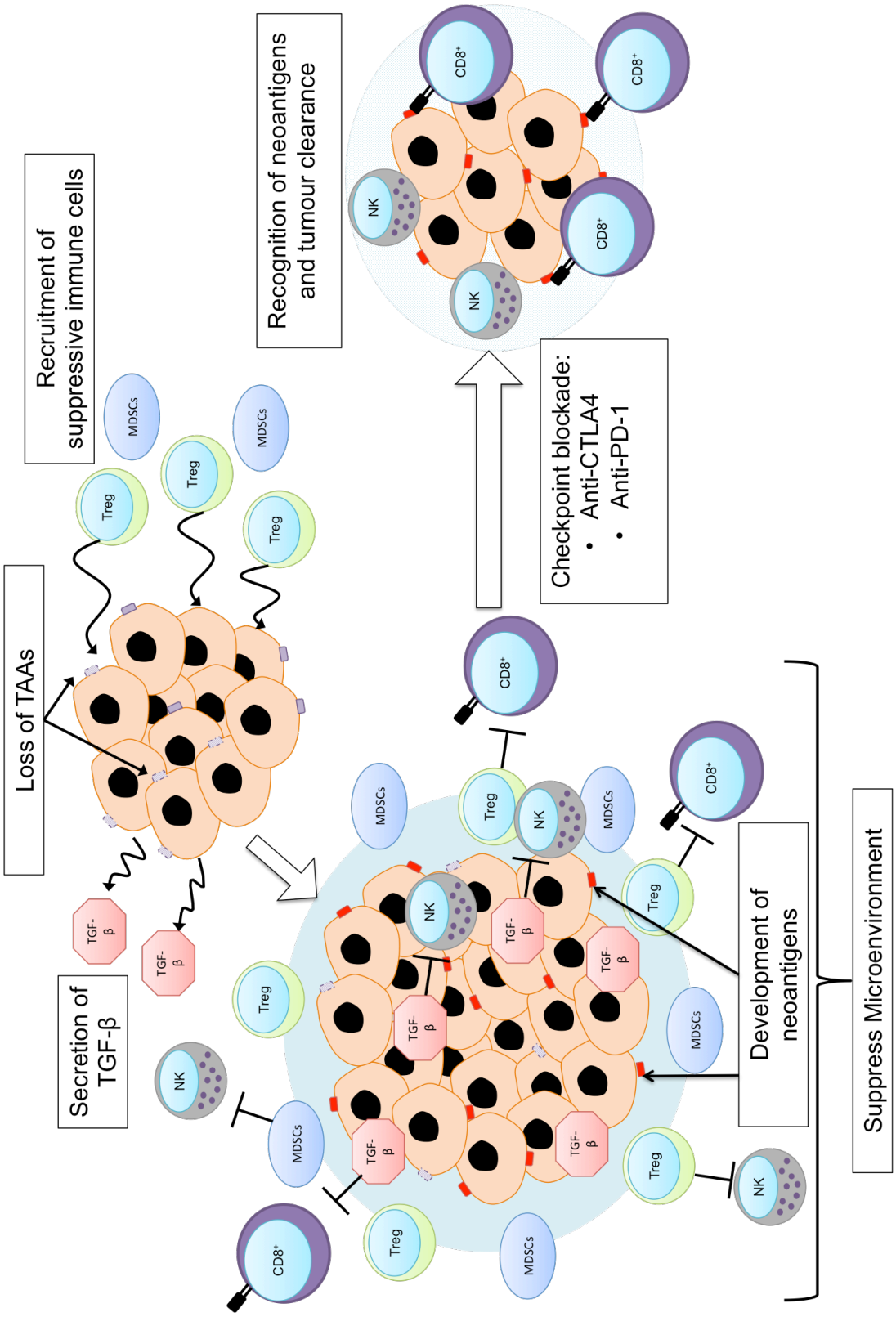

Figure 1.1| Exploiting neoantigen development. The loss of TAAs, recruitment of suppressive immune cells and secretion of TGF-β by tumour cells creates an immunosuppressive microenvironment within the tumour preventing immune clearance. Within the suppressive microenvironment further mutations within tumour cells lead to the generation of neoantigens. Checkpoint blockade such as anti-CTLA-4 or anti-PD-1 antibodies reverse immunosuppression creating the opportunity for neoantigen recognition and immune-mediated tumour clearance.

Exome sequencing and MHC epitope prediction algorithm software has recently shed light on elusive neoantigens. Investigation of an MCA-derived tumour from a RAG2 knockout mouse highlighted a neoantigen arising from the mutation in the gene encoding Spectrin-β2, which normally functioned as an immunodominant rejection antigen (Matsushita et al. 2012). Tumour cells lacking the Spectrin-β2 mutation were able to avoid immune clearance and were selected for growth when transplanted with clones expressing the functional Spectrin-β2, solidifying the notion of TAAs and neoantigens in the process of immune-mediated tumour cell clearance (Matsushita et al. 2012). Interestingly, this phenomenon has also been demonstrated in a clinical setting, where expansion of tumour cells lacking neoantigens is observed in patients after immunotherapy treatment (Nicholaou et al. 2011; von Boehmer et al. 2013). Therefore, when using neoantigens and TAAs as targets during immunotherapy, more than one must be taken into account to avoid selection of weakly immunogenic tumour cells (Mittal et al. 2014).

1.1.3 Inflammation in cancer

It has been widely accepted that inflammation plays a role in tumorigenesis and was incorporated into Hanahan and Weinberg's revised hallmarks of cancer in 2011 (Hanahan and Weinberg 2011; Raposo et al. 2015). There are four main types of inflammation that can contribute to tumorigenesis. Firstly, inflammation arising in response to an infectious agent such a *Helicobacter pylori* can result in the development of mucosa-

associated lymphoid tissue (MALT) lymphoma or gastric carcinoma in humans (De Falco et al. 2015). Secondly, patients with immune-mediated diseases have increased incidence of related cancers, for example inflammatory bowel disease (IBD) and colon cancer (Francescone et al. 2015). Other subclinical inflammatory diseases leave patients with a predisposition to cancers, for example obese patients have a higher risk of liver cancer (Calle and Kaaks 2004). Finally, inflammation occurring as a result of environmental carcinogens such as smoke pollution is also notably correlated with increased cancer incidence (Cohen and Pope 1995).

There are a variety of different mechanisms by which inflammation can initiate tumour growth, with many arising from the transition from acute inflammation to chronic inflammation (reviewed by Coussens and Werb 2002). This results in the upregulation of reactive oxygen species (ROS) and reactive nitrogen intermediates (RNI) that ultimately lead to DNA mutations and inhibit intrinsic mismatch-repair mechanisms (Waris and Ahsan 2006). This genomic instability can initiate tumorigenesis, while the presence of DNA mutations further drives inflammation supporting tumour progression (Ohnishi et al. 2013). Inflammation at the site of a growing tumour supports angiogenesis and the epithelial to mesenchymal transition (EMT), a process necessary for the metastasis of cancer cells (discussed in section 1.2) (Raposo et al. 2015).

The overlapping intrinsic and extrinsic pathways of inflammation and cancer share transcription factors, cytokines and chemokines involved in the recruitment of leukocytes to the tumour (Mantovani et al. 2008). Furthermore, the production of immunosuppressive cytokines in the tumour

microenvironment supports immune evasion and recruits other suppress immune cell subsets such as Tregs, myeloid derived suppressor cells (MDSCs) and tumour promoting macrophages (Balkwill et al. 2005).

1.1.3.1 The role of NF-κB and IL-6 in tumour promoting inflammation

The transcription factor NF-κB and the cytokine IL-6 have both been heavily implicated in the switch from acute wound-healing inflammation to tumour-promoting chronic inflammation (Raposo et al. 2015). The constitutive expression of NF-κB is a hallmark of chronic inflammation and is also documented in many cancer types (Chaturvedi et al. 2011; Karin 2008). Haematological malignancies and lymphomas, such as non-Hodgkin's Lymphoma (NHL), display dysregulation and chronic activation of the NF-κB signaling pathway, resulting in the upregulation of anti-apoptotic proteins such as Bcl-2 promoting tumour cell survival and other chromosomal mutations (Brien et al. 2007; Escarcega et al. 2007; Hiscott et al. 2001; Karin 2006). The constitutive expression of NF-κB has been highlighted as a main mechanism of resistance against chemotherapeutic agents, with some p53-targeted therapies causing the activation of the NF-κB pathway (Brien et al. 2007; Das and White 1997). NF-κB could be used as a target for anti-cancer therapies as inhibition of the transcription factor has been shown to improve the efficacy of and reduce resistance to anti-cancer agents both *in vivo* and *in vitro* (Nakanishi and Toi 2005). However, as NF-κB plays an essential role in many different signaling pathways, possible off-target effects might cause toxicity (Hoesel and Schmid 2013).

IL-6 has both anti- and pro-inflammatory roles depending on the signaling pathways it induces (Yao et al. 2014). IL-6 can be described as an inflammation amplifier due to its interaction with NF-κB in a positive amplifying loop (Atsumi et al. 2014). Phosphatase and tensin homologue (PTEN) and p53 knockdown induces IL-6-mediate STAT3 and NF-κB signaling in a triple negative model of breast cancer, which can initiate EMT in cancer stem cells (Kim et al. 2015). IL-6 has also been shown to be involved in the maturation of DCs and other APCs and can promote the expression of MHC (Hsiao et al. 2008). However, IL-6-mediated small Rho GTPase and STAT3 signaling pathways can induce the differentiation of DCs into regulatory DCs (DCregs) (Zhong et al. 2014).

1.1.3.2 Macrophages, inflammation, and cancer progression

Tumour associated macrophages (TAMs) are accepted to be involved in angiogenesis, tumour cell proliferation and metastasis (discussed further in Section 1.2) (Raposo et al. 2015). The phenotype of TAMs determines whether they have a pro- or anti-tumour response. While macrophages have a wide phenotypic spectrum with varying functions, their classification can be simplified to “M1” and “M2”. The classical M1 phenotype, induced by microbial products or IFN-γ, exhibits anti-tumour effects. However in most human cancers, the macrophage phenotype is weighted towards an M2 phenotype (Sica et al. 2006).

An M2 phenotype is induced by Treg or tumour derived cytokines, such as colony stimulating factor 1 (CSF-1), IL-10, IL-4, IL-6, TGF-β and prostaglandin E2 (PGE2) (Mantovani et al. 2002; Sica et al. 2006). These

macrophages promote angiogenesis through the secretion of pro-angiogenic factors (such as VEGF, angiopoietins and prostaglandin E2 (PGE2)), stimulate proliferation of tumour cells through production of epidermal growth factor (EGF), platelet derived growth factor (PDGF), hepatocyte growth factor (HGF), and basic fibroblastic growth factor (bFGF) (Klimp et al. 2001; Lewis and Murdoch 2005; Sunderkötter et al. 1991). Furthermore, M2 macrophages have increased production of PGE2, nitric oxide and H_2O_2 resulting in direct cytotoxic and suppressive activity on T cells (Klimp et al. 2001; Sica et al. 2006).

1.1.4 Cancer immunotherapy

There is a vast array of different immunological mechanisms involved in tumorigenesis and tumour clearance, and while we are still investigating the events underpinning immune-mediated tolerance to self-antigens, a plethora of mechanisms can be targeted for cancer therapies.

A highly personalized immunotherapy involves the *ex vivo* expansion of patient tumour infiltrating anti-tumour lymphocytes that are subsequently re-infused in a process known as adoptive cell therapy (ACT) (Rosenberg and Restifo 2015). Additionally, the isolated infiltrating lymphocytes can be engineered to express T cell receptors (TCRs) or chimeric antigen receptors (CARs) specific to TAAs (Rosenberg and Restifo 2015). In clinical trials, this therapy has proven most successful in melanoma patients whereby 50% of patients exhibited a response with 22% eliciting complete responses (Hinrichs and Rosenberg 2014). In a study using genetically engineered

TCR expressing lymphocytes specific to the melanoma-melanocyte antigen Melan-A, tumour regression was observed in patients (Morgan et al. 2006). CAR therapy has also been trialed in patients with B cell lymphoma. T cells expressing a CAR against CD19 lead to remission in patients with the disease, with 67% of patients being in sustained remission (Kochenderfer et al. 2010; Maude et al. 2014). However, difficulties arise when targeting self-antigens as on-target off-tumour toxicities are observed (Johnson et al. 2009).

The existence of TAAs has also given rise to the use of cancer vaccines and was originally demonstrated in 1991 by the recognition of a melanoma antigen MAGE-A1 by T cells (van der Bruggen et al. 1991). While many TAAs have since been identified, the majority of antigens used for cancer vaccination are derivatives of male testis antigens (Vigneron et al. 2013). The expression of these antigens is restricted to the male germ line, however many of them appear to be overexpressed in tumours. While some of these vaccines appear to have limited efficacy most likely due to the difficulty in overcoming self-tolerance, the addition of immune adjuvants such as IL-2 has seen some improvement (Makkouk and Weiner 2015). GVAX is a whole tumour cell cancer vaccine that consists of two irradiated prostates cancer cell lines that express Granulocyte-Macrophage Colony Stimulating Factor (GM-CSF). While whole cell tumour vaccines give rise to the opportunity of eliciting immune responses to many different TAAs present on the cancer cells, little change to overall survival was observed in a GVAX clinical trial (Makkouk and Weiner 2015).

The use of DCs pulsed with TAAs as a cancer vaccine has also been explored and has shown the most promise. In 2010, the US Food and Drug Administration (FDA) approved an antigen-pulsed DC cancer vaccine called Provenge for the treatment of metastatic prostate cancer. This vaccine consists of DCs pulsed with a prostatic acid phosphatase fusion protein and GM-CSF, which demonstrated increased survival in three separate Phase III clinical trials (Higano et al. 2009; Kantoff et al. 2010; Kissick and Sanda 2015; Small et al. 2006). While chronic antigen exposure can cause T cell exhaustion in response to a cancer vaccine thereby decreasing its efficacy, the combination of cancer vaccines with therapies to bypass T cell exhaustion show promise (Kissick and Sanda 2015).

Co-stimulatory molecules are used in conjunction with tumour-antigen MHC complexes to stimulate naïve T cells and initiate an anti-tumour immune response. While engagement of these co-stimulatory molecules initially leads to increased proliferation and expansion of specific T cells, negative feedback loops kick-in to prevent the uncontrolled and harmful T cell responses (Quezada and Peggs 2013; Salomon and Bluestone 2001; Sharma and Allison 2015). Checkpoint inhibition therapy aims to target the co-stimulatory molecules in order to prevent inhibition of T cell responses and circumvent T cell exhaustion. Cytotoxic T Lymphocyte Antigen 4 (CTLA-4) is an inhibitory molecule that interacts with CD80 and CD86 on APCs. The co-stimulatory molecule CD28 on T cells that normally interacts with CD80 and CD86 is outcompeted by CTLA-4 in order to downregulate T cell responses (Krummel and Allison 2011; Walunas et al. 1994). Mouse studies also indicated that CTLA-4 was implicated in dampening an anti-tumour

immune response, and CTLA-4 blockade resulted in tumour rejection (Krummel and Allison 1996; Leach et al. 1996). In humans, the CTLA-4 blocking antibody Ipilimumab was approved for use by the FDA after successful clinical trials in melanoma patients (Hodi et al. 2010; Robert et al. 2011). However, while 20% patients treated with Ipilimumab had increased survival, approximately 60% patients observed immune related adverse events (irAE) (Hodi et al. 2010; Schadendorf et al. 2015).

It was initially hypothesised that Ipilimumab targeted CTLA-4 expression on T cells, however CTLA-4 is also constitutively expressed on Tregs in both humans and in mice (Krummel et al. 1996; Read et al. 2000; Takahashi et al. 2000; Walunas et al. 1994; Wing et al. 2008). Therefore, anti-CTLA-4 could act by depleting Tregs thereby removing anti-tumour immune suppression (Read et al. 2006). Further investigations found that inhibition of CTLA-4 on both T cells and Tregs was required for tumour rejection, and while CTLA-4 blockade results in expansion of both T lymphocyte subsets, the ratio of Treg: T cell was ultimately increased in the tumour (Curran and Allison 2009; Liakou et al. 2008; Quezada et al. 2006; Schmidt et al. 2008; Shrikant et al. 1999; Waitz et al. 2012). Quezada and colleagues also demonstrated that CTLA-4 blockade-mediated Treg depletion was dependent on the presence of Fc receptor expressing macrophages within the tumour (Simpson et al. 2013).

A second checkpoint molecule was described in 2000 called Programmed cell Death receptor 1 (PD-1) (Freeman et al. 2000). While PD-1 is expressed on activated T cells, it is mainly expressed on Tregs, B cells, NKT cells and monocytes (Greenwald et al. 2004). PD-1 is activated on

these cells when interacting with one of its two ligands PD-L1 and PD-L2 and interferes with TCR signaling (reviewed in (Greenwald et al. 2004). While PD-L2 is mainly expressed on activated macrophages and DCs, PD-L1 is expressed on T cells and B cells as well as DCs and macrophages. PD-L1 expression has also been shown in some human tumours in response to T cell derived IFN-γ (Dong et al. 2002; Zou and Chen 2008). Mouse models revealed that PD-1 blockade resulted in increased T cell-mediated anti-tumour immunity, and the FDA approved a humanized anti-PD-1 antibody in 2014 known as Pembroluzimab (Dong et al. 2002; Fife et al. 2009; Hamid et al. 2013; Iwai et al. 2002; Robert et al. 2014b; Topalian et al. 2012; Topalian et al. 2014). Pembroluzimab was correlated with good responses in melanoma patients, however like CTLA-4 also had high irAE (approximately 79%) with some patients developing autoimmune diabetes (Hamid et al. 2013; Martin-Liberal et al. 2015). Following from this, a second anti-PD-1 antibody called Nivolumab was approved by the FDA for the treatment of metastatic melanoma and non-small cell lung carcinoma (NSCLC) (Robert et al. 2014a). Interestingly the combination of anti-CTLA-4 and anti-PD-1 therapies has demonstrated better outcome than either single therapy in preclinical studies (Curran et al. 2010). A phase I clinical trial observed over 80% regression of metastatic melanoma in around 50% of patients treated (Wolchok et al. 2013). A study by Zelenay *et al* in 2015 demonstrated the use of a COX2 inhibitor with PD-1 blockade (Zelenay et al. 2015). COX1 and COX2 are important for the production of PGE2, a growth factor involved in the survival, growth, migration, metastasis and immunosuppressive activities of cancer cells (Wang and DuBois 2010) and

are often overexpressed in many different cancer types such as colorectal cancer (CRC), breast, gastric, pancreatic and lung (Dannenberg and Subbaramaiah 2003; Wang and DuBois 2010). Zelenay and colleagues found that loss of COX2 expression in a murine melanoma cell line $Braf^{V600E}$ shifted the inflammatory profile, leading to a decrease in IL-6 and CXCL1 and an increase in anti-tumour immune mediators IFN-γ, T-bet, CXCL10 and IL-12. The subsequent inhibition of COX by aspirin in combination with anti-PD-1 antibody greatly increased $Braf^{V600E}$ tumour rejection, even when the inoculum of tumour cells was too great for anti-PD-1 alone to cause regression (Zelenay et al. 2015). Not only does this study solidify the impact of inflammation on tumour progression, but also suggests a use for COX inhibitors to amplify the effects of checkpoint blockade.

1.2 Metastasis

While there have been great advances in the treatment of primary cancers in patients, the development of metastasis is still responsible for around 90% of patient deaths (Chaffer and Weinberg 2011; Seyfried and Huysentruyt 2013). The term metastasis is used to describe the spread of cancer cells originating from a primary tumour to distant sites, leading to seeding and new metastatic lesion growth (Seyfried and Huysentruyt 2013).

1.2.1 Metastatic Cascade

In order for metastasis to occur, cells from a primary tumour must detach and complete the steps dictated in the metastatic cascade

(Chambers et al. 2002; Duffy et al. 2008; Seyfried and Huysentruyt 2013). Primary tumours must undergo the process of angiogenesis not only to support the tumours metabolic needs but also to allow intravasation of tissue-invading tumour cells into circulation (Chambers et al. 2002; Wyckoff et al. 2000). Once the circulating tumour cells have reached their destined organ, extravasation occurs depositing cells into the surrounding tissue. From here, cells undergo proliferation and initiate angiogenesis, creating a niche for metastatic cell survival (Chambers et al. 2002; Scully et al. 2012). An overview of the metastatic cascade is demonstrated in Figure 1.2.

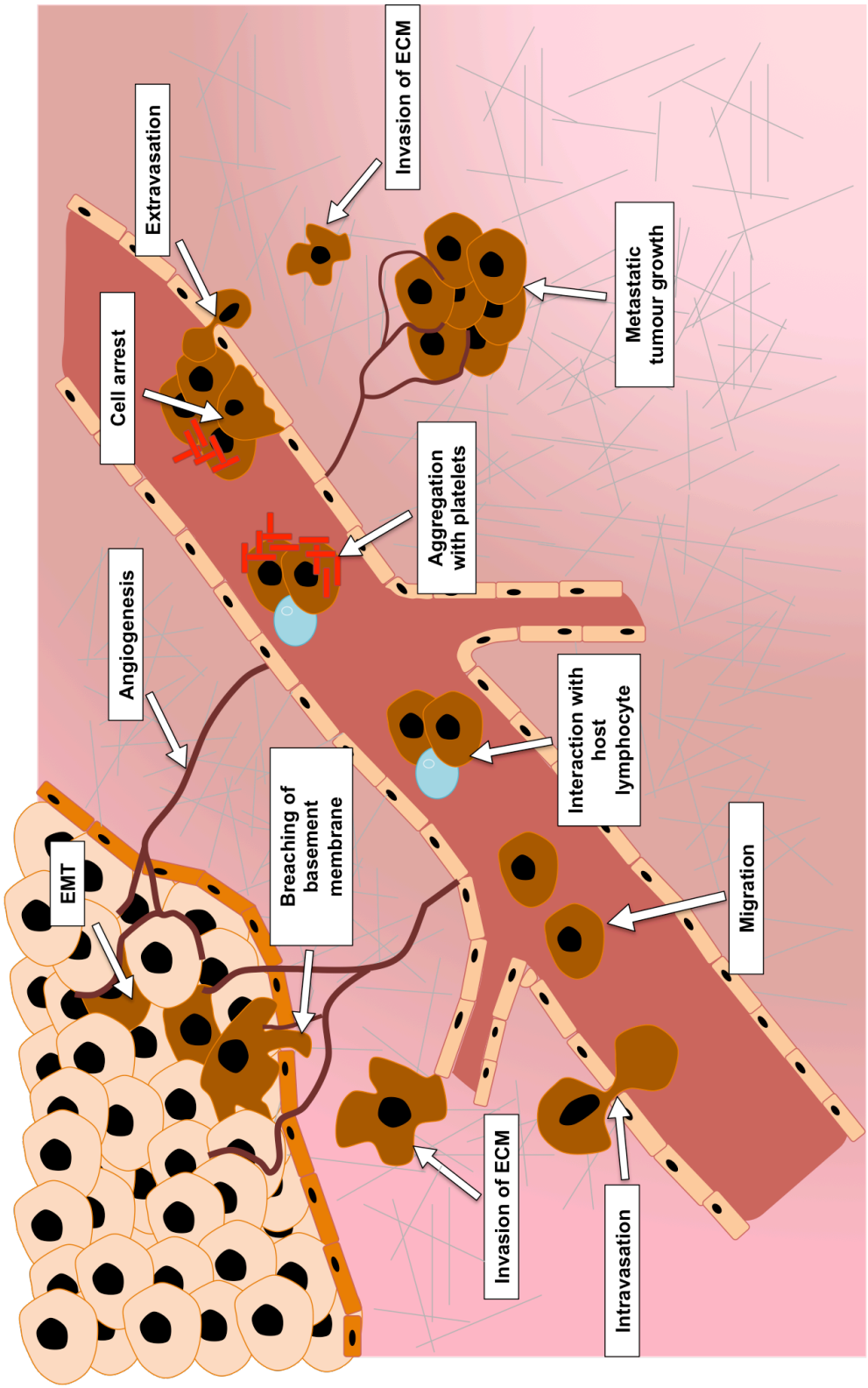

Figure 1.2| The metastatic cascade. The metastatic cascade describes all the steps a metastasizing cell has to complete to form distant site metastases. First, cells must undergo the epithelial to mesenchymal transition and then pass through the basement membrane. Once the basement membrane has been breached, the metastatic cells invade the ECM and intravasate into blood vessels (pictured) or lymphatic vessels. Metastatic cells then migrate through circulation, aggregating with platelets until cell arrest at the endothelial wall. Cells then extravasate the blood vessel and invade the ECM of the secondary organ before seeding and proliferating to form a secondary tumour. Finally, the new metastatic site induces angiogenesis.

1.2.1.1 Invasion

The first stage of the metastatic cascade is the invasion of tumour cells into the surrounding tissue. This is achieved through alterations in cell-cell interactions and between cells and the Extracellular Matrix (ECM) (Scully et al. 2012). The cadherin family plays a vital role in the initial invasion step of metastasis (Bacac and Stamenkovic 2008). E-cadherin, important in the maintenance of adherens junctions in epithelial cells, acts as a tumour suppressor and prevents the detachment of tumour cells (Wendt et al. 2011). Experiments have shown that inhibition of E-cadherin through the use of mAbs can promote an invasive phenotype in epithelial cells, whereas the addition of E-cadherin into invasive carcinoma cells reversed this (Vleminckx et al. 1991). In breast cancer patients, the loss of E-cadherin has been associated with progression, metastasis, and a poor prognosis (Kowalski et al. 2003; Scully et al. 2012). During EMT cells can undergo a cadherin switch from E-cadherin to N-cadherin, which promotes a more motile and invasive phenotype in epithelial cells (Bacac and Stamenkovic 2008; Scully et al. 2012; Wheelock and Johnson 2003). In mice, Kotb *et al* showed that the switch of E-cadherin for N-cadherin on breast epithelial cells leads to the formation of fibrosis in the mammary glands and eventually to the development of malignant breast tumours (Kotb et al. 2011).

While the EMT is an important step in the metastatic cascade, the ECM must be degraded in order for tumour cells to complete invasion into the surrounding tissue. Integrins are transmembrane adhesion receptors that can be found on components of the ECM and mediate the adherence of tumour cells to the ECM (Li and Feng 2011; Mego et al. 2010). It has been

shown that some integrins, such as αvβ1 and α3β1, play a role in degrading the ECM by upregulating certain matrix metalloproteinases (MMPs) allowing the invasion of tumour cells into the surrounding tissues (Mitchell et al. 2010; Rolli et al. 2003). Other MMPs work independently of integrins to enzymatically degrade the ECM, further promoting tissue invasion. Once epithelial carcinoma cells have undergone EMT to resemble long fibroblastic-like cells they are able to move through pores within the degraded ECM following a low resistance route (Provenzano et al. 2008; Rösel et al. 2008; Scully et al. 2012). From here, these cells can begin the intravasation stage of metastasis either through the vasculature or lymphatics.

1.2.1.2 Intravasation

The process of angiogenesis within the primary tumour not only supplies the tumour with oxygen and glucose but also provides an opportunity for intravasation of invading tumour cells (Chambers et al. 2002; Scully et al. 2012). While intravasation can also occur within the lymphatics, the main route is through haematogenous intravasation (Bacac and Stamenkovic 2008; Chiang et al. 2016). Each tumour type has varying methods of intravasation, and can occur via a passive or active mechanism. Ultimately tumours that intravasate into the lymphatics eventually drain into the circulatory system but during this process come into contact with different lymph nodes, which in some cancers are the first point of metastasis (Bacac and Stamenkovic 2008; Chiang et al. 2016). The route of intravasation of tumour cells is dictated by various factors, namely the

availability of blood or lymphatic vessels. Blood vessels have tight endothelial junctions proving difficult to pass through, and once tumour cells are inside the blood vessel they are exposed to high blood flow and pressure. Lymphatics are easier to intravasate as they are designed for the passage of cells in and out of the vessels. The limiting factor for this method of intravasation is the ability of tumour cells to move through the ECM and reach the lymphatic vessels (Chiang et al. 2016).

There are a number of different *in vivo* models for the investigation of tumour cell intravasation. Transparent fluorescent transgenic Zebrafish can successfully be used to visualise intravasation through high-resolution imaging (Moore and Langenau 2012). Murine models can also be used to directly visualise intravasation through the use of intravital multiphoton imaging of fluorescently labeled tumour cells (Chiang et al. 2016).

1.2.1.3 Circulation and extravasation

Once tumour cells have undergone intravasation they must survive in circulation until the point of extravasation is reached. This involves resisting stress-induced destruction from fast blood flow and escaping immune clearance. Tumour cells express oligosaccharides that correspond to various selectins (Bacac and Stamenkovic 2008). These lectins can be found on platelets and endothelial cells, such as P-selectin and E-selectin, and on the surface of leukocytes, such as L-selectin (Rosen 2004; Sackstein 2005). The expression of these selectin ligands on tumour cells allows aggregation of platelets and leukocytes to the tumour cells and can also promote adherence of tumour cells to activated endothelium (Mannori et al. 1995;

Rosen 2004). Integrins have also been shown to play a part in the adhesion of tumour cells to the endothelium. A study by Taichman *et al* showed that tumour cells expressing α4β1 integrin were able to adhere to VCAM-1 on activated endothelial cells (Taichman et al. 1991). Once tumour cells have arrested on the endothelium, they proliferate and disrupt the capillary wall (Chambers et al. 2002). From here it is then possible to infiltrate the surrounding tissues.

1.2.2 Differing hypotheses of specific-site metastasis

1.2.2.1 Seed and soil hypothesis

In 1889, Stephen Paget first proposed the seed and soil hypothesis of metastasis after analysis of over 900 autopsies of patients with primary and secondary tumours. It was noticed that there was a pattern to the location of organs that developed secondary tumours, which led him to develop the hypothesis that the seed (metastasizing cells) must be compatible with the soil (site of metastatic tumour growth) (Paget 1889). This was further evidenced through the review of clinical data by Sugarbaker and, later, Weiss (Sugarbaker 1979; Weiss 2000).

This hypothesis has come under scrutiny after intravital microscopy showed tumour cells aggregated to platelets and leukocytes can block capillaries and arrest against the endothelial walls. Tumour cells can then proliferate and disrupt the capillary wall and invade the local parenchyma (Bacac and Stamenkovic 2008; Chambers et al. 2002; Chambers et al. 1998-1999). This is due to the size restrictions of capillaries. While white

blood cells can pass through small capillaries and arrest using cadherins and integrins, tumour cells arrest in the capillaries as a result of their large size. It is possible to speculate therefore that the site-specific metastases development is not due to homing of tumour cells but rather the suitability of the secondary site for metastases proliferation and angiogenesis.

1.2.2.2 Chemokine-mediated hypothesis

Chemokines and their respective receptors are heavily involved in homing of lymphocytes to different organs and also tumours (discussed in Section 1.3.4.2) and have recently been shown to play a potential role in metastasis (Bacac and Stamenkovic 2008; Chambers et al. 2002). In breast cancer, tumour cells were found to express CXCR4 and CCR7 chemokine receptors with their ligands expressed at key sites of metastasis, such as the lungs, liver, lymph nodes and spleen (Muller et al. 2001). Further analysis of the human breast cancer cell line MDA-MB-231 injected into SCID mice along with human CXCR4 blocking antibody revealed fewer lung metastases after 28 days (Muller et al. 2001). Interactions of chemokines with their receptors initiates intracellular signaling resulting in actin polymerization and development of pseudopodia, as well as activation of the RAS/MAPK pathway (Chambers et al. 2002). In many human cancers, RAS genes are often mutated or activated through other mechanisms and influence the proliferation-apoptosis balance in favour of cell growth (Clark and Der 1995). Recent studies have shown that liver micrometastases induced with RAS-transformed cells survived and maintained metastatic growth better than their control counterparts (Koop et al. 1996; Varghese et al. 2002).

While studies suggest a key role for chemokines in metastasis, ultimately the size and shape of metastasizing cancer cells limits their ability to recirculate once they have arrested in a capillary and therefore raises doubts about their importance in tumour cell homing. However, chemokine interactions could be an important determining factor of tumour cells extravasation, proliferation and survival at specific organ sites (Chambers et al. 2002).

1.2.2.3 Genetically determined metastatic homing

Another postulated hypothesis regarding organ-specific metastasis is that homing to new metastatic sites is, in part, genetically determined (Bacac and Stamenkovic 2008). Investigation of lung-colonizing B16 melanoma cell gene expression revealed the upregulation of RhoC, a protein in the Rho-GTPase family normally associated with cell proliferation and cytoskeletal remodeling (Clark et al. 2000; Van Aelst and D'Souza-Schorey 1997). In the human breast cancer cell line MDA-MB-231, repeated intravenous injection led to the isolation of daughter cell lines exhibiting a pattern of gene expression specific not only to generalized metastasis, but also to the particular organs within which they had seeded and grown (Minn et al. 2005). Another study demonstrated that overexpressed genes in cell lines able to metastasize to bone were associated with membrane-bound and secreted molecules within the bone microenvironment (Kang et al. 2003). While the induced expression of a single one of these overexpressed genes in MDA.MD-231 failed to initiate bone metastasis, the combination of three

or more bone metastasis-associated genes in this cell line successfully promoted metastasis to bone (Kang et al. 2003).

Each of these hypotheses has some merit in the context of metastasis. It is widely accepted that Stephen Paget's idea of site-specific metastasis holds true whereby the site at which metastases develop must have the correct microenvironment, however the idea of chemokine-dependent homing of metastasizing cells to distant organs remains unclear. While it is evident that chemokines play a role in metastasis, it is not known whether the expression of chemokine receptors by tumour cells aids cells extravasation after cell arrest within the capillaries. Evidence exists to support each of the three hypotheses, suggesting a combination of all 3 must occur for successful metastasis.

1.2.3 The metastatic niche

The notion of site-specific metastasis is supported by the development of distant-site metastatic niches. Similar to stem cell niches, metastatic niches provide the optimal environment for the seeding, proliferation and ultimate survival of metastasizing cells, however they lack structural organization observed in stem cell niches (Descot and Oskarsson 2013).

The pre-metastatic niche is formed at distant sites ahead of cancer cell colonization under the influence of growth factors, cytokines, exosomes and enzymes secreted by the primary tumour (Psaila and Lyden 2009). The subsequent remodeling of ECM, vasculature and lymphatics create an

environment conducive to cancer cell extravasation and seeding (Descot and Oskarsson 2013; Psaila and Lyden 2009). Matrix metalloproteinases (MMPs) and other enzymes are able to remodel the ECM leading to an increase in stromal fibronectin and retention of recruited vascular endothelial growth factor (VEGF)R1^{+} bone marrow derived cells (BMDCs) (Kaplan et al. 2005).

Studies have also shown metastasizing cells are able to take advantage of already established stem cell niches. For example, cancer cells have been shown to colonize the osteoblastic niche of hematopoietic stem cells in the metastasis of prostate cancer cells to bone (Shiozawa et al. 2011). With the overlap of signaling pathways involved in both pluripotency and cancer cell propagation, such as Wnt, Notch, PI3K and JAK-STAT, the stem cell niche provides many benefits to metastasizing cells (Dreesen and Brivanlou 2007). Interestingly, endothelial cells have also been implicated in maintaining cancer stem cell phenotype in CRC through the induction of the Notch signaling pathway (Lu et al. 2013). Further evidence for the involvement of endothelial cells in metastasis was revealed in a xenograft mouse model of breast and melanoma cell metastasis to brain, which showed maintenance of cancer cell-endothelial cell contact long after extravasation (Carbonell et al. 2009; Kienast et al. 2010). While it is clear that the utilization of stem cell niches and involvement of endothelial cells play a role in the development of metastases, the precise mechanisms are yet to be described (Descot and Oskarsson 2013).

Upon formation of the metastatic niche, mechanisms of disease progression begin to unfold. The invasive front of the metastatic niche is the

site at which the newly formed secondary tumour meets the stroma, and is constantly moving (Friedl et al. 2012). Tumour cells at the invasive front undergo EMT as described in Section 1.2.1.1 allowing invasion of surrounding stroma and progression of metastatic disease (Thiery et al. 2009). While the invasive front is highly vascularized, newly formed blood vessels are underdeveloped and leaky, preventing oxygen delivery to certain parts of the tumour (Vaupel et al. 2001). This leads to the formation of hypoxic pockets, an environment that promotes cancer stem cell phenotypes (Lu and Kang 2010).

1.2.3.1 The niche ECM

The ECM in the metastatic niche develops an optimal structure for the progression and outgrowth of metastases (Descot and Oskarsson 2013). While investigation into the specific components of the niche ECM is ongoing, its general overall structure appears much different to ECM in homeostatic conditions (Descot and Oskarsson 2013; Sleeman 2012). The composition of the ECM undergoes both changes in constitution and deposition of new ECM components. The recruitment of fibroblasts and fibroblast-like cells plus the deposition by primary tumour cells leads to the accumulation of fibronectin, which is required for the attachment of cancer cells and BMDCs (Kaplan et al. 2005). Other ECM components, such as periostin and tenascin-c, are also key factors in the reconstitution of the niche ECM. Periostin is involved in retention of tenascin-c in the ECM through binding this factor along with fibronectin and collagen type I (Kii et al. 2010; Vogelstein et al. 2013). Both periostin and tenascin-c are strong

promoters of Notch and Wnt signaling pathways promoting stem cell like properties and remodeling, and have also been shown to promote metastasis to the lung (Oskarsson et al. 2011).

Matrix proteins, heparin and heparin sulfate within the ECM are able to bind and retain growth factors and cytokines such as GM-CSF, HGF, interleukins, TGF-β, and EGFs (Taipale and Keski-Oja 1997). Furthermore, the structure of the ECM is conducive to cancer cell adhesion. The activation of focal adhesion kinase (FAK) by type 1 collagen and by integrin surface receptors on cancer cells leads to PI3K and MAPK cell signaling promoting cancer cell survival (Chiarugi and Giannoni 2008). Furthermore, FAK also regulates EMT through TGF-β signaling and ECM adhesion causing disruption of E-cadherin interactions in CRC (Avizienyte et al. 2002; Cicchini et al. 2008).

1.2.3.2 The secreted cytokine milieu of the metastatic niche

The induction and maintenance of EMT at the invasive front is essential for the progression of metastatic disease (Descot and Oskarsson 2013). Cytokines such as TGF- β and hepatocyte growth factor (HGF) are both strong inducers of EMT, with HGF also promoting stem cell like properties in already differentiated cancer cells by strengthening the Wnt signaling pathway (Janda et al. 2002; Vermeulen et al. 2010).

Inflammatory cytokines have also been implicated in promoting the progression of metastasis. In breast cancer, the production of IL-6 by osteoblasts promotes outgrowth of bone metastases, while PI3K signaling initiated by CXCL12 and IGF1 further stimulate metastatic outgrowth (Sethi

et al. 2011; Zhang et al. 2009). Inflammatory cytokines also recruit inflammatory monocytes and myeloid progenitors to the site of lung metastases from breast cancer through CCL2 and CXCL1/2 chemokines (Acharyya et al. 2012; Qian et al. 2011). Furthermore, inflammatory myeloid progenitors also maintain a stem cell like state in cancer cells, preventing upregulation of differentiated cell markers and therefore immune recognition and destruction (Landsberg et al. 2012).

Cancer cells as well as the niche parenchyma in lungs can secrete the calcium binding S100 proteins (Descot and Oskarsson 2013). During the formation of the pre-metastatic niche, TNFα, TGF-β and VEGF-A secretion by the primary tumour leads to upregulation of S100A8/9 and recruitment of CD11b myeloid cells along the CXCL1/2 axis (Hiratsuka et al. 2006; Hiratsuka et al. 2008; Lukanidin and Sleeman 2012).

Microvesicles around 30-100nm in diameter known as exosomes have also recently been implicated in metastasis (Descot and Oskarsson 2013). Exosomes released from melanomas have been shown to prime BMDCs for a pro-metastatic phenotype through the delivery of Met receptors (Peinado et al. 2012). Exosomes have also been shown to induce expression of growth factors such as VEGF-A and remodeling enzymes such as MMP2 and MMP9 at the pre-metastatic niche (Grange et al. 2011; Jung et al. 2009; Peinado et al. 2011). Additionally, exosomes have also been implicated in mediating suppression of anti-tumour immune responses (Valenti et al. 2007). A study by Clayton and colleagues in 2011 described the expression of the ectonucleosidases CD39 and CD73 by cancer derived exosomes that led to an increase in extracellular adenosine (Clayton et al.

2011). Conversion of 5'AMP to adenosine by exosomes resulted in the inhibition of T cell activity in an A2A-receptor dependent manner, similar to Treg mediated suppression discussed in Section 1.3.3.2. (Clayton et al. 2011).

1.2.3.3. The role of MMPs and other remodeling enzymes in the metastatic niche

MMPs have an important role in the remodeling of the ECM at the primary tumour site in order for invasion to occur (Descot and Oskarsson 2013; Sleeman 2012). Similarly, MMPs as well as other remodeling enzymes like cathepsins have an important role at the metastatic niche. MMPs cleave domains of ECM components that can subsequently interact with integrins and other surface receptors thereby initiating intracellular signaling (Descot and Oskarsson 2013). For example, in mammary gland involution MMP2 cleaves an EGF-like fragment from the basement membrane protein LM-332, which subsequently binds to EGFR and initiates MAPK signaling (Schenk et al. 2003). These cleaved domains can also be involved in immune cell recruitment. The degradation of collagen by MMPs produces tripeptide Pro-Gly-Pro, which initiates CXCR1/2 mediated recruitment of neutrophils to the lungs (Weathington et al. 2006). As the structure of the ECM allows retention of growth factors, MMP enzymatic activity releases these growth factors such as TGF-β thus promoting proliferation and survival of cancer cells (Dallas et al. 2002). In mammary carcinoma models, MMP2 and MMP9 are able to cleave latent TGF-β in the

pre-metastatic niche and hypoxic areas resulting in cancer invasion and angiogenesis (Yu and Stamenkovic 2000).

The state of hypoxia causes secretion of lysyl oxidase (LOX) enzyme in response to hypoxia inducible factor (HIF)-1, which in turn leads to stiffening of the matrix by the formation of crosslinks between collagen fibres (Erler et al. 2006). This LOX dependent ECM stiffening ultimately promotes MAPK and PI3K signaling through focal adhesions. The presence of matrix stiffening is often associated with aggressive tumours and a poor prognosis (Levental et al. 2009). A hypoxic state in the metastatic niche also recruits $VEGFR1^+$ BMDCs and $CD11b^+$ myeloid cells, while also maintaining stem cell like properties of cancer cells (Du et al. 2008; Lin and Yun 2010; Lu and Kang 2010). It is postulated therefore that the hypoxic state in the metastatic niche promotes metastatic outgrowth by encouraging the proliferation of the cancer stem cell population (Sleeman 2012).

1.2.4 The role of the immune system in metastasis

Cells of the immune system play important roles in the prevention of metastasis and destruction of tumour cells, however they have also been implicated in aiding the progression of disease (Kitamura et al. 2015).

Macrophages have been implicated in both tumour suppression and tumour progression. Macrophages are recruited to the tumour site through the production of cytokines such as colony stimulating factor 1 (CSF-1), VEGF-A, CCL2 and CXCL12 (Cook and Hagemann 2013; Lee et al. 2013). Once at the tumour site, these tumour associate macrophages (TAMs) can

suppress $CD8^+$ T cell cytotoxic activity through the expression of programmed death ligand 1 (PD-L1) and recruitment of Tregs via CCL22 (Curiel et al. 2004; Kuang et al. 2009). Macrophages have been implicated in aiding angiogenesis and have been shown to be associated with new blood vessels, aiding dissemination of metastatic cancer cells (Kitamura et al. 2015). In a mouse model of breast cancer, the depletion of macrophages impaired the onset of angiogenesis thereby leading to suppression of PyMT cell metastasis to the lungs (Lin et al. 2006; Lin et al. 2001). TAMs promote angiogenesis through the secretion of VEGF-A, and knock out of the *Ets2I* gene in TAMs leads to the upregulation of thrombospondin 1 and 2 (Zabuawala et al. 2010). TAMs are also involved in invasion and intravasation of tumour cells as intravital microscopy exhibits the association of disseminating tumour cells and TAMs during intravasation in PyMT tumours (Wyckoff et al. 2004; Wyckoff et al. 2007). The secretion of EGF by TAMs enhances the invasive qualities of tumour cells through the stimulation of invapodium formation (Zhou et al. 2014). TAMs also aid the adhesion of tumour cells to the ECM through the secretion of CCL18 and osteonectin (Chen et al. 2011; Sangaletti et al. 2008). The production of cathepsin B and S by TAMs in a mouse model of pancreatic cancer has also been shown to promote angiogenesis and the metastasis of tumour cells (Gocheva et al. 2010). The induction of TAM-like phenotype in tumour infiltrating macrophages have not yet been fully characterized, however recent studies have demonstrated the role of $CD4^+$ T cells in this process (Kitamura et al. 2015). The secretion of IL-4 by $CD4^+$ Tcells increases the production of EGF by TAMs, which is associated with invasion of tumour cells (DeNardo et al.

2009). Furthermore, the production of IL-4 by tumour cells also increases the production of cathepsins by TAMs promoting angiogenesis (Gocheva et al. 2010). The production of GM-CSF by human breast tissue alters the phenotype of macrophages to a TAM-like phenotype, which has been shown to be required for the occurrence of metastasis in a xenograft mouse model (Su et al. 2014). COX2 inhibition by Etodolac suppresses the expression of VEGF-A and MMP9 by TAMs, preventing the metastasis of breast cancer cells to the lungs in a mouse model (Na et al. 2013). Interestingly, the histidine-rich glycoprotein overexpression in TAMs skews their polarization to anti-tumour from pro-tumorigenic through the down-regulation of placental growth factor (PGF) thereby inhibiting metastasis by normalizing the structure of leaky blood vessels (Rolny et al. 2011). Collectively, these suggest that the roles of macrophages in tumour progression or suppression are heavily dependent on the tumour microenvironment (Kitamura et al. 2015).

Similarly, neutrophil contribution to tumour immunity is also tumour-dependent. Neutrophils have been implicated in the promotion of angiogenesis and cell migration (Kitamura et al. 2015). A mouse model of melanoma demonstrated that UV light stimulation promoted the recruitment of neutrophils to the tumour site to enhance angiogenesis leading to an increase in metastasis (Bald et al. 2014). Conversely, in a murine model of spontaneous breast cancer, the depletion of neutrophils was correlated with increased metastatic foci within the lungs (Granot et al. 2011). Moreover, neutrophils isolated from tumours in mice were found to kill tumour cells *in vitro* in an H_2O_2-dependent manner. The adoptive transfer of these anti-

tumour neutrophils into tumour bearing mice suppressed the development of lung metastases (Granot et al. 2011).

$CD11b^+$ $Gr1^+$ MDSCs are also recruited to the tumour site through CXCL5 or GM-CSF as shown by a mouse model of pancreatic cancer (Bayne et al. 2012). At the invasive front, MDSCs can promote invasion of tumour cells through expression of MMPs (Yang et al. 2008). MDSCs have also been shown to suppress the production of cytokines by T cells *in vitro* and the use of GR1 neutralizing antibody decreases the frequency of MDSCs while increasing the presence and function of NK cells in a subcutaneous model of lung cancer in mice (Srivastava et al. 2012; Yang et al. 2008). This ablation of MDSCs also prevents the metastasis of tumour cells from the subcutaneous site to the lungs. However, GR1 neutralizing antibodies are not specific to MDSCs and can also suppress monocytes and neutrophils (Sawant et al. 2012).

The adaptive immune subset also plays a role in metastasis. Tregs are recruited to the primary tumour site by CCL22 and CCL5 (Curiel et al. 2004; Tan et al. 2009; Tan et al. 2011; Yang et al. 2012). The secretion of TNF increase lung metastasis in a melanoma mouse model by causing the expansion of Tregs (Chopra et al. 2013). Furthermore, the suppression of NK cell cytotoxicity in a TGF-β-dependent manner by Tregs further promotes metastasis (Smyth et al. 2006b). The role of Tregs in tumour development is further discussed in Section 1.3.4.

A study in the murine breast cancer model PyMT revealed that the loss of TGF-β signaling led to an increase in CXCL1 and CXCL5 thereby recruiting MDSCs to the tumour site (Novitskiy et al. 2011). This in turn led to

the accumulation of Th17 cells due to the secretion of IL-6, IL-23 and TGF-β by MDSCs. In a positive feedback loop, the secretion of IL-17 by Th17 cells further recruited MDSCs to the tumour site thereby increasing immunosuppression and ultimately leading to increased metastasis to the lungs (Novitskiy et al. 2011). Conversely, Th17 cells can also recruit DCs and cytotoxic cells to the tumour site, suggesting that the role of Th17 cells in tumour immunity is dependent on the tumour environment in the same manner as TAMs and neutrophils (Zou and Restifo 2010).

Finally, B cells expressing CD25 and B220 known as B-regs also play a role in metastasis (Kitamura et al. 2015). In an intravenous 4T1 murine breast cancer model, an increase in $CD25^+$ $B220^+$ B-regs was observed. The administration of B220 depleting antibody in this model resulted in fewer lung metastases (Olkhanud et al. 2011). It has been postulated that B-regs act by converting $CD4^+$ T cells to Tregs via the secretion of TGF-β, although more investigation is needed (Olkhanud et al. 2011).

The recruitment of suppressive cell types to the tumour allows tumour cell survival and dissemination into circulation as shown by different tumour models. It is also clear that the role of immune cells in cancers is dependent on the tumour microenvironment, with a variety of cytokine and chemokine expression by tumour cells influencing the type of immune cells recruited. Further investigation and understanding of the mechanisms involved in recruitment and suppression on different tumour models would pave the way for effective immunotherapy treatments in cancer and metastasis.

1.3 Regulatory T cells

1.3.1 Discovery of Tregs

Tregs are described as $CD4^+$ $CD25^+$ $Foxp3^+$ T cells and develop in the thymus during positive and negative selection. The idea of the thymus as the site of a suppressive T cell subset development was first postulated in the 1960s, when thymectomy between day 2 and day 4 of life led to autoimmune destruction of ovaries in neonatal mice (McIntire Kr Fau - Sell et al. 1964; Nishizuka and Sakakura 1969). It was Sakaguchi and colleagues in 1995 that discovered a suppressive $CD25^+$ subset of $CD4^+$ T cells that prevent the onset of autoimmunity in thymectomized mice. It was also observed that when $CD4^+$ T cells were adoptively transferred into thymectomized mice without the $CD25^+CD4^+$ subpopulation, autoimmune disease was still present (Sakaguchi et al. 1995).

CD25 is not specific to this suppressive subset of T cells and is also upregulated on all activated T cells. The forkhead transcription factor Forkhead Box Protein 3 (Foxp3), found on the X-chromosome, was identified as a specific maker of Tregs (Fontenot et al. 2003; Hori et al. 2003; Khattri et al. 2003). A loss-of-function mutation in the *foxp3* gene locus was discovered to be responsible for the autoimmunity in Scurfy mice and for the onset of IPEX (immunodysregulation, polyendocrinopathy, enteropathy, X-linked syndrome), an inherited autoimmune disorder in humans (Bennett et al. 2001; Brunkow et al. 2001; Wildin et al. 2001). Furthermore, while Foxp3 expression was primarily limited to $CD4^+CD25^+$ Tregs, retroviral expression of Foxp3 in $CD25^-CD4^+$ T cells *in vitro* and transgene induction of Foxp3 *in*

vivo promoted suppressive activity and expression of Treg associated markers such as CD25, GITR and CTLA-4 (Fontenot et al. 2003; Hori et al. 2003; Khattri et al. 2003). While in mice Foxp3 expression is specific to $CD4^+$ Treg cells, activated human T conventional cells also transiently upregulate Foxp3 without acquiring suppressive activities or a Treg-like phenotype (Fontenot et al. 2005b; Gavin et al. 2006).

1.3.2 Development of Tregs

1.3.2.1 Thymic Tregs (tTregs)

Tregs develop during positive and negative selection in the thymus. T cell progenitors migrate from the bone marrow to the subcapsular zone of the thymus where they expand as double negative (DN) cells and begin to express TCRs (Overgaard et al. 2015). Upon migration back to the medulla of the thymus, these early stage lymphocytes begin their double positive (DP) stage and express both CD4 and CD8 (Germain 2002). During this time, DP cells undergo selection in the thymus determined by the signal strength received by thymic APCs. High avidity interactions between TCR and peptide MHC (pMHC) complex lead to negative selection of thymocytes, whereas low to medium affinity leads to positive selection (Workman et al. 2009). The DP thymocytes subsequently differentiate into either the CD4 or CD8 lineage, depending on the expression of certain transcription factors (Overgaard et al. 2015).

Of the CD4 single positive (CD4SP) lineage, thymic derived Tregs are thought to develop from immature $CD24^{hi}CD4^+CD8^-$ thymocytes, although a

small proportion have been identified as having been developed from DP cells (Kitagawa et al. 2017; Lee and Hsieh 2009). These immature CD4SP cells undergo strong TCR and CD28 co-stimulation to generate tTreg precursor cells with a $CD25^{+}GITR^{+}Foxp3^{-}CD4SP$ phenotype (Lio and Hsieh 2008). These tTreg precursors undergo further stimulation through TCR binding and IL-2 to differentiate into a $Foxp3^{+}$ tTregs with a stable DNA methylation pattern (Kitagawa et al. 2017; Lio and Hsieh 2008). Some studies have shown, however, that IL-2 is not necessarily required for tTreg cell differentiation, as mice with IL-2 knockdown only experience a 50% decrease in numbers of tTregs (D'Cruz and Klein 2005; Fontenot et al. 2005a). In 2017, Shimon Sakaguchi and colleagues showed that the presence of Treg Super Enhancers (SEs) precede the expression of Foxp3 in tTreg precursors and are associated with Treg genes such as *Foxp3, Ctla4* and *Il2ra*. Furthermore, it was also observed that Foxp3 is not require for the induction of Treg-associated genes, but enhances an established Treg gene expression pattern (Kitagawa et al. 2017).

1.3.2.2 Peripherally derived Tregs (pTregs)

Tregs can also be induced outside of the thymus from naïve $CD4^{+}$ T cells. This induction occurs through exposure to stimulatory cytokines, such as IL-10 and TGF-β, and strong TCR signaling with suboptimal co-stimulation (Plitas and Rudensky 2016). The *Foxp3* cis-regulatory element conserved non-coding sequence (CNS) 1, required for the induction of pTregs, contains a retrotransposon normally found in placental mammals suggesting a role of pTregs in maternal-neonatal tolerance (Samstein et al.

2012). It has also been shown that CNS knock-out mice that do not develop pTregs did not develop severe autoimmunity, but instead developed spontaneous Th2 responses at mucosal sites and inflammation associated with asthma and allergic airways (Josefowicz et al. 2012). These data suggest that while tTregs are involved in self-tolerance, pTregs are involved in tolerance to non-self antigens (Plitas and Rudensky 2016).

1.3.3 Function of Tregs

Tregs promote self-tolerance and prevent autoimmune responses through the suppression of other immune cell subsets. In the presence of APCs *in vitro,* Tregs are functionally capable of suppressing the proliferation and cytokine production of naïve Tcells, while *in vivo* Tregs suppress the effector activities of $CD8^+$ and $CD4^+$ Tcells (Sakaguchi et al. 2008; Takahashi et al. 1998; Thornton and Shevach 1998).

There are four main mechanisms described for Treg-mediated suppression, either acting directly on effector cells or APCs or indirectly through suppressive cytokines.

1.3.3.1 Suppression through inhibitory cytokines

Inhibitory cytokines, such as IL-10, TGF-β, and IL-35 appear to have differing suppressive functions *in vivo* and *in vitro.* The anti-inflammatory cytokine IL-10 *in vivo* has been shown to be important for control of Experimental Autoimmune Encephalomyelitis (EAE), a murine disease homologue of human multiple sclerosis, inflammation at mucosal sites and

infection (Schmidt et al. 2012). Conversely a suppressive function of Treg-generated IL-10 could not be identified through the use of *in vitro* suppression assays (Schmidt et al. 2012).

While TGF-β has been shown to be required for induction of pTregs *in vivo,* its suppressive ability remains controversial. Although TGF-β deficient Tregs have been shown to suppress conventional T cells *in vitro,* Treg-mediated control of colitis *in vivo* has been shown to require TGF-β (Izcue et al. 2009; Read et al. 2000). Surface-bound TGF-β has also been shown to play a role in cell-cell contact-mediated suppression (Nakamura et al. 2001). In a model of diabetes, Tregs expressing membrane-tethered TGF-β were able to control $CD8^+$ T cell infiltration into islet therefore delaying the onset of disease (Green et al. 2003).

IL-35 is a member of the IL-12 heterodimeric cytokine family formed from the Epstein-Barr virus induced gene *Ebi3* and p35 (or *Il12a*). This recently described inhibitory cytokine is preferentially expressed by, and required for suppressive activity of, Tregs (Collison et al. 2007). Both *Ebi3* and *Il12a* deficient Tregs not only had reduced regulatory function *in vitro* but also failed to cure IBD *in vivo* (Collison et al. 2007).

1.3.3.2 Metabolic disruption-mediated suppression

The upregulation of IL-2Rα (CD25) is a classic hallmark of Tregs. While IL-2 is required for the differentiation of tTregs and for their maintenance, Tregs do not secrete IL-2 themselves. An interesting hypothesis postulated that high-level expression of CD25 allowed Tregs to “scavenge” IL-2 thus depriving local actively proliferating effector T cells

leading to cytokine deprivation-mediated apoptosis (de la Rosa et al. 2004; Duthoit et al. 2004; Fontenot et al. 2005a; Pandiyan et al. 2007; Thornton and Shevach 1998). Recent studies have shown, however, that depletion of IL-2 alone is not sufficient in preventing the suppression of effector T cells by Tregs (Oberle et al. 2007).

CD39 and CD73 are ectoenzymes expressed on the surface of Tregs generating pericellular adenosine and adenosine derivatives that can activate the A2A receptor on effector T cells and suppress their function (Borsellino et al. 2007; Deaglio et al. 2007; Kobie et al. 2006). Not only does the activation of A2A receptors suppress T cell function, it also promotes the secretion of TGF-β and inhibits production of IL-6; a cytokine that promotes differentiation of naïve CD4 cells into a Th17 rather than a Treg phenotype (Oukka 2007; Zarek et al. 2008).

1.3.3.3. Suppression through direct cytotoxicity

Human Tregs express granzyme B upon activation and can directly kill activated effector cells as part of the perforin/granzyme cell death pathway (Grossman et al. 2004; Hoves et al. 2010). While this pathway is a principle cytotoxic mechanism performed by NK cells and CTLs upon intracellular pathogens, it has also been shown to be a potential mechanism of suppression executed by Tregs (Grossman et al. 2004; Hoves et al. 2010).

Murine Foxp3^{+} Tregs have also been shown to upregulate granzyme B upon activation (Shevach 2009). It has been reported that granzyme B-deficient murine Tregs have decreased suppressive activity *in vitro,* and the

upregulation of granzyme B allows killing of effector cells by Tregs in a perforin-independent granzyme B-dependent manner (Gondek et al. 2005). In 2010 Boissonnas *et al* used two-photon microscopy to show the killing of DCs by Tregs using perforin-dependent mechanisms in a tumour-draining lymph node (Boissonnas et al. 2010).

1.3.3.4 Suppression through dendritic cell targeting

Tregs can also suppress through inhibition of APCs therefore preventing the activation of effector T cells (Vignali et al. 2008). The cell surface protein CTLA-4 is constitutively expressed on both murine and human Foxp3$^+$ Tregs and has been shown to play an important role in the suppressive effects of Tregs (Read et al. 2000; Takahashi et al. 1998). It has been reported that by removing the function of CTLA-4 through either blocking antibodies or use of CTLA-4-deficient Tregs, the suppression of DCs was reduced (Oderup et al. 2006; Serra et al. 2003). Moreover, autoimmunity induced by CLTA-4 deficiency or CTLA-4 blockade can be improved by the addition of WT Tregs (Bachmann et al. 1999; Takahashi et al. 2000). While CTLA-4 deficiency causes systemic autoimmunity, CTLA-4 deficient Tregs exhibit suppressive functions both *in vitro* and *in vivo* through cytokine-mediated mechanisms (Read et al. 2006; Tang et al. 2004).

Surface bound CTLA-4 interacts with the co-stimulatory molecules CD80/CD86 on DCs and the subsequent ligation of these molecules leads to upregulation of indoleamine 2,3-dioxygenase (IDO), a potent regulatory enzyme that catabolizes tryptophan into proapoptotic metabolites, ultimately leading to cell cycle arrest of effector T cells (Fallarino et al. 2003; Mellor

and Munn 2004). In addition, CTLA-4 has also been shown to remove CD80/CD86 from the surface of APCs through trans-endocytosis, thereby preventing costimulation to APCs (Qureshi et al. 2011).

Finally, surface-expressed lymphocyte-activation gene 3 (LAG-3); a CD4 homologue, can bind to MHC II with very high affinity (Huang et al. 2004; Workman and Vignali 2005). This interaction between LAG-3 and MHC II on DCs induces an immunoreceptor tyrosine-based activation motif (ITAM)-mediated inhibitory signaling pathway leading to the suppression of DCs immunostimulatory functions (Liang et al. 2008).

1.3.4 Role of Tregs in Cancer

1.3.4.1 Tregs in anti-tumour immunity

Robert North first postulated the involvement of suppressive-like cells in anti-tumour immunity in the 1980s [reviewed in (Gallimore and Godkin 2008)]. North and colleagues showed that while an anti-tumour immune response was mounted in response to Meth A tumours (an MCA-induced tumour cell line); tumour growth could not be fully prohibited due to activity of suppressor T cells. Furthermore, through measuring concomitant immunity (described as the ability to reject a second inoculum of the original tumour cell line) it was observed that anti-tumour immune responses deteriorated over time concurrent with increased suppressive T cell activity (Gallimore and Godkin 2008; North and Bursuker 1984). Further investigation led to the characterization of these suppressor T cells as $CD4^+$ CD8- cells, with the use of CD4-depleting antibodies leading to successful tumour regression

(Awwad and North 1988). The work by North and colleagues first demonstrated the ability of Tregs to suppress an anti-tumour immune response, and with subsequent identification of CD25 and a specific Treg marker by Sakaguchi in 1995, further investigation into the extent of Treg suppression commenced (Gallimore and Godkin 2008; Sakaguchi et al. 1995).

Many studies have shown that depletion of $CD25^+$ cells ultimately results in generation of an anti-tumour immune response. CD25 depleting monoclonal antibodies were used to induce $CD8^+$ T cell and NK cell anti-tumour responses not only in the Meth A tumour model, but also in other tumour cell line derived models (Onizuka et al. 1999; Shimizu et al. 1999). It was also found that concomitant immunity could be induced after depletion of $CD25^+$ Tcells (Turk et al. 2004). While prophylactic depletion of $CD25^+$ T cells was able to successfully control tumour growth, CD25 depleting antibodies given at the time of tumour challenge were not. As activated T cells express CD25, this effect was most likely due to depleting of anti-tumour $CD25^+$ T cells as well as Tregs (Jones et al. 2002; Li et al. 2003; Onizuka et al. 1999; Quezada et al. 2008; Shimizu et al. 1999; Sutmuller et al. 2001). However, it was possible to promote tumour regression of an established tumour through intra-tumoural injection of CD25-depleting antibodies (Yu et al. 2005).

The identification of Foxp3 as a specific Treg marker allowed exclusive depletion of Tregs without affecting effector T cells. The development of diphtheria toxin receptor transgenic mice by Rudensky and Sparwasser (discussed in Section 1.5.1) allows the depletion of $Foxp3^+$ cells

expressing the Diphtheria Toxin Receptor through administration of Diphtheria Toxin (Kim et al. 2007; Lahl et al. 2007). Subsequent studies using these transgenic mice have demonstrated that specific depletion of $Foxp3^+$ cells not only prevents tumour development but also results in regression of an established primary tumour initiated by injection of a tumour cell line or the carcinogen MCA (Hindley et al. 2012; Klages et al. 2010; Li et al. 2010; Teng et al. 2010). The progression of these collective studies initiated by North and colleagues demonstrate the capability of Tregs to suppress anti-tumour immune responses and open doors for potential Treg-specific cancer therapies.

1.3.4.2 Enrichment of Tregs at the tumour site

The enrichment of Tregs in different cancers has been well documented for both human and murine tumours. The normal ratio of conventional T cells to Treg in homeostatic conditions becomes unbalanced in cancer patients, and an increase in Tregs can be observed in both the peripheral blood and the tumour microenvironment in cancers like pancreatic, lung, breast, liver and colorectal tumours (Betts et al. 2007; Hindley et al. 2012; Nishikawa and Sakaguchi 2010; Quezada et al. 2011; Scurr et al. 2012; Wilke et al. 2010). The increased presence of Tregs in cancer patients can indicate a good or poor prognosis depending on the type of cancer. In ovarian carcinomas, breast cancers, and gastric cancer an increase in Treg numbers is correlated with poor survival (Bates et al. 2006; Curiel et al. 2004; Perrone et al. 2008; Sato et al. 2005). Contrastingly however, in inflammation driven cancers the presence of Tregs correlates

with a good prognosis, in which Tregs are thought to exert suppression of pro-tumour inflammation (Ruffell et al. 2010). Similarly, in Hodgkin's lymphoma the presence of Tregs is also consistent with improved survival (Álvaro et al. 2005). In CRC, the presence of tumour-infiltrating Tregs have been correlated with an improved outcome, however tumour antigen specific Tregs in CRC have been shown to suppress an anti-tumour response (Bonertz et al. 2009; Scurr et al. 2012). Importantly, altering the ratio of conventional T cells (Tconv) to Tregs is associated with a better prognosis. In B16 melanoma challenged mice, treatment with CTLA-4 blockade and GVAX vaccine significantly increases Tconv cells in comparison to Tregs, resulting in tumour rejection (Quezada et al. 2006).

There have been several studies to show chemokine-mediated Treg enrichment at the tumour site (Ondondo et al. 2013). Treg surface-expressed inflammatory cytokine receptors, such as CCR4, CCR5 and CXCR3, have been shown to be involved in intra-tumoural infiltration of Tregs (Iellem et al. 2001; Sather et al. 2007). Both CCL22 and CCL17, which are ligands for CCR4, have been shown to be upregulated in ovarian carcinomas and human breast cancers (Curiel et al. 2004). In mouse models, the disruption of CCL22/CCL17-CCR4 axis leads to a decrease in Treg infiltration and increases anti-tumour immune responses (Ishida et al. 2006; Pere et al. 2011). Not only do CCL5 levels in tumours correlate with dampened $CD8^+$ T cell responses, but CCL5 along with CCL3 and CCL4 level in mouse lymphomas were increased upon myeloid derived suppressor cell (MDSC) infiltration (Schlecker et al. 2012). This in turn led to enhanced $CCR5^+$ Treg recruitment into the tumour. Similarly, $CXCR3^+$ $Foxp3^+$ Tregs

have also been observed in human ovarian, CRC and hepatocellular carcinomas (Redjimi et al. 2012; Yang et al. 2011). However, both CCR5 and CXCR3 are upregulated on activated T cells. The CXCR3 ligands CXCL9, CXCL10, and CXCL11 bind IFN-γ and allow homing of activated effector cells (Ondondo et al. 2013). It is important to note, however, that while these chemokine axes described recruit Tregs to the tumour site, they also recruit effector T cells and are associated with a good prognosis in many cancers (Ondondo et al. 2013). Furthermore, a study conducted in our lab showed Treg cells utilized many different overlapping chemokine axes during homing to MCA-induced tumours, showing a lack of a specific chemokine axis for Treg recruitment (Ondondo et al. 2015).

While both pTreg and tTregs can suppress an anti-tumour immune response, the extent of each subset's contribution remains unclear. A study by Valzasina *et al* showed the adoptive transfer of Thy1.1 $CD4^{+}CD25^{-}$ T cells into tumour-bearing mice led to the conversion of these cells into functional $Foxp3^{+}$ $CD25^{+}$ $CD4^{+}$ Tregs (Valzasina et al. 2006). Other studies have shown that the secretion of TGF-β by tumour cells and other immune cells such as DCs can also induce differentiation into pTregs at the tumour site (Ghiringhelli et al. 2005; Liu et al. 2007). However, the difficulty in identification of pTregs and tTregs arises from the lack of specific markers for each subset (Ondondo et al. 2013). While Helios and Nrp1 are expressed on tTregs and not pTregs, they are also expressed on activated T cells. However, by using Helios and Nrp1 as makers for tTregs, studies have shown that Tregs present in both murine and human carcinomas are predominantly tTregs (Bui et al. 2006; Curiel et al. 2004; Ghiringhelli et al.

2005; Hansen et al. 2012; Teng et al. 2010; Wainwright et al. 2011). Furthermore, our own lab has previously shown that Tregs accumulating in MCA tumours are Helios expressing tTregs (Colbeck et al. 2015; Hindley et al. 2012).

1.3.5 Tregs in metastasis

As previously described, the presence of Tregs in some cancers is correlated with a poor prognosis. Similarly, the presence of Tregs in primary tumours in breast, gastric, prostate, CRC, and lung cancers have also been associated with metastasis development (Decker et al. 2012; Fu et al. 2013; Huen et al. 2013; Lal et al. 2013; Recchia et al. 2013; Takenaka et al. 2013; Zhou et al. 2013). Breast cancer patients exhibit increased Treg enrichment with progression from normal breast, to ductal carcinoma *in situ* (DCIS) to invasive ductal carcinoma (IDC), whereas intratumoural infiltration of $PD1^{+}$ $Foxp3^{+}$ Tregs in patients with clear cell renal cell carcinoma (CCRCC) is correlated to metastasis relapse (Kang et al. 2013; Lal et al. 2013; Takenaka et al. 2013). Patients with metastatic castration-resistant prostate cancer (mCRPC) have been shown to have higher levels of $CD4^{+}CD25^{+}CD127^{low/-}$ cells in their peripheral blood in comparison to healthy donors (Huen et al. 2013). Furthermore, Tregs from mCRPC patient peripheral blood mononuclear cells (PBMCs) were compared to healthy donor Tregs from PBMCs and were found to have overexpression of C-FOS, C-JUN, DUSP1, and RGS-1 involved in T cell proliferation and inhibition of cellular migration (Huen et al. 2013). Accumulation of systemic and intratumoural Tregs has

therefore been correlated with development of distant site metastases in several cancers (Halvorsen et al. 2014).

1.3.5.1 Enrichment of Tregs in metastasis

In the same manner as the primary tumours, Treg enrichment associated with metastasis is cancer-type dependent (Halvorsen et al. 2014). Patients with breast, gastric and papillary thyroid cancer (PTC) display increased Treg enrichment in lymph nodes from patients with metastatic disease in comparison to non-metastatic diseased lymph nodes (Faghih et al. 2014; French et al. 2012; Kashimura et al. 2012; Mansfield et al. 2009). PTC patients with metastatic disease also exhibit an increase in PD-1 expressing T cells, a marker of T cell exhaustion as well as a mechanism of suppression by Tregs, and therefore the combined presence of $Foxp3^+$ Tregs and $PD\text{-}1^+$ T cells is suggested as a biomarker of aggressive or recurrent disease (French et al. 2012). In patients with previously untreated breast cancer, the accumulation of $CD4^+CD25^+CD127^{low/-}$ Tregs in lymph nodes has been associated with the decrease in pro-inflammatory cytokines IL-17 and IFN-γ, leading to the hypothesis that in this case Tregs promote an anti-inflammatory pro-tumorigenic state (Faghih et al. 2014). Contrastingly, the presence of $CD4^+CD25^{high}$ cells in the peritoneal metastases of ovarian carcinoma patients is correlated with a good prognosis, suggesting possibilities for Tregs to promote metastasis regression in some tumours (Tsiatas et al. 2009).

As tissue biopsies and samples are restricted to primary tumours, PBMCs and lymph nodes, there is little information about metastases-harboring organs in human patients (Halvorsen et al. 2014). However, mouse models have demonstrated the presence of Tregs at distant sites of metastasis in murine breast cancer (4T1 and 4T1.2) and melanoma (B16F10) (Abadi et al. 2013; Biragyn et al. 2013; Chopra et al. 2013; Dalotto-Moreno et al. 2013; Ghochikyan et al. 2014; Kim et al. 2014; Olkhanud et al. 2011).

1.3.5.2 Metastasis-promoting functions of Tregs

While the functions by which Tregs can promote the progression of a primary tumour have been described, their ability to promote metastasis is poorly understood (Halvorsen et al. 2014). In both human and murine cancers, the expression of COX2 and PGE_2 is associated with metastasis progression (Brudvik et al. 2012; Karavitis et al. 2012). In CRC, tumour expression of COX2 is much higher than surrounding healthy tissue and PGE_2 levels in peripheral blood is also elevated (Yaqub et al. 2008). PGE_2 promotes tumour progression by stimulating cell proliferation, angiogenesis, and invasion of tissue by tumour cells (Brudvik et al. 2012; Fujino et al. 2011). In one study, the inhibition of COX2 by indomethacin resulted in the prevention of $CD4^+CD25^-CD127^{dim/-}$ Treg-mediated suppression of cytotoxic responses against CEA (a colorectal antigen) (Brudvik et al. 2012). Similarly, a study using a murine model of CRC showed that tumour cells expressing COX2 were involved in PGE2-mediated Treg recruitment, promoting metastasis to bone (Karavitis et al. 2012).

The expression of Nrp1 by Tregs stabilizes their phenotype thereby enhancing their anti-tumour immune suppressive abilities (Delgoffe et al. 2013). In a murine study, the ablation of Nrp1 expressing Tregs slowed tumour growth in a number of different tumour models and reduced lung metastasis in a B16 melanoma model. Furthermore, developed lung metastases in these mice exhibited increased infiltration of IFN-γ and TNF-α expressing $CD8^+$ T cells (Delgoffe et al. 2013). Interestingly, both $CD4^+CD25^+$ cells isolated from stage III and IV ovarian cancer patient PBMCs and murine $Foxp3^+$ Tregs isolated from spleens were found to secrete VEGF-A *in vitro* (Facciabene et al. 2011). This study potentially suggests a role for Tregs to promote metastasis in addition to their immunosuppressive capabilities, however further study is required (Halvorsen et al. 2014).

The secretion of CCL22 and CCL17 by lung metastases has been shown to recruit Tregs resulting in the apoptosis of NK cells in a beta-galactoside-binding protein (b-GBP)-dependent manner (Olkhanud et al. 2009). Furthermore, the accumulation of Tregs was observed at metastatic sites in the B16F10 murine melanoma model. In this study, while the administration of TNF resulted in metastases enriched for TNFR2 expressing Tregs and less infiltration of $CD8^+$ effector cells, the ablation of $Foxp3^+$ cells through administration of DTx reversed this effect (Chopra et al. 2013).

Most studies investigating the migration and accumulation of Tregs in metastatic foci have been in pre-clinical models and therefore further study is required to understand whether the same is true for Treg enrichment in

cancer patients. Nonetheless, collectively these studies suggest a role for Tregs in metastasis progression and therefore provide opportunities for Treg-targeted treatment of metastasis (Halvorsen et al. 2014).

While Tregs are generally associated with poor outcome of some cancer and therapies targeting Tregs such as checkpoint inhibition currently show promising results, there is still little evidence to suggest whether depletion of Tregs can promote immune control of metastasis. The availability of transgenic mouse models and spontaneously metastasizing murine carcinoma cell lines allow us to address this question.

1.4 4T1 Murine Mammary Carcinoma Model

1.4.1 Development of the 4T1 cell line

4T1 is a murine mammary carcinoma that closely mimics stage 4 triple-negative human breast cancer. It is a subpopulation of the 410.1 cell line that was originally derived from a spontaneous tumour that arose in a female BALB/C mouse nursed on a C3H parent (BALB/BfC3H) (Dexter Dl Fau - Kowalski et al. 1978; Pulaski and Ostrand-Rosenberg 2000). Both of the subpopulations derived from the parent line (4T1 and 4T07) are resistant to thioguanine (H Heppner et al. 2000). 4T1 tumour cells grow well both in culture and *in vivo,* and spontaneously metastasizes to multiple organs from a single primary tumour (Lelekakis et al. 1999; Pulaski and Ostrand-Rosenberg 1998).

1.4.2 Suitability of 4T1 for metastasis investigation

Of the two subpopulations derived from 410.1, 4T1 spontaneously metastasizes via the haematogenous route to the lungs, liver, bone and brain (Aslakson and Miller 1992; H Heppner et al. 2000). The resistance of 4T1 to thioguanine allows the detection of metastatic colonies by the clonogenic assay (Pulaski and Ostrand-Rosenberg 2000). In this method, organs thought to be harboring metastatic 4T1 colonies are mechanically and enzymatically digested and subsequently incubated with 6-thioguanine-supplemented growth media (described in Chapter 2). Only 4T1 cells survive the incubation period and grow colonies, which can be stained with methylene blue and counted. The resistance of 4T1 to 6-thioguanine arises from a loss-of-function mutation in the *HPRT* gene. In normal cells, HPRT recycles 6-thioguanine into its nucleotide form, which when incorporated into DNA is toxic to cells. Although present in 4T1 cells, HPRT is inactive preventing incorporation of 6-thioguanine and therefore cell toxicity (Lepage 1963).

The main advantage of 4T1 over other animal models of metastasis is that it spontaneously metastasizes from a primary tumour in a manner similar to human breast cancer. In human breast cancer cases, the lungs are the first sites of metastasis (up to 77% of cases) after which secondary tumours can be found in the liver (Amer 1982; Kamby et al. 1987; Pulaski and Ostrand-Rosenberg 1998). Similarly, like some human breast cancers, 4T1 is also poorly immunogenic and triple negative for common breast cancer markers. Combined, these traits of 4T1 make this cell line suitable for investigating metastasis in clinically relevant situation. Furthermore, as 4T1

cells are normally injected subcutaneously around the mammary fat pads, they can easily be surgically excised mimicking the treatment of human breast cancer (Pulaski and Ostrand-Rosenberg 2000). As 4T1 was a cell line derived from a tumour with other non-metastatic subpopulations, it is also a useful model for examination of metastasis-associated genes (Christensen et al. 1998).

1.4.3 Growth of 4T1 *in vivo*

Subcutaneous 4T1 tumours grow uniformly in BALB/C mice, even after low cell numbers are injected, and continue to grow rapidly (Pulaski and Ostrand-Rosenberg 2000). Mice bearing 4T1 tumours have also been reported to display splenomegaly due to the increase in MDSC number and granulocytic infiltration (duPre and Hunter Jr 2007). It has also been observed that 4T1 tumours constitutively express genes associated with GM-CSF and G-CSF (duPre and Hunter Jr 2007). The number of 4T1 cells injected subcutaneously dictates the growth of primary tumours. If fewer cells are injected into the mammary fat pads, for example 7×10^3, tumours are not palpable until day 14 to day 21, whereas an inoculation volume of 1×10^6 cells gives palpable tumours between day 4 and day 7. It is reported that even though the primary tumour growth increases with higher inoculation cell number, the number of metastatic colonies observed does not significantly increase (Pulaski and Ostrand-Rosenberg 2000).

Collectively, the specific traits of 4T1 in comparison to other subpopulations of 410.1 create a robust animal model to investigate varying aspects of metastasis.

1.5 DEpletion of REGulatory T cell animal model

1.5.1 Development of DEREG mice

DEpletion of REGulatory (DEREG) T cell mice are a strain of BALB/C mice that were genetically engineered in the Sparwasser lab to express the Diphtheria Toxin Receptor (DTR) on their Tregs (Lahl et al. 2007). The DEREG strain was developed using a Bacterial Artificial Chromosome (BAC); a large fragment of genomic DNA containing a desired gene and their corresponding regulatory sequences. For the generation of these mice, a BAC containing the *foxp3* locus and a DTR-eGFP fusion protein inserted into the first exon of the *foxp3* gene was inserted into a fertilized oocyte of mice (Lahl et al. 2007). Transgenic mice developed in this manner have advantages and disadvantages in comparison to knock-in or knockout mice. BAC-transgenes only take 3-6 months to generate, compared to 1-2 years for knock-in/out transgenics, and have a medium technical difficulty. However, the genomic insertion site is not known with BAC-transgenes as the BAC is randomly inserted into the genome (Sparwasser and Eberl 2007).

Through injection of Diphtheria Toxin (DTx) the Tregs of DEREG mice can be ablated. This allows investigation of different homeostatic and disease states in the absence of Tregs.

1.5.2 Depletion of Tregs through DTx

The administration of DTx to DEREG mice has been shown to selectively deplete Foxp3$^+$ Tregs (Lahl et al. 2007). As the BAC encodes the DTR transgene under the regulation of the *foxp3* promoter, only cells with endogenous Foxp3 expression express the DTR. The receptor-binding domain of DTx binds to the DTR on Foxp3$^+$ cells allowing entry into the cell where, in order to become active, the polypeptide is "nicked" at an arginine-rich site (Li et al. 2013). Once activated, the catalytic domain of DTx catalyzes the transfer of adenosine-diphosphate (ADP)-ribose to EF-2, an elongation factor that promotes the translocation of ribosomes. This blocks protein synthesis and ultimately kills the cell (Sandvig and Olsnes 1981; Zovickian et al. 1987).

Due to genetic silencing, not all Foxp3$^+$ Tregs express the DTR. As a result, there is a remaining baseline level of Tregs after DTx administration (approximately 10%) (Lahl et al. 2007). This low-level of Tregs prevents mice from the development of severe autoimmunity, which is observed in Foxp3-DTR knock-in transgenic mice (Kim et al. 2009a; Kim et al. 2007; Mayer et al. 2014a). Recently, it has been observed that continued treatment with DTx in DEREG mice causes an anti-DTx antibody response resulting in Tregs returning to pre-treatment levels (Wang et al. 2016).

1.5.3 Examples of documented uses of DEREG mice

DEREG mice provide a convenient mouse model for the investigation of Tregs in homeostasis and in disease. In 2014, Berod *et al* used DEREG mice to explore the involvement of Tregs in *Mycobacterium bovis* because of

the low-level of remaining Tregs preventing autoimmunity. They observed that after Treg depletion in DEREG mice, a niche of DTx-insensitive Tregs were able to expand. While these mice had worse pathogen burden in comparison to DEREG x Foxp3^{GFP} mice (in which total Treg ablation is achieved upon DTx treatment), rapid development of severe autoimmunity was prevented (Berod et al. 2014). The GFP reporter gene found under the regulation of the Foxp3 promoter in DEREG mice can also be exploited as demonstrated by the study conducted by Lahl *et al* in 2009. In this study, DEREG mice were crossed with scurfy-mutant (sf) mice to locate "would-be" Tregs in order to investigate the potential self-reactive TCRs on nonfunctional Tregs (Lahl et al. 2009). DEREG mice have also been used to investigate the role of Tregs in malarial infection. Abel *et al* found that after ablation of Tregs in *Plasmodium yoelii*-infected DEREG mice, there was an increase in activate T cells and a decrease in parasitic burden (Abel et al. 2012). The role of Tregs in allergic airways has also been investigated using DEREG mice. While the absence of Tregs does not aggravate allergic airway inflammation, it was found that Foxp3^{+} Tregs were required for Schistosoma mansoni-mediated suppression of allergic airway inflammation (Baru et al. 2012; Layland et al. 2013). Tregs have also been shown to suppress Th2 immunity during *Cryptococcus neoformans* infection. In a study performed by Schulze *et al* in 2014, it was observed that the number of Foxp3^{+} Tregs increased in BALB/C wild type mice after intranasal infection with *C. neoformans* and after Treg depletion in *C. neoformans*-infected DEREG mice a stronger allergic inflammation response was detected along with increased mucus production, IgE production, fungal

burden and GATA-3^{+} Th2 cell presence (Schulze et al. 2014). These studies collectively demonstrate the versatility and durability of the DEREG model for the investigation of the varying roles of Tregs.

1.6 PET/CT imaging

PET/CT imaging has been used to diagnose tumours and metastatic lesions for a number of years. Each of the two components were developed separately; CT was developed in the early 1970s and PET was developed over a number of years between 1969 and 1985 (Gerd and Joel 2006; Hounsfield 1973). The dual technique was first developed in 1991 by Townsend and colleagues and became a working prototype with help from Ron Nutt in 1998 (Kinahan et al. 1998; Townsend et al. 1993). Clinical trials performed using the original prototype found that the combination of PET and CT allowed more precise identification of tumours, and furthermore was able to distinguish malignant lesions from surrounding tissue (Charron et al. 2000; Kluetz et al. 2000; Meltzer et al. 2000).

1.6.1 Principles of PET/CT imaging

1.6.1.1 Computed Tomography

PET/CT imaging combines two separate imaging techniques of Positron Emission Tomography (PET) and Computed Tomography (CT). In a CT, the subject is placed in the centre of a moving circular rig (gantry) consisting of an X-ray emitter and X-ray detector set at 180° to each other. With the subject in the middle, the X-ray emitter fires X-rays at the subject

creating an image on the detector (Figure 1.3). Different densities of tissues within the body absorb X-rays of different energies. As ionizing X-ray beams penetrate tissues of lower densities, such as internal organs, small fractions of the beams are absorbed while the remaining pass through the tissue to be received by the X-ray detector (Ohlerth and Scharf 2007). Conversely, in the more dense tissues of the body such as the skeleton, only the highest X-ray energies pass through to the detector. The attenuated beams that hit the detector after passing through the subject are compared to the original X-ray beam intensity giving an attenuation value in Hounsfield Units (HU) (Ohlerth and Scharf 2007). All attenuation values are normalized to that of water, 0 HU, as X-rays can pass through water with very little attenuation. The attenuation values of body tissues are plotted relative to water on the HU scale ranging from -950 for the air space in the lungs to >250 for compact bone (Berry 2002; Kalendar 2005; Ohlerth and Scharf 2007; Wegener 1993). The values on the HU scale can be assigned to shades of grey in order to be visually displayed on a reconstructed CT image (Ohlerth and Scharf 2007).

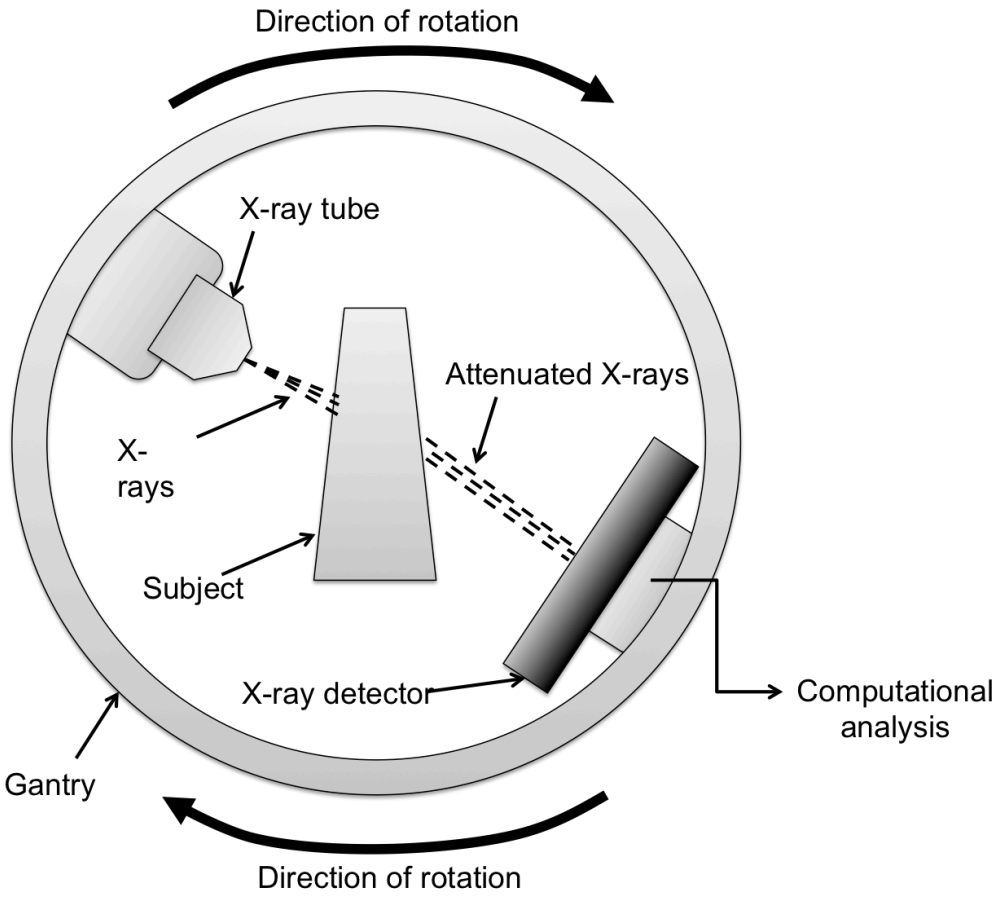

Figure 1.3| Components of CT scanning. X-rays of varying energies are fired from an X-ray tube towards a subject. As the X-rays pass through the subject, the X-rays are attenuated and are received by the X-ray detector. The gantry completes a 360 rotation of the subject taking X-ray images at a set number of projections. The data collected by the X-ray detector throughout a full scan is then reconstructed to produce a CT image.

1.6.1.2 Positron Emission Tomography

PET imaging uses scintillation crystals to detect β-decay of a radioisotope. An unstable radioisotope, such as Fluorine^{18} (F^{18}), decays to emit a positron that travels a distance between 1-2 mm before coming into contact with an electron. These particles annihilate each other, emitting two γ−rays along a straight angle to be detected by the scintillation crystals. The scintillation crystals are coupled to a photon multiplier tube that amplifies the signal in order for computer algorithms to calculate the point of annihilation (Figure 1.4) (Vaquero and Kinahan 2015). It is then possible to create a PET image detailing the positions of radioactivity in the subject being scanned. Using reconstruction and data analysis software, the PET image can be mapped onto the corresponding CT image, allowing identification of areas of increased radioactivity uptake. PET image data is initially read in Bq, which looks at the radioactive decay occurring across the subject. This can be converted into the Standardised Uptake Value (SUV), the calculation of which can be found in Chapter 2. This measurement takes into account the weight of the subject, the amount of radioactivity injected, the time at which the radioactivity was injected and the time of the scan. All other measurements used in clinical and preclinical scanning are derivatives of the SUV.

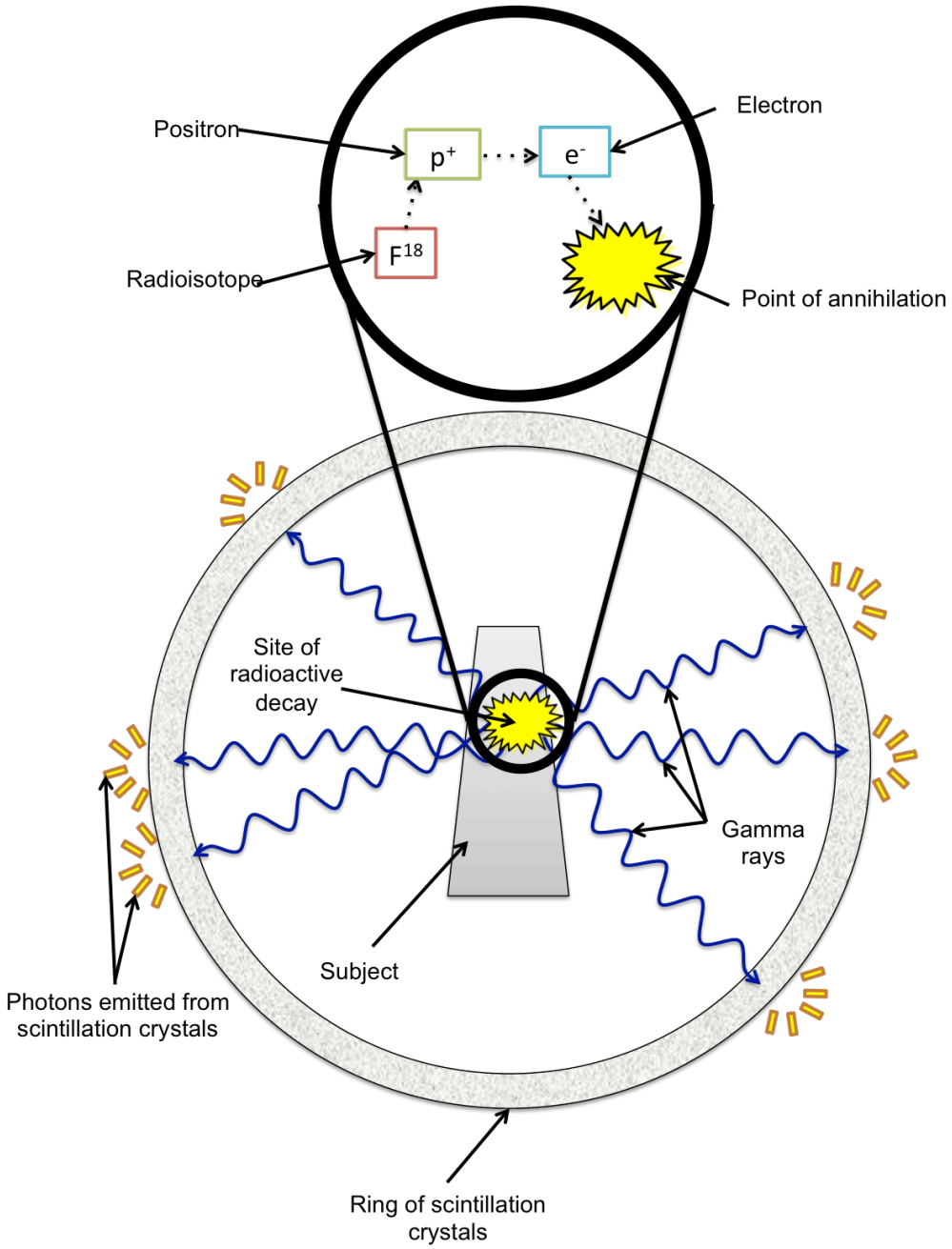

Figure 1.4| Components of PET scanning. A radioactive tracer undergoes β-decay to emit a positron. The positron travels until it comes into contact with an electron at which point annihilation occurs and photons are emitted as gamma rays along a straight angle. These photons are detected by a ring of scintillation crystals, which are coupled to photon multiplier tubes that amplifies the signal received. Computer algorithms use the activated scintillation crystals to determine the point of radioactive decay and reconstruct the PET image.

1.6.2 Clinical PET/CT imaging

The main use of PET/CT imaging in clinical medicine uses a radioactive glucose analogue known as F^{18} Fluoro-deoxyglucose (FDG) to detect malignant tumours. This technique exploits the Warburg Principle which postulates that cancer cells experience increased glucose metabolism (Warburg 1956; Warburg et al. 1924). Therefore, in a PET/CT scan tumour cells exhibit an increase uptake of FDG compared to surrounding tissues, allowing identification of malignant lesions. F^{18} is also commonly used in clinical PET/CT imaging due to its short half-life of 109.8 minutes. This means that 24 hours after administration of FDG, radioactive decay is no longer detectable within the patient and therefore poses less of a risk to the patient. FDG PET/CT is commonly used to measure different cancers, such as prostate, lymphoma, bladder and breast cancers, (Fonager et al. 2016; Hu et al. 2015; Hulikal et al. 2015; ÖZtÜRk and Karapolat 2015) as well as the detection of metastases (Joshi et al. 2013; Lee et al. 2012; Nogami et al. 2015). F^{18} has also been investigated for use as part of Fluoromethylcholine (FCH) for lymph node staging of prostate cancer, where limited success was observed when analysing lymph nodes but scans were able to detect bone metastases (Poulsen et al. 2012). Other radioisotopes have also been used in PET/CT scanning. Gallium^{68} (Ga^{68}) labeled DOTATATE has been used to target somatostatin receptor (SSTR), specifically SSTR2, in PET/CT scanning in order to detect benign and malignant thyroid tumours, gastro-entero-pancreatic neuroendocrine tumours, and bone metastases arising from pancreatic neuroendocrine tumours (Goel et al. 2014; Nockel et al. 2016; Sadowski et al. 2016).

1.6.3 Preclinical PET/CT imaging

While clinical PET/CT imaging focuses on detection of malignancies within patients, preclinical PET/CT can be used for much wider purposes. Lee *et al.* in 2013 used FDG PET/CT to measure the growth of a subcutaneous B16 melanoma xenograft in BALB/C nude mice and found it to be a more accurate measurement tool than calipers (Lee et al. 2013). FDG PET/CT has also been investigated for use in monitoring the progression of pulmonary infections in rabbits and in mice. This study was performed for up to 38 weeks in rabbits and up to 14 in mice and it was found that FDG PET/CT was useful for longitudinal investigation of pulmonary infections (Bagci et al. 2013). F^{18} has also been used for different tracers in order to monitor cell migrations, for example N-[2-(diethylamino)ethyl]-^{18}F-5-fluoropicolinamide or ^{18}F P3BZA has been used to trace retinal pigment epithelial cells in the treatment of Parkinson's disease in rats (Bu et al. 2014). Amino acid based radiotracers have been developed for preclinical PET/CT based on their experimental applications, for example F^{18} – fluorothymidine (FLT) can be used to monitor cell proliferation (Rendon et al. 2016) and F^{18} – fluoropropyl-L-glutamate (FSPG) can be used to visualise intracranial activity (Mittra et al. 2016). The ability to radiolabel monoclonal antibodies (mAbs) allows specific imaging of target tissues and thus the study of certain disease progression, such as prostate cancer and lymph node metastasis (Hall et al. 2012).

1.7 Hypothesis and Aims

The hypothesis of this project states that the recruitment of Tregs to the site of a primary tumour suppresses an anti-tumour immune response and results in the progression of tumour growth and metastasis. I hypothesise that the depletion of Tregs promotes an anti-tumour immune response and prevents/slows the progression of metastasis.

The aims of this PhD thesis were:

1. To deplete Tregs in a genetically engineered mouse model in order to investigate the effect of Treg depletion on metastasis
2. To develop an *in vivo* imaging technique in order to visualise the progression of metastasis over a period of time in a single mouse
3. To investigate the immune microenvironment of primary tumours in order to determine its “association” with metastasis.

Chapter 2

2 Materials and Methods

2.1 Materials and Reagents

2.1.1 Mice and Cell Lines

The murine mammary carcinoma cell line 4T1 was obtained from ATCC (CRL-2539).

DEREG mice were a kind gift from Prof Rick Maizels at The University of Edinburgh, originally developed by Prof Tim Sparwasser.

Wild type (WT) female 6-8 week old Balb/c mice were obtained from Envigo Laboratories or Charles River Laboratories.

2.1.2 Cell Culture

Complete Roswell Park Memorial Institute Medium (RPMI) from Life Sciences supplemented with 2 mM L-Glutamine, 1 mM sodium pyruvate, 50 µg/ml penicillin streptomycin, and 10% foetal calf serum all from Sigma Aldrich.

0.05% Trypsin/EDTA, (1X), from Gibco Life Technologies.

2.1.3 Induction of primary tumour growth

29G insulin syringes from BD biosciences.

Diphtheria toxin diluted to a 5 µg/kg in Phosphate Buffered Saline (PBS) at pH7 from Gibco Life Technologies.

Digital Calipers from Vet Tech.

Ear Punch from Vet Tech.

2.1.4 Surgical removal of the primary tumour

100% isoflurane from Prima Healthcare.

Metacam from Boehringer Ingelhein.

Vetbond tissue glue from 3M Animal Care Products.

Vicryl Rapide undyed braided absorbable suture 4-0 from Ethicon

Woven Swabs from Premier

Latex surgical gloves size 7 from Encore

Hydrex antibacterial scrub from Ecolab

Industrial Methylated Spirit 70% v/v from Ecolab

Cotton buds from Universal

Hair clippers from Contura

Cardiff Aldasorber Scavenger cartridge from Shirley Aldred and Co.

29G insulin syringes from BD Biosceinces

2.1.5 PET/CT Scanning

Fluoro-deoxy-glucose (FDG), containing the radioisotope Fluorine^{18} was made either on site by Cardiff University Positron Emission Tomography Imaging Suite (PETIC) or delivered by Alliance Medical Molecular Imaging LTD.

100% Isoflurane (as above)

Omnipaque contrast agent from GE Healthcare containing 350mg Iodine/ml, injected neat 100 µl intraperitonealy (i.p) and 100 µl intravenously (i.v)

Saline solution 0.9% w/v for intravenous infusion (B. Braun Melsungen AG)

Mediso nanoScan® PET/CT scanner

2.1.6 Clonogenic Assay

Hanks Balanced Salt Solution (HBSS) from Sigma Aldrich

Collagenase type IV from Sigma Aldrich, 50 mg dissolved in 2 of 1X HBSS

Collagenase type I from Sigma Aldrich, 50 mg dissolved in 25 ml of 1XHBSS

Hyaluronidase from Sigma Aldrich, 50 mg, plus Bovine Serum Albumin (BSA) from Sigma Aldrich, 25 mg, dissolved in 25 ml of 1X HBSS

Iscove's Modified Dulbecco's Medium (IMDM), supplemented with 10% FCS, penicillin/streptomycin, and L-Glutamate as before

60 mM 6-thioguanine in Sodium Hydroxide stock solution, diluted to 60 µM in 10% IMDM media

9 cm diameter Nuclon tissue culture plates, Thermo Fischer Scientific

2.1.7 Immunofluorescence Staining

OCT from CellPath

99% Acetone (ice cold) from Fischer Scientific

1X PBS (made in house)

ImmEdge™ PAP-pen from Vector Laboratories

Avidin Biotin blocking kit from Vector Laboratories

2.5% Horse Serum from Vector Laboratories

2.5% Goat Serum from Vector Laboratories

1% Bovine Serum Albumin (Sigma Aldrich) in 1X PBS

1% Paraformaldehyde, made from 8% stock solution (40 g of PFA [Fischer Scientific] in 500 ml distilled water)

0.3M glycine from Sigma Aldrich

Vectashield containing DAPI nuclear stain from Vector Laboratories

2.1.8 Immunohistochemical Staining

10% Formalin Solution from Sigma Aldrich

Xylene

70%, 90% and 100% Ethanol

1X Tris-EDTA

1X PBS

ImmEdge™ PAP-pen from Vector Laboratories

3% H_2O_2/MeOH made from 30% w/v H_2O_2 from Fischer Scientific

2.5% Horse Serum (as above)

2.5% Goat Serum (as above)

Rat Impress reagent from Vector Laboratories

Mouse Impress Reagent from Vector Laboratories

Rabbit Impress Reagent from Vector Laboratories

Impress-DAB Chromogen from Vector Laboratories

Impress-VIP Chromogen from Vector Laboratories

Vector-SG Chromogen from Vector Laboratories

Haematoxylin from Sigma Aldrich

Scotts Reagent from Thermo Shandon

DPX from Fischer Scientific

2.1.9 Flow Cytometry

Microvette Lithium Heparin tubes from Starstedt

Number 24 Scalpels from Swann Morton

Red Blood Cell Lysis buffer X10 from Biolegend

Complete RPMI (as above)

96-well U-bottomed plates from Nuclon

PBS (as above)

FACs buffer made in house

Fixation/permeabilisation buffer from eBiosciences

BDCanto

BDFortessa

2.2 Methods

2.2.1 Induction of 4T1 primary tumour

2.2.1.1 4T1 cell culture

4T1 tumour cells were defrosted in a water bath heated to 37°C for up to 90 seconds. Tumour cells were then transferred into a 15 ml Falcon tube containing 5 ml RMPI medium supplemented with 10% Foetal Calf Serum

(FCS) (R10). The cell suspension was then centrifuged at 1500 rpm for 5 minutes, and the resulting cell pellet was re-suspended in a further 5 ml R10 medium. Tumour cells were transferred into a T25 flask containing 10 ml R10 medium and were incubated at 37°C 5% CO_2 for 24 hours. The following day, the supernatant was removed from the flask and cells were washed with 1x PBS to remove any excess media before the addition of 3 ml Trypsin EDTA. The cells were incubated with the Trypsin for 5-10 minutes, after which time 7 ml R10 medium was added to inactivate the enzyme. The resulting cell suspension was then centrifuged at 1500 rpm for 5 minutes and the cell pellet was re-suspended in 5 ml R10. One milliliter cell suspension was added to 30 ml fresh R10 in a T175 flask. Cells were split up to 3 times a week, and were left to grow for 3-6 passages before being injected into mice.

2.2.1.2 4T1 injection and growth

On the day of injection, 4T1 cells were counted using a haemocytometer and made up to a concentration of $1x10^6$/ml in PBS. Mice were scruffed and injected subcutaneously (s.c) with $1x10^5$ 4T1 cells (100 µl cell suspension) around the mammary fat pads of the lower left quadrant. At day 5, injection was accepted to be successful if a small tumour could be palpated. Tumours were measured from day 7 up to 3 times per week until the tumour was resected or until the mouse was sacrificed. Two perpendicular measurements were taken of the tumour from which the volume was calculated.

2.2.2 *In Vivo* Treg depletion

Diphtheria toxin (DTx) was injected i.p at a concentration of 5 μg/kg every other day. For assessing the effects of Treg depletion on the primary tumour, DTx was injected i.p from the day the primary tumour was palpable (day 5). For assessing the effects of Treg depletion on metastasis, mice were injected with DTx twice before surgery on day 0 (day -4 and day -2).

2.2.3. Surgical removal of primary tumour

Surgical instruments were all purchased from VetDirect under the instruction of the Named Veterinary Surgeon (NVS). Twenty-four hours before surgery, surgical instruments were sorted into bags (1 set per mouse) and autoclaved. Each surgical set contained the following instruments; 1x Strabismus Scissors (straight, blunt/blunt), 1x Mayo Scissors (straight, blunt/blunt), 1x Needle Holding Forceps, 1x Rat-toothed Forceps, 1x Iris Micro-dissecting Forceps, and 2-3x Bulldog Clamps. Each set was wrapped in EcoDrape, placed in an autoclave bag and sealed with autoclave tape. Paper towels were also placed in autoclave bags (3x towels per bag) for sterilization to dry hands with before donning surgical gloves. Before surgery, recovery cages containing Vet Bed were allowed to warm in a heating chamber set to 37°C. Tumours on each mouse were measured before induction of anaesthesia through isoflurane in an anaesthetic box. Once the mouse was unconscious, it was placed on a facemask supplied with O_2 and isoflurane to maintain anaesthesia while the surgery area was prepped. The tumour and the surrounding area were shaved using Wella

hair clippers, and the area was swabbed 2x with Hibiscrub antibacterial wash and 2x with Surgical Spirit. Each mouse was also injected subcutaneously (s.c) with 0.5 mg/mL Metacam, a local anaesthetic to prevent pain upon waking. Preparation was performed by a surgical assistant while the surgeon scrubbed up following complete aseptic techniques. The autoclaved bag containing the surgical instruments was tipped out onto the surgical work area, along with a sterile operation cover in which a hole was cut to fit around the tumour. Using the rat toothed forceps, the subcutaneous tumour was lifted up and small incisions around the base of the tumour were made with the strabismus scissors. Any blood vessels connected to the tumour were clamped for up to 1 minute (or when no blood was seen) using the bulldog clamps. Fatty tissue connecting the tumour to the intraperitoneal muscle was teased apart using the blunt ends of the strabismus scissors and the tumour was removed and placed in either Neutral Buffered Formalin Solution (NBFS) or OCT. The wound was closed with horizontal mattress stitches using Vicryl *rapide* absorbable braided sutures, and the mouse was placed in the heated recovery chamber until consciousness was regained. Mice were checked on every hour for up to 4 hours, then every 12 hours to assess the wellbeing of the animals and the strength of the sutures. Surgical instruments were soaked in warm water and washed with Hibiscrub, then were left to air dry.

2.2.4. PET/CT imaging

2.2.4.1 Scanning

Tumour bearing mice were transferred into the pre-clinical PETIC (PET/CT Imaging Centre) facility up to 3 days before scanning. On the day of scanning, the Mediso nanoScan PET/CT scanner was calibrated using Na^{22} point source of 1 MBq. Each mouse was warmed for at least 1 hour prior to scanning to deactivate brown fat activity at 37°C, and was injected i.p with 100 µl Omnipaque iodine contrast agent before induction of anaesthesia with isoflurane. Once unconsciousness had been achieved, mice were placed on a warmed mouse bed in the PET/CT scanner upon which O_2 and isoflurane were supplied via a facemask. $Fluorine^{18}$-incorporated fluoro-deoxyglucose (FDG) (made in-house) was made up to 10-14MBq in an insulin syringe, along with 100 µl Omnipaque, and was then injected i.v via the tail vein. Fifteen minutes after the i.p injection of Omnipaque, a whole body, semicircular CT scan was performed at 70 KVp x-ray energy, with 720 projections and a 300 ms exposure time. Thirty minutes after the i.v injection of FDG and Omnipaque, a 60-minute static PET scan with respiratory gating was performed. The breathing rate of each mouse was recorded using a breathing pad placed underneath the animal, allowing a respiratory trace to be calculated. Trigger delays were set using MC2B software on the respiratory trace, allowing the Nucline™ program to exclude decay data observed within a complete respiratory cycle (inhalation and exhalation). Upon completion of the PET scan, the mouse was removed from the bed and placed in the heated recovery chamber until waking. All scanned mice were kept in a scantainer for 24 hours after scanning until

complete radioactive decay of the FDG, when mice were returned to the normal housing rooms in the PETIC facility.

2.2.4.2 Analysis of PET/CT imaging

Scans performed on the old Gamma Medica Triumph II PET/CT/SPECT scanner were co-registered on VIVID software (Gamma Media Ideas) and analysed on PMod3.3 software. Later scans acquired on the Mediso nanoScan PET/CT scanner were automatically co-registered upon scan reconstruction on Nucline software (Mediso). Scans were then analysed on Vivoquant^{TM} software (Invicro). Regions of Interest (ROIs) were drawn in 3D around organs thought to be harboring metastatic 4T1 cells using different spline and contour tools. For each ROI, the maximum Standardised Uptake Value (SUVmax), Hot Pixel Average (HPA) and Total Lesion Glycolysis (TLG) were calculated along the parameters detailed in table 2.1.

Table 2.1| Parameters used to analyse ROIs in PET/CT scans

Parameter	Calculation	Units of measurement
SUV	Image derived radioactivity concentration at t=0 (Injected dose at t=0/body weight)	g/ml
SUVmax	The pixel with the highest value of SUV in a given area (ROI)	g/ml
Hot Pixel Average	The mean of the 5 pixels with the highest SUV in a given area (ROI)	g/ml
Total Lesion Glycolysis	Average SUV of the whole ROI X ROI volume	g/ml*cm^3

2.2.5. Clonogenic assay

Organs suspected to harbor metastatic 4T1 cells in mice (brain, lungs, liver and draining LN) were harvested after animals were culled by CO_2. Organs were immediately submerged in HBSS and transported on ice into a class II Hepa-filtered hood. Each organ (except the draining LN) was removed from the HBSS and transferred into a 6-well tissue culture plate using a Pasteur pipette, and mashed using the end of a 2 ml syringe. The mashed organs were then transferred into a 15 ml Falcon tube containing 2.5 ml of a specific collagenase cocktail. Brains and lungs were added to a collagenase IV cocktail and livers were added to a collagenase I cocktail along with 2.5 ml of Hyaluronidase. Each well containing a mashed organ was washed with 2.5 ml of HBSS twice and added to the corresponding 15 ml Falcon. Brains were incubated in a shaking water bath at 37°C for 120 mins, lungs were incubated on a rotating arm at 4°C for 75 mins, and livers were incubated in a shaking water bath at 37°C for 20-30 mins. After the incubation period, each sample was passed through a 70 μm nylon cell strainer washed with HBSS before centrifugation at 1500 rpm for 5 mins at room temperature. The resulting supernatant was discarded and the cell pellet was washed 2-3 times depending on its size. Each pellet was then re-suspended in 10 ml of 6-TG media, then plated on a 9 cm tissue culture plate and left to incubate for 14 days at 37°C and 5% CO2. Draining LNs were removed from the HBSS like the other organs, but were immediately mashed through a 70 μm nylon cell strainer directly into 10 ml of 6-TG media in a 9 cm tissue culture plate, and were then left to incubate in accordance with the other organs. After the incubation period, the remaining media was

removed from each plate and any resulting cell colonies were fixed to the plate with 5 ml of methanol for 5 mins. Each plate was then washed with sterile water, stained with 5 ml methylene blue dye for 5 mins before a final wash with sterile water. The resulting blue colonies were then counted once the plate was completely dry, with each colony representing one metastatic cell.

2.2.6. Immunofluorescence

2.2.6.1 Staining frozen sections

Organs expected to harbor 4T1 metastatic cells were placed in OCT (optimum cutting temperature compound), frozen on dry ice and then kept at -80°C until required. Each sample was cut at 5 µm sections on a Cryostat and placed on a frosted glass microscope slide before being left to air-dry for 1-24 hours. Slides were fixed in ice-cold acetone for 10 minutes before being washed 3 x 3 minutes in 1x PBS. To prevent non-specific binding, a blocking step was performed in which either 2.5% Normal Horse Serum or 2.5% Normal Goat Serum was incubated with each section for 30 minutes at room temperature. Primary antibodies were made up to the desired concentrations in 1% BSA/PBS, and were incubated with the sections overnight at 4°C. A list of primary antibodies used is detailed in table 2.2. The following morning, slides were washed 3x 3 minutes in 1x PBS. Secondary antibodies were made up to the appropriate concentrations in the same way as the primary antibodies and then centrifuged at 13 000 rpm for 10 minutes at 4°C in order to remove aggregates. Slides were then incubated with the secondary

antibodies for 30-60 minutes at room temperature. Slides then underwent 3 washes in 1x PBS at 3 minutes each before being fixed in 4% PFA (paraformaldehyde) for 10 minutes at room temperature. Any excess PFA was then quenched by incubation with 0.3Molar glycine (in PBS) for a further 10 minutes at room temperature. Slides were washed for a final 3 times in 1x PBS as before being mounted in Vectashield containing DAPI (4, 6-diamidino-2-phenylindole). The coverslips were then sealed to each slide with clear nail varnish to prevent movement of the coverslip and the sample sections underneath.

2.2.6.2 Immune cell infiltration quantification on frozen sections

Frozen tumour sections were stained with fluorescent conjugated antibodies targeting $CD8^+$ $CD3^+$, $CD4^+CD3^+$, and $Foxp3^+CD3^+$ cells. Sections were viewed on a fluorescence microscope and positive cells were counted by eye per high power field of view. For each section, 10 high power fields of view were enumerated and from this an average was calculated.

Table 2.2| Antibodies used in Immunohistochemistry and Immunofluorescence staining

Target Antigen	Clone	Conjugate	Isotype	Supplier	Final concentration (µg/ml)
Primary antibodies					
CD3	-	Purified	Rabbit Poly	Dako	0.6
Foxp3	FJK-165	Purified	Rat IgG2a	eBioscience	1
CD4	RM4-5	Purified	Rat IgG2a	Biolegend	1
CD8	53-6.7	Purified	Rat IgG2a	eBioscience	1
B220	RA3-6B2	Purified	Rat IgG2a	Biolegend	1
Secondary antibodies					
Rat IgG	-	Alexa Fluor 488	Donkey IgG	Life Technologies	1
Rabbit Ig	-	Alexa Fluor 568	-	Life Technologies	1
Streptavidin	-	FITC	-	Biolegend	1
Rat IgM		Alexa Fluor 594	-	Life Technologies	1
Rat IgG	-	Alexa Fluor 555	-	Life Technologies	1
Isotype control antibodies					
Rat IgG2a	RTK2758	Purified	-	Biolegend	See primary
Rat IgM	RTK2118	Purified	-	Biolegend	See primary
Rat IgM	RTK2118	Biotinylated	-	Biolegend	See primary
Rabbit Ig		Purified		AbCam	See primary
Mouse IgG1		Purified		AbCam	See primary

2.2.7. Immunohistochemistry

2.2.7.1 Staining paraffin embedded sections

Tumours, lungs and draining LNs taken from DEREG mice were placed in bijoux tubes containing 5 ml 10% formalin solution for up to 1 month before being embedded in paraffin. Each sample was cut into 5 µm-thick sections on a Leica Microtome and mounted onto a glass slide, and any excess wax was melted off at 60°C. Slides were then completely de-waxed through 3 x 5 minute washes with xylene and then rehydrated in descending alcohol washes (100% MeOH, 90% MeOH, 90% MeOH, and 70% MeOH) at 3 minutes each. Antigen retrieval was performed by microwaving slides in pre-warmed 10 mmol/L Tris, 1 mmol/l EDTA at pH9 for 8 minutes, after which time slides were left to cool for 30 minutes before being equilibrated in 1x PBS. Any endogenous peroxidase activity was quenched using 3% H_2O_2/MeOH for 5 minutes at room temperature before slides were washed 3 x 3 minutes in 1x PBS. To prevent non-specific binding, slides were incubated with 2.5% Normal Horse Serum for up to 30 minutes at room temperature. Specific primary antibody solutions were made up to the suitable concentration in 1% BSA/PBS solution, and were incubated with each slide overnight at 4°C. A list of antibodies used can be found in table 2.2. The following day, slides were washed 3 x 3 minutes in 1x PBS. Primary antibodies were then detected using an ImmPRESS Horse Radish Peroxidase polymer detection kit during a 30-minute incubation with each slide, after which time slides were washed a further 3x 3 min in 1x PBS. The detected antibodies were then detected using Impact DAB (3, 3'-diaminobenzidine; brown), Impact VIP (Very Intense Purple; purple) or

Vector SG (grey). Slides were rinsed twice in dH_2O and then counterstained in Haematoxylin for up to 1 minute. Once slides had been rinsed with running tap water, they were then dehydrated in ascending alcohols (70% MeOH, 90% MeOH, 90% MeOH, 100% MeOH) for 3 minutes each and then 3 x 5 minute washes with xylene. A coverslip was then mounted onto each slide using DPX (distyrene, a plasticiser, and xylene) and slides were left for up to 1 hour at 60°C for the DPX to set. Sections were then imaged on Zeiss Axio Observer Z1 or scanned on Zeiss Axio Scan.Z1 slide scanner.

2.2.7.2 Quantification of T cell infiltration in paraffin sections

Paraffin embedded tumour sections were stained with antibodies targeting $CD8^+$, $Foxp3^+$, and $CD3^+$ cells. Slides were scanned on a Zeiss Axio Scan.Z1 slide scanner and analysed using Zen software. A grid was placed over each section and 10 squares were enumerated and an average was calculated.

2.2.8 Flow Cytometry

2.2.8.1 Phenotyping DEREG mice

Mice were ear coded when they reached 4 weeks old, and were subsequently tail-tipped under local anaesthetic. Blood from the tail-tip was collected in a Microvette lithium heparin-containing tube in order to prevent clotting, and tubes were stored on ice for up to 45 minutes. Each blood sample was then stained with APC-Cy 780 conjugated anti-mouse CD4 antibody (eBioscience) and was left to incubate for 1 hour on ice. Samples

were then re-suspended in 200 µl 1x Red Blood Cell (RBC) lysis buffer (made from 10x stock solution) and run on a BD FACsCanto flow cytometry machine. Up to 200 000 events were captured, and DEREG positive mice were identified as having GFP^+ (FITC) $CD4^+$ cells. The gating strategy is shown in figure 2.1.

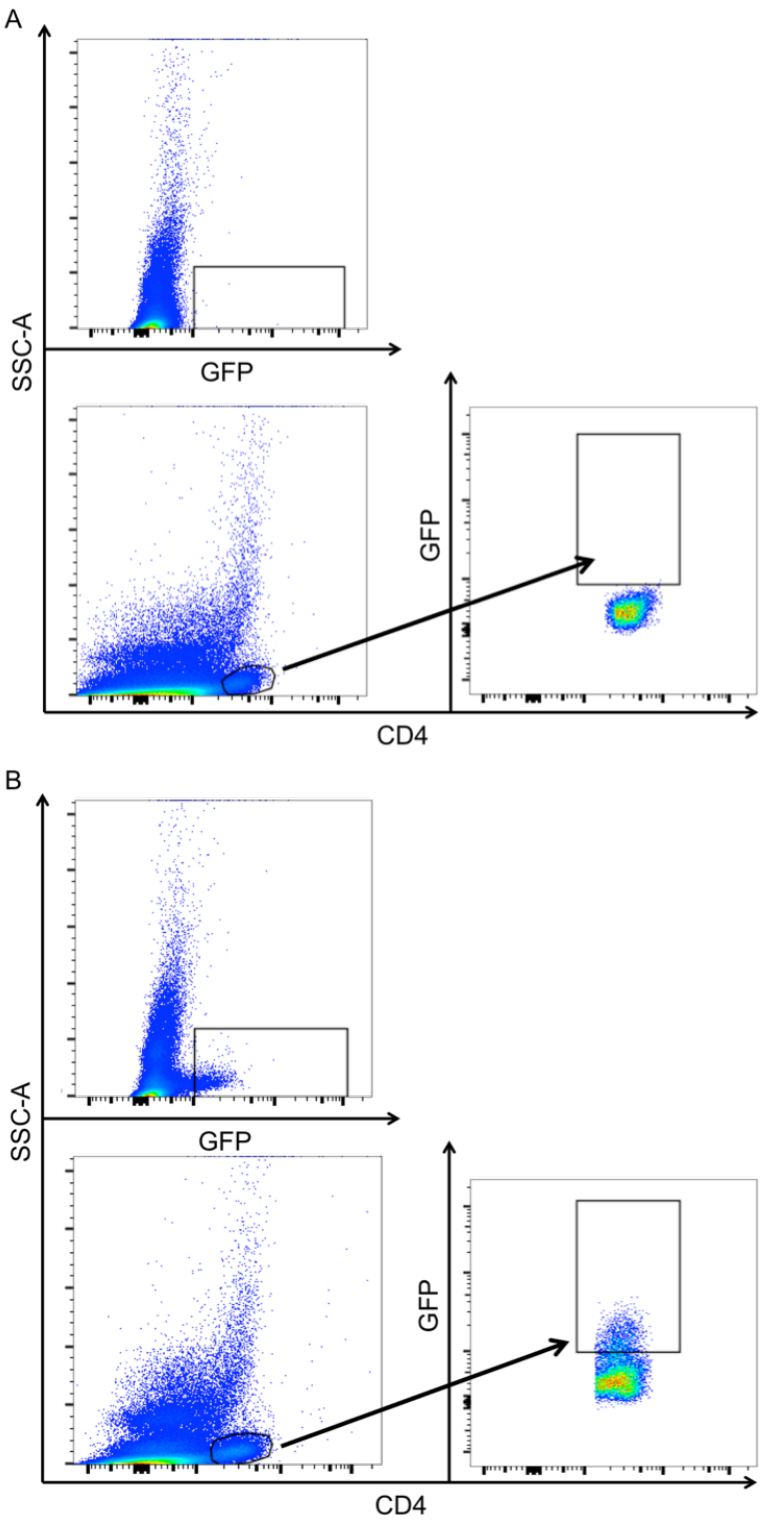

Figure 2.1| Gating strategy for determining the phenotype of DEREG litters. Plots were initially gated on GFP versus side scatter area (SSC-A) and then on CD4 versus SSC-A. From the $CD4^+$ population, a new plot was created as CD4 versus GFP and a gate was drawn around $CD4^+GFP^+$ population. (A) Shows the gating strategy for a DEREG negative mouse. (B) Shows the gating strategy for a DEREG positive mouse.

2.2.8.2 Looking for Tregs in DEREG mice

DEREG and WT Balb/c mice were sacrificed and their spleens and LNs were harvested. In a multiwell plate, spleens and LNs were homogenised using the base of a syringe plunger. The homogenised tissues were then re-suspended in complete RPMI medium and passed through a 70 µm cell strainer. Cell suspension were then centrifuged 1500 rpm for 5 minutes, the supernatant discarded, and the resulting cell pellet was re-suspended in complete RPMI and washed through centrifugation as before. Red blood cells from the homogenised spleens were lysed using RBC lysis buffer, 5 ml of which were added to each cell suspension for 90 seconds. After this time, 20 ml of RMPI was added to stop the reaction and cells were subsequently centrifuged at 1500 rpm for 5 minutes and the supernatant was discarded.

The single cell suspensions were plated in a 96-well u-bottomed plate at a density of $5x10^5$ – $1x10^6$ cells per well. Cells were washed twice using PBS and were subsequently stained for dead cells using a fixable dead cell staining kit (LIVE/DEAD Aqua by INVITROGEN). LIVE/DEAD was diluted 1/10 in PBS and 3 µl were added to each cell-containing well and the plate was incubated in the dark at room temperature for 15 minutes. Cells were then washed twice in PBS through centrifugation at 1500 rpm for 3 minutes before Fc receptors were blocked using diluted anti-CD16/32 antibody. Plates were left to incubate in the dark for 10 minutes at 4°C, after which time cells were washed a further 2 times in FACS buffer. Antibody master-mixes of surface stains were made up to the desired concentrations and were added at 25-50 µl per well and left to incubate in the dark for up to an

hour at 4°C. A list of surface antibodies used can be found in table 2.4. After incubation, cells were then permeabilised using fixation/permeabilisation buffer (eBioscience) overnight and subsequently stained with intracellular antibodies as before. Flow cytometric data was analysed using FlowJo software, the gating strategy can be found in figure 2.2.

Table 2.3| Antibodies used for flow cytometry staining

Target Antigen	Clone	Conjugate	Supplier	Stock concentration	Final concentration (µg/ml)
Surface antibodies					
CD4	RM4-5	APC-Cy-780	eBioscience	0.2 mg/ml	2
CD25	PC61	PE	BD Pharmingen	0.2 mg/ml	4
B220	RA3-6B2	PE	BD Pharmingen	0.2 mg/ml	4
CD8	53-6.7	PECy7	eBioscience	0.2 mg/ml	4
CD3	17A2	APC-Cy-780	eBioscience	0.2 mg/ml	2
Intracellular antibodies					
Foxp3	FJK-16s	PECy7	eBioscience	0.2 mg/ml	4

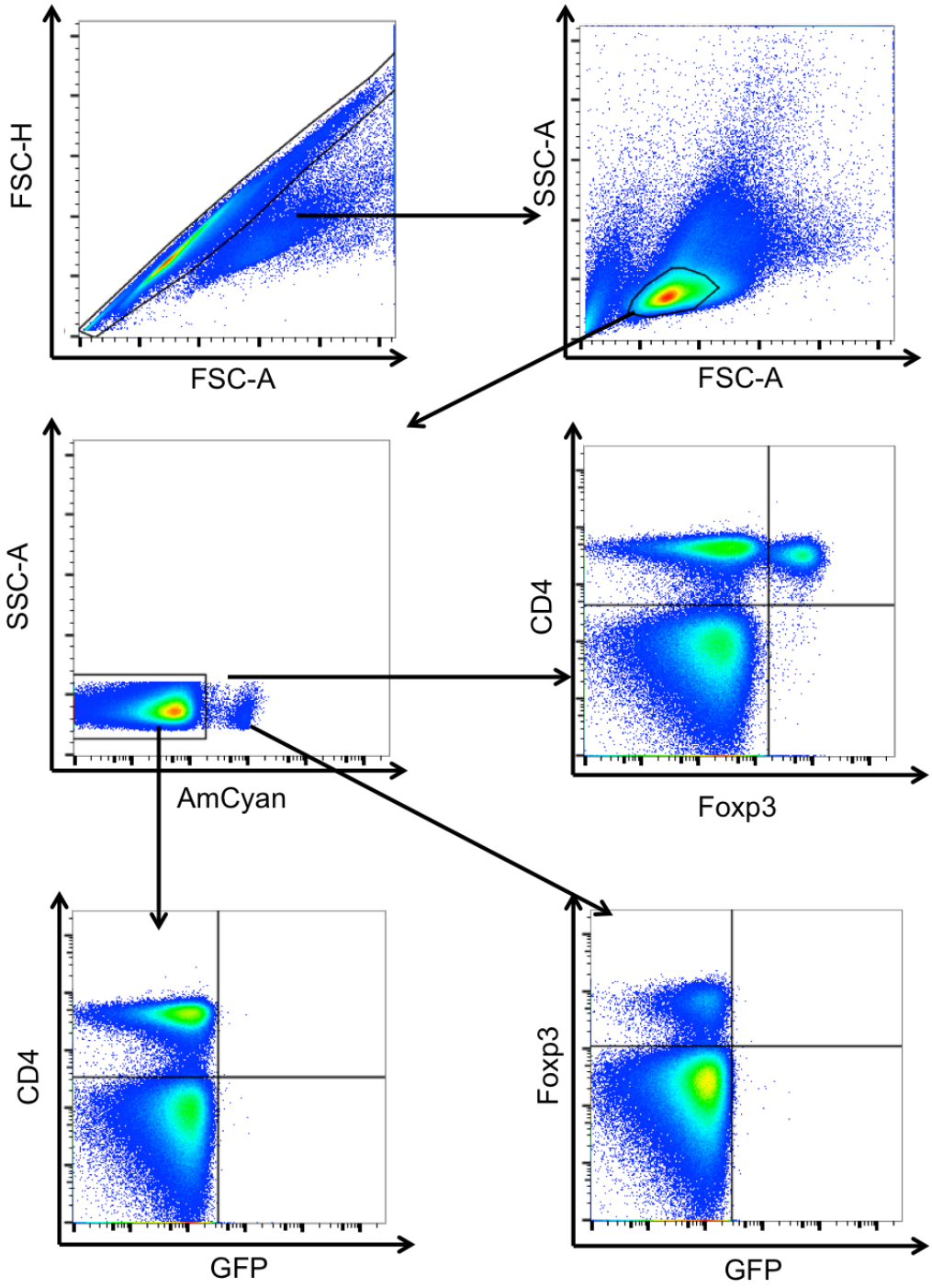

Figure 2.2| Gating strategy for Treg analysis. Initially, cells were plotted as forward scatter area (FSC-A) versus forward scatter height (FSC-H) in order to gate on single cells and exclude doublet cells. From this population, cells were plotted as FSC-A versus SSC-A and a gate was drawn around the lymphocyte population. From the lymphocyte population, cells were plotted as AmCyan (LIVE/DEAD) versus SSC-A to select living cells. The living cell population could then be plotted as Foxp3 versus CD4, GFP versus CD4 and GFP versus Foxp3.

2.2.9 Statistical Analysis

All statistical analysis was performed on GraphPad Prism™ software. Details of each statistical test performed are presented in Figure legends.

Chapter Three

3 Results: Optimising preclinical PET/CT imaging to monitor progression of 4T1 metastasis in mice.

3.1 Introduction

There are two different imaging components that make up PET/CT; Positron Emission Tomography (PET) and Computed Tomography (CT). CT uses X-rays to build up a 3D image of a scanned subject, while PET uses scintillation crystals to detect annihilation positrons emitted from a decaying radioactive isotope. In combination, these two components create an image detailing different structures and tissues within the human body.

The most common use of PET/CT exploits the Warburg effect, in which tumour cells have increased glycolysis in comparison to surrounding tissues (Warburg 1956). In medicine, the radioactive glucose analogue fluoro-deoxyglucose (FDG), containing the radioisotope Fluorine^{18}, is injected intravenously into patients and is taken up by highly metabolically active tissues such as tumours. Scintillation crystals in the PET scanner detect the decay of F^{18} generating a map of radioactivity that, through the use of computer algorithms, can be plotted onto the CT of the patient. This allows identification of malignant lesions without the use of invasive surgery.

The use of PET/CT as a combined imaging technique was conceived in 1991 by Townsend and colleagues, and was further developed into a working prototype in 1998 with help from Ron Nutt (Kinahan et al. 1998; Townsend et al. 1993). Combined PET/CT was created in order to obtain

clinically relevant PET and CT images in a single session, and using the original prototype, a number of clinical trials were conducted involving the scanning of cancer patients (Charron et al. 2000; Kluetz et al. 2000; Meltzer et al. 2000). In the case of head and neck cancers, it was found that PET/CT was able to distinguish between malignant lesions and the surrounding muscle tissue (Kluetz et al. 2000), and the combination of PET and CT allowed for more precise localization of tumours for further radiotherapy (Charron et al. 2000; Meltzer et al. 2000).

The use of PET/CT in preclinical models has been described for a number of different disease models, such as certain tumours, brain abnormalities and respiratory infections, as well as imaging cell recruitment and changes in metabolism (Chapter 1) (Bagci et al. 2013; Bu et al. 2014; Lee et al. 2013; Mittra et al. 2016; Park et al. 2015; Rendon et al. 2016). Figure 3.1 details the process of CT and PET imaging in a preclinical scanner.

It has been shown that solid tumours can be imaged over time in mice using FDG PET/CT. While FDG PET/CT imaging in humans has a high rate of success when diagnosing metastasis, in mice this has not been quantified (Charron et al. 2000; Kluetz et al. 2000; Meltzer et al. 2000). I aimed to successfully optimize both PET and CT imaging on the Gamma Medica Triumph II PET/CT/SPECT scanner and subsequently, following refurbishment and updating of the imaging facility, the Mediso nanoScan PET/CT scanner, for assessing the progression of metastatic disease in mice. Specifically, metastatic disease was assessed in DEREG mice injected with 4T1 murine mammary carcinoma. Mice were injected

subcutaneously close to the mammary fat pad with $1x10^5$ 4T1 cells and tumours were left to grow for 14 days before being surgically resected. After tumour removal, the mice undergo a series of PET/CT scans in order to monitor metastasis progression. This chapter describes optimisation of both Gamma Medica and Medico scanners as well as use of the relevant acquisition and data analysis software.

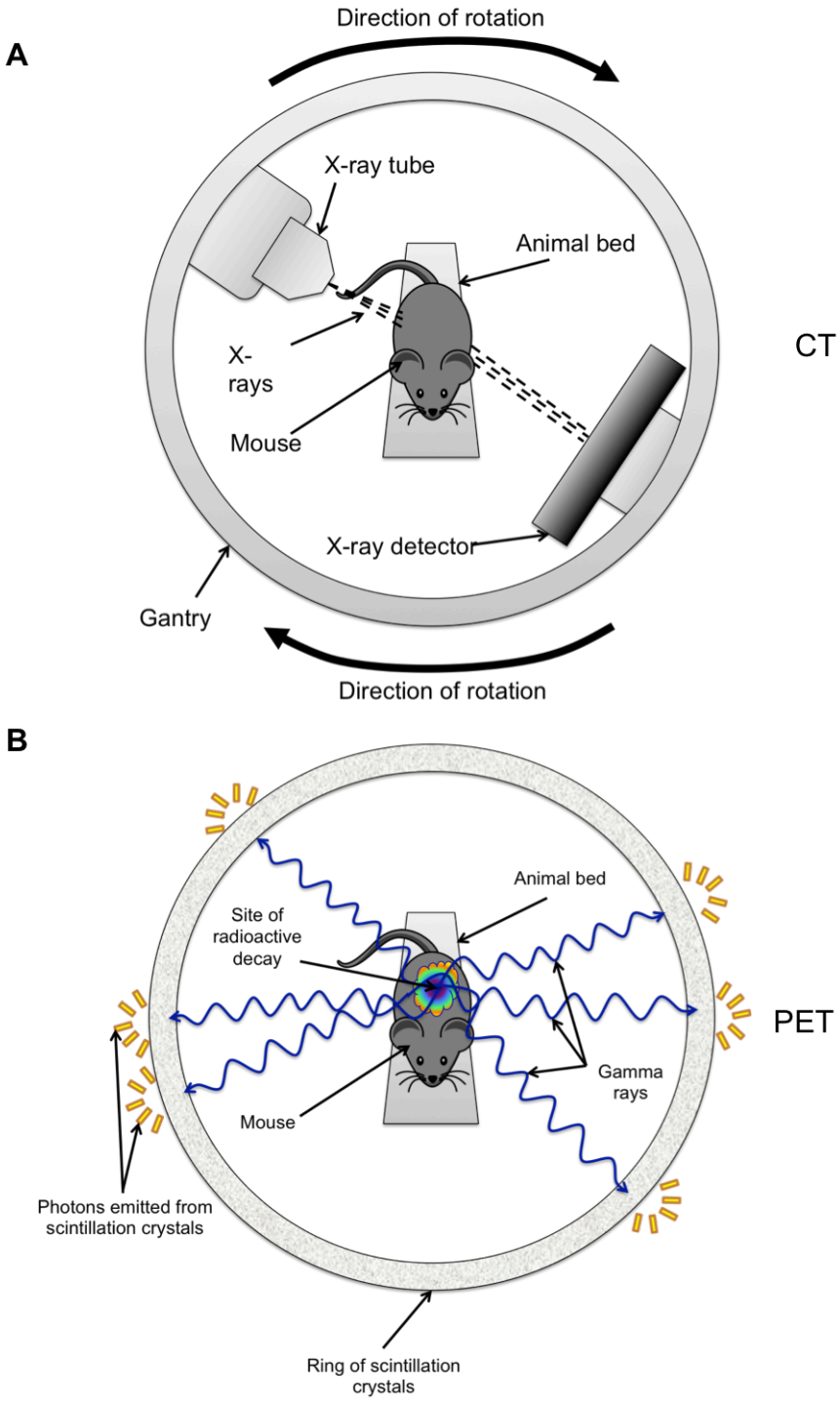

Figure 3.1| Diagrams detailing the process of CT and PET scanning. (A) A mouse is placed on the animal bed in the centre of the gantry. X-rays are emitted from the x-ray tube at the mouse and are detected on the other side of the gantry by the x-ray detector. The gantry rotates 360 degrees emitting x-rays towards the mouse until a full rotation has been completed. (B) The mouse sits in the centre of the scintillation crystals while the radioactive isotope decays emitting gamma rays at 180° to one another. Gamma rays are detected by the scintillation crystals, which cause emission of photons that are amplified by a photon multiplier tube. The point at which photons are emitted from the scintillation crystals is analysed by a computer, which calculates the point the original decay occurred

3.2 Results: Altering different parameters of CT scans allows definition of soft tissues

The ability to differentiate between the soft tissues in a CT scan is vital for enabling Regions Of Interest (ROIs) to be drawn around tissues predicted to harbor metastatic cells. There are many different parameters of CT scans that can be optimized in order to increase the resolution of different areas of the scanned subject such as the skeleton, cardiovascular architecture or abdominal organs. An overview of the CT parameters optimized can be found in Table 3.1.

CT optimisations were performed on both the Gamma Medica Triumph II PET/CT/SPECT scanner and the Mediso nanoScan PET/CT scanners. When comparing the scans from Triumph II scanner to the nanoScan scanner, it was observed that even without the use of a contrast agent, the contrast of the CTs obtained with nanoScan showed definition of tissue not visible using the Triumph II (Figure 3.2). Thus, CT parameters were optimized using the Mediso nanoScan unless stated otherwise.

Table 3.4| CT parameters for optimisation on the Mediso nanoScan.

CT Parameter	Options Available	Overall Effect on CT
X-ray energy	35KVp, 50KVp, 70KVp	Soft tissue definition and contrast
Binning	1:1, 1:4, 1:16	Final resolution of CT
Projection number	360, 480, 720	Final resolution of CT
Contrast agent	Iohexol, Aurovist™	Soft tissue definition and contrast

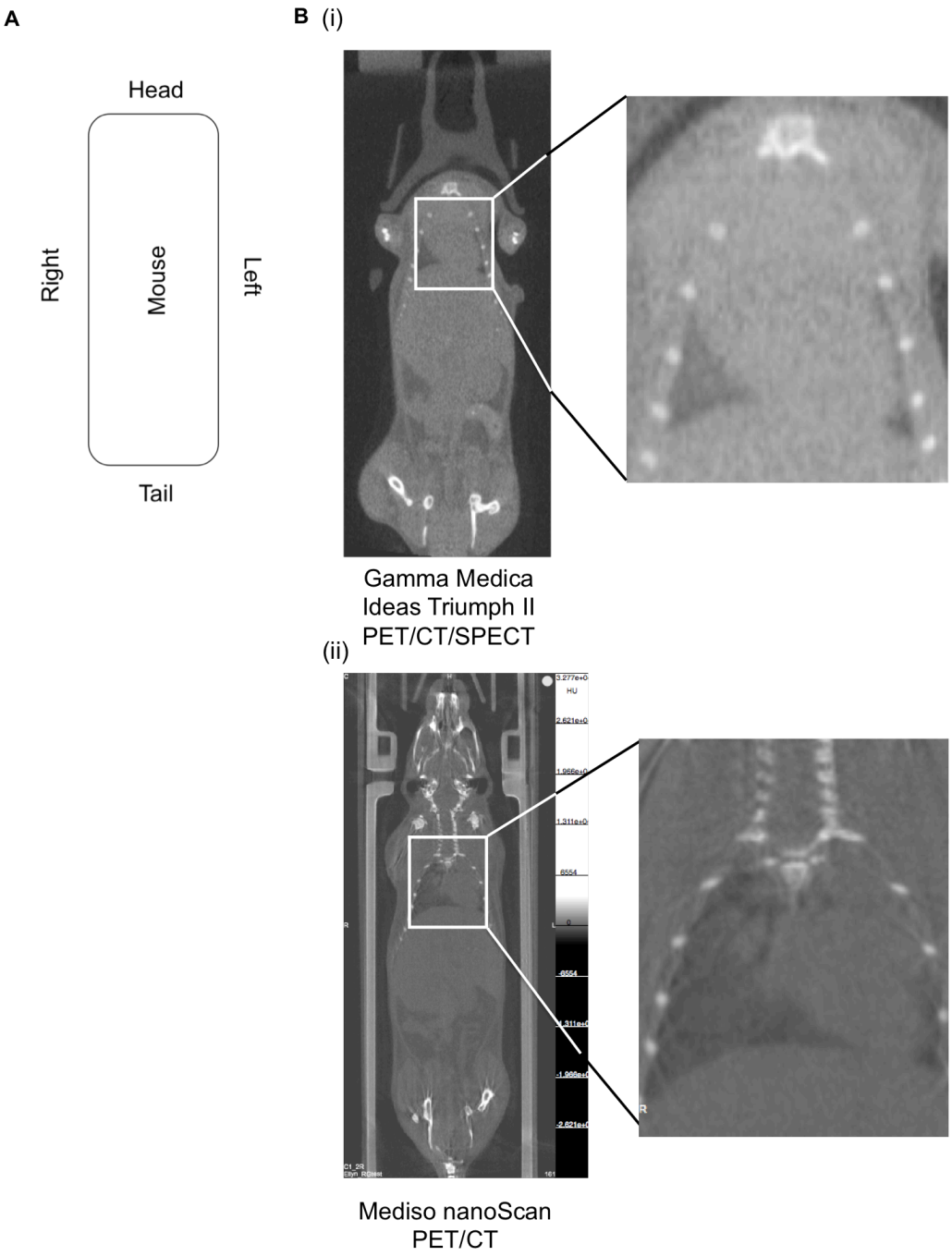

Figure 3.2| The Mediso nanoScan PET/CT scanner produces clearer, higher resolution CT images with enhanced soft tissue contrast than the Gamma Medica Triumph II PET/CT/SPECT scanner. (A) Indicates the orientation of the scanned mice in (B). (B) Shows two mice scanned under the optimized protocol for the Gamma Medica Triumph II (i) and the Mediso nanoScan (ii). The white box highlights the increased resolution of CT acquired on the nanoScan PET/CT scanner.

3.2.1 Optimisation of X-ray energy

The strength of X-rays used in the acquisition of a CT scan determines which tissues are most visible in the final image. X-rays of different energies (measured in KVp, where KVp is the peak kilovoltage applied across the X-ray tube) are differentially absorbed by tissues within the body. Low X-ray energy (35 KVp) can be absorbed by soft tissues such as the internal organs but cannot penetrate bone, whereas high X-ray energy (70 KVp) penetrates most tissues. Different X-ray energies were tested in order to ascertain the optimum energy for soft tissue definition. On the Gamma Medica Triumph II, a single female BALB/c mouse was anaesthetised, placed on a warmed rat bed in the PET/CT scanner and subjected to 3 CT scans at X-ray energies: 60KVp, 50KVp and 45KVp. No difference was observed in soft tissue definition between the different X-ray energies thus the default setting of 60KVp was used for all subsequent scans performed using the Gamma Medica Triumph II.

X-ray energies of 35KVp, 50KVp and 70KVp were subsequently tested for the Mediso nanoScan PET/CT scanner. Whilst all X-ray energies were absorbed by the soft tissues of the mouse, the lower X-ray energies of 35KVp and 50KVp were not absorbed by bone and instead were subject to beam hardening, creating a “glowing” effect around the bone appearing as streaks on the CT image (Figure 3.3). Artifacts, such as these arising from the ribcage can obscure the air space within the lungs, hindering accurate delineation of the lung. An X-ray energy of 70KVp allowed absorption of X-rays by the bone as well as the soft tissues, reducing such artifacts (Figure 3.3). Therefore, 70KVp X-ray energy was used for all subsequent CT scans.

3.2.2 Optimising the projection number

The number of projections refers to the number of image slices taken in a full 360 rotation of the gantry. For example, a scan performed with 360 projections means an image is taken at every degree the gantry is turned. Increasing the number of projections increases the final resolution of the images obtained. Since the Mediso nanoScan allows projection number to be set at 360, 480 or 720, 720 projections were selected to enable clear identification of small structures within the chest cavity.

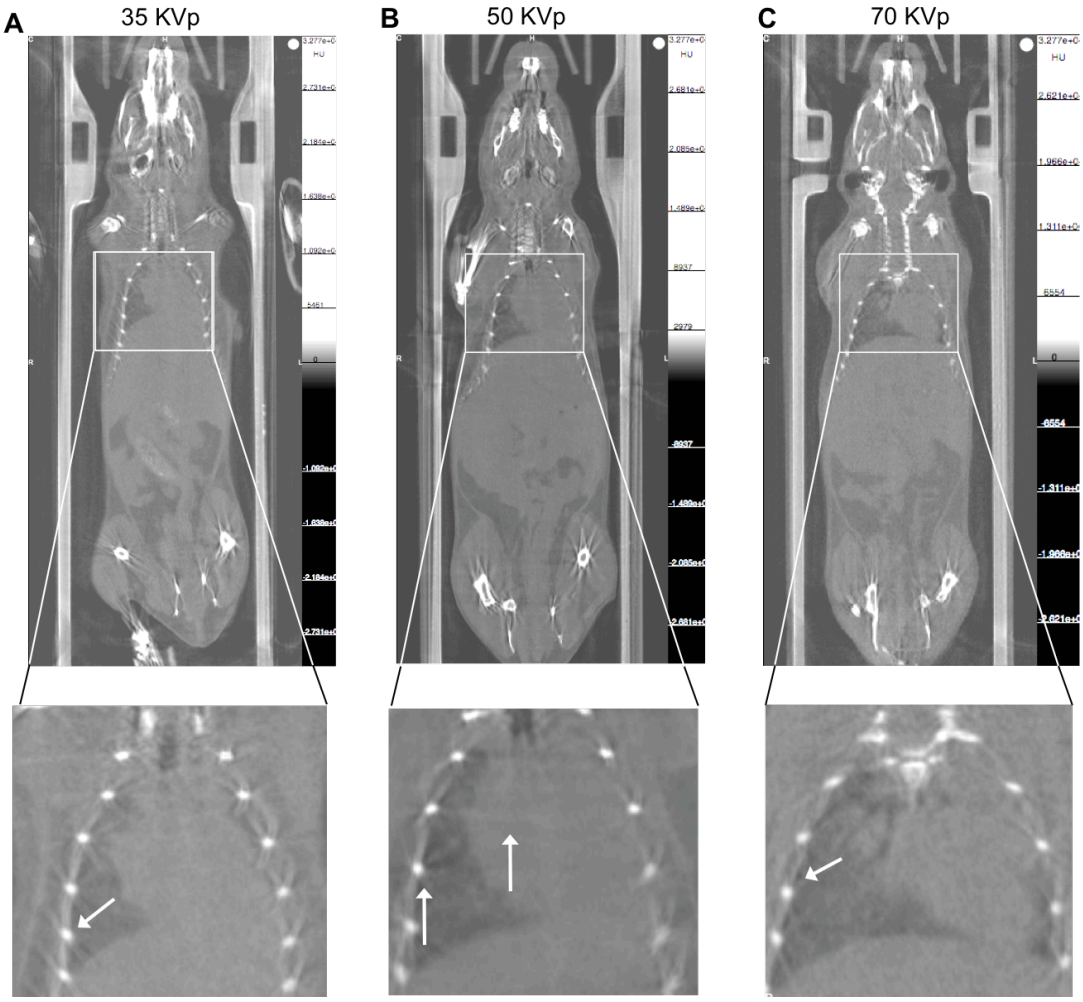

Figure 3.3| Changes in X-ray energy voltages highlight different aspects of a scanned subject. Resulting CT scans of the same naïve mouse scanned at different X-ray energy voltages for the same period of time on the Mediso nanoScan scanner. The mouse was anaesthetised and placed on the animal bed in the scanner and subsequently underwent 3 consecutive 3-minute scans at the voltages indicated above. On each of the 3 scans, white arrows indicate the beam hardening effect seen at lower voltages, where a "glowing" effect is seen around bone. The brightness of each image has been artificially increased by 26% using Microsoft PowerPoint™ in order to fully reveal the extent of artifacts.

3.2.3 Optimising the Binning process.

Using the Nucline™ software, it is also possible to change the resolution of the CT image created by altering the binning process. Binning is the process of assigning pixels picked up by the X-ray detector to pixels in the projections that make up the final reconstructed CT image, where acquisition of a CT image at a 1:1 binning means that for every pixel detected by the X-ray detector, 1 pixel is finally created in the reconstructed CT image (described in Figure 3.4). Images collected at a 1:1 binning are most likely to produce the best resolution CT images but also a higher signal to noise ratio. In addition, collection of data at a 1:1 binning requires large amounts of computer space and has a longer CT reconstruction time, which restricts the throughput of mice in an experiment. To explore whether higher binning could be used, a CT scan of a naïve BALB/c mouse, performed using the Mediso nanoScan, was reconstructed at a 1:4 binning and 1:1 binning (Figure 3.5). While more background noise was observed with a 1:1 binning, definition of some structures within the abdomen and the chest cavity were clearly lost as a result of the 1:4 binning, as indicated by the white arrows at (i) in the chest cavity and (ii) in the abdominal cavity. Consequently, all CT scans were acquired at a 1:1 binning.

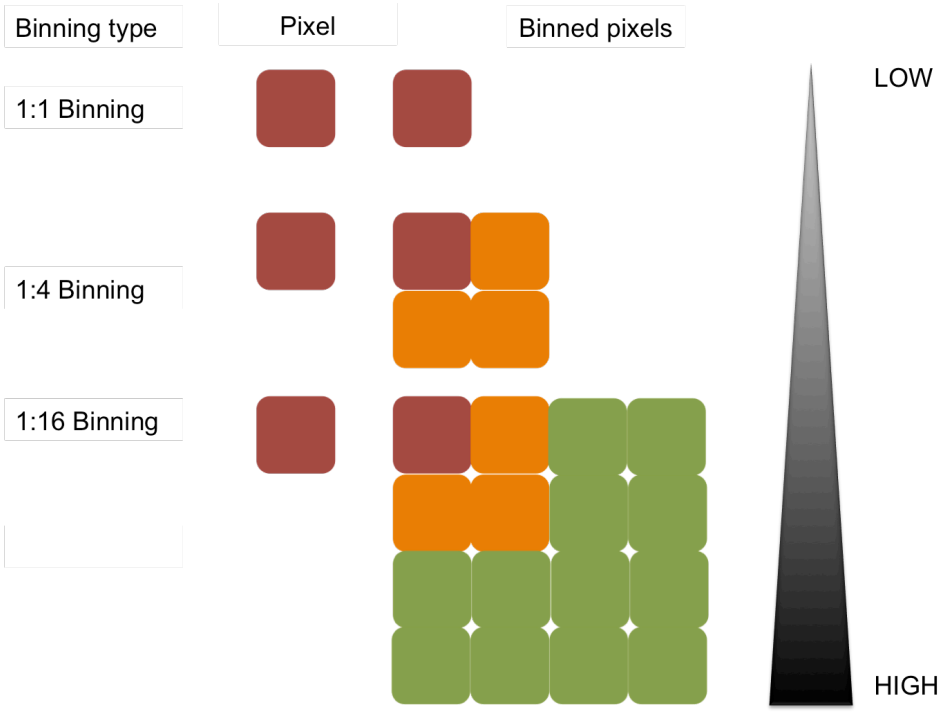

Figure 3.4| A diagram describing the process of binning during CT acquisition. During the acquisition of a CT scan, each pixel or group of pixels can be assigned to a single pixel in the reconstructed image. The lower the binning the better the resolution of the final reconstructed CT scans.

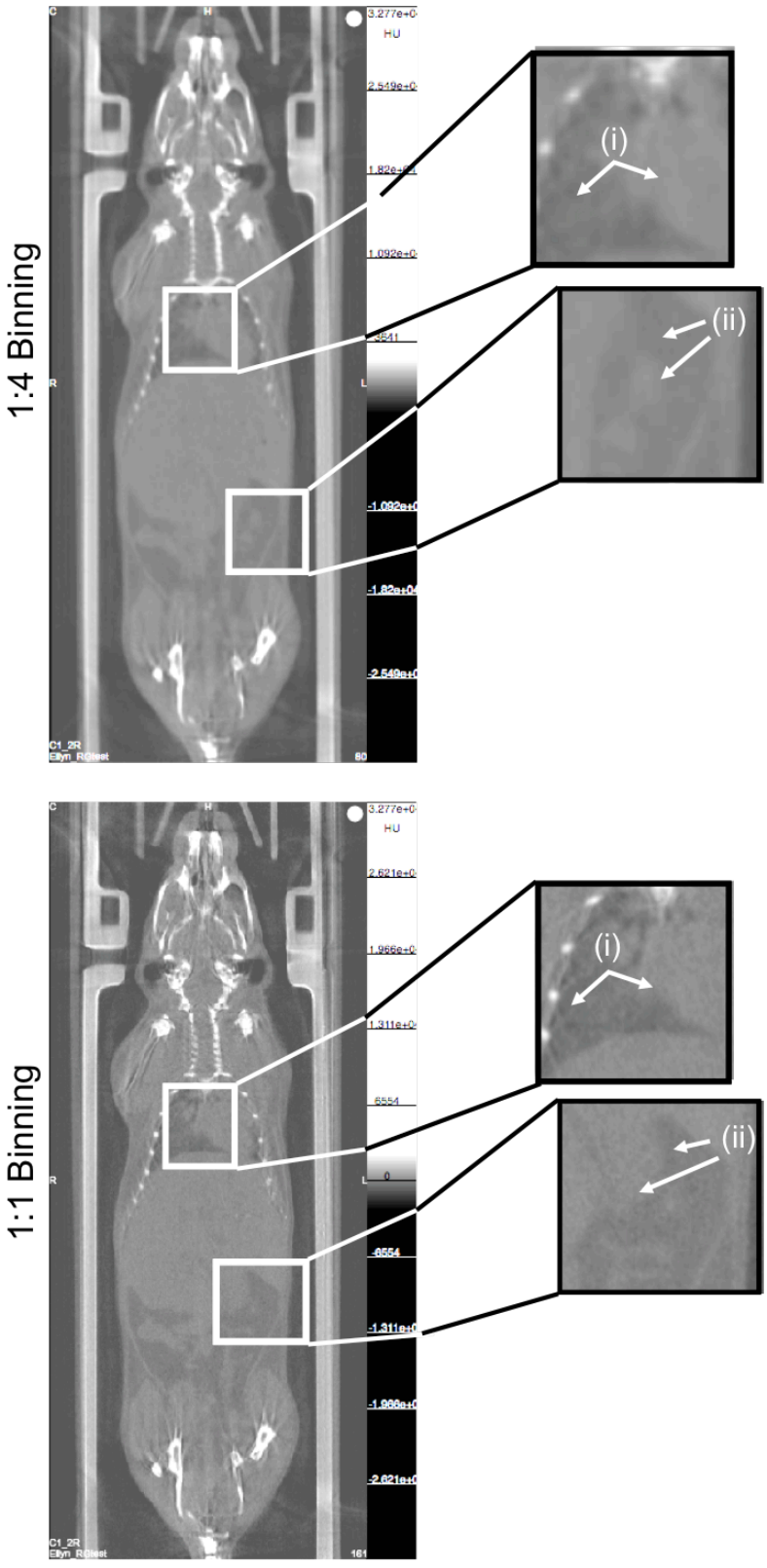

Figure 3.5| The binning process enhances the resolution of the final reconstructed CT image. A CT image acquired at 1:1 binning and subsequently reconstructed at 1:1 binning and 1:4 binning. White arrows indicate the difference in contrast between the heart and lungs (i) and some soft tissues in the abdominal cavity (ii). Each image has been artificially brightened by 26% using Microsoft PowerPoint™ to fully highlight the contrast observed in binning techniques.

3.2.4 Optimising the use of contrast agents for CT

In order to distinguish between the soft tissues, it is standard clinical practice to use a nonionic iodine contrast agent called Iohexol (trade name Omnipaque) (Cacayorin et al. 1983). In patients, Iohexol is injected intravenously to highlight the vasculature or taken orally to highlight gastro-intestinal structures (Wiklund et al. 1994). In the case of preclinical studies, a contrast agent named AuroVist^{TM} has been highlighted as a useful tool to highlight the vascular system which in the case of the study described here, could be particularly useful for increasing the contrast between the heart and the lungs in the chest cavity (Darin et al. 2013). Thus, both contrast agents were compared.

3.2.4.1 Iohexol

In humans, fat surrounds the internal organs offering “natural” contrast between soft tissues. This is not the case in mice, therefore injection of contrast agent both intraperitonealy and intravenously was deemed necessary to differentiate between the soft tissues in the abdominal cavity and the chest cavity. Female mice were untreated or injected i.p with 100 µl Iohexol before induction of anaesthesia and 100 µl Iohexol i.v thereafter. Fifteen minutes later, mice underwent a CT scan using the previously described protocol. By comparing the two CT scans with and without Iohexol, sharper contrast between the lungs and the heart [Figure 3.6 (B)(i)], increased detailing of the heart [Figure 3.6 (B)(ii)] and greater soft tissue definition within the abdominal cavity [Figure 3.6 (B)(iv)] was observed in the Iohexol treated mice. Moreover, use of Iohexol enabled differentiation

of the diaphragm and liver and more detailed image of the peritoneal cavity [Figure 3.6 (B)(iii)]. No artifacts were observed as a result of Iohexol use.

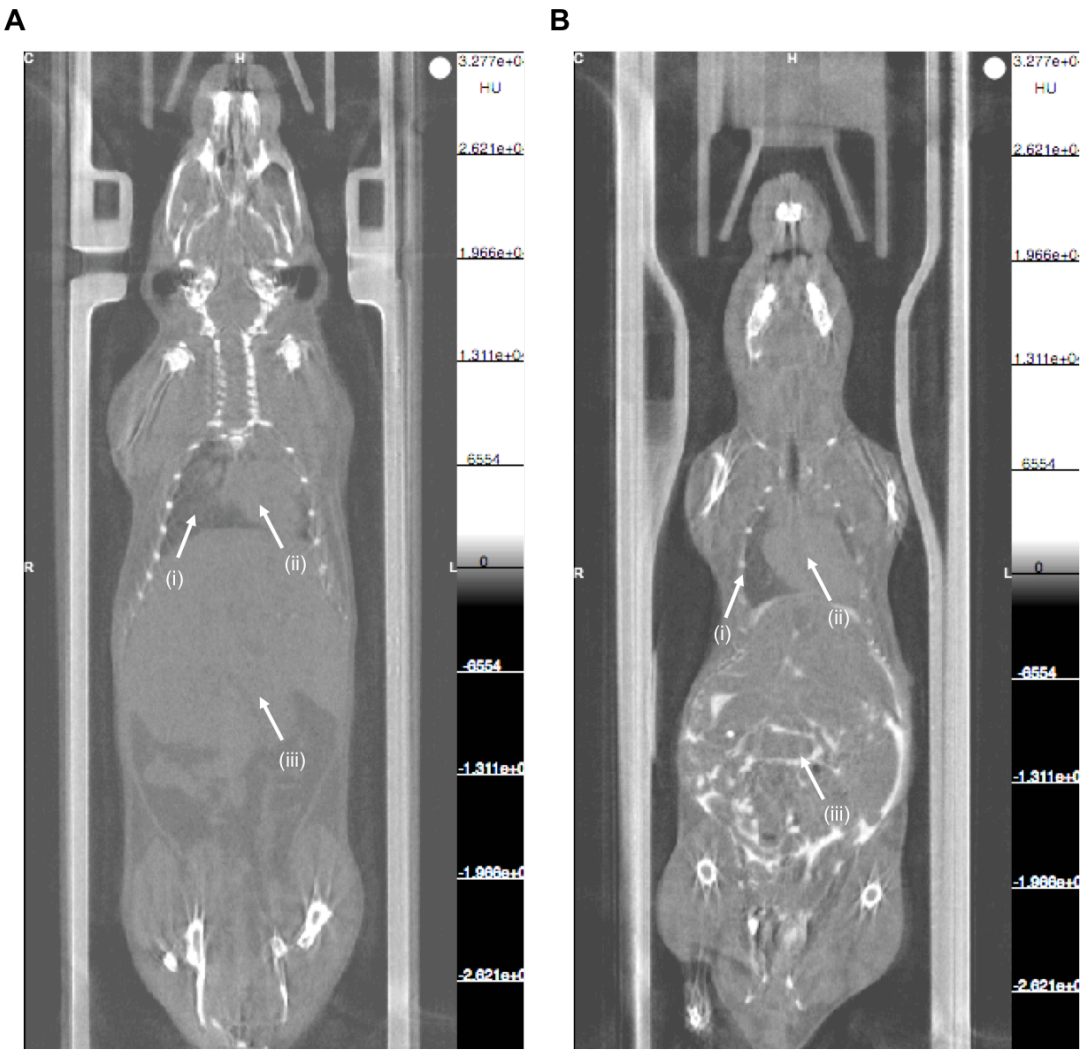

Figure 3.6| Using the iodine contrast agent Iohexol aids differentiation of soft tissues. CT scans of mice taken on Mediso nanoscan PET/CT scanner. Each mouse was scanned at 70 KVp for 3 minutes (A) without and (B) with Iohexol contrast agent. The notation (i) indicates the chest cavity, where an increased contrast between the air space and the cardiovascular system is observed in mouse administered with Iohexol. (ii) Indicates the detail of the heart and (iii) shows Iohexol in the contrast achieved within the abdomen after i.p administration. The brightness of each image has been artificially increased by 26% using Microsoft PowerPoint™ in order to fully demonstrate the differences seen in CT images after the use of contrast agent.

3.2.4.2 Aurovist

Use of the gold-nanoparticle contrast agent AuroVist^{TM}, described for use as a vascular contrast agent (Darin et al. 2013; Hainfeld et al. 2006), was also explored and compared to Iohexol.

Three age matched littermate mice were warmed for >1 hour at 37°C before being anaesthetised and injected i.v with approximately 10MBq of FDG plus 100 µl of AuroVist^{TM} at a concentration of 100 mg/ml. A CT scan was then performed using the previously described protocol; followed 15 mins later with a PET scan.

The scans in Figure 3.7 show that Aurovist^{TM} increased the contrast between the heart and the lungs in comparison to no contrast agent, but the level of contrast was not superior to Iohexol. As Iohexol was freely obtained in-house, it became the contrast agent of choice for all subsequent scans.

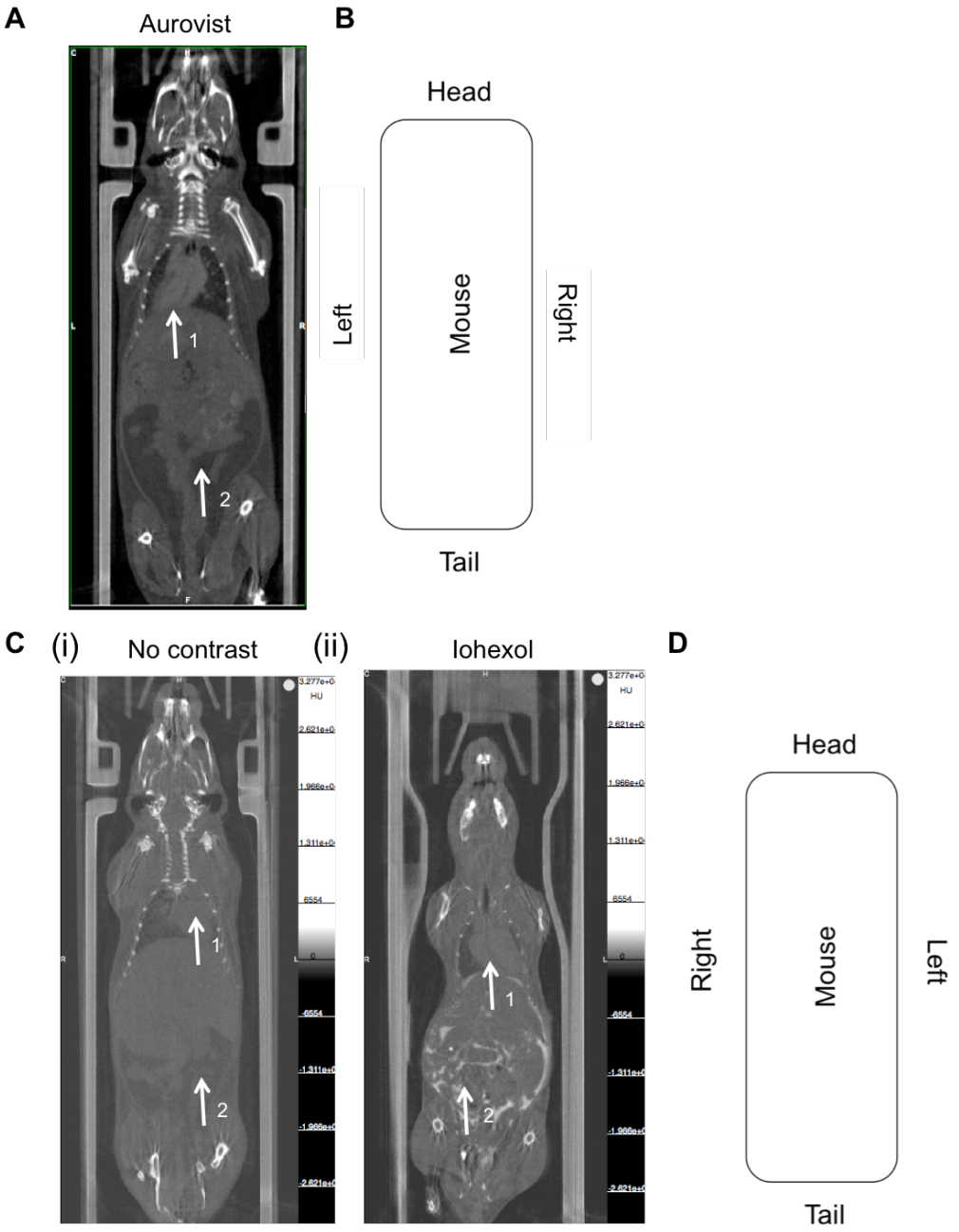

Figure 3.7| Gold nanoparticle contrast agent Aurovist highlights vasculature in mice. (A) shows CT scan of a mouse injected i.v with Aurovist in the orientation shown in (B). (C) Shows CT scans of a mouse with no contrast administered (i) and with Iohexol contrast agent (ii) in the orientation shown in (D). The white arrows show the difference in contrast at the heart (number 1) and the abdomen (number 2).

3.3 Results: Optimisation of PET imaging shows areas of high metabolic activity.

Optimal PET/CT imaging of small animals requires warming of the animal to body temperature before induction of anaesthesia and injection of FDG (Fueger et al. 2006). Mice have a higher proportion of brown fat than humans in order to maintain body heat. This is important as mice have a small surface area to volume ratio and can lose body heat quickly. The main areas rich in brown fat lie around the neck and shoulder blades, and when active these areas have a large glycolytic output (Hu et al. 2010; Wang et al. 2012). Consequently, on a FDG PET scan areas of brown fat appear highly radioactive, and can obscure changes in metabolic activity in other organs. By warming mice to their natural body temperature, brown fat begins to deactivate and therefore does not uptake FDG at the same rate as more metabolically active organs (Fueger et al. 2006; Wang et al. 2012). This is illustrated in Figure 3.8.

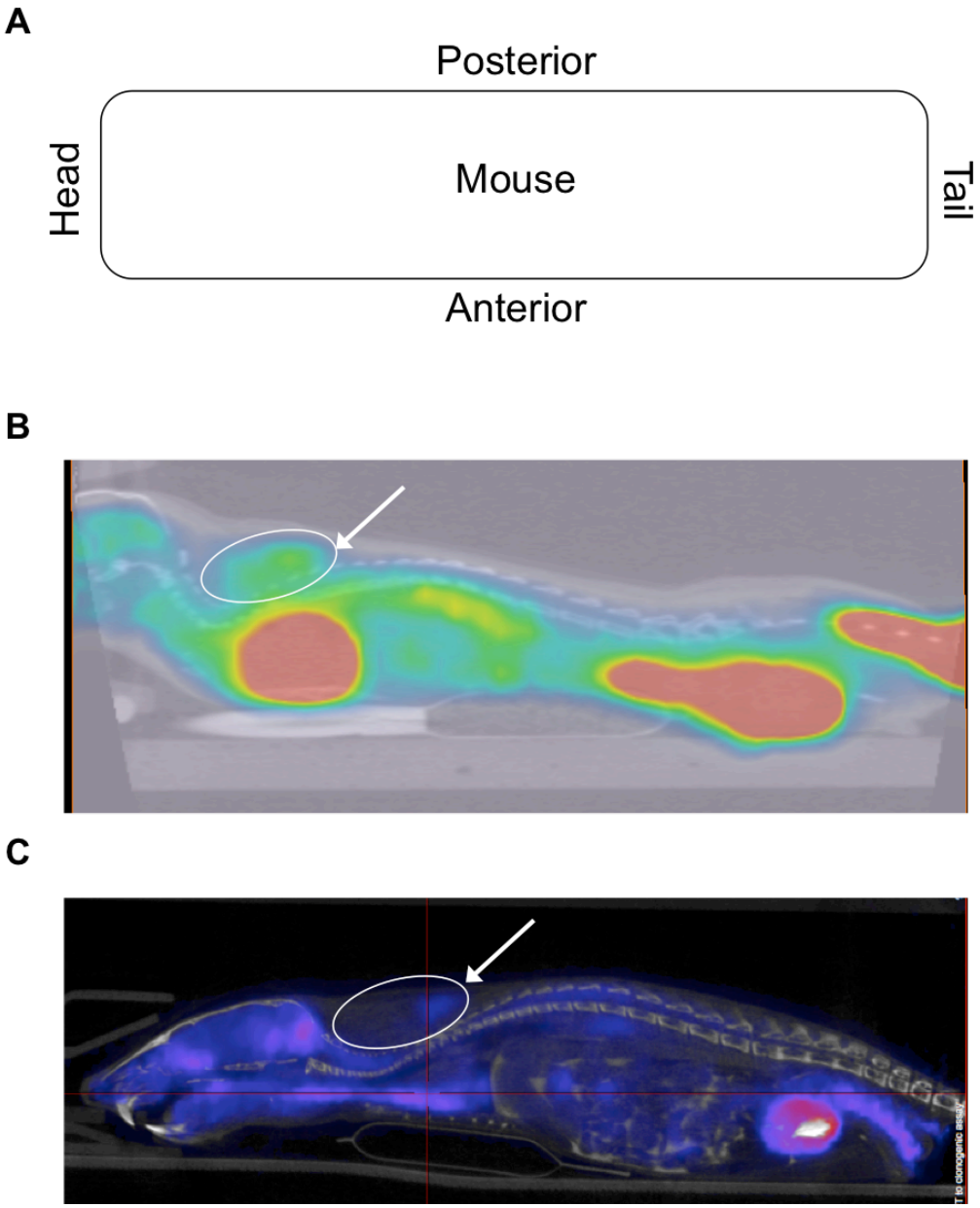

Figure 3.8| Warming mice to their natural body temperature prevents the uptake of FDG by brown fat. (A) Indicated the orientation of the mice in the scans in (B) and (C). (B) Shows a scan taken on the Gamma Medica Triumph II of a mouse that has not been warmed before scanning. A white oval and arrow highlights the area of brown fat around the neck and shoulder blades. (C) Shows a scan taken on the Mediso nanoScan of a mouse warmed for >1 hour before scanning. The white arrow and oval indicates the area of brown fat.

3.3.1 Optimisation of FDG administration

To identify the most appropriate technique for administering FDG, i.v versus i.p injection was compared. Mice were warmed for at least 1 hour before being anaesthetised and injected i.p with approximately 10MBq of FDG and placed on a warmed mouse bed ready for scanning on the Gamma Medica Triumph II scanner. A CT scan was performed first as previously described, followed by a 15 minute PET scan 1 hour after the initial i.p injection in order to allow sufficient uptake of FDG by tissues. An example of a reconstructed PET/CT scan after an i.p injection of FDG is shown in Figure 3.9. The reconstructed image shows a large area of radioactivity around the site of injection [Figure 3.9 (A) in pink and (B) in green), which was almost indistinguishable from surrounding organs such as the bladder. A second method of FDG administration was then tested, where mice were warmed, anaesthetised and subsequently injected i.v with approximately 10MBq FDG before undergoing CT and PET scan as before. As shown in Figure 3.10, no injection site artifacts were observed and therefore, FDG was administered via the tail vein for all future scans.

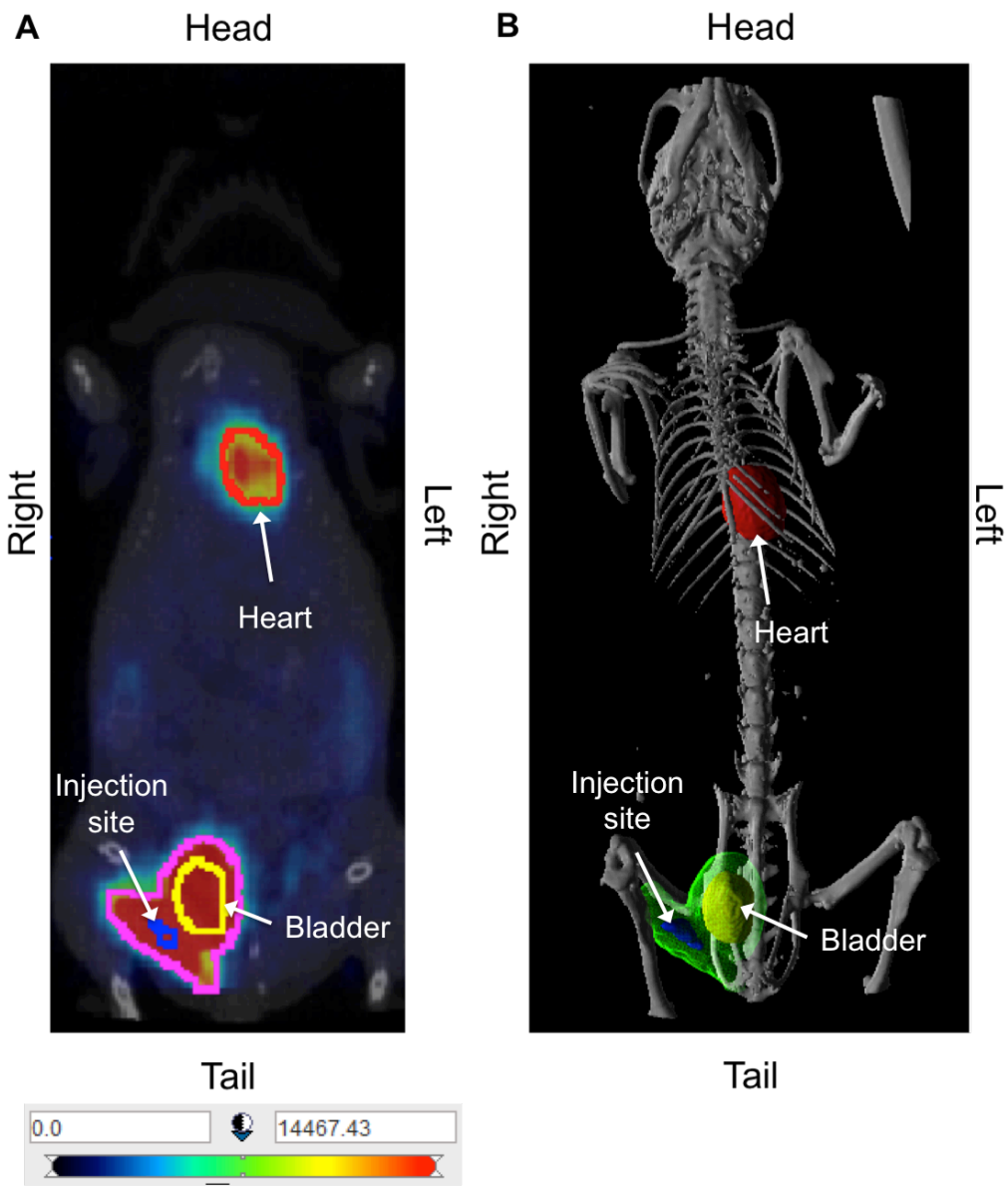

Figure 3.9| FDG injected i.p leaves an area of high radioactivity on PET/CT images. (A) A 2D PET/CT image taken using Gamma Medica Triumph II of a mouse injected i.p with 10 MBq of FDG, with the range of radioactivity seen in the PET scan given in Bq/ml on the scale bar below. ROIs have been drawn around the heart in red, the bladder in yellow, and the injection site in blue. The pink ROI indicates the size of the area of radioactivity from both the bladder and the injection site. (B) A 3D image created using Pmod3.3 software of the mouse with ROIs from (A). The area in green indicates the pink ROI in (A).

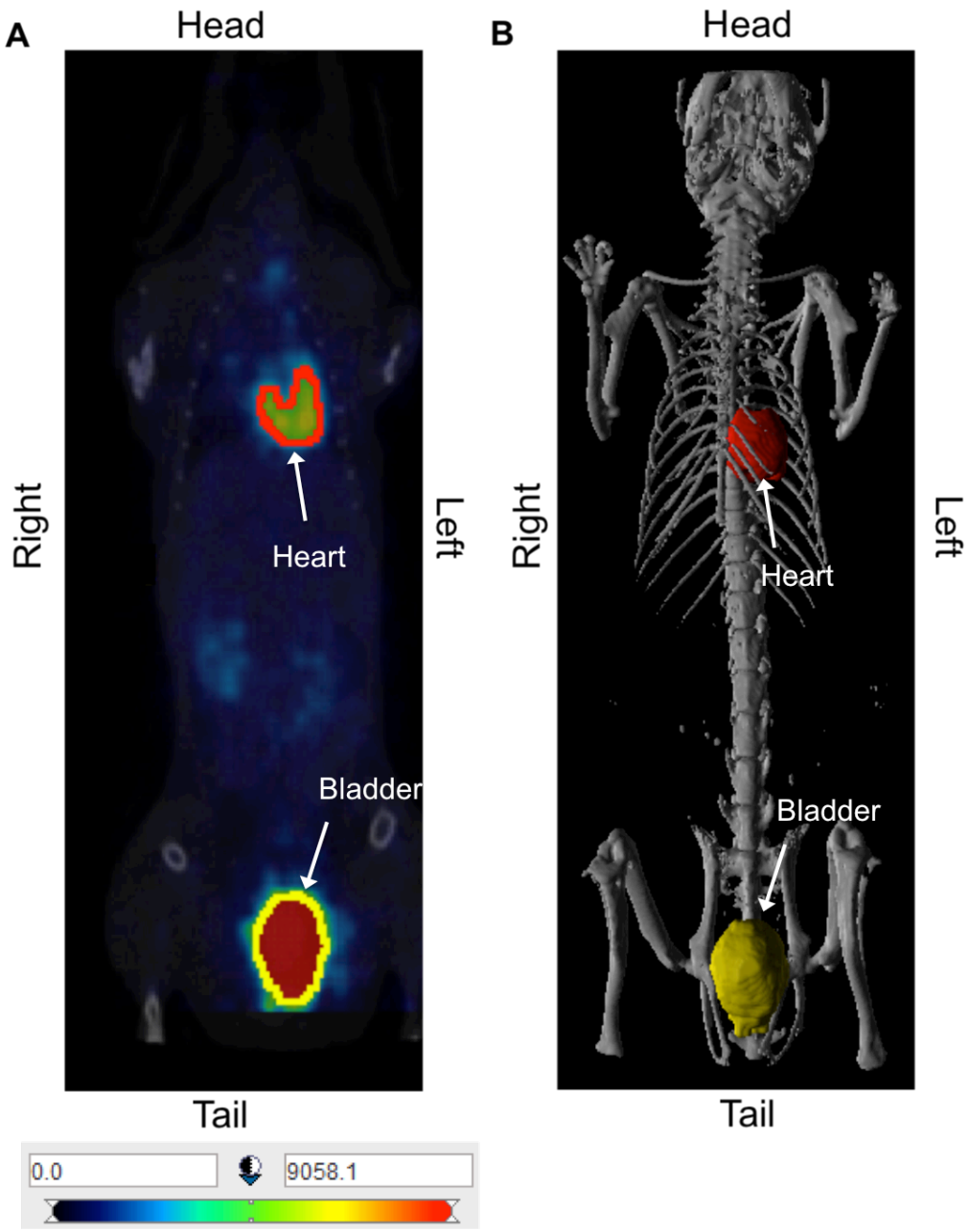

Figure 3.10| Administration of FDG via the tail vein gives a cleaner PET/CT scan than i.p administration. A 2D PET/CT image taken on the Gamma Medica Triumph II (A) and a 3D image created using Pmod (B) of a mouse injected i.v with approximately 10 MBq of FDG. The range of radioactivity seen in (A) is given in Bq/ml in the scale bar below the scan. ROIs are drawn around the bladder in yellow in (A) and solid yellow in (B), and the heart in red (A) and solid red (B).

3.3.2 Optimisation of respiratory gating

On the Mediso nanoScan PET/CT scanner, respiratory gating can be used to prevent the movement of the chest from obscuring the finer structures within the chest cavity. A breathing pad is placed under the mouse on the scanning bed that monitors the breathing rate in breaths per minute (bpm) and creates a trace as shown in Figure 3.11. The MC2B software gates around a complete breathing cycle (inhalation and exhalation) indicated by the white box in Figure 3.11 (i) and excludes data collected during this time [between points (ii) and (iii)] from the final reconstructed PET image, requiring scans to be run for longer. To enable use of respiratory gating, FDG uptake time was reduced to 30 minutes and PET scan time was increased to 60 minutes. A comparison of a respiratory-gated scan and a non-gated scan of the same mouse is shown in Figure 3.12. A reduction in the diameter of radioactivity around the heart was observed after respiratory gating, as shown by the measurements in Figure 3.12 (B). This allows for greater accuracy when drawing ROIs around the heart and the lungs. Therefore, respiratory gating was used on all subsequent PET scans.

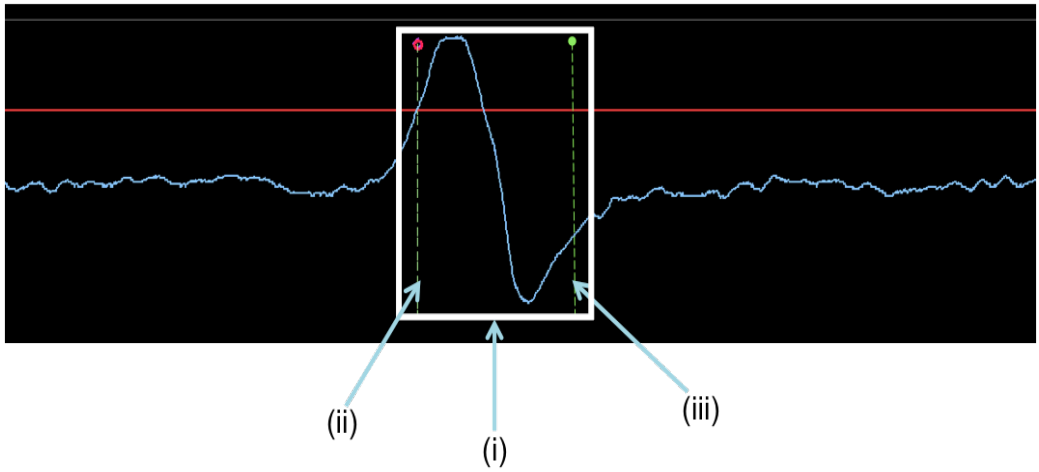

Figure 3.11| MC2B software monitors the breathing rate of the subject being scanned creating a trace. The blue line indicates the breathing trace picked up by the breathing pad placed underneath the subject and the white box at (i) indicates a full breathing cycle. A threshold is set by the red line that, when breached, triggers the MC2B software to begin measuring inhalation at (ii). A trigger delay can be set manually to signify the end of the breathing cycle shown at (iii).

A (i) No respiratory gating (ii) With respiratory gating

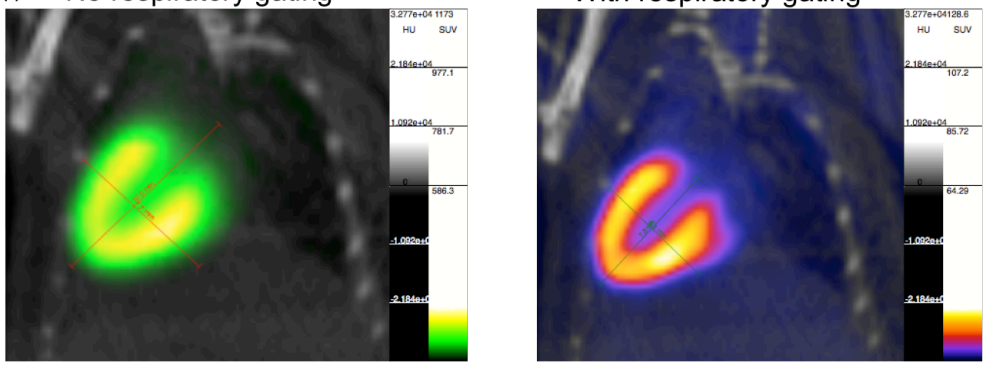

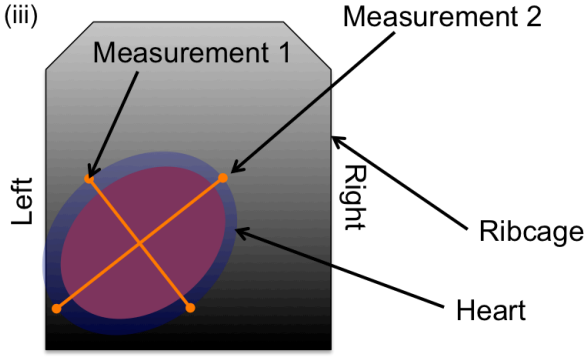

B

Gating	Measurement 1	Measurement 2
No Respiratory Gating	7.7mm	10.0mm
With Respiratory Gating	6.8mm	7.8mm

Figure 3.12| Respiratory gating creates cleaner images of the heart in PET/CT scanning. (A) Shows a PET/CT scan where the PET has been reconstructed with respiratory gating (i) and without respiratory gating (ii). Two perpendicular measurements have been taken across the highly radioactive region of the heart, a diagram of which is shown in (iii). The table in (B) details the two measurements taken across the heart in both the respiratory-gated reconstruction and non-gated reconstruction.

3.4 Results: Regions of interest can be drawn around areas thought to harbor metastasizing 4T1 tumour cells.

The possibility of using PET/CT imaging to monitor progression of tumour growth and metastasis was then investigated. In the case of the tumour used in this study, i.e. the 4T1 mammary carcinoma cell line that metastasizes to the lung, it was important that consistent and reliable ROIs could be drawn around the lungs. The possibility of using VivoQuant software (InviCro) to achieve this goal was examined. VivoQuant automatically imports data from both the PET and the CT images collected on the Nucline^{TM} software, then co-registers the reconstructed images and pre-processes the PET image data from Bq/ml to Standardised Uptake Value (SUV).

3.4.1 Drawing Lung ROIs

When looking solely at the PET image data the radioactivity is highest through the heart, as this organ has a high metabolic expenditure even under anaesthesia. Consequently, the lungs appear to have low or background radioactivity in comparison, creating difficulty when drawing lung ROI from PET data alone. However, there is a large contrast on the CT scan between the black empty air space of the lungs and the grey soft tissue of the heart. Therefore, the CT scan can be used to draw the lung ROI. This is done on VivoQuant by selecting the lightest and darkest points of the lungs on the CT to be set as the upper and lower thresholds within which the 3D

ROI is drawn. The PET image is then overlaid onto the CT image with the lung ROI allowing the SUV data to be calculated as shown in Figure 3.13.

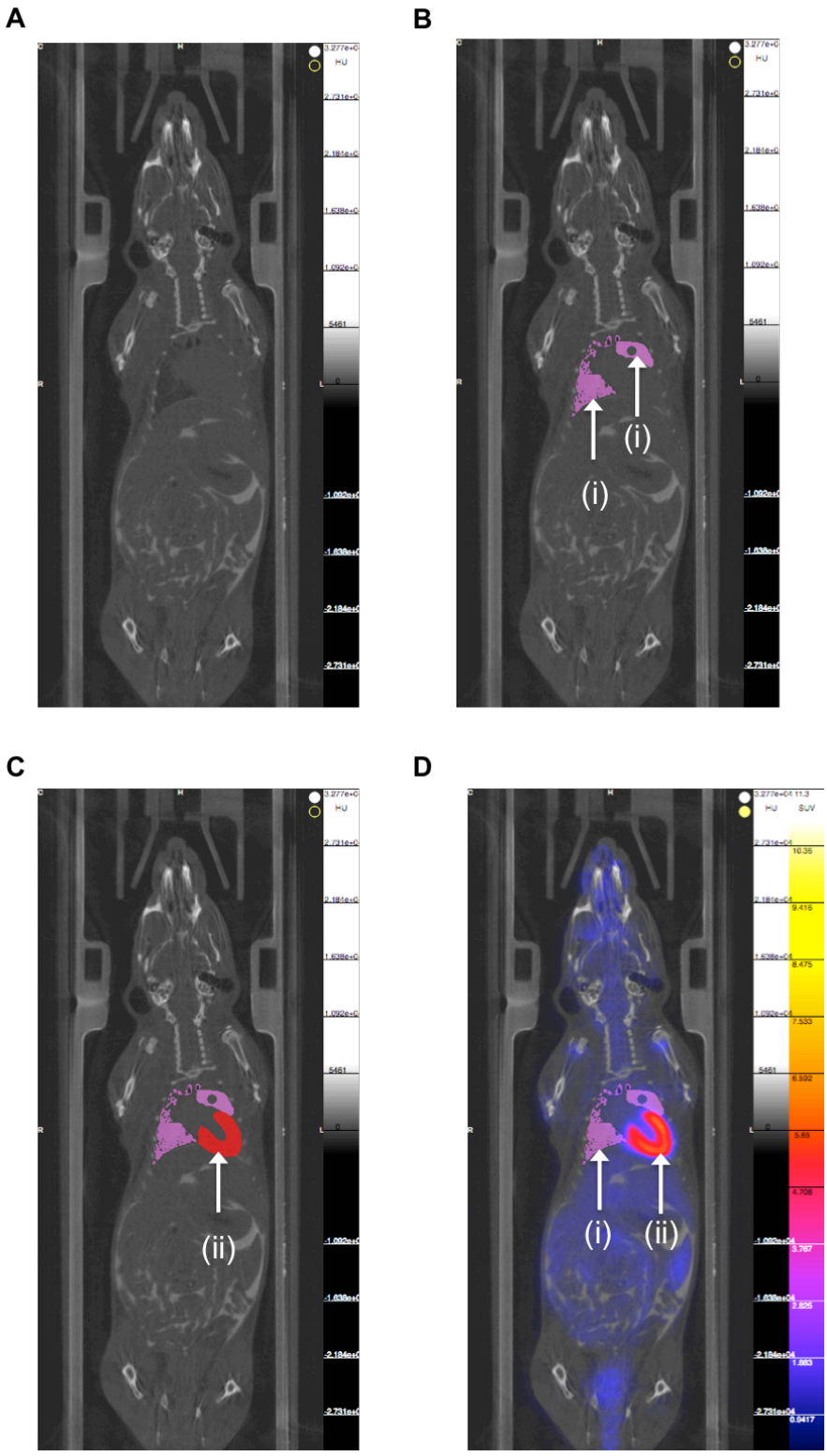

Figure 3.13| CT scans can be used to draw regions of interest (ROIs) in areas low in radioactivity. A set of example scans taken on the Mediso nanoScan of a mouse showing the stages of drawing lung ROIs. (A) Shows the CT scan without ROIs. (B) ROIs of the lungs were drawn with the connected thresholding tool on VivoQuant software; shown in lilac and indicated by a white arrow (i). (C) The heart ROI can be imported from the PET scan and imposed on the CT scan; shown in red and indicated by a white arrow (ii). (D) The lung ROI can be seen clearly when the PET is imposed on the CT scan and will measure values used in PET.

3.4.2 Drawing soft tissue ROIs

ROIs can also be used to exclude organs of high metabolic activity that do not harbor 4T1 metastasis from data analysis, such as the heart. The heart ROI is drawn on the PET image data by selecting the highest and lowest SUV values to be set as the upper and lower thresholds between which the ROI is drawn in 3D (Figure 3.14 and 3.15).

Excretory organs such as the bladder and the kidneys are also observed as areas of high radioactivity. These organs are very good indicators of FDG metabolism within the mouse. ROIs can be drawn around the kidneys and the bladder using the same technique as the heart and can be monitored over different scans.

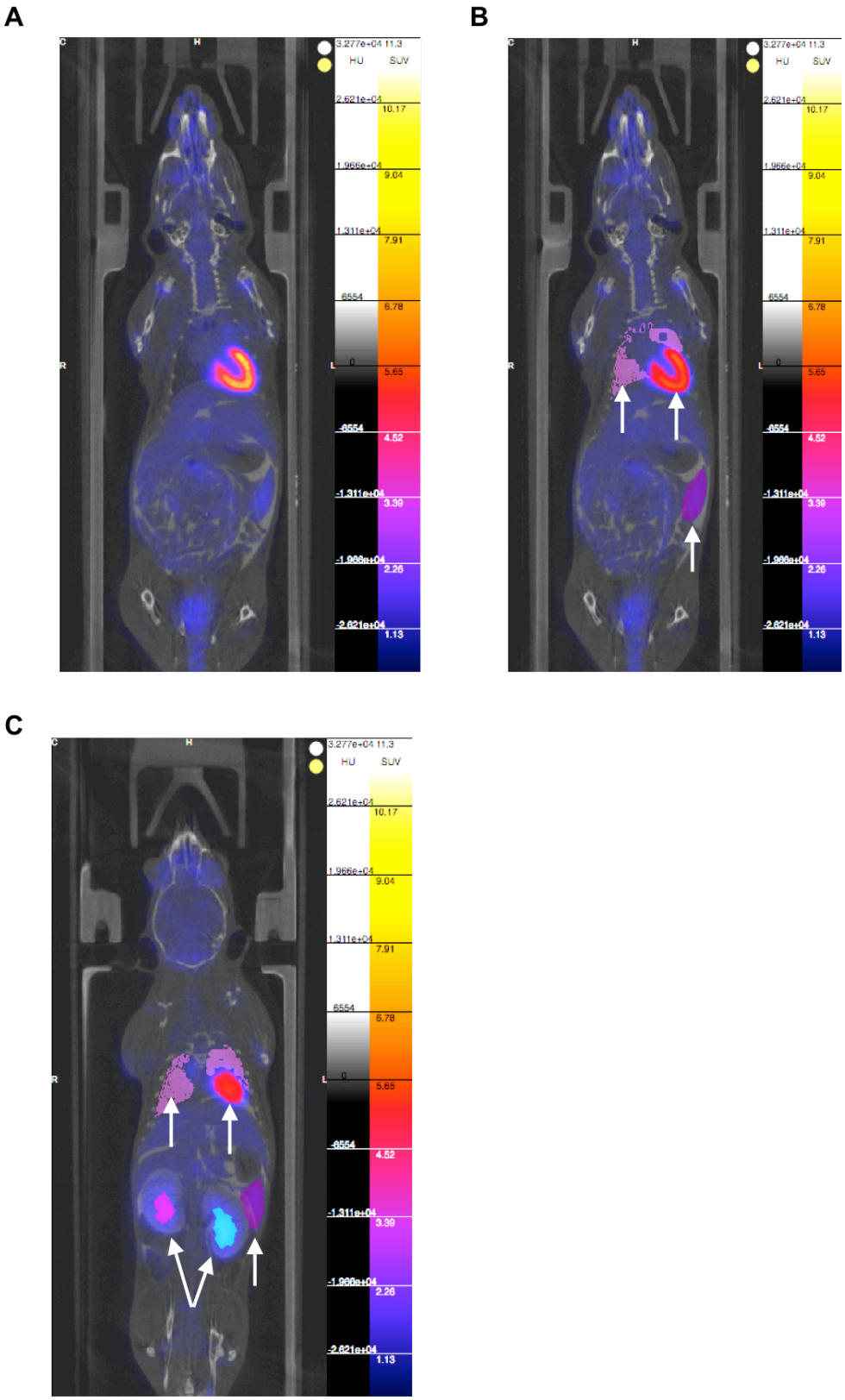

Figure 3.14| ROIs can be drawn on the PET data using the connected thresholding tool. Examples of a PET/CT scan taken on the Mediso nanoScan of a tumour-bearing Treg-replete mouse after drawing of ROIs. (A) Shows the original PET/CT scan with no ROIs drawn. (B) Shows the ROIs visible in the plane, all indicated by white arrows. The lungs are shown in lilac, the heart in red and the spleen in purple. (C) Shows the addition of the kidney ROIs in magenta and cyan.

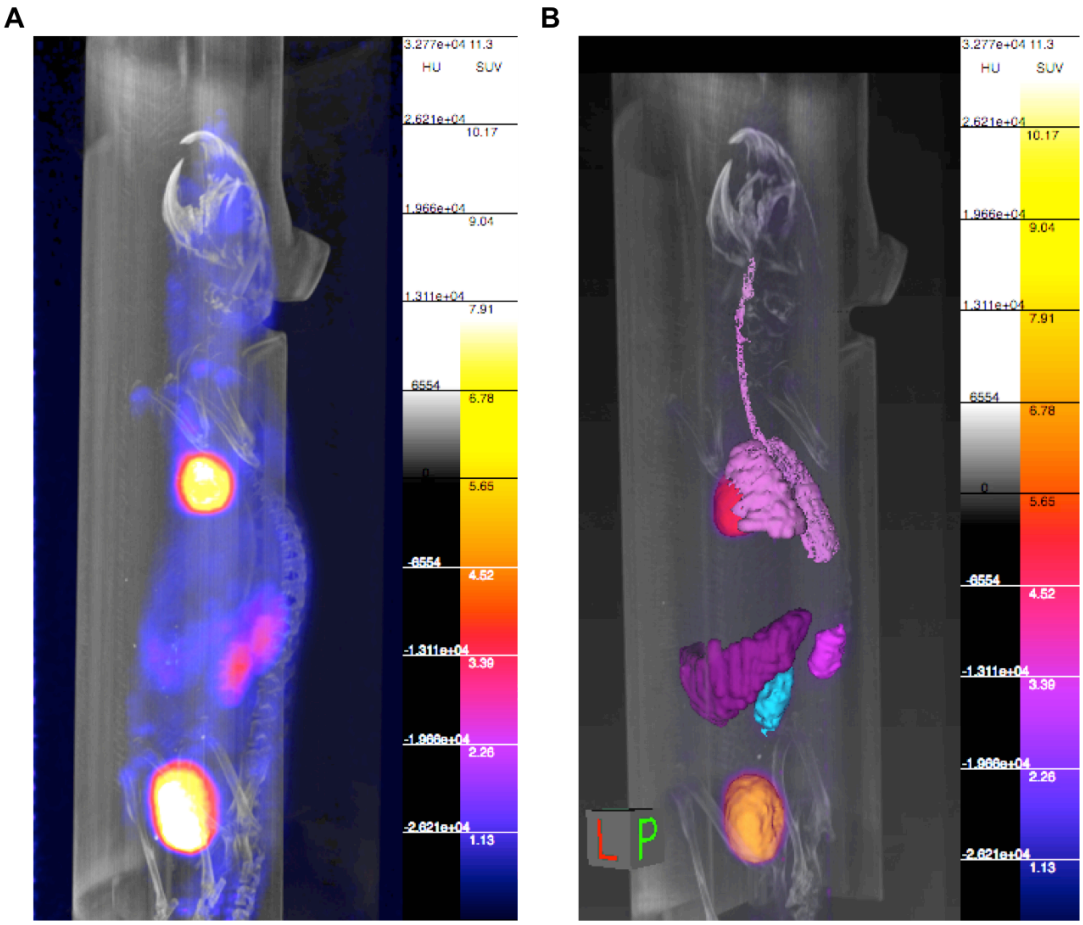

Figure 3.15| VivoQuant software can create 3D renderings of PET/CT data and ROI positions. (A) Shows a 3D Maximum Intensity Projection (MIP) image of the PET/CT image shown in Figure 3.15. (B) Shows the 3D rendering of the ROIs drawn in Figure 3.5 on a MIP image.

3.5 Results: PET/CT image data can be quantified in different ways

All PET/CT image data stems from the SUV, which is calculated using the equation detailed in Table 3.2. The SUV takes into account the animal's weight, the injected dose of radioactivity, the time of radioactivity administration and the time of the scan. In medicine, it is standard practice to use the maximum SUV measured in a ROI (SUVmax) when describing levels of radioactivity within a tissue. However, this is an inaccurate way of quantifying changes in radioactivity in mice. The resolution of PET images are the same in humans and in mice. Due to the obvious size difference between humans and mice a pixel in a mouse covers a larger area of tissue than in a human, meaning the SUVmax of a ROI has a higher chance of being an anomaly in a mouse because of its size. Therefore, SUVmax is a suboptimal way of analysing data collected from pre-clinical PET/CT scans.

Another method of PET analysis is the Hot Pixel Average (HPA), in which an average of the five "hottest" (most radioactive) pixels of a ROI is calculated. However, if the hottest pixel is an anomaly then the overall HPA increases.

Total Lesion Glycolysis (TLG) is the only measurement that takes into account the size of the ROI being analysed. A ROI TLG is calculated by multiplying the average SUV by the ROI area, showing the radioactivity uptake over the entire organ. The calculations and units of each of the three described parameters can be found in Table 3.2. Figure 3.16 shows the TLG of different ROIs of a tumour-bearing mouse. In this study the development of micrometastases in distant organs are being analysed, which as

described previously cannot be individually identified in PET/CT imaging. Therefore by looking at the changes in the TLG, the average SUV can be measured over time within a set area where metastasis is likely to occur. For all future scans, TLG was used to investigate metastasis progression.

Table 3.5| The calculations of different parameters for analysing PET data

Parameter	Calculation	Units of measurement
SUV	Image derived radioactivity concentration at t=0 / (Injected dose at t=0/body weight)	g/ml
SUVmax	The pixel with the highest value of SUV in a given area (ROI)	g/ml
Hot Pixel Average	The mean of the 5 pixels with the highest SUV in a given area (ROI)	g/ml
Total Lesion Glycolysis	Average SUV of the whole ROI X ROI volume	$g/ml*cm^3$

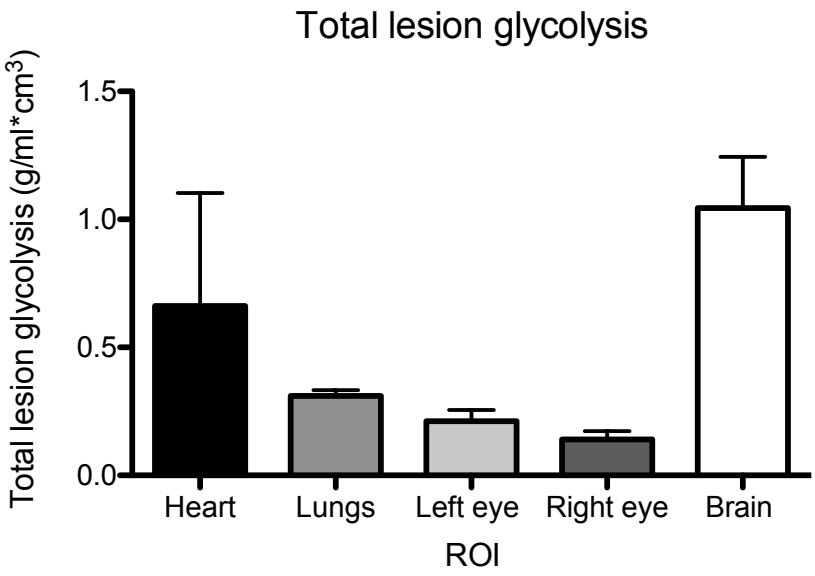

Figure 3.16| TLG is used to analyse PET/CT images. The graph shows the TLG of 5 different ROIs of a tumour-bearing female Balb/c mouse.

3.6 Results: Imaging 4T1 tumours and metastasis

3.6.1 Imaging primary 4T1 tumours

The protocols optimized for the Gamma Media Triumph II PET/CT/SPECT scanner and the Mediso nanoScan PET/CT scanner where subsequently used to image primary and metastasized 4T1 tumours. Mice were warmed in a heating box for at least one hour before Iohexol was administered both i.p and i.v as previously described. Ten MBq of FDG was administered i.v after induction of anaesthesia and a PET/CT scan was performed as before.

Large primary tumours were observed around the lower left abdominal quadrant on the PET/CT images, an example of which is shown in Figure 3.17. A 3D model of the mouse shows a lack of radioactivity uptake in the centre of the tumour, which is suggestive of necrosis.

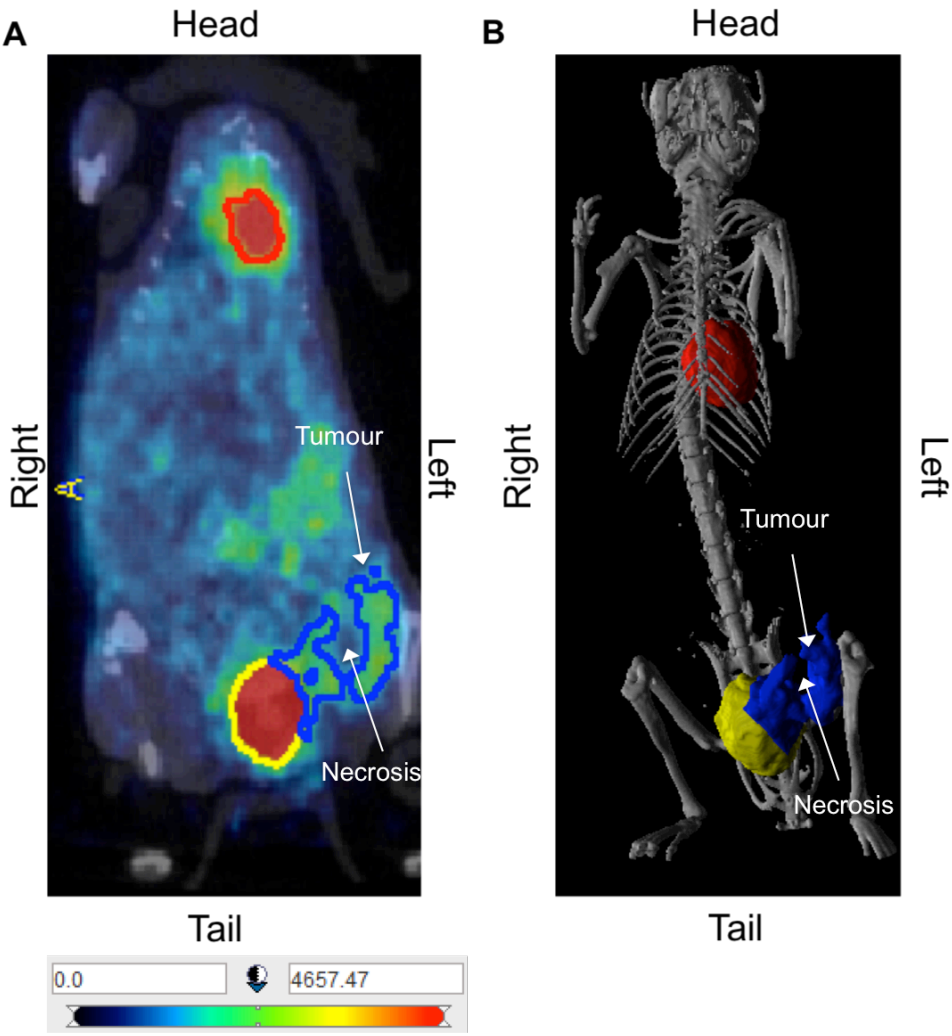

Figure 3.17| Solid primary tumours can be imaged using PET/CT. A 2D (A) and 3D (B) PET/CT image taken of a solid tumour bearing mouse using the Gamma Medica Triumph II scanner and analysed using Pmod software. The range of radioactivity in the scan shown in (A) is given in Bq/ml in the scale bar below the scan. ROIs are drawn on both images as an outline (A) or a solid volume (B). Bladder is drawn in yellow, heart in red and the primary tumour drawn in blue. A white arrow indicates the area of necrosis within the tumour.

3.6.2 Imaging 4T1 metastasis

In order to keep the area of the lung ROI constant allowing for a direct comparison of TLG between scans, the ROI drawn on the initial PET/CT scan was reoriented and transposed onto consecutive scans. An example of reorientation can be seen in Figure 3.18.

Metastasis progression was then monitored in mice after tumour resection. Three days after surgery, all mice were scanned following the optimized protocol for the nanoScan PET/CT scanner. Mice were scanned once a week for 3 weeks in total, with the initial scan taken as baseline. Three consecutive scans from a representative mouse are shown in Figure 3.19 with ROIs drawn around the lungs, heart, kidneys and bladder. The TLG of the lungs was measured over all three scans and a progressive increase was observed. Upon sacrifice of the mouse there were no large tumour nodules, however the clonogenic assay revealed micrometastases (examined in more detail in Chapter 4). This suggests that the increase in TLG seen over 3 weeks within the lungs could be due to the progression of 4T1 metastasis.

In some cases, metastatic nodules form on the lungs and the ribcage in the later stages of metastasis, examples of which can be found in Figure 3.20. These appear in later scans, and using VivoQuant software can be reoriented and transposed onto previous scans in the same way as lung ROI. Figure 3.20 shows the increase in TLG over time from metastatic nodule.

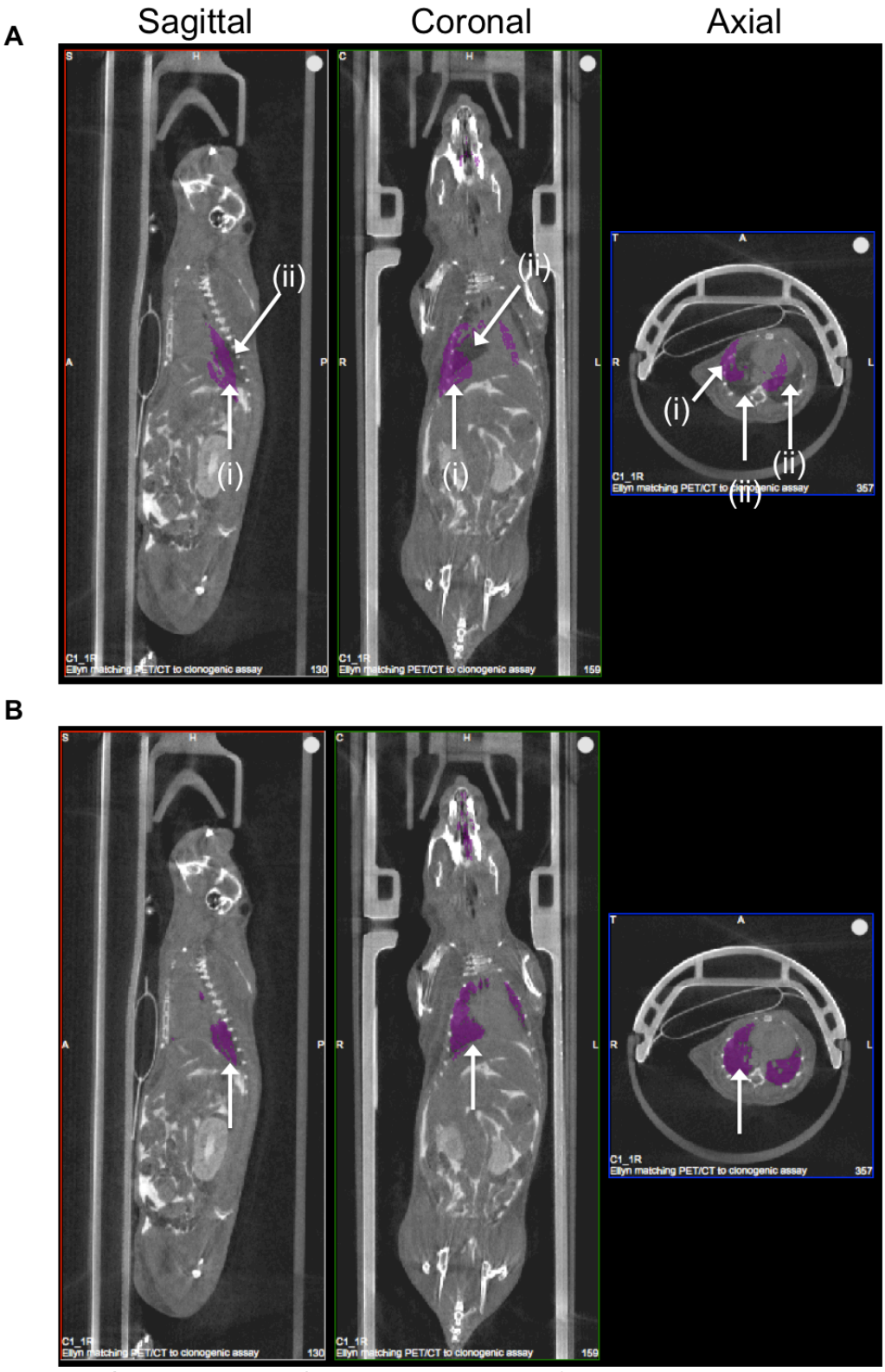

Figure 3.18| Baseline lung ROI can be reoriented to fit lung area on proceeding scans. Second CT scan of a mouse scanned on the Mediso nanoScan 14 days after the baseline scan shown in the sagittal, coronal and axial plane. (A) CT scan with the baseline lung ROI (i) imposed onto the image, where the darker air space is shown at (ii). (B) The lung ROI shown by a white arrow reoriented to fit the air space of the lungs shown in (A).

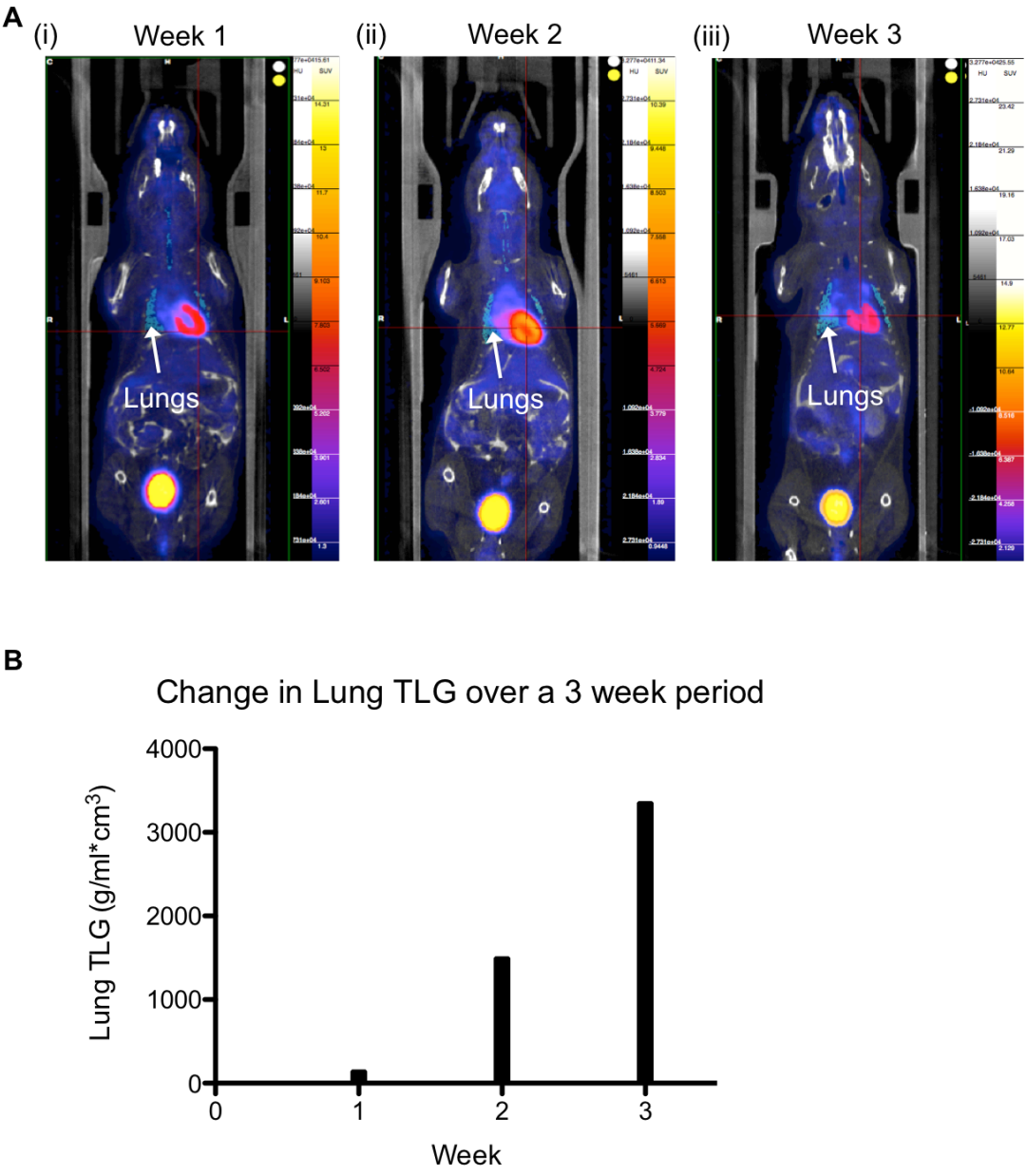

Figure 3.19| Changes in TLG can be observed in the lung ROI of a Treg-replete metastasis-bearing mouse. A single Treg-replete metastasis-bearing mouse was scanned using the Mediso nanoScan on the same day each week for 3 weeks. Each of the scans are shown in (A) week 1 (i), week 2 (ii) and week 3 (iii). The lung ROI (drawn in light sea green and indicated by a white arrow) was drawn on the scan shown in (A) (i) and then reoriented onto images (ii) and (iii). (B) Shows the TLG of the lung ROI in each scan.

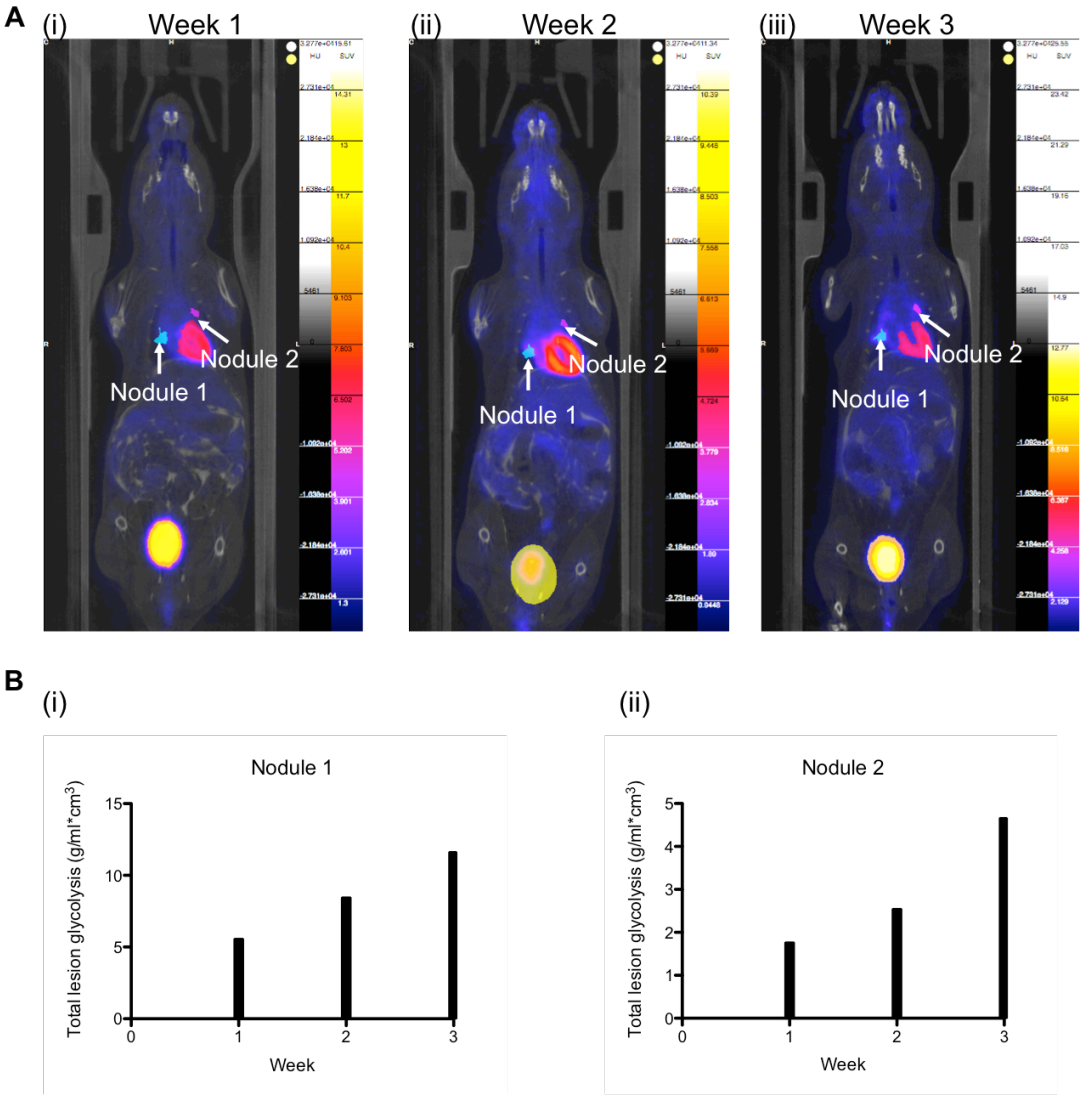

Figure 3.20| Metastatic nodules appearing on later scans can be retrospectively transposed onto previous scans to monitor changes in TLG. A Treg-replete metastasis bearing DEREG mouse was scanned once a week for 3 weeks. (A) PET/CT data was analysed on VivoQuant software and ROIs drawn around nodule 1 (cyan) and nodule 2 (magenta) on the final scan (iii) were retrospectively transposed onto scans from week 1 and 2 [(i) and (ii) respectively]. (B) The TLG was calculated for nodule 1 (i) and nodule 2 (ii) on each scan.

3.7 Discussion

PET/CT imaging has been used since the 1990's for clinical diagnosis of cancer and metastasis, and therefore had a potential to be applied to preclinical metastasis studies (Kinahan et al. 1998; Townsend et al. 1993). The changing of PET/CT scanners mid- project hindered the optimisation of PET/CT imaging for this purpose in our lab. However, the Mediso nanoScan PET/CT scanner was found to be superior to the Gamma Medica Triumph II PET/CT/SPECT scanner, along with the upgrade in analysis software.

Through altering CT scan parameters, it was possible to achieve a high quality CT scan displaying differentiation between soft tissues and smaller structures within the chest cavity. In order to achieve this, it was shown that CT scans should be performed with 70 KVp X-ray energy, 720 projections and 1:1 binning. Along with i.p and i.v administration of Iohexol, this protocol created CT images with a high resolution and contrast definition between soft tissues.

When using increased X-ray KVp and projection number during a CT scan, the subject receives a higher radiation dose of approximately 13.5 cGy. This raises the possibility of biological effects occurring as a result of the increased radiation. It is widely accepted that high doses ionizing radiation can create DNA mutations with a potential to cause cancer. Interestingly, studies have shown that small doses of ionizing radiation (in the region of 1.2-100 mGy) have a conditioning effect on mice, thereby reducing the distinct biological effects of high dose radiation (1-2 Gy) on DNA (Nenoi et al. 2015). Conversely, targeted high dose radiation can be used to treat some tumours. The radiation doses used for radiation therapy

are in the region of 20Gy (McGinnis et al. 2016), whereas the radiation dose received during a CT scan using the optimized protocol is more than 100 fold lower. Therefore, the radiation dose received by mice during CT scanning is not high enough to cause detrimental effects to DNA. However, to further decrease the risk of ionizing radiation, the Field Of View (FOV) of the CT is increased to encapsulate the entire subject. This allows the radiation to be spread across the subject rather than being focused on a single area.

The progression of metastasis was measured through drawing ROIs around organs potentially harboring 4T1 cells. It was shown that it is possible to draw ROIs on the CT scan or the PET scan using different contouring tools on VivoQuant software. As the lungs are the first place 4T1 cells generally seed during metastasis it was important to keep this ROI constant throughout scans. By using the lung ROI drawn on the baseline scan and reorienting it to fit the subsequent scans, it was therefore possible to measure the change in TLG of the same area over time. The opposite was done with ROIs that appear in the later scans, in that they could be superimposed onto earlier scans and the change in TLG was measured over time. This is important for lymphoid organs such as the spleen and the LNs as they show an increase in metabolic activity during Treg depletion (discussed further in Chapter 4), and in the later stages of metastasis it has been shown using the clonogenic assay that 4T1 cell colonies are present in inguinal LNs.

The best parameter to measure the progression of metastasis is TLG in comparison to the SUVmax, a standard clinical practice for measuring

ROIs on a PET/CT scan, and the HPA. Both of these parameters have a higher risk of anomaly due to the size of the subject being scanned, and while the SUVmax and HPA look at the highest level of radioactivity within a ROI, only the TLG takes into account its area.

Through optimisation of PET/CT scanning and image analysis, it was possible to visualise solid primary tumours and large metastatic nodules found in the lungs and ribcage. In addition, through utilizing the lung ROI from the baseline scan, it was possible to measure the change in TLG over time, where an increase in TLG is indicative of metastasis.

PET/CT imaging is not without its limitations. FDG PET/CT imaging is not specific to cancer cells, as shown by the high levels of radioactivity seen in organs such as the heart, kidneys and bladder. While the location of large solid tumours within a mouse is clear, micro-metastases cannot be identified through their increase in glycolytic activity with such clarity. The radiolabelling of specific antibodies has proven to be a promising area, with human HER2 antibodies being investigated for use in imaging cancer in mice (Denis-Bacelar et al. 2016). However, as 4T1 is a triple negative breast cancer cell line it is not possible to use 4T1-specific radiolabelled antibodies to image metastasis.

In conclusion, the techniques described in this chapter have demonstrated successful optimisation of PET/CT imaging using both the Gamma Medica Triumph II PET/CT/SPECT scanner and the Mediso nanoScan PET/CT scanner. This technique was therefore be used to measure the progression of metastasis in Treg-depleted and Treg-replete mice after primary tumour resection, described in Chapter 4.

Chapter Four

4 Results: Investigating the effects of Treg depletion on the growth of a primary tumour and the progression of metastasis

4.1 Introduction

Regulatory T cells (Tregs) are a subset of $CD4^+$ cells that also express Foxp3 and CD25 (Sakaguchi et al. 1995). Tregs have a suppressive phenotype and play a major role in maintaining peripheral tolerance. Loss of Tregs leads to fatal autoimmune and inflammatory disorders in humans and in mice (Brunkow et al. 2001; Lahl et al. 2007). While Tregs are important in maintaining immune homeostasis, they have also been implicated in suppressing anti-tumour immune responses, whereby recruitment of Tregs to the tumour site provides an immune-suppressive niche preventing immune-mediated clearance of the tumour (Gallimore and Sakaguchi 2002). In humans, studies have shown an enrichment of Tregs in certain tumours such as ovarian, breast, pancreatic and lung, and their presence is generally correlated with a bad prognosis (Cheng et al. 2016; Hanagiri et al. 2013; Knutson et al. 2015; Xu et al. 2010). Previously, studies in mice have shown that the ablation of Tregs in mice leads to the control of primary tumour growth, although this effect has not been investigated in the context of metastasis, which remains the main cause of fatality amongst cancer patients (North 1982; North and Awwad 1990).

DEREG mice expressing DTR on their Tregs can be used to investigate the depletion of Tregs on the progression of metastasis. The

triple negative murine breast cancer model 4T1 metastasizes spontaneously from a primary tumour in the same manner as human stage IV breast cancer (discussed in Chapter 1 Section 1.5) and is therefore a robust model to investigate development of metastasis. The resistance of 4T1 to 6-thioguanine can be exploited to detect metastatic colonies in distant organs as described in Chapter 1.

In vivo imaging can also be used to image tumour progression in 4T1-bearing mice. PET/CT exploits the Warburg principle of increased glycolytic activity of tumour cells (Warburg 1956) by measuring the uptake of a radioactive glucose analogue F^{18}-Fluorodeoxyglucose (FDG) by different tissues. The optimisation of this technique for analysis of metastasis was described in Chapter 3.

Few studies have examined the effect of Treg depletion on the progression of triple negative breast cancer metastasis in a resection model. Therefore, experiments described in this Chapter aimed to investigate the effect of Treg depletion on the growth of a primary 4T1 tumour and on the progression of metastasis. This investigation was undertaken using 2 methods of metastasis analysis: the clonogenic assay and PET/CT imaging. The experiments tested the hypothesis that depletion of Tregs controls the growth of a primary tumour and limits the progression of metastasis.

4.2 Results: Depletion of Regulatory T cells can be achieved in DEREG positive mice through administration of diphtheria toxin

In order to determine the efficiency of Treg depletion of DTx in the DEREG mice, two doses of DTx were compared. Female naïve DEREG mice were left untreated or treated with 10 µg/kg or 5 µg/kg DTx injected i.p on day 0. Upon sacrifice on day 2, spleens and LNs were harvested from the mice and cells were stained for CD4, Foxp3, CD25 and GFP as shown in Figure 4.1. A Wild Type (WT) Balb/c mouse was injected with 100 µl PBS for comparison in which no depletion of Tregs was observed as expected. Interestingly, only 85% of the $CD4^+$ $Foxp3^+$ cells in untreated DEREG mice expressed GFP (Figure 4.2C). This could be explained by gene silencing of the BAC, indicating that not all $Foxp3^+$ cells can be depleted via DTR. A significant depletion of Tregs is achieved however, using both doses of DTx. Therefore, to avoid adverse effects, the lowest effective dose of 5 µg/kg was used in all subsequent experiments.

The remaining 15% of Foxp3 positive cells that do not express the DTR and are therefore refractory to depletion by DTx, expand to eventually repopulate the Treg pool (Figure 4.3). This expansion of DTR^- Tregs in DEREG mice has previously been shown to confer protection against systemic autoimmunity that is observed in DTR knock-in mice after prolonged DTx treatment (Mayer et al. 2014b). Interestingly, an expansion of GFP^+ DTR^+ Tregs was also observed in mice after 3 weeks of DTx treatment, showing development of resistance to DTx by DEREG mice.

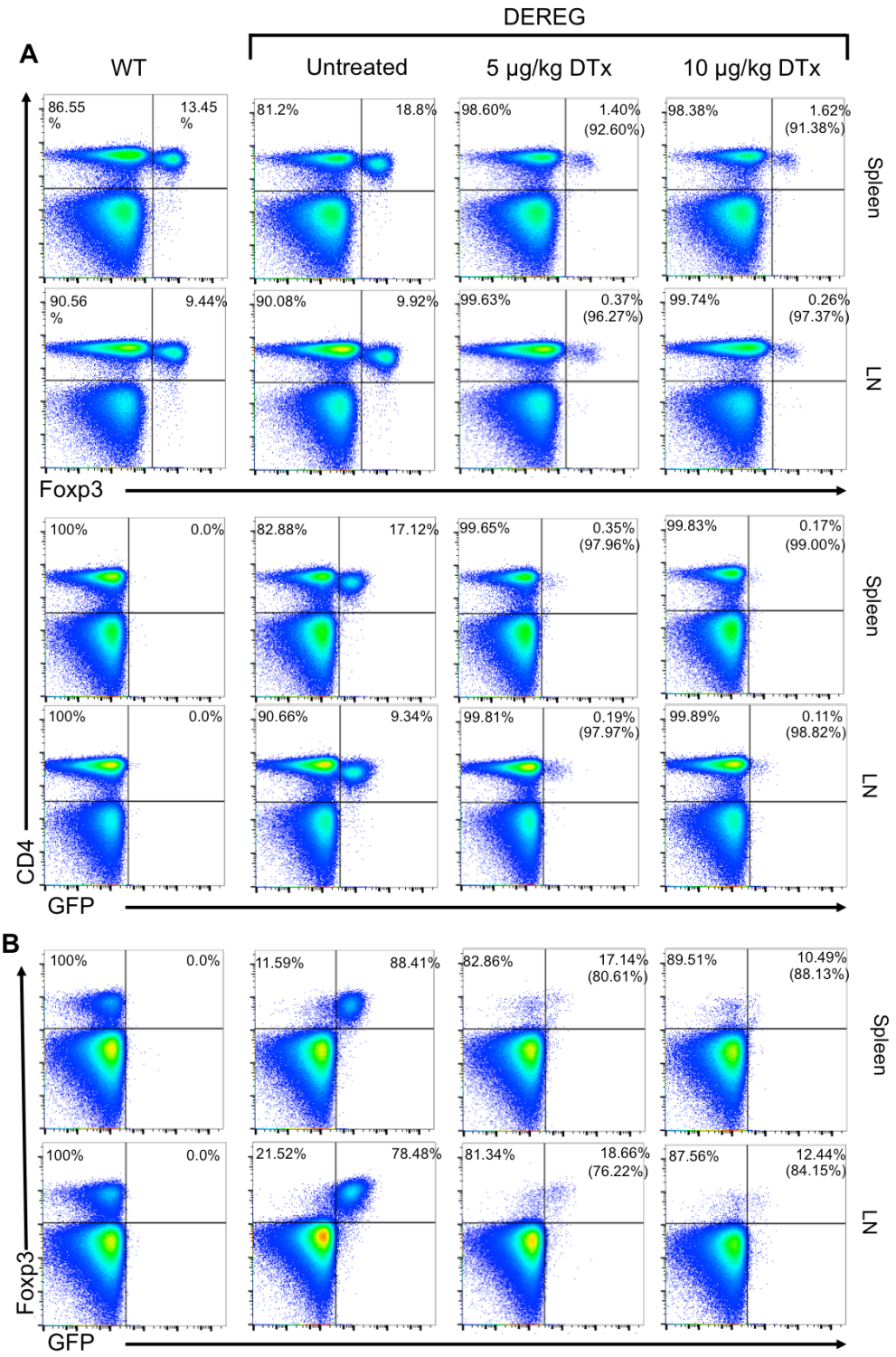

Figure 4.2| Injection of DTx causes successful depletion of Tregs in DEREG mice. DEREG mice were left untreated (n=2) or treated with either 5 µg/kg (n=2) or 10 µg/kg (n=2) of DTx to deplete Tregs. Two days later, cells from spleens and inguinal LNs stained for CD4, Foxp3, and GFP fluorescence was detected on the FITC channel. Lymphocyte populations were gated as described in Chapter 2. (A) $CD4^+Foxp3^+$ or $CD4^+GFP^+$ cells as a percentage of the total $CD4^+$ population (top right quadrant), and percentage depletion of cells after DTx treatment is shown in brackets. (B) $Foxp3^+GFP^+$ cells as a percentage of total $Foxp3^+$ population (top right quadrant), with the percentage depletion of cells after DTx treatment in brackets.

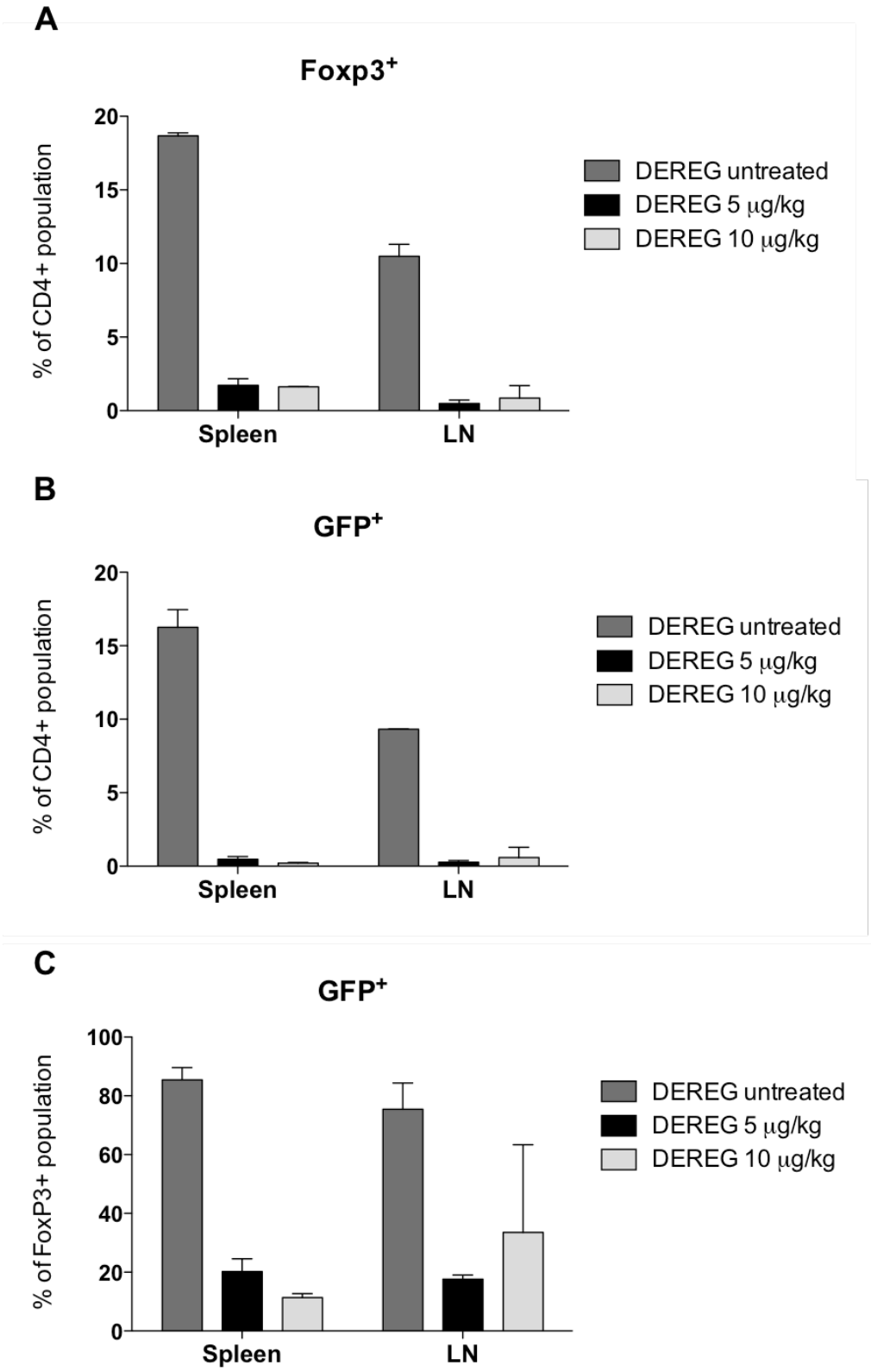

Figure 4.3| Injection of DTx causes successful depletion of Tregs in DEREG mice. All data shown are averages of n=2 from figure 4.1 (A) Shows the proportion of $Foxp3^+$ cells as a percentage of $CD4^+$ cells in an untreated DEREG mouse and DEREG mice given 5 μg/kg or 10 μg/kg DTx. (B) Shows the proportion of GFP^+ cells as a percentage of $CD4^+$ cells in the same mice and (C) shows the proportion of GFP^+ cells as a percentage of $Foxp3^+$ cells.

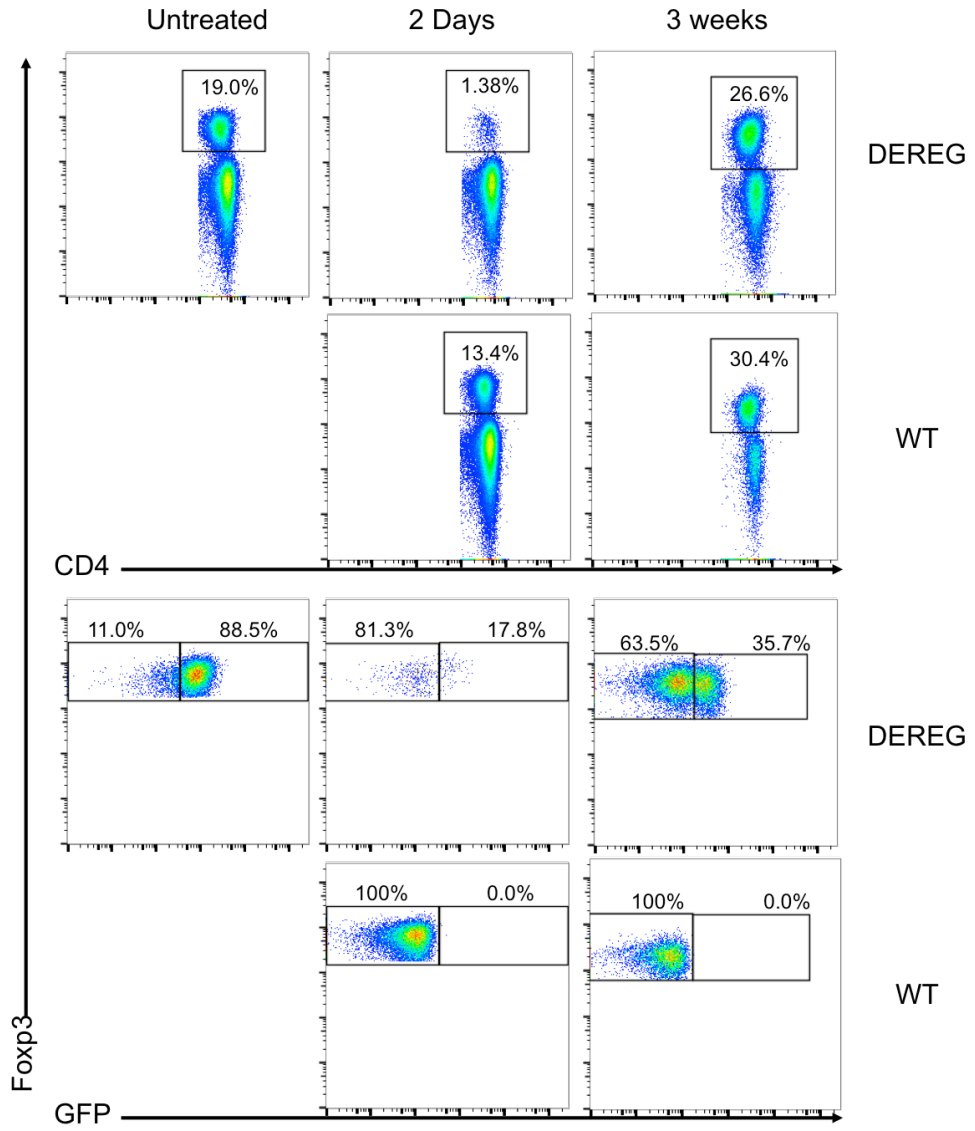

Figure 4.4| Restoration of Tregs after 3 weeks of DTx treatment. WT and DEREG mice were sacrificed 2 days [(n=2)(n=2) respectively] or 3 weeks [(n=1)(n=4) respectively] post DTx treatment. Cells from spleens and LNs were stained for CD4, Foxp3 and GFP. Examples of a WT Balb/c mouse, a DEREG mouse treated with 5 μg/kg DTx, and an untreated DEREG mouse are shown above. The top panel shows the $Foxp3^{+}CD4^{+}$ cell populations and the bottom panel shows the $GFP^{+}CD4^{+}$ cell population of the same mice. Percentages show the gated population as a percentage of the CD4 population.

4.3 Results: Using the clonogenic assay to quantify 4T1 metastasis

Metastatic colonies were assessed using the clonogenic assay as described in Chapter 2 and outlined in Figure 4.4. In order to demonstrate the reliability of this technique, mice bearing 4T1 tumours were sacrificed and the lungs, liver, draining LN, and brain were harvested for analysis of metastases. Once the cell suspensions had been prepared as previously described, samples were plated and incubated with 6-TG media for 14 days. Metastatic colonies were observed in the lungs and in some of the draining LNs, however no metastases were found in the brain or the liver. This was not unexpected however, as brain metastases occur in the later stages of the disease (Pulaski and Ostrand-Rosenberg 2000). As the lungs are the first sites of metastasis in the 4T1 model, clonogenic assay analyses of these organs gave the best indication of metastasis control. Therefore, the lungs were the main focus for metastasis experiments. In some cases, lungs would show metastatic tumour nodules that would result in a densely packed clonogenic assay plate. In this circumstance the plate was split into quarters, and one quadrant was counted and then multiplied by 4 in order to calculate the total number of metastatic colonies on the plate. Examples of positive metastasis and negative metastasis plates can be seen in Figure 4.5.

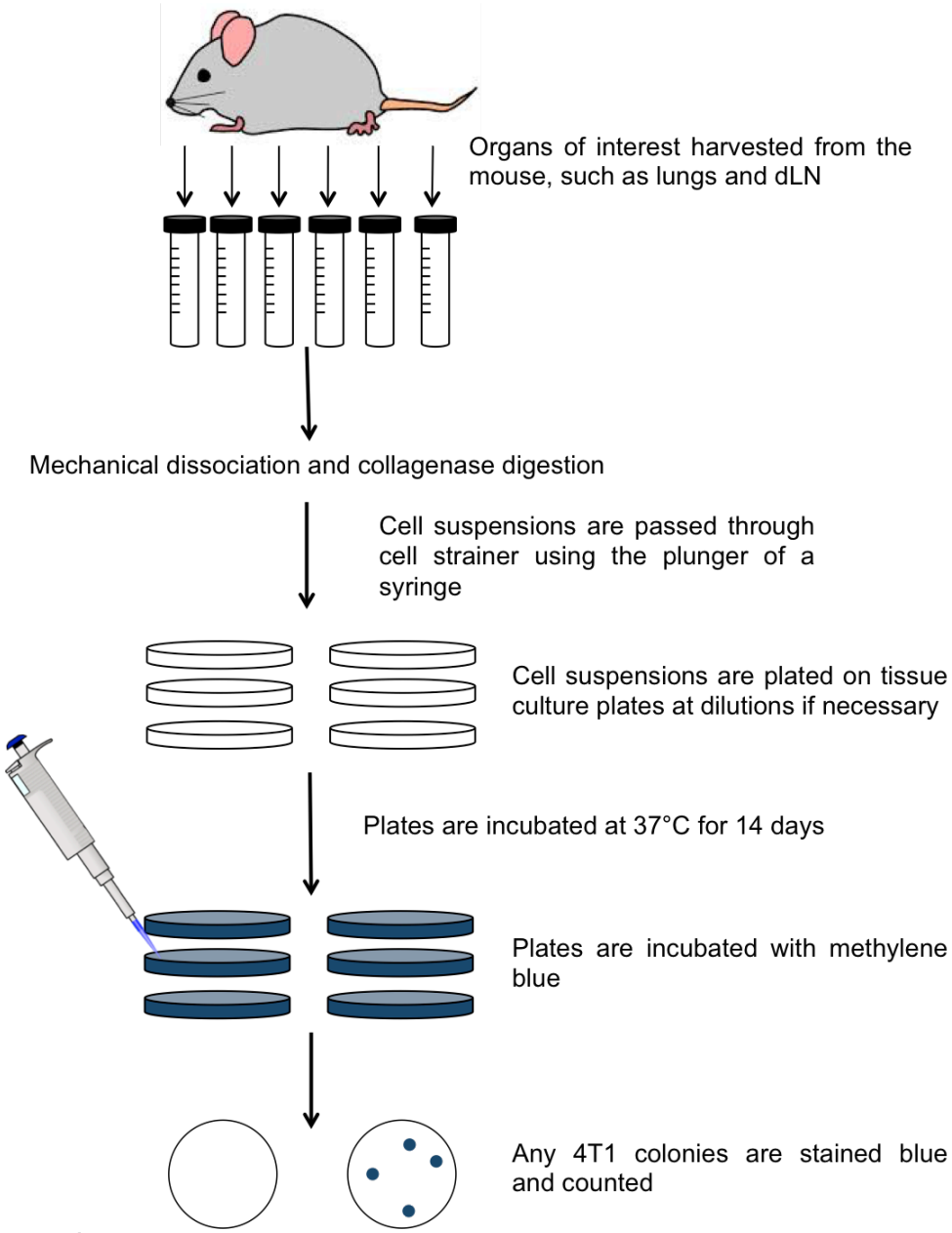

Figure 4.4| The clonogenic assay is used to detect micrometastases in distant organs of tumour bearing mice. This figure shows the process of the clonogenic assay, resulting in blue 4T1 colonies on a tissue culture plate that are subsequently counted. Each blue colony represents 1 metastatic cell.

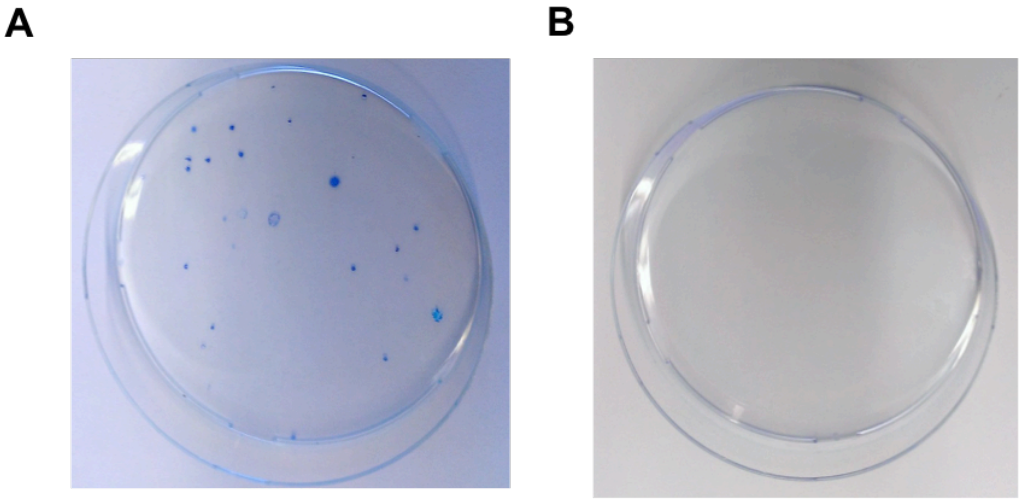

Figure 4.5| 4T1 metastatic colonies are stained blue. (A) Shows a positive clonogenic assay plate with blue 4T1 colonies. (B) Shows a negative clonogenic assay plate without any 4T1 colonies.

4.4 Results: Depletion of Tregs cannot control metastasis induced through intravenous injection of tumour cells

Some studies have investigated control of lung metastasis established through i.v administration of tumour cells. Using this method, tumour cells locate to the lungs immediately therefore establishing metastatic disease independently of a primary tumour. Bos *et al.* have shown the growth of the breast cancer cell line PyMT in the lungs after i.v administration can be controlled through depletion of Tregs (Bos et al. 2013).

To determine whether this was also the case in the 4T1 model, lung metastasis after i.v administration of the cells was assessed. Eighteen mice were split into 2 groups that received either $5x10^5$ or $1x10^5$ 4T1 cells injected i.v on day 0 in order to establish the number of cells required for tumour take. Three mice from each group were harvested on day 7, day 10 and day 14, and lungs, liver, and inguinal LNs were harvested for clonogenic assay analysis [Figure 4.6 (A)]. The mice that received $5x10^5$ cells became sicker in a shorter period of time with only 1 mouse surviving to day 14. All mice receiving $1x10^5$ cells survived. Analysis of lung clonogenic assay plates exhibited almost complete covering with 4T1 metastatic colonies, with further colonies being found in the liver (Figure 4.7). Histological samples of lungs bearing 4T1 metastatic nodules indicated almost complete occlusion of the lungs as a result of tumour growth (Figure 4.8).

In order to prevent development of respiratory distress in mice as a result of overloading of lungs with 4T1 metastatic cells, the number of cells injected i.v was reduced to $1x10^4$ per mouse. DEREG positive mice and DEREG negative littermate controls were injected i.v with the revised

number of cells on day 0 and were subsequently treated every other day with 5 μg/kg DTx from day 7 until sacrifice on day 17 (Figure 4.6 B)

Clonogenic assay analysis was performed on the lungs upon sacrifice, revealing no significant difference in the number of metastatic 4T1 colonies observed in Treg-depleted and Treg-replete mice, as shown in Figure 4.9. This could be due to the sheer numbers of cells establishing metastatic niches in the lungs. Due to the systemic dissemination of 4T1 tumour cells and their preferential localization to the lung, a potential anti-tumour immune response may possibly be unable to clear the tumour burden before health deterioration of the mouse due to its rapid growth. Fewer cells arriving at the lungs via spontaneous metastasis from a primary tumour may present different challenges to the immune system than the large number of cells arriving in the lungs through i.v administration, and may not overwhelm the lungs in the same manner. Therefore, the effect of Treg depletion on metastasis was then investigated on spontaneous metastasis occurring from a primary tumour.

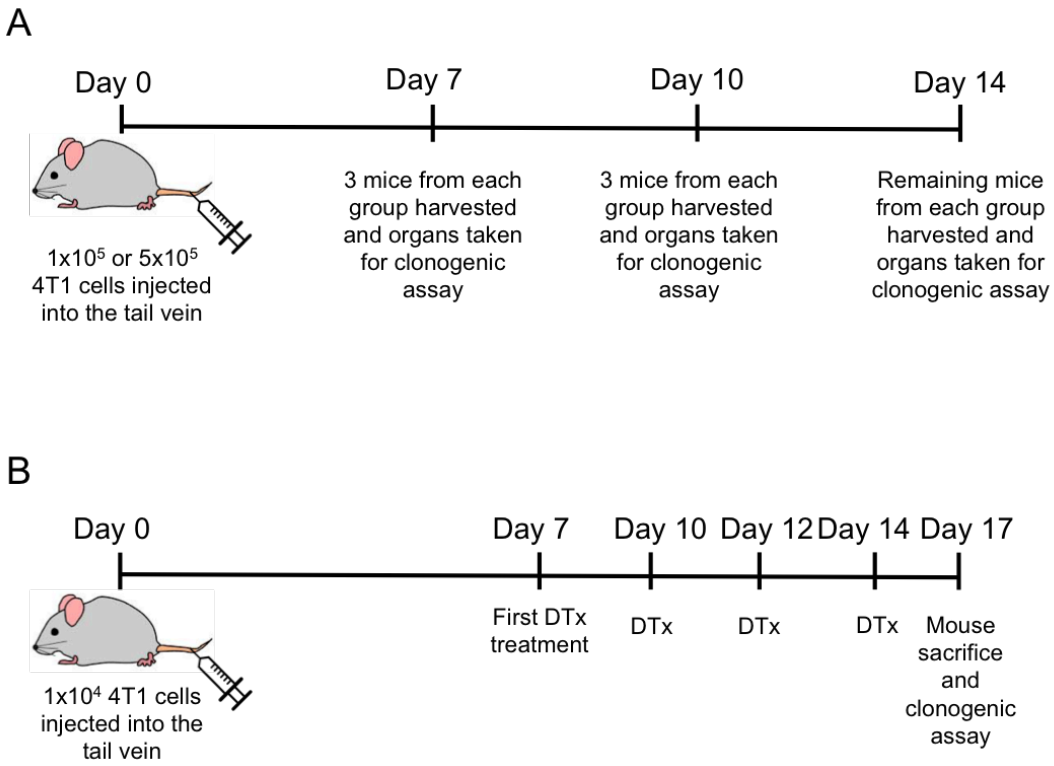

Figure 4.6| Investigating the effect of Treg depletion on a tail vein model of metastasis. (A) Shows the experimental timeline used to measure the establishment of lung metastasis after tail vein injection of 4T1 cells. (B) Shows the experimental timelines investigating the effect of Treg depletion on the development of metastasis from tail vein inoculation of 4T1 cells.

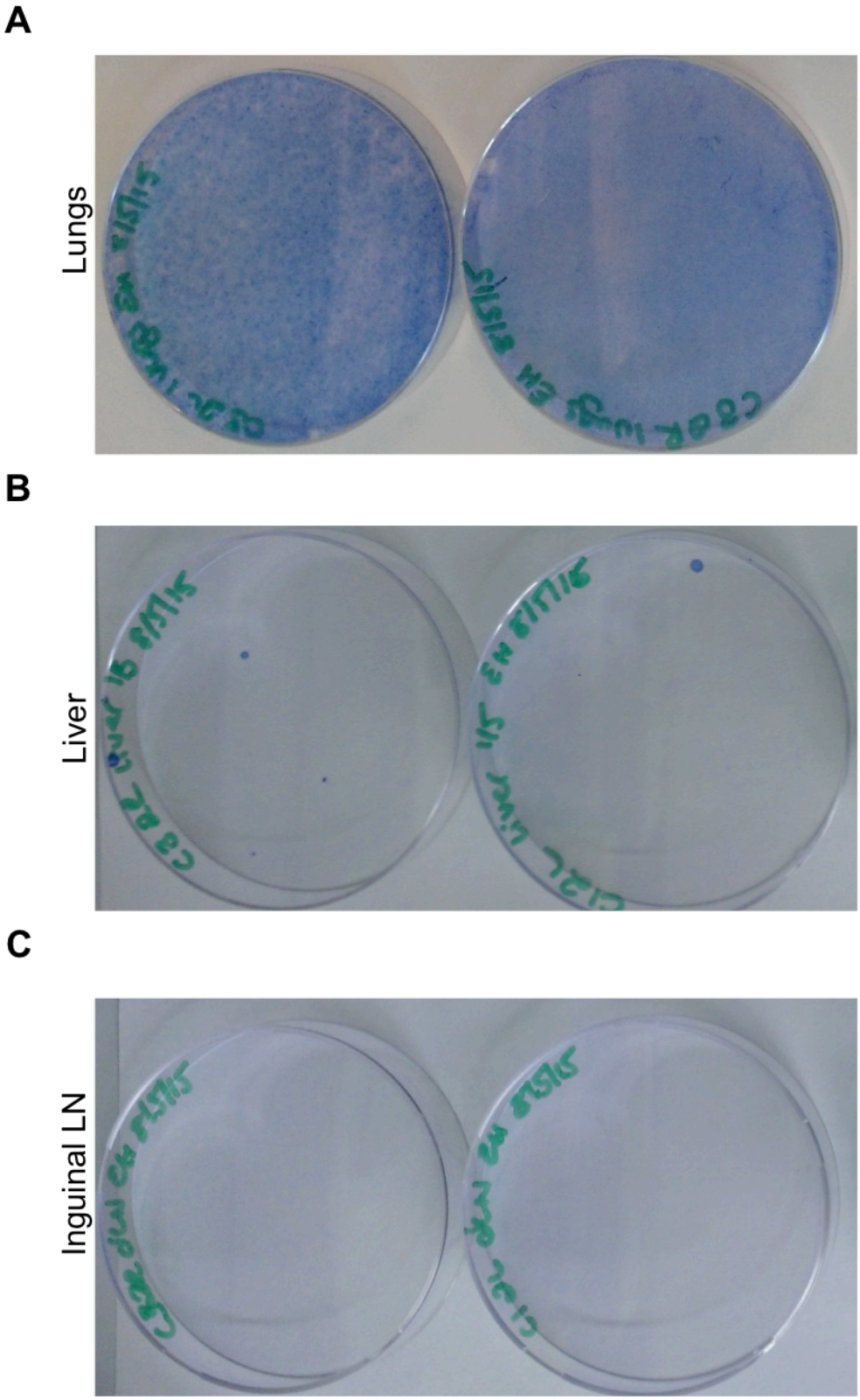

Figure 4.7 | 4T1 metastases are found in different organs after tail vein administration than from a s.c tumour. Examples of clonogenic assay plates showing metastasis in the lungs (A), the liver (B), and the inguinal LN (C) from mice with tail vein induced metastasis.

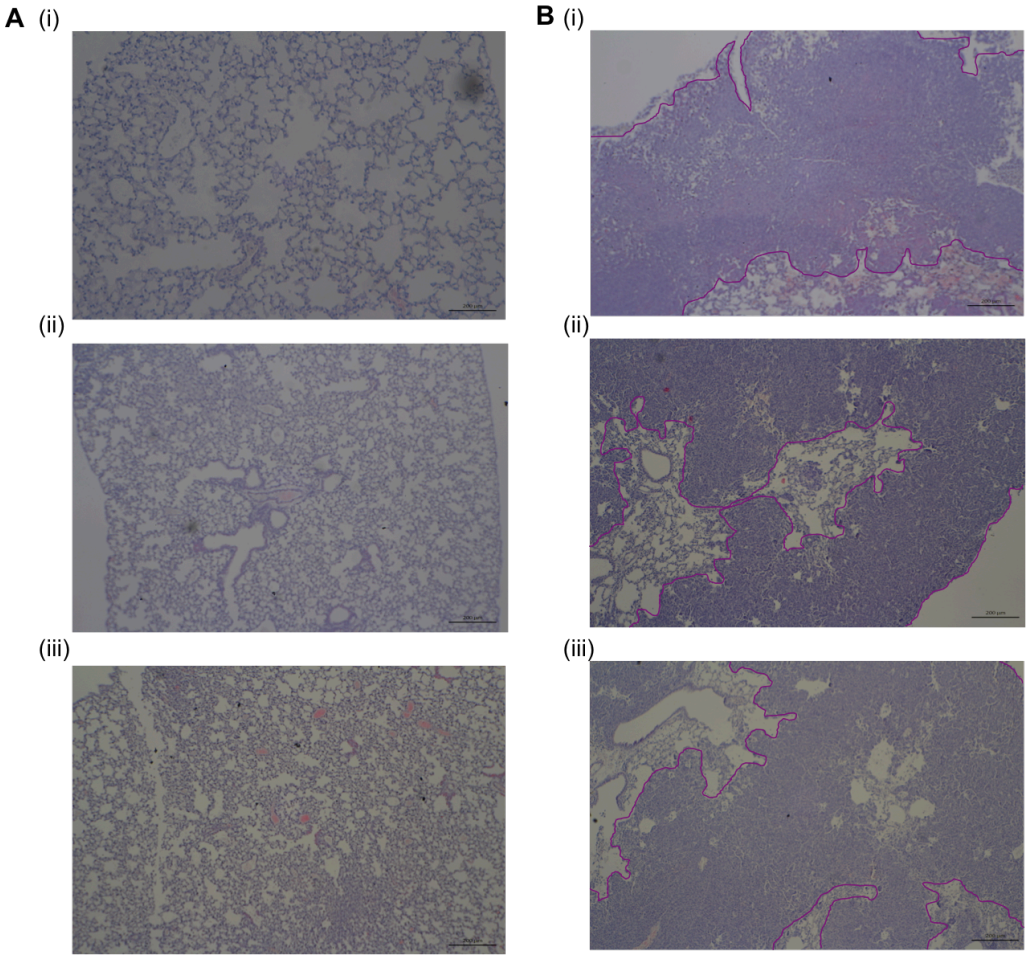

Figure 4.8 | Tail vein induced metastasis cause occlusion of the lungs. Examples of Haematoxylin and Eosin (H&E) staining of lungs from naïve healthy mice (A) compared to lungs of mice that have tail vein induced metastasis after injection of $1x10^5$ 4T1 cells (B). Tumour areas are identified by purple lines in (B).

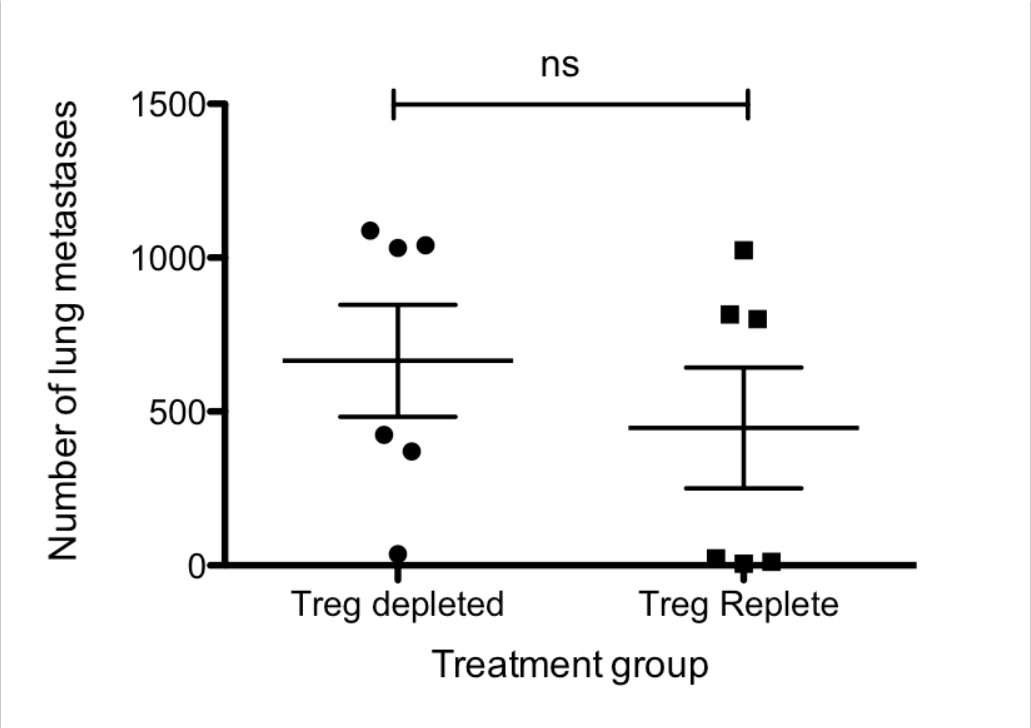

Figure 4.9| Treg depletion does not control the progression of metastasis of tail vein induced metastasis. The number of lung metastases detected using the clonogenic assay in Treg-depleted and Treg-replete mice injected i.v with $1x10^4$ 4T1 cells. An unpaired t-test was performed giving a p value of p=0.4338

4.5 Results: Treg depletion causes regression of a primary tumour

In order to analyse the growth of 4T1 tumours, mice were injected subcutaneously with $1x10^5$ 4T1 cells close to the mammary fat pads. 4T1 cells were first palpable on day 5 after injection and were large enough to begin measuring on day 7. Tumours were measured up to 3 times a week using digital calipers, taking two perpendicular measurements across the tumour. 4T1 tumours grew in 100% of injected mice, and all tumours grew uniformly until sacrifice (Figure 4.10). Due to rapid tumour growth, small necrotic areas prone to scabbing and ulceration were often observed in the centre of the tumour. Mice were checked every other day for development of necrosis and were sacrificed if a crater-like appearance or discharge was observed.

Previous studies have shown that the immune response induced as a result of Treg depletion can control the growth of a primary tumour in mice (Hindley et al. 2012). To assess this in the context of the 4T1 model, 6-8 week-old DEREG positive mice and their negative littermate controls were injected s.c with 4T1 cells on day 0. When the tumours were first palpable on day 5, mice were injected i.p with 5 μg/kg of DTx every other day until sacrifice on day 21; the full experimental timeline can be found in Figure 4.11 (A). Tumours were measured 3 times a week, at the same time as DTx was administered. Tumour growth curves are shown in Figure 4.11 (B). 4T1 tumours in Treg-replete mice grew uniformly as before, whereas 4T1 tumours in Treg-depleted mice began to regress after day 10, with some tumours demonstrating complete regression. Not only does this recapitulate

the findings seen in other studies, but this also shows that the initial depletion of Tregs and resulting expansion of effector T cells is enough to initiate an anti-tumour immune response even though Tregs begin to expand and return to normal levels after 3 weeks of depletion. Therefore, it was hypothesised that metastasis occurring spontaneously from a primary tumour could be controlled through Treg depletion in the same manner as the primary tumour growth.

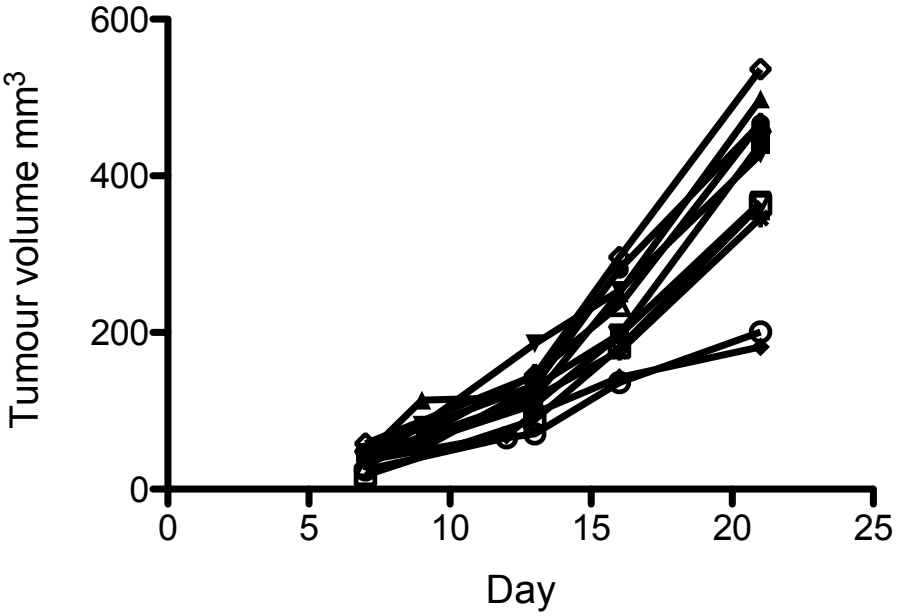

Figure 4.10| 4T1 tumours grow uniformly in WT Balb/c mice. Female 6-8 week old female Balb/c mice were injected subcutaneously with $1x10^5$ 4T1 cells on day 0 and developing primary tumours were measured from day 7 over a 3-week period. The graph shows the volume of the 4T1 tumours over time.

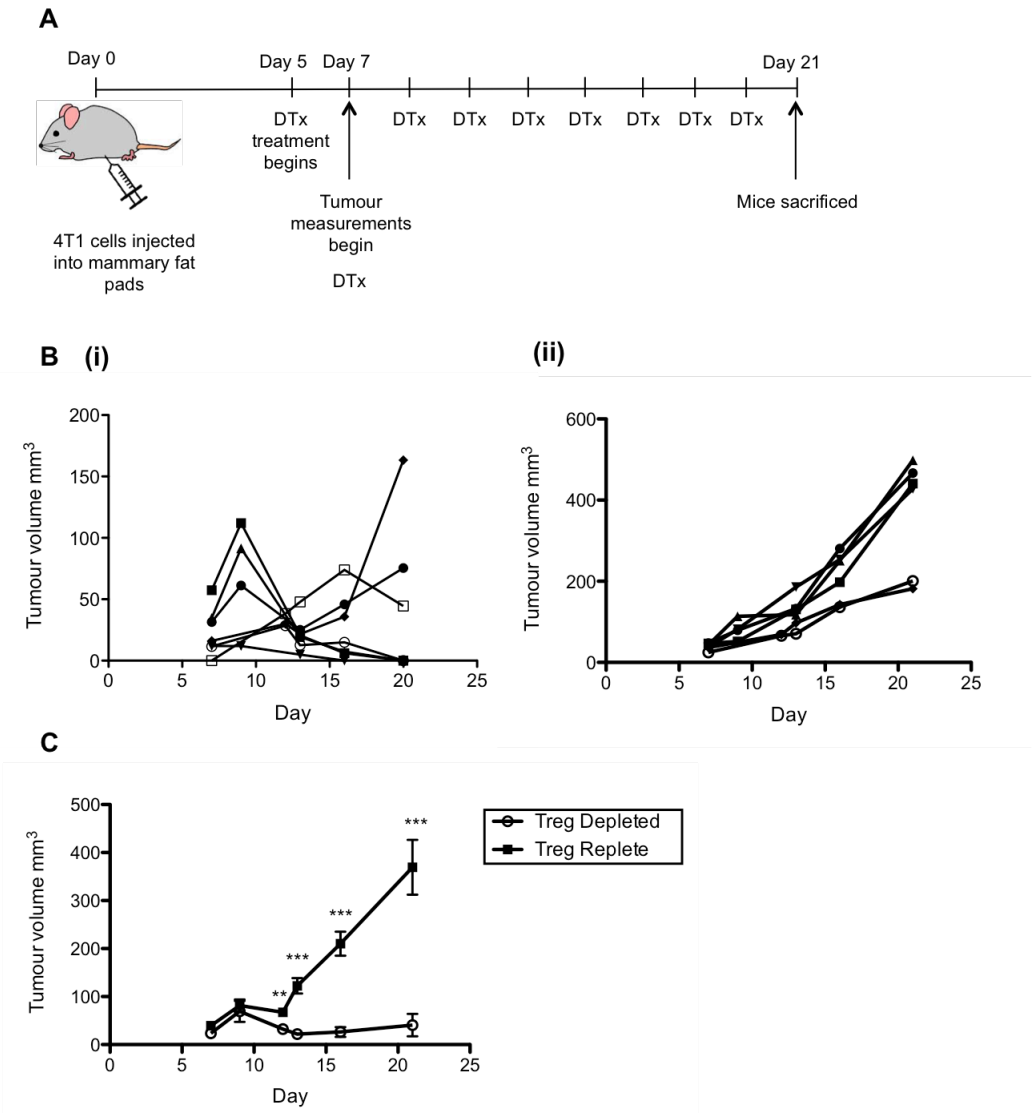

Figure 4.11| Depletion of Tregs can control the growth of a primary tumour. (A) Shows the experimental timeline of the experiment investigating the effect of Treg depletion on a primary tumour. The graphs in (B) show the tumour volume over time of (i) Treg-depleted mice and (ii) Treg-replete mice. (C) Shows the average tumour volumes over time of Treg-depleted and Treg-replete mice. The statistical analysis in (C) is an unpaired two-tailed t test at each time point, giving the following values: day 12 p=0.0034, day 13 p=<0.0001, day 16 p=<0.0001, and day 21 p=0.0002.

4.6 Results: Relationship between 4T1 metastasis and the size of the primary tumour

In clinical cases of mammary carcinoma, it is standard practice to resect a primary tumour as long as it is operable. In this study therefore, to analyse metastasis in a clinically relevant setting, 4T1-bearing mice underwent surgery to resect their primary tumours. This technique also serves to improve the welfare of the animals. Resecting the primary tumour prevents infection and ulceration of the necrotic area, while also ensuring the primary tumour does not become so large as to hinder the movement of the mouse.

In order to successfully analyse the control of metastasis conferred through Treg depletion, it was necessary to establish at what point metastasis occurred and thus at what point to resect the primary tumour. To do this, Balb/c mice were injected s.c with $1x10^5$ 4T1 cells as before and resulting primary tumours were resected at varying tumour volumes. Mice were then left for a maximum of 14 days after resection before sacrifice, at which point the lungs were taken for analysis of metastatic burden using the clonogenic assay. Whilst primary tumour volume and numbers of lung nodules were not significantly associated, replotting the data as shown in Figure 4.12 indicates that to achieve metastatic tumours in > 80% of mice, primary tumours should be over 125 mm^3 in volume or 5 mm in diameter. It is important to note that not all tumour-bearing mice go on to develop detectable metastatic disease and some mice develop more metastatic colonies than others. Therefore, the primary tumours were resected once both perpendicular measurements had crossed the lower threshold. This

gave a high chance of metastasis at the time of resection, but also meant the tumour was small enough to prevent the development of necrotic ulceration and to lower the risk of reduced mobility of the mice.

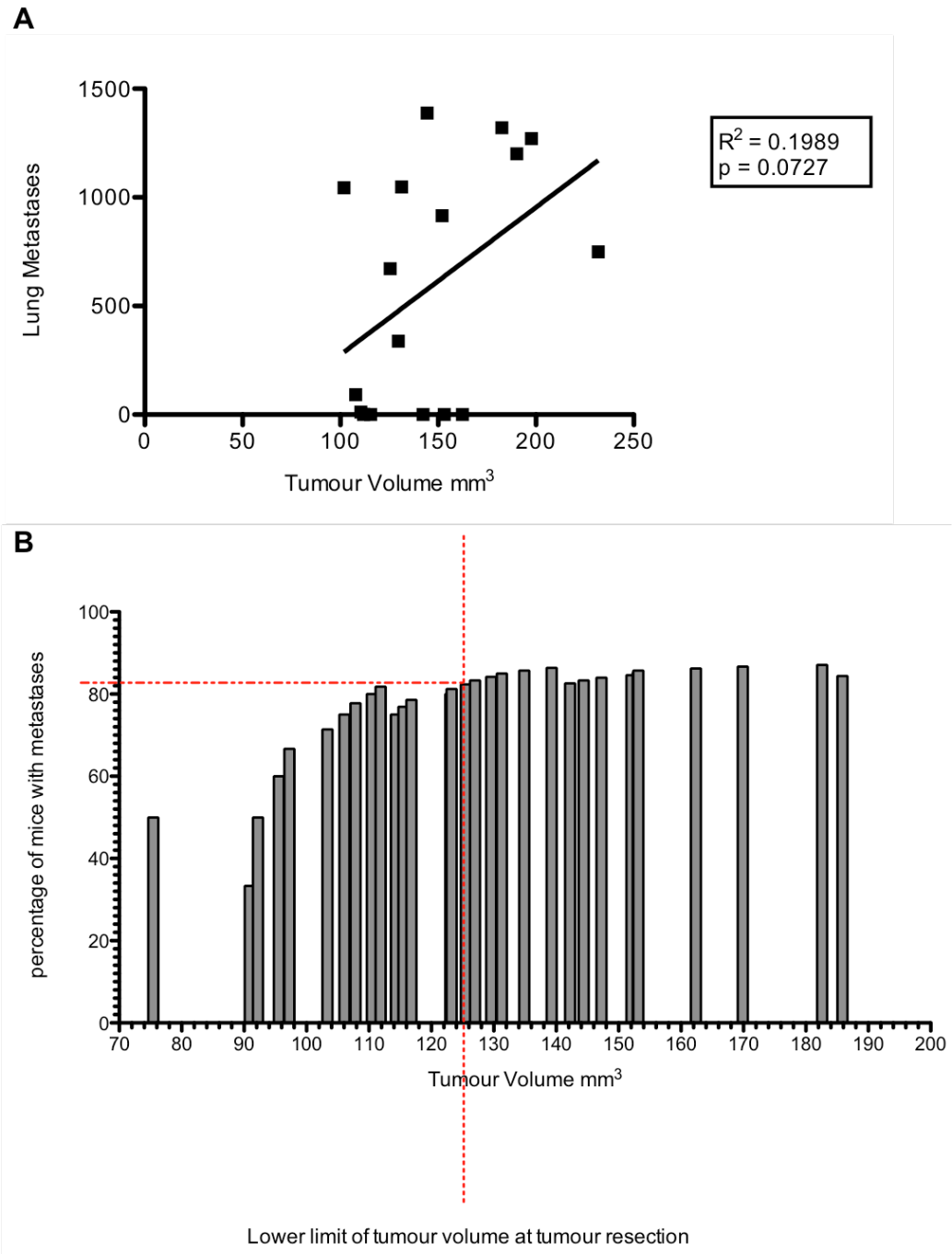

Figure 4.12| 4T1 metastasis development and it's relationship to tumour volume at the point of resection. 4T1 tumour-bearing mice underwent surgery to resect primary tumours at different volumes, and were sacrificed 10 days later. Lungs were harvested and metastatic burden was analysed using the clonogenic assay. (A) Shows the number of lung metastases in mice when tumours were resected at different volumes. (B) Shows the percentage of mice with ≥1 metastatic colony when tumours were resected at different tumour volumes. Linear regression was performed on the data set and the R^2 and p values are given in the box to the right of the graph. The dotted red line indicates the lower threshold for the tumour volume at the time of resection.

4.7 Results: Treg depletion can promote control of metastatic disease

Once the time point of tumour resection had been established, it was necessary to investigate the effect of depleting Tregs before and after resection on the progression of metastasis. In a pilot experiment, 10 female 6-10 week old DEREG mice were split into 3 groups and injected s.c with $1x10^5$ 4T1 cells. Each of the 3 groups then underwent a different treatment plan described in Figure 4.13. Briefly, mice in group 1 (Treatment before surgery – TS) were given 2 rounds of DTx treatment before the primary tumour was resected on day 14. Group 2 (Surgery before Treatment - ST) and group 3 (No Treatment - NT) were treated with DTx or PBS respectively 24 hours after tumour resection. Mice in all groups then received treatment every other day until sacrifice on day 24, when the lungs were harvested and taken for clonogenic assay. Primary tumour growth was measured in each treatment group, and the average tumour growth can be found in Figure 4.14(A). It was observed that in the T-S group tumour growth was slower than in the other two groups and did not reach 125 mm^3 in volume at the time of resection. Upon sacrifice on day 24, lungs were taken for clonogenic assay analysis. Significantly fewer metastatic colonies were observed in mice treated with DTx before surgery and after surgery than mice that received no treatment, however there was not a significant difference between mice treated before or after surgery. The data indicates that as a pilot experiment conducted with a small number of mice, it was difficult to observe significant differences between the S-T and T-S group. For

pragmatic reasons, the protocol of Treg depletion before surgery was adopted for all future metastasis experiments.

In each of these experiments mice were phenotyped and split into DEREG positive and DEREG negative littermate controls. All mice in an experiment were treated with DTx in order to eliminate the possibility of non-specific effects of DTx on tumour metastasis. Figure 4.15 shows the cumulative data from repeated metastasis experiments, from which significantly fewer metastatic lung nodules were observed in Treg-depleted mice when compared to Treg-replete mice. Similar control was observed in the primary tumour growth of these mice. Figures 4.16 and 4.17 show the tumour growth curves and tumour growth rates of both Treg-depleted and Treg-replete mice before and after 2 rounds of DTx treatment started on day 10. Figure 4.16 (B) shows no significant difference in the overall tumour growth rates of Treg-replete mice after treatment with DTx. Contrastingly, Figure 4.17 shows a significant decrease in tumour growth rate after DTx administration in Treg-depleted mice. Interestingly, this difference is also observed in Treg-depleted mice that did not develop metastatic disease but not in mice that did [Figure 4.17 (F) and (D) respectively], suggesting that mice with slowed primary tumour growth rate were also those that controlled development of metastasis.

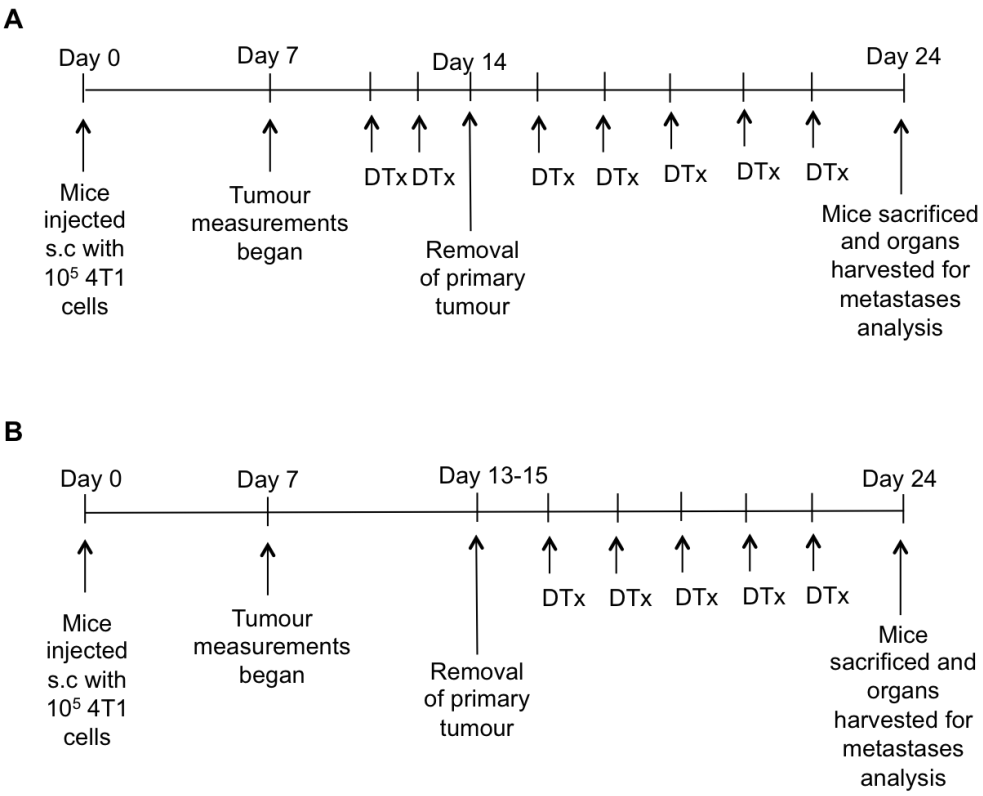

Figure 4.13| Depleting Tregs before and after resection of a primary tumour. (A) Shows the experimental timeline for the Treatment before Surgery group (TS) and (B) shows the experimental timeline for the Surgery before Treatment group (ST) and the No Treatment group (NT).

A

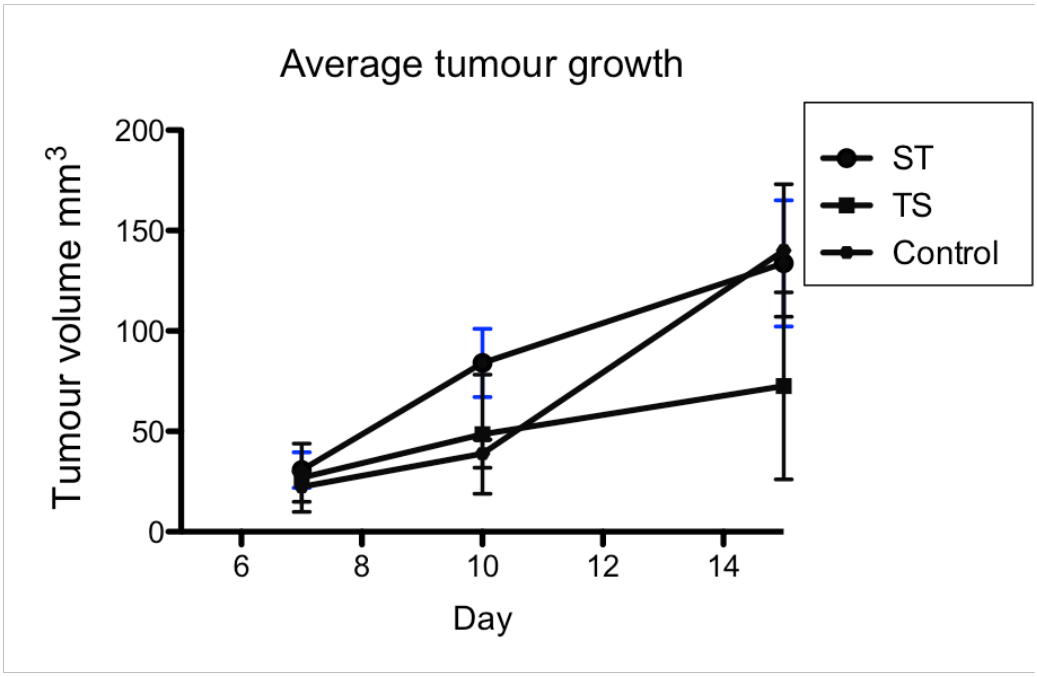

B

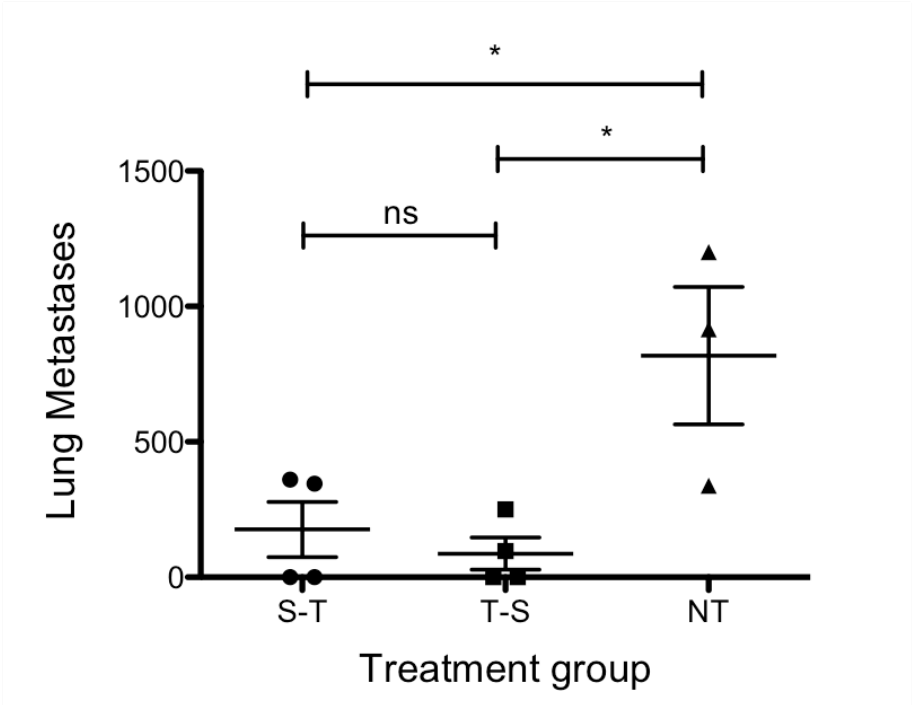

Figure 4.14| Depleting Tregs before primary tumour resection results in fewer metastatic colonies. (A) Shows the average tumour volume over time of each treatment group. (B) Shows the number of lung metastases per group. Statistical analysis performed was a t-test. P values are as follows: p=0.4773 for S-T vs. T-S, p=0.0222 for T-S vs. NT and p=0.0465 for S-T vs. NT. Post-hoc power analysis calculations were 11.5%, 65.1%, and 80.1% for S-T vs. T-S, S-T vs. NT, and T-S vs. NT respectively.

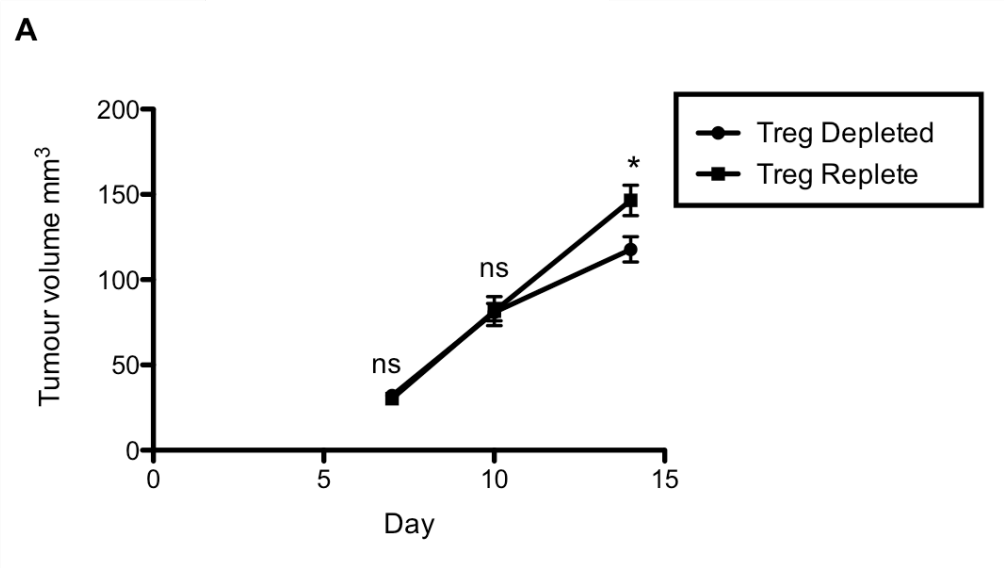

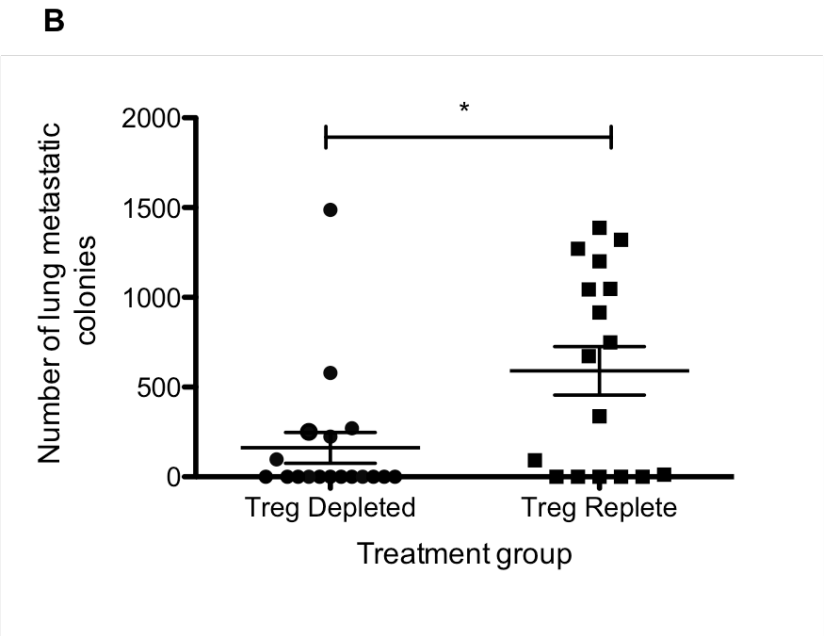

Figure 4.15| Treg depletion is able to control the progression of metastatic disease in Treg-depleted mice. (A) The average primary tumour growth over time of Treg-depleted and Treg-replete mice. An unpaired test was performed at each time point giving the p values as follows: p=0.6284, p=0.9502, and p=0.0176. (B) The number of metastatic colonies observed in the lungs of Treg-depleted and Treg-replete mice using the clonogenic assay. A Mann-Whitney test was performed on the data set giving a p value of p=0.0162.

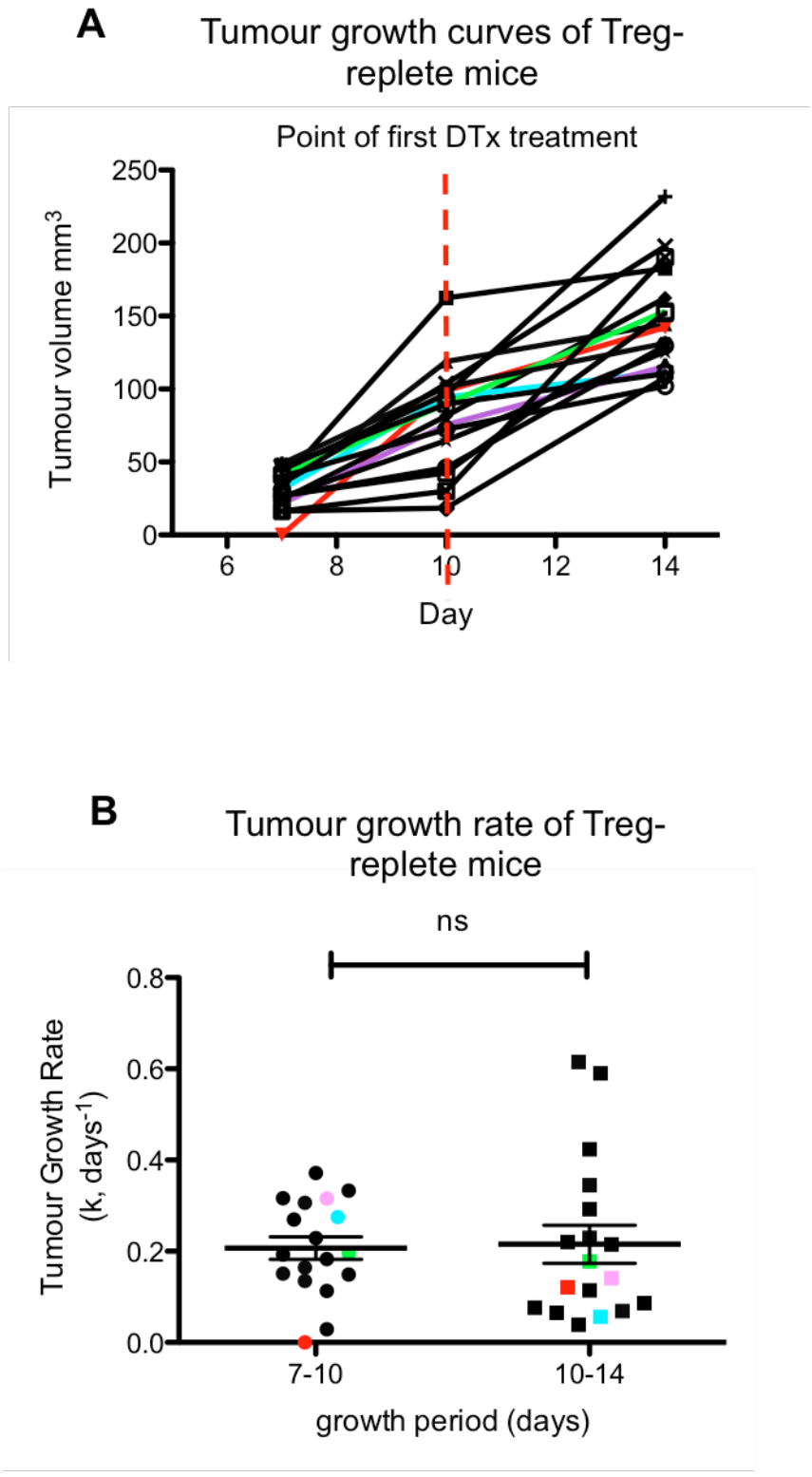

Figure 4.16| Treatment with DTx before primary tumour removal does not affect the tumour growth rate in DEREG littermate control mice. (A) Primary tumour growth curves of DEREG littermate control mice. The growth rate of primary tumours before and after DTx treatment is shown for all mice (B). Paired t tests were performed on the data sets in (B) giving a p value of p=0.8879. Coloured lines and data points represent Treg-replete mice that did not develop metastasis. Dotted red line indicates first DTx treatment.

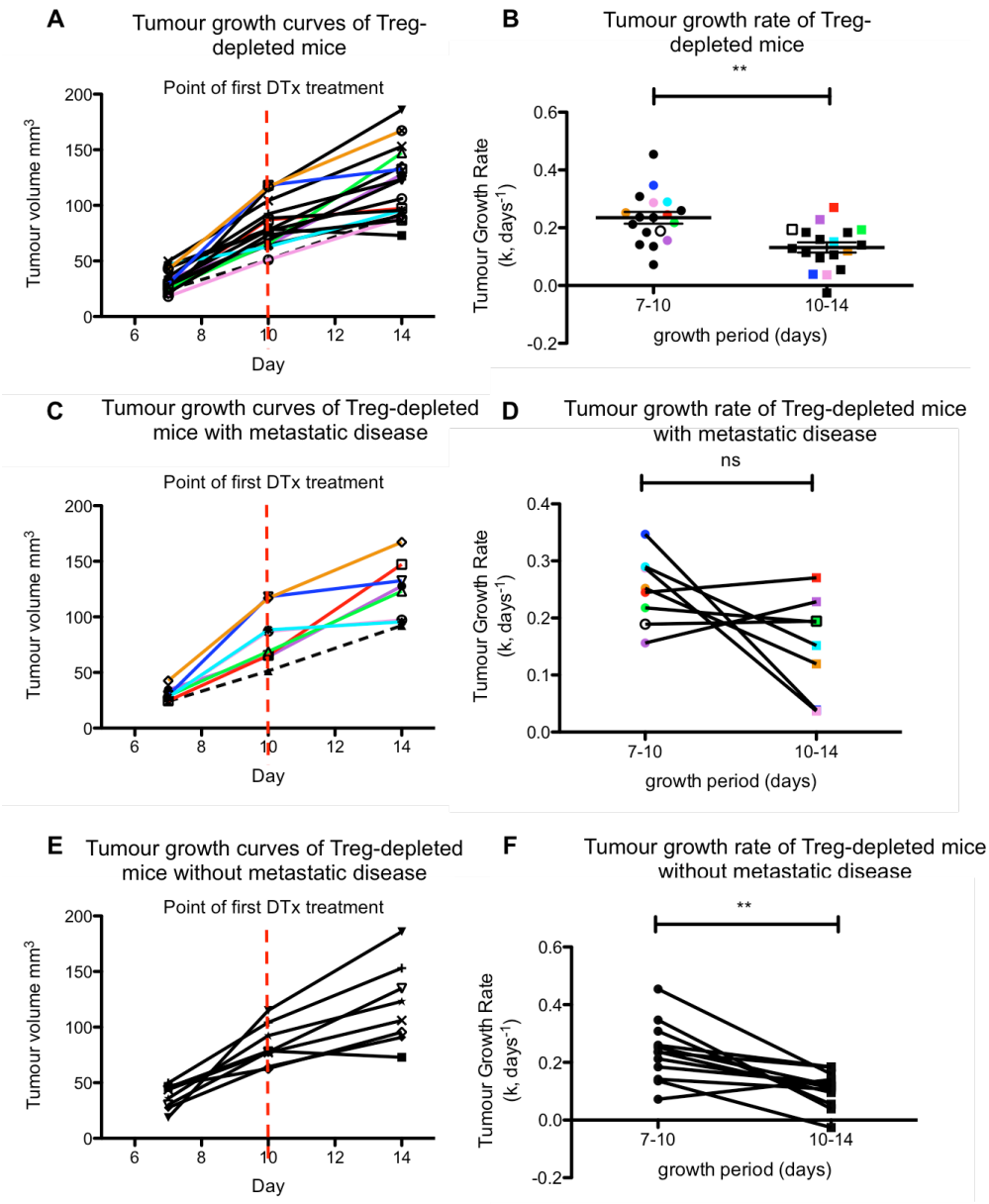

Figure 4.17| Depletion of Tregs before primary tumour removal slows tumour growth rate in mice that do not develop metastasis. (A) Primary tumour growth curves of DEREG mice that developed metastatic disease (C) and those that did not (E). The growth rate of primary tumours before and after DTx treatment is shown for all mice (B), mice that developed metastasis (D), and mice that did not develop metastasis (F). Paired t tests were performed on the data sets in (B), (D), and (F) giving p=0.0017, p=0.0929 and p=0.0022 respectively. Dotted red lines on (A), (C), and (E) indicate first DTx treatment.

4.8 Results: Using PET/CT imaging to quantify 4T1 metastasis

The main limitation of the clonogenic assay is information on metastasis progression can only be gained at a single time-point. Therefore it was hypothesised that through the use of PET/CT as an *in vivo* imaging technique, information could be gathered about the progression of metastasis over time in a single mouse. While PET/CT imaging has been described for use in imaging of primary tumours and different metabolic diseases, little is known about its potential for imaging metastasis. The optimisation of this technique can be found in Chapter 3.

In order to determine whether PET/CT was suitable for imaging 4T1 metastasis, the ability to image solid primary 4T1 tumours was examined. Briefly, tumour-bearing mice were warmed for one hour at 37°C in a heated recovery box and injected i.p with 100 µl Iohexol contrast agent prior to induction of anaesthesia. Once anaesthetised, mice were injected i.v with approximately 100 MBq of F^{18}-FDG and a further 100 µl Iohexol. Mice were placed on a heated mouse bed in the PET/CT scanner and underwent a 15-minute CT followed by a 60-minute PET scan. PET and CT scans were reconstructed and analysed on Pmod 3.3 software.

Primary tumours were observed in DEREG mice PET/CT images as shown by the 3D model in Figure 4.18(A). Interestingly, the 3D model of a primary tumour shows a lack of radioactivity in the centre. This is most likely due to tumour necrosis, as dead tissue in the centre of the primary tumour will not take up FDG.

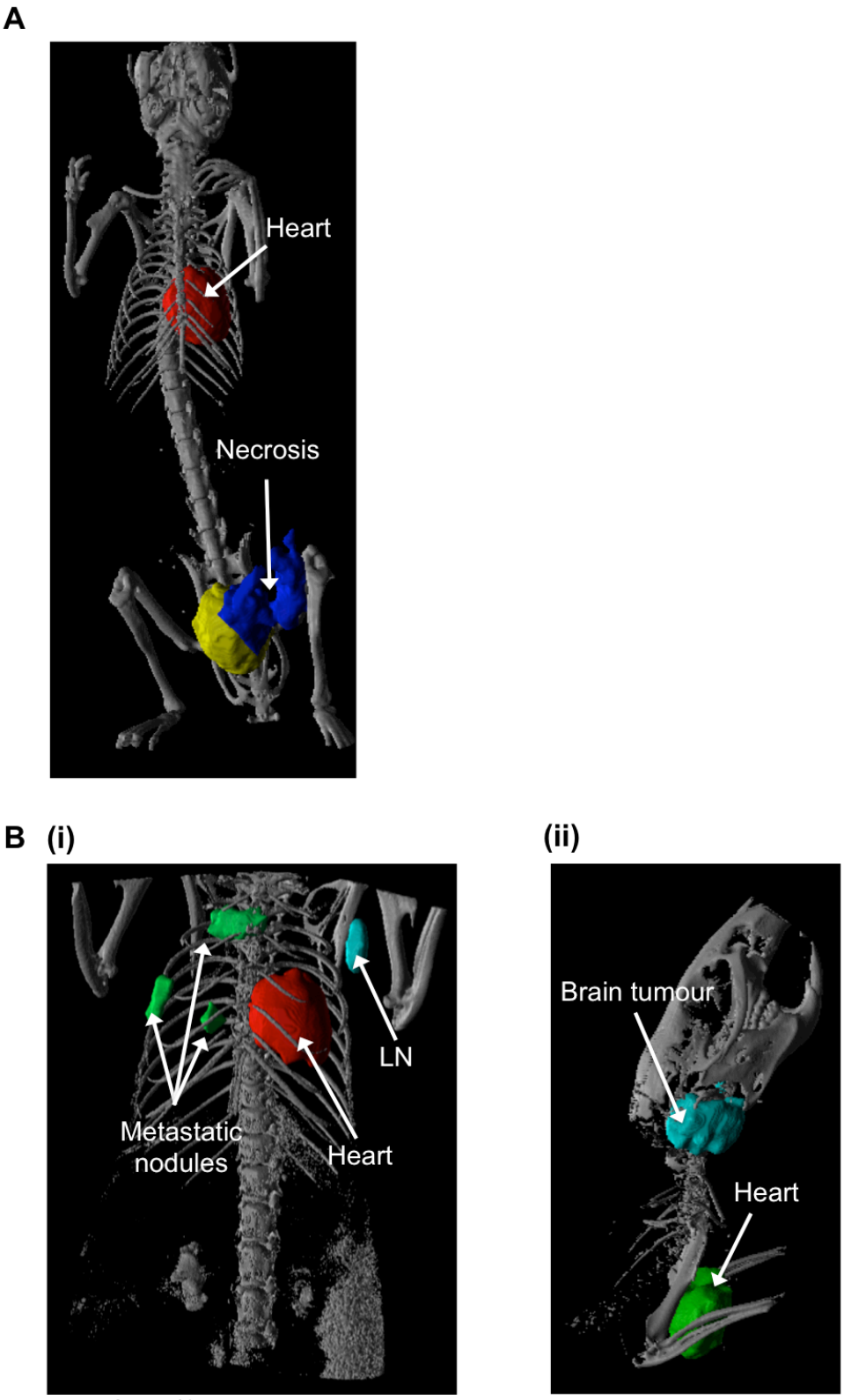

Figure 4.18| PET/CT scanning can be used to image tumours and metastatic nodules in DEREG mice. Tumour-bearing and metastasis-bearing mice were scanned using the Gamma Medica Triumph II PET/CT/SPECT scanner and resulting imaged were analysed using Pmod3.3 software. (A) Shows a tumour-bearing mouse with 3D ROIs drawn for the heart in red, the bladder in yellow and s.c tumour in blue. (B) Shows metastatic nodules in (i) the chest cavity in green and in (ii) the skull in blue.

In order to detect metastases within the lungs, mice were imaged after resection of the primary tumour using the Mediso nanoScan^{TM} PET/CT scanner. After being transferred into the PETIC preclinical scanning facility 24 hours after surgery and 3 days prior to the initial PET/CT scan, mice were imaged once a week for up to 3 weeks and sacrificed 24 hours after the final scan. Upon sacrifice, lungs were harvested for analysis of metastasis using the clonogenic assay.

PET/CT scans of mice in the later stages of metastatic disease show solid tumour nodules within the chest cavity and, in one case, within the skull [Figure 4.18 (B)]. However, the development of micrometastases in the lungs during the early stages of disease cannot be seen by eye on a PET/CT image. It is therefore necessary to draw a ROI around the lungs on the first PET/CT scan that can be transposed onto subsequent scans, in order to measure changes in different parameters within a constant area.

In Chapter 3 the different measures of radioactivity uptake were discussed. Due to the lack of visualization of micrometastases by eye on a PET/CT image, it was hypothesised that any overall change in radioactivity uptake over an entire ROI could be measured through the TLG (g/ml*cm^3), which is calculated by the product of the area of the ROI and the average SUV, rather than at specific sites through the SUVmax or HPA, which looks at the most radioactive point or the average of the 5 most radioactive points respectively. To test this, Treg-depleted mice and Treg-replete mice were scanned once after primary tumour removal and once 2 weeks later. Lung ROIs were drawn on week 1 scan and transposed onto the week 3 scan, and the TLG was calculated for each ROI and compared to naïve mice

(Figure 4.19). Interestingly, naïve mice had a higher lung TLG when compared to Treg-depleted and Treg-replete mice. This appears paradoxical, especially when comparing PET/CT images of a naïve (A) and metastasis-bearing Treg-depleted mouse (B) in Figure 4.20 where there appears to be less spread of radioactivity in the naïve mouse in comparison to the Treg-depleted mouse, with most of the radioactivity being taken up by the heart, bladder and kidneys.

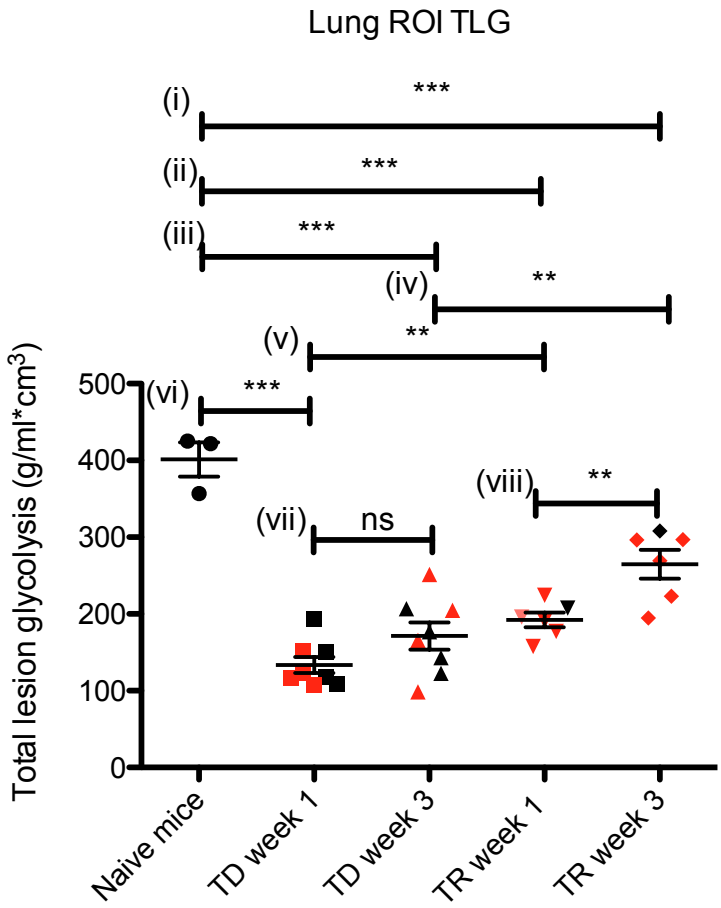

Figure 4.19 | Lung ROI TLG is higher in naïve mice compared to experimental mice. Naïve mice, Treg-depleted (TD), and Treg-replete (TR) mice were scanned once or twice and lung ROIs were drawn on PET/CT images. TLG was calculated for each lung ROI and plotted on the graph above. A one-was ANOVA was performed on the data sets giving the following p values: (i) p=0.0032 (ii) p=<0.0001, (iii) p=<0.0001, (iv) p=0.0037, (v) p=0.0018, (vi) p=<0.0001, (vii) p=0.0696 and (viii) p=0.0078. Red data points indicate mice found to have metastatic colonies using the clonogenic assay.

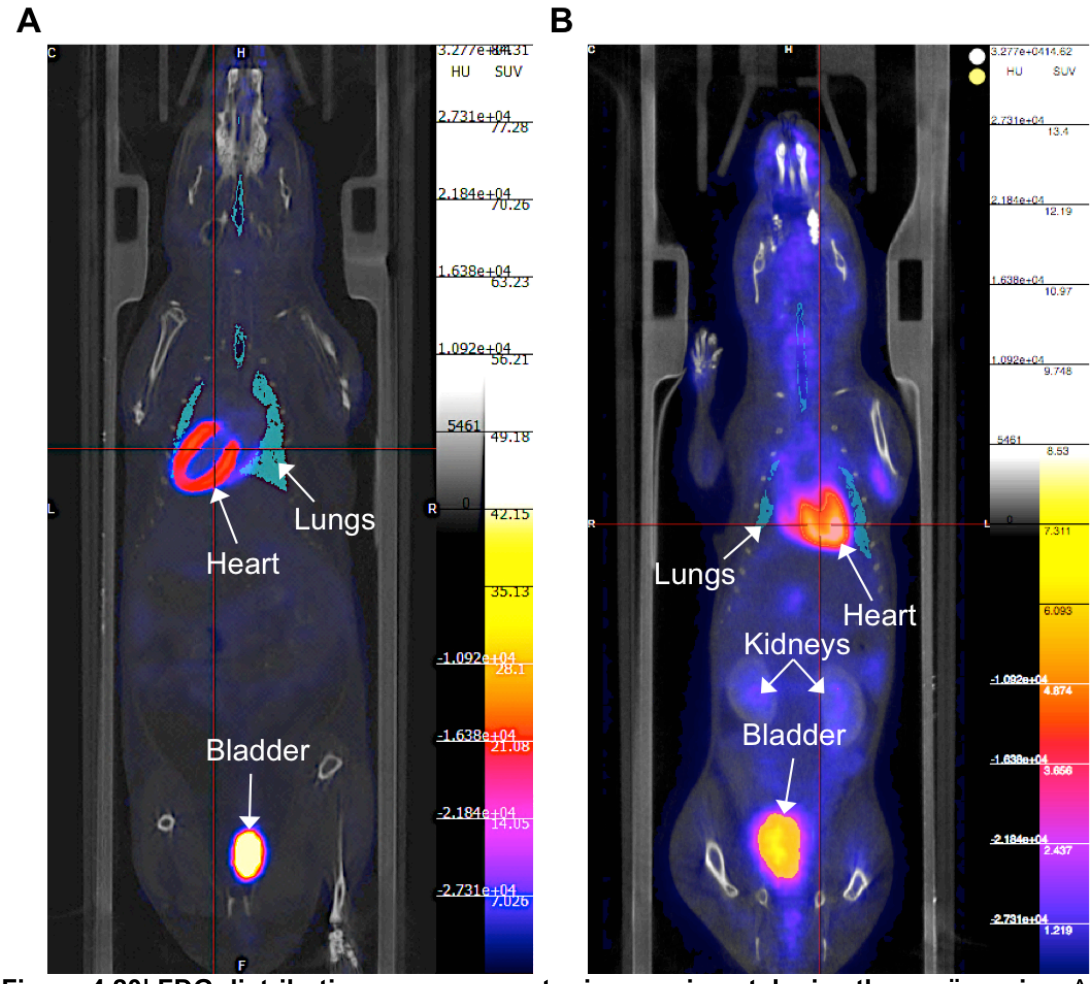

Figure 4.20| FDG distribution appears greater in experimental mice than naïve mice. A PET/CT scan of a naïve mouse (A) and a Treg-depleted experimental mouse 1 week after primary tumour removal (B). FDG distribution is shown as SUV.

In order to investigate why the lung TLG was higher in the naïve mice, the parameters of TLG (ROI volume x average SUV) were considered. Its boundaries and its density define the ROI volume of a given tissue. Since the lung is characterized by the prevalence of air filled spaces and thus a lower tissue density than surrounding bone, it is reasonable to conclude that the ROI volume would be higher in naïve mice than experimental mice, whose lung air space could be occluded by cancer cells. A calculation of ROI volume indicated a larger volume in naïve compared to experimental mice (Figure 4.21). The ROI values are used to calculate the SUV thus impacting on the final TLG values.

While the equation for the calculation of SUV takes into account the weight of the subject, the time at which the radioactivity was injected, the amount of radioactivity injected and the time at which the scan was performed, it does not account for the distribution of FDG throughout the subject. As FDG is excreted from the body in the same manner as glucose, the radioactivity of the kidneys is a good indicator of FDG metabolism. Therefore, normalizing all ROI TLG by the average TLG of the kidney ROIs would remove variability of FDG metabolism. Figure 4.22 shows that after normalizing to the kidney ROI TLG, there is no difference between the lung ROI TLG in naïve mice and experimental mice in the week 1 scan and the week 3 scan. This shows that even though mice had developed metastatic disease (indicated by red data points) the increase in radioactivity uptake, measured in TLG, could not be detected above background.

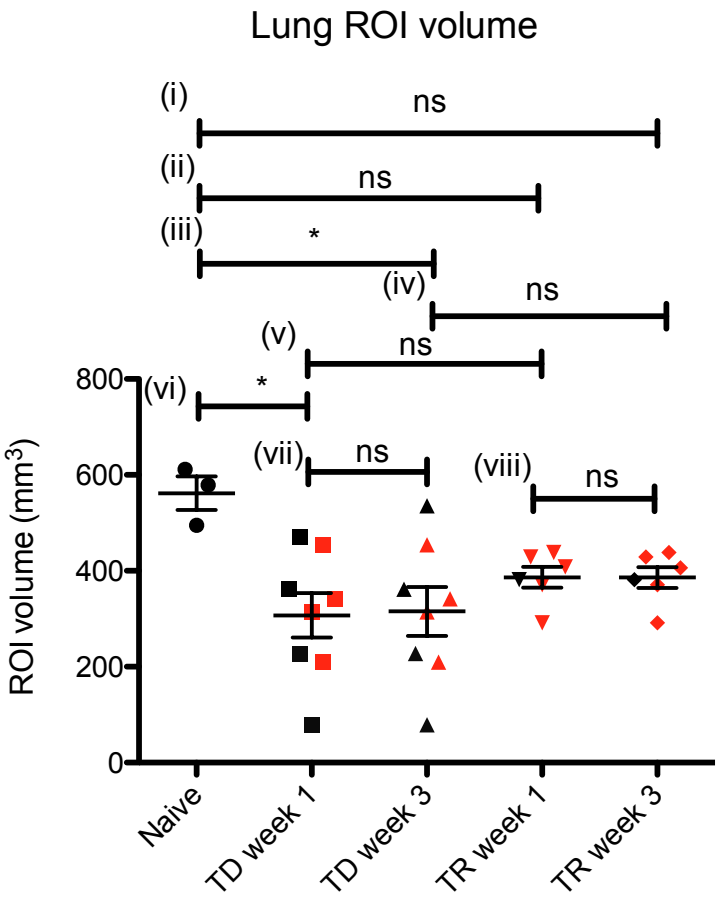

Figure 4.21| Naïve mice have increased Lung ROI volume compared to experimental mice. Lung ROI volumes were compared using a one-way ANOVA was performed to compare lung ROI volume of naïve mice to each experimental group giving the following p values: (i) p=0.2390, (ii) p=0.2413, (iii) p=0.0258, (iv) p=0.7933, (v) p=0.7184, (vi) p=0.0202, (vii) p=0.9999, (viii) p=0.9999

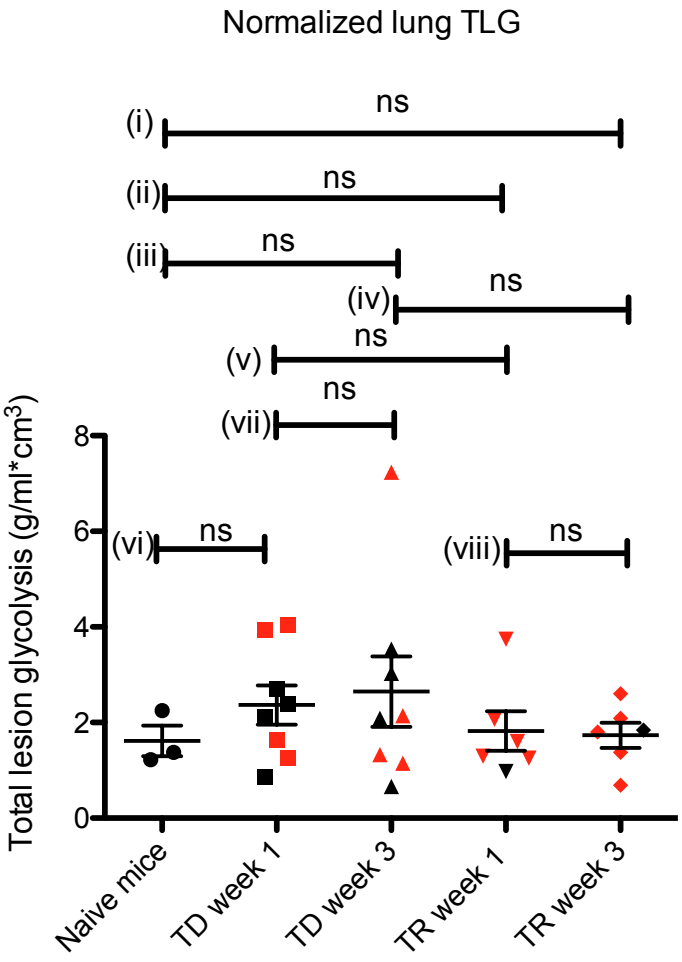

Figure 4.22| Normalizing TLG of ROIs to the average kidney ROI TLG allows accurate comparison between groups. Changes in lung ROI TLG were compared using a one-way ANOVA giving p values as follows: (i) p=>0.9999, (ii) p=0.995, (iii) p=0.7924, (iv) p=0.7325, (v) p=0.9441, (vi) p=0.9221, (vii) p=0.6457, (viii) p=0.8707. Red data points indicate mice found to have metastatic colonies using the clonogenic assay.

Hounsfield Units (HU), described in Chapter 1, are used to differentiate between tissues in a CT scan. Low HU corresponds to empty airspace, whereas high HU corresponds to dense tissue. As it was not possible to detect lung metastases using TLG, it was hypothesised that a change in mean HU of a lung ROI would indicate occlusion of the lungs and therefore development of metastases. Figure 4.23 shows the mean HU of lung ROIs from naïve and experimental mice. Naïve mice had the lowest HU, representing more empty airspace in the lungs in comparison to experimental mice. In both Treg-depleted and Treg-replete mice, there was a significant increase in mean HU between the scans at week 1 and week 3 indicating a decrease in airspace and an increase in tissue area. The decrease in airspace could not however be accounted for by cancer cells as some mice with an increase in mean HU above that observed in naïve mice were tumour-free upon clonogenic assay analysis. Table 4.1 shows the probability that the increase in HU is due to metastasis for Treg-depleted and Treg-replete mice. Out of 6 Treg-depleted mice that displayed an increase in HU between week 1 and week 3, 50% of mice developed metastatic colonies in the lungs shown by clonogenic assay. Comparatively, 5 out of 6 Treg-replete mice developed metastasis and showed an increase in HU, showing an 83% chance that an increase in HU is due to metastasis in this treatment group. While the increase observed in HU is a good indicator of metastases, it is difficult to determine whether the occlusion of the lungs is due to inflammation as a result of an induced immune response or the development of metastatic colonies. Figure 4.24 shows the lungs of a mouse with an increase in HU and no metastasis at week 1 and week 3

compared to a mouse with an increase in HU with metastatic disease. Looking by eye at these images, it is not possible to identify tissue inflammation or metastases. Treg-depletion in an otherwise naïve DEREG mouse leads to a dramatic increase in uptake of FDG by lymphoid organs due to systemic inflammation as shown in Figure 4.25. This further demonstrates the difficulties faced when determining the causes of lung occlusion. This coupled with the lack of information gained by the TLG of the lung ROIs, at the time points measured it is difficult to accurately determine the cause of lung occlusion without later confirmation from the clonogenic assay. However, with increased numbers it might be possible to assign a probability of metastatic disease as a cause of lung occlusion.

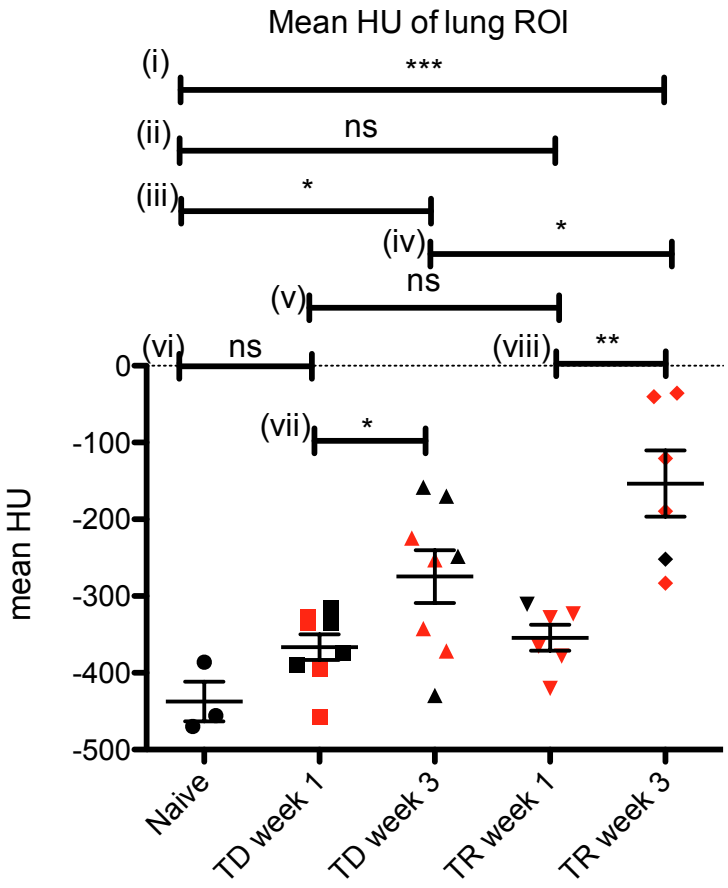

Figure 4.23| HU increase in mice with occluded lungs. The mean HU of lung ROIs of naïve mice was compared to experimental mice. A one-way ANOVA was performed to compare mean HU of lung ROI of naïve mice to each experimental group giving the following p values: (i) p=0.0001, (ii) p=0.5436, (vii) p=0.0196, (iii) p=0.0294, (iv) p=0.0471, (v) p=0.9983, (vi) p=0.6451, (viii) p=0.0060. Red data points indicate mice found to have metastatic colonies using the clonogenic assay.

Table 4.6|Probability of an increase in HU of lung ROI is as a result of metastases.

Group	n	Increased HU (n=)	Occurrence of Metastases (n=)	Percentage (%)	Probability of metastases
Treg-depleted	8	6	3	50	0.50
Treg-replete	6	6	5	83.33	0.83

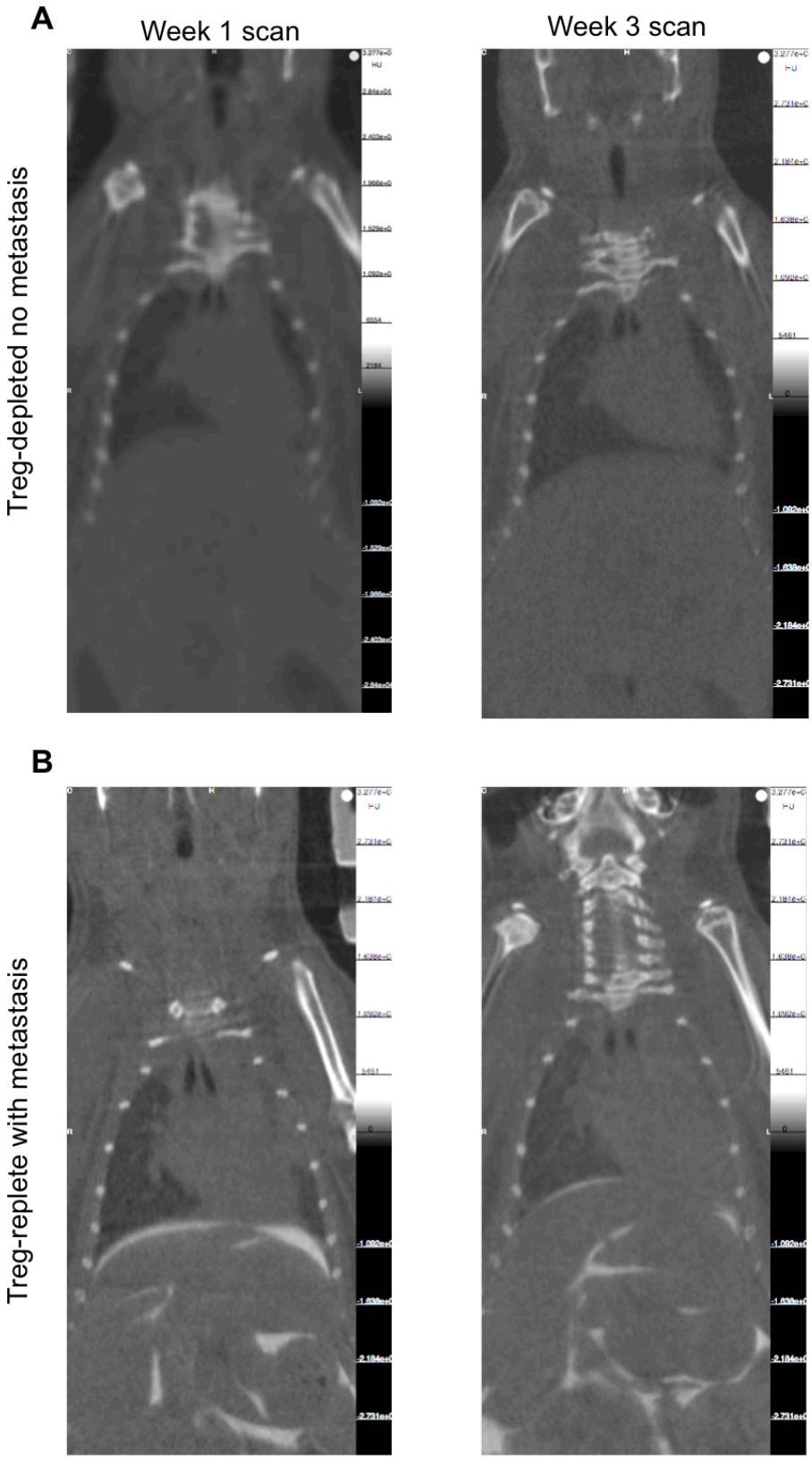

Figure 4.24| Increase in HU and occlusion of the lung cannot distinguish between inflammation and metastases development. Treg-depleted and Treg-replete mice underwent a PET/CT scan at week 1 and at week 3. (A) Shows the two scans of Treg-depleted mouse that did not develop metastasis but had an increase in HU between week 1 and week 2. (B) Shows the two scans of a Treg-replete mouse that developed metastases and had an increase in HU between week 1 and week 2.

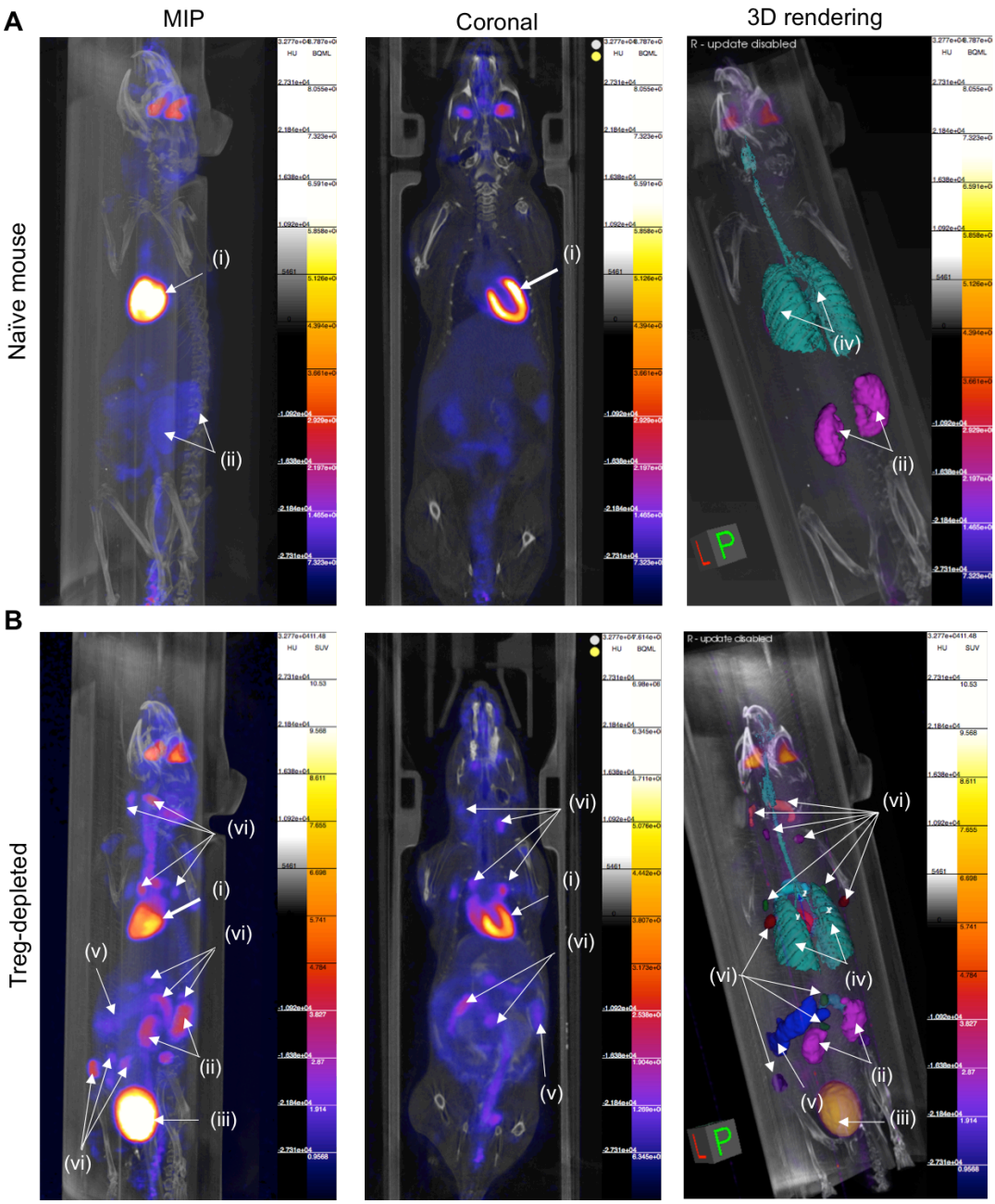

Figure 4.25| Depletion of Tregs in a DEREG mouse leads to increased uptake of FDG by lymphoid organs. A naïve DEREG (A) and a Treg-depleted DEREG mouse (B) underwent a PET/CT scan on the Mediso nanoScan™ PET/CT scanner. Scans were reconstructed using Nucline™ software and analysed on VivoQuant™ software. The Maximum Intensity Projection (MIP), coronal plane, and a 3D rendering with ROIs are shown for each mouse. ROIs are indicated by white arrows and labeled as follows: (i) heart, (ii) kidneys, (iii) bladder, (iv) lungs, (v) spleen, and (vi) lymph nodes.

4.9 Discussion

The aims of the experiments in this chapter were to examine the effect of Treg depletion on the growth of a 4T1 tumour and the progression of its metastasis using both *in vitro* and *in vivo* techniques.

Initial experiments showed that Treg depletion did not result in better control of metastasis induced through intravenous injection of tumour cells even when low doses of tumour cells were used. It was not possible to reduce the dose further as this would have resulted in variable tumour-take in control animals.

The effect of Treg depletion on spontaneous metastasis was therefore investigated. Not only did this allow for a more clinically relevant experimental set-up, this metastasis model also prevented the overloading of lungs with 4T1 cells leading to occlusion and respiratory difficulties. It was hypothesised that as primary tumour control was promoted through Treg depletion, metastasis progression could be controlled in the same mouse.

In clinical cases, metastasis arises from a primary tumour where small numbers of cells detach and migrate to distant sites. The 4T1 tumour cell line is highly metastatic and from the experiments described in this Chapter has been shown to spontaneously metastasize from a primary tumour >125 mm^3 in diameter. In each metastasis experiment, all primary tumours were resected once a volume of >125 mm^3 had been reached as preliminary experiments indicated that metastasis would have occurred in >80% of animals bearing such tumours.

Using this experimental model, significantly less metastatic colonies were observed in Treg-depleted mice than Treg-replete mice with many

Treg-depleted mice developing very few or no metastatic colonies. Out of 18 Treg-depleted mice only 8 developed metastasis, 7 of which had a colony count of <1000 (ranging from 1-579). Conversely, 15 out of 17 Treg-replete mice developed metastasis, 6 of which had >1000 colonies with a maximum colony count of 1388 (Figure 4.26). I went on to evaluate whether there was a link between the ability of the mice to control primary tumour growth and metastases. When the Treg-depleted group was split into mice that did and did not develop metastasis, it was observed that there was no significant difference in the overall growth rate of primary tumours in mice that developed metastatic colonies whereas a significant decrease in primary tumour growth rate was observed in those which did not develop metastatic colonies. When the same analysis was performed on Treg-replete mice no significant difference was found in the tumour growth rates before and after DTx treatment and no relationship was observed between primary tumour growth rates and development of metastases. This indicates that the control observed over primary tumour growth and metastasis progression occurs as an effect of DTx mediated Treg depletion and suggests a difference in the anti-tumour immune response generated in individual mice as a result of Treg-depletion (explored further in Chapter 5).

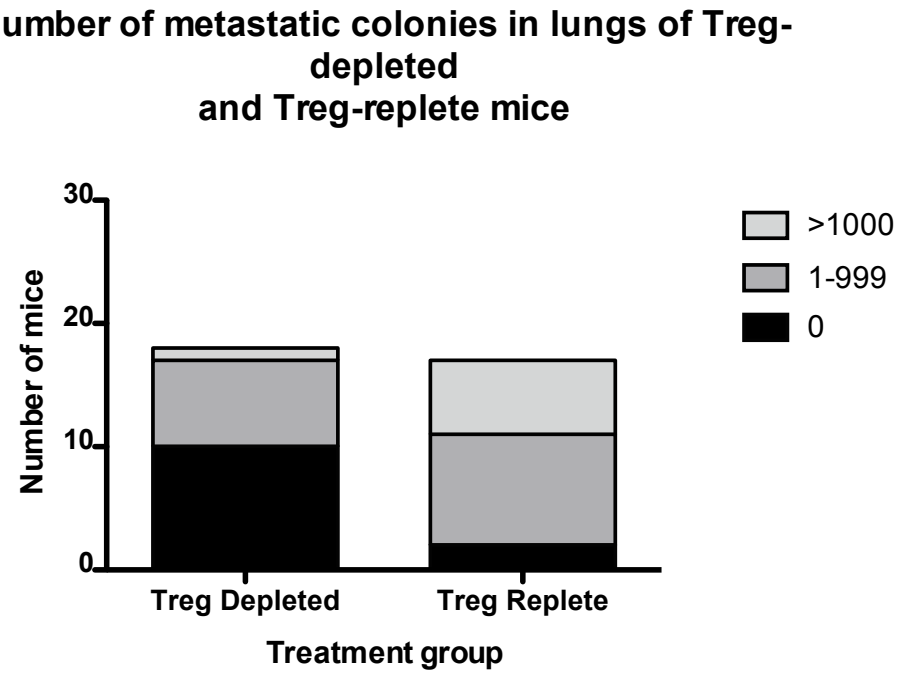

Figure 4.26| Significantly fewer metastatic colonies are observed in the lungs of Treg depleted mice compared to Treg replete mice. The number of Treg-depleted and Treg-replete mice that did and did not develop metastasis was compared using a Fischer's exact test. Treg-depleted vs. Treg-replete mice that developed more than 1000 metastatic colonies gave a significant p value of p=0.0063, while mice that developed between 1-999 colonies gave a p value of p=0.0540.

While the clonogenic assay gives a good representation of metastatic colonies in the lungs of DEREG mice, this method is not without limitations. The method described by Pulaski *et al.* in 2000 states that one colony represents one metastatic cell. However while all tissues are homogenised in the same way for the same length of time, there is no way to determine how many cells initially form a colony. For example, a cluster of metastatic cells from a single niche could be broken up during the homogenizing process to form small clusters or single cells that will each form an individual colonies on the clonogenic assay plate, giving the impression of more metastatic colonies in the lungs of DEREG mice. A further limitation of the clonogenic assay is metastasis progression is only measured at a single time point. Therefore mice must be sacrificed at multiple time points in order to monitor metastasis progression over time. Not only does this increase the number of mice required for an experiment, it also means progression of the disease is not measured in a single mouse. In order to address these limitations, PET/CT was investigated for use as an *in vivo* imaging technique to measure metastasis over time.

PET/CT imaging was successful in visualizing solid primary tumours and large metastatic nodules within the chest cavity. Mice were scanned up to 3 times over a 3-week period, with the initial scan taken after primary tumour resection. In order to accurately measure changes in FDG uptake between scans, the lung ROI was drawn on the initial scan and transposed onto subsequent PET/CT images, as discussed in Chapter 3, allowing the ROI volume to remain constant throughout analysis. It was originally hypothesised that an increase in FDG uptake by the lungs could be detected

through changes observed in the TLG. In human patient scans, the SUVmax is used to identify malignant metastatic nodules. However, these metastatic nodules can be identified on a CT image, which is not possible for the micro-metastatic colonies observed in this mouse model. Therefore it is necessary to identify an increase in FDG uptake over an entire ROI using the TLG. Initially it was observed that naïve mice had higher TLG than experimental mice. Further investigation found that the ROI volume and average SUV were also both higher in naïve mice than experimental mice. As described in Results 4.8, I concluded that as the lung ROI is defined by the tissue density, which in turn is defined by the empty airspace within the lungs, problems arise in the case of identifying mouse lung micrometastases. At the time of the initial scan, experimental mice have already had treatment and have begun to develop micrometastases. Therefore mice will have less empty air space and a higher tissue density resulting in lower ROI volumes used to detect changes in SUV. Thus, whilst PET can be used to identify large lesions in experimental mice, the technique is not sensitive enough to detect micrometastases. It was hypothesised that the CT could be used to detect changes in tissue structure within the lungs over time. The mean HU of lung ROIs of naïve mice were significantly lower than Treg-depleted mice at week 3 and Treg-replete mice at both time points, confirming naïve mice have larger empty air space than experimental mice. There was also a significant increase in mean HU between scans at week 1 and week 3 in both treatment groups, indicating an increase in tissue area within the lungs. While all but one mouse developed metastatic colonies in the Treg-replete group, this was not the case with Treg-depleted mice even though a

significant increase in HU was observed. It is reasonable to speculate that this increase in tissue area could be due to inflammation arising from Treg depletion although currently it is not possible to distinguish between inflammation and metastases using HU alone. Differences between increases in HU due to inflammation and development of metastases might become apparent after repeated scanning. Such an approach is however unfeasible due to high costs and animal welfare issues.

In conclusion PET/CT scanning can successfully image solid primary tumours and large metastatic nodules, but through PET imaging alone it is not possible to detect micrometastases. Changes in HU of lung ROI show potential for detecting micrometastases, as both Treg-replete and Treg-depleted mice show increases in HU over time. While only 50% of Treg-depleted mice with an increase in HU were confirmed to have micrometastases, this extended to over 80% in Treg-replete mice. If it was possible to take an absolute baseline scan before tumour induction or Treg-depletion, and continue scanning past week 3, it is possible that increases in HU due to inflammation would plateau whereas micrometastases would continue to increase in HU. Nonetheless, the increases observed in these two experimental groups further confirm the results concluded from the clonogenic assay.

The experiments conducted in this chapter have shown that Treg depletion can induce the control of metastasis progression in mice. The metastasis experiments were conducted after a pilot experiment suggested that commencing Treg depletion before primary tumour resection was able to promote control over 4T1 metastasis. However, as small numbers of mice

were used in this experiment and no significant difference was observed between the number of metastatic colonies between Treg-depleted groups, further investigation is required to analyse the effect of Treg depletion post-resection in comparison to pre-resection. Current clinical practice for breast cancer patients in most cases is to remove the primary tumour before administering adjuvant chemo- and immunotherapies for treatment of potential metastasis. Neo-adjuvant chemotherapies are currently being investigated for use in resectable liver metastases, osteosarcomas, adenoneuroendocrine carcinomas and some breast cancers (discussed in Chapter 1) (Ayez et al. 2015; Gu et al. 2015; Kim et al. 2009b; Song et al. 2012), although neo-adjuvant immunotherapies have not been extensively examined in patients. Therefore it is important to further investigate the efficacies of neo-adjuvant and adjuvant Treg depletion on the development of metastases in murine breast cancer in order for translation into a clinical setting.

Chapter 5

5 Results: Investigating the levels of immune cell infiltration into primary tumours after Treg depletion

5.1 Introduction

As the data presented in Chapter 4 demonstrated that depletion of Tregs was able to promote the control of 4T1 metastasis, the infiltration of T cells into the primary tumour was subsequently investigated under the hypothesis of mice that went on to develop metastasis had a lower immune cell infiltration in the primary tumour in comparison to mice able to promote control of metastasis after Treg depletion.

In cancer patients, the presence of effector T cells within the tumour microenvironment is generally associated with a good prognosis and better patient outcome. In a mouse model of MCA induced tumours in our lab, the rejection of a primary tumour has been associated with increased infiltration of T cells after Treg depletion (Hindley et al. 2012). In line with this, the presence of Tregs at the tumour site has been associated with a poor prognosis in most cancers apart from those induced through inflammation (Bates et al. 2006; Curiel et al. 2004; Perrone et al. 2008; Ruffell et al. 2010; Sato et al. 2005). The ratio of Tregs:T cells has been shown to be important in promoting tumour rejection as demonstrated by the inhibition of immune checkpoints as discussed in Chapter 1 (Quezada et al. 2006).

In this Chapter, primary tumours resected from Treg-depleted and Treg-replete mice were analysed for the presence of T cells and Tregs.

Lymphocyte infiltration was compared between treatment groups and between mice that did and did not develop metastases within each treatment group.

5.2 Results: Prolonged Treg depletion leads to an increase in T cell infiltration in the primary tumour

In order to analyse the lymphocyte infiltration into primary tumours in response to Treg depletion, 6-8 week old female DEREG mice were injected s.c with $1x10^5$ 4T1 cells on day 0. Mice were treated with DTx every other day as previously described from day 5 until sacrifice on day 21. Frozen sections were cut at 5 μm thickness and subsequently stained for CD8, CD4, CD3, and Foxp3 as described in Chapter 2. Examples of immunofluorescence staining are shown in the Appendix Figure C.

Figure 5.1 shows the number of infiltrating $CD8^+CD3^+$, $CD4^+CD3^+$ and $Foxp3^+CD3^+$ cells per high power field of view (HPFOV). It was observed that there was a significant increase in both $CD8^+CD3^+$ and $CD4^+CD3^+$ infiltrating cells in Treg-depleted mice in comparison to Treg-replete, which is consistent with overall slowed growth and regression of the primary tumour as shown in Chapter 4. Interestingly however, there was no significant difference between the number of $Foxp3^+CD3^+$ cells in the primary tumour between Treg-depleted and Treg-replete mice. At the time of tumour harvest mice had received 8 DTx doses over a 2-week period, which as described in Chapter 4 could be enough time to allow Treg cells to recover.

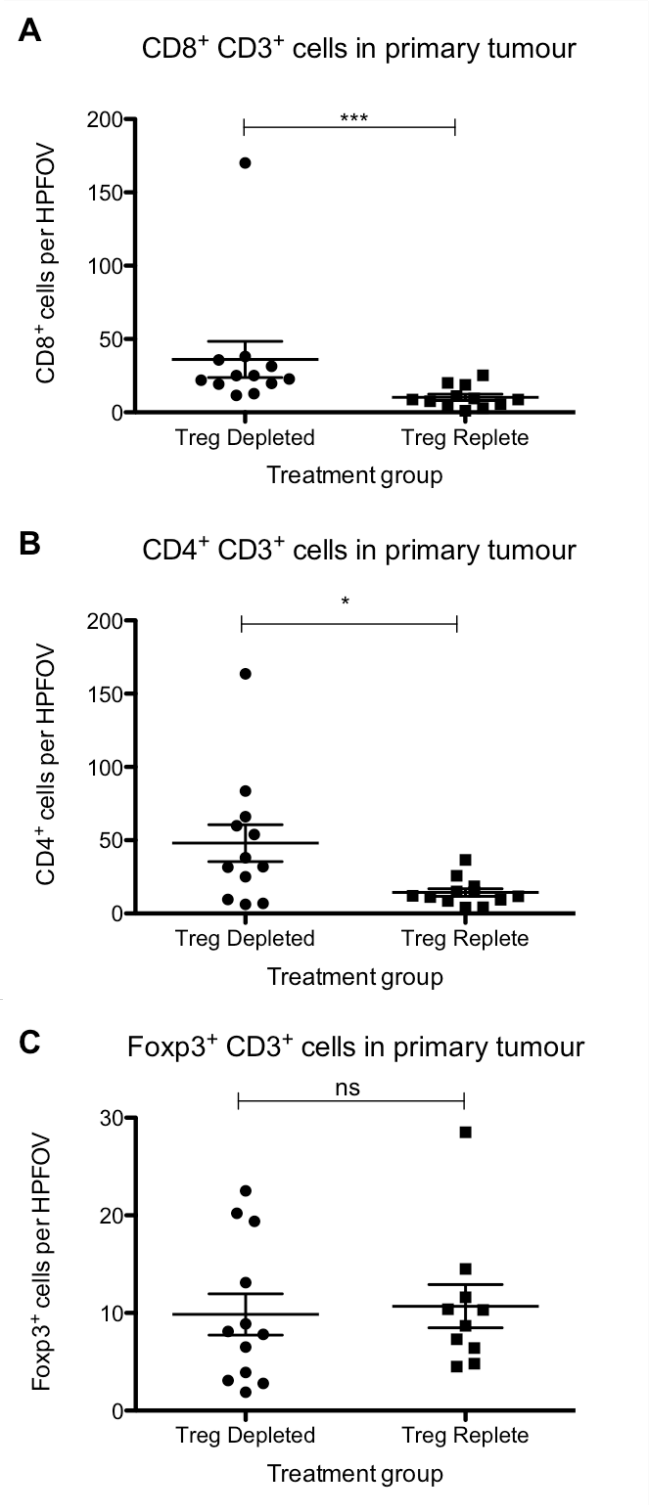

Figure 5.1| Prolonged Treg-depletion leads to increase infiltration of $CD8^+$ and $CD4^+$ cells. 4T1 tumours were induced in mice on day 0. Mice were treated every other day from day 5 with DTx until sacrifice on day 21. Primary tumours were frozen in OCT and sections were stained for CD8, CD4, CD3 and Foxp3. (A) The number of $CD8^+CD3^+$ cells per High Power Field Of View (HPFOV) in Treg-depleted and Treg-replete tumours. (B) The number of $CD4^+CD3^+$ cells per HPFOV. (C) The number of $Foxp3^+CD3^+$ cells per HPFOV. A Mann-Whitney test was performed on all the data giving p value of p=0.0009 (A), p=0.0226 (B), and p=0.5752 (C).

5.3 Results: Two doses of DTx are not enough to alter T cell infiltration in primary tumours

As a significant increase was observed in primary tumour T cell infiltration after Treg depletion, the immune cell infiltration of primary tumour removed during surgery was investigated. Mice were injected with 4T1 cells as before and resulting tumours were measured from day 7. DTx treatment commenced on day 10 and primary tumours were resected on day 14 after 2 doses of DTx. Tumours were fixed in 10% formalin solution and subsequently embedded in paraffin wax for cutting and staining, following the protocol outlined in Chapter 2.

Two serial sections were stained as follows: section 1 stained for $CD8^+$ cells, and $CD3^+$ cells and section 2 was stained for $Foxp3^+$ cells, $CD3^+$ cells blood vessels. Slides were subsequently scanned using a high-resolution digital Zeiss Axio Scan.Z1 slide scanner and immune cell infiltration was analysed as depicted in Figures 5.2 and 5.3. Figures 5.4-5.7 show examples of primary tumours from a Treg-replete metastasis-bearing mouse, Treg-replete metastasis-free mouse, Treg-depleted metastasis-bearing mouse, and a Treg-depleted metastasis-free mouse respectively.

Firstly, the number of $CD8^+$ cells, $Foxp3^+$ cells and $CD8^-Foxp3^-CD3^+$ cells observed per HPFOV were compared between Treg-depleted and Treg-replete mice (Figure 5.8). $CD3^+$ cells that were negative for both Foxp3 and CD8 were used as an indicator of $CD4^+$ T cell numbers. No significant difference was observed between the treatment groups for any immune subset, including $Foxp3^+$ cells. Each treatment group was further divided into

mice that went on to develop metastases and those that did not, the results of which are shown in Figures 5.9 and 5.10.

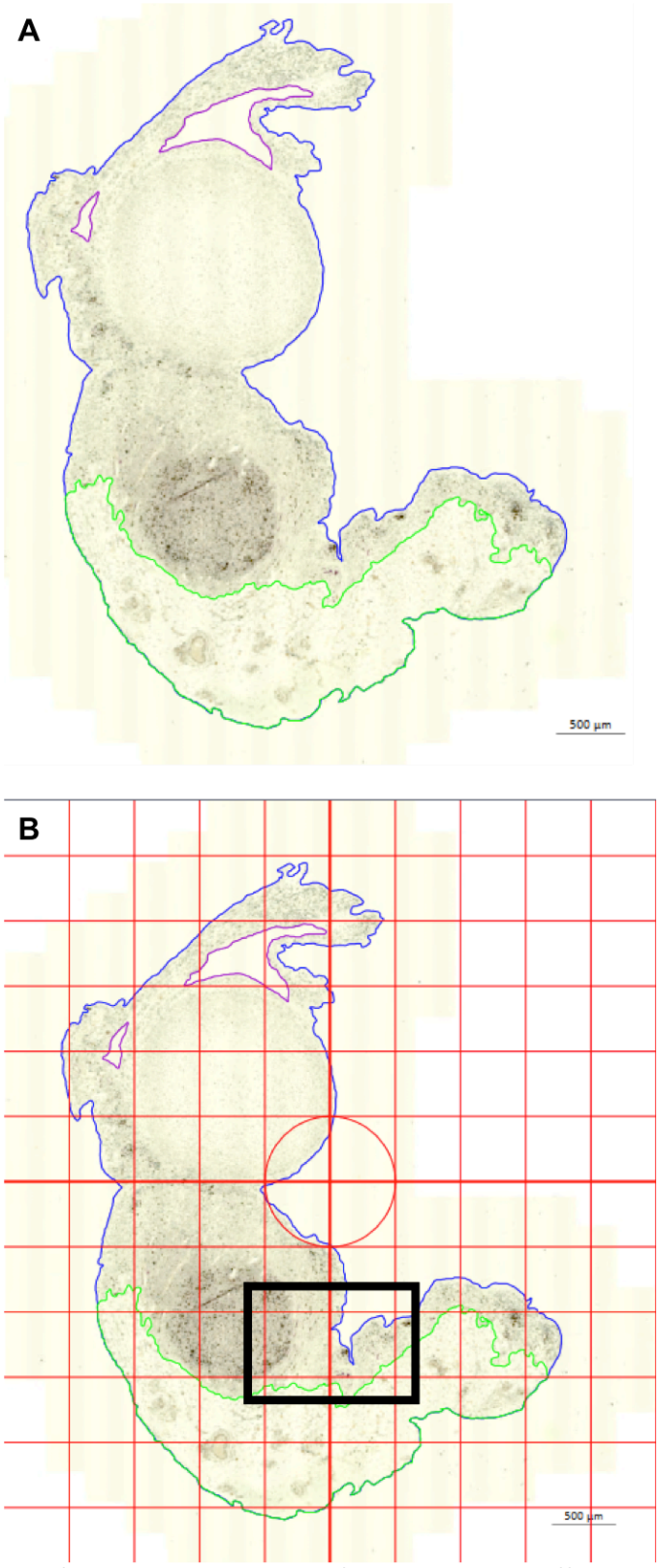

Figure 5.2| Quantifying immune cell infiltration in paraffin sections of primary tumours. (A) A low power image of a primary 4T1 tumour removed at day 14 from a mouse. The total area of tissue is drawn around in blue, the peritumoural tissue is drawn around in green and any holes in the tissue are drawn around in purple. A grid is placed over the image as shown in (B) and 10 squares are used to count immune cell infiltration. The black square indicates the area used in Figure 5.3.

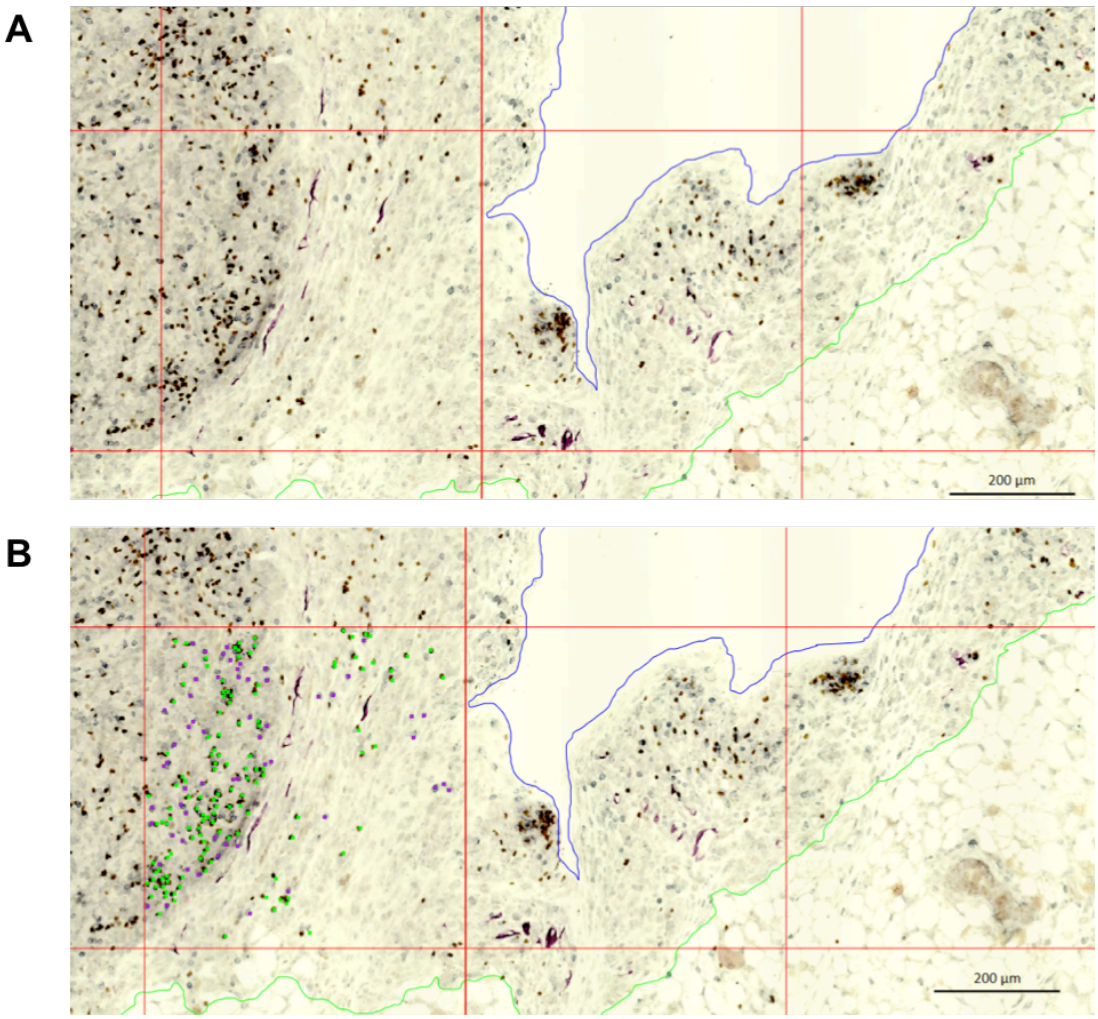

Figure 5.3| Quantifying immune cell infiltration in paraffin sections of primary tumours. (A) And (B) show the enlarged section depicted by the black box in Figure 5.2(B). (B) $Foxp3^+$ cells are counted in green and $CD3^+$ cells counted in purple.

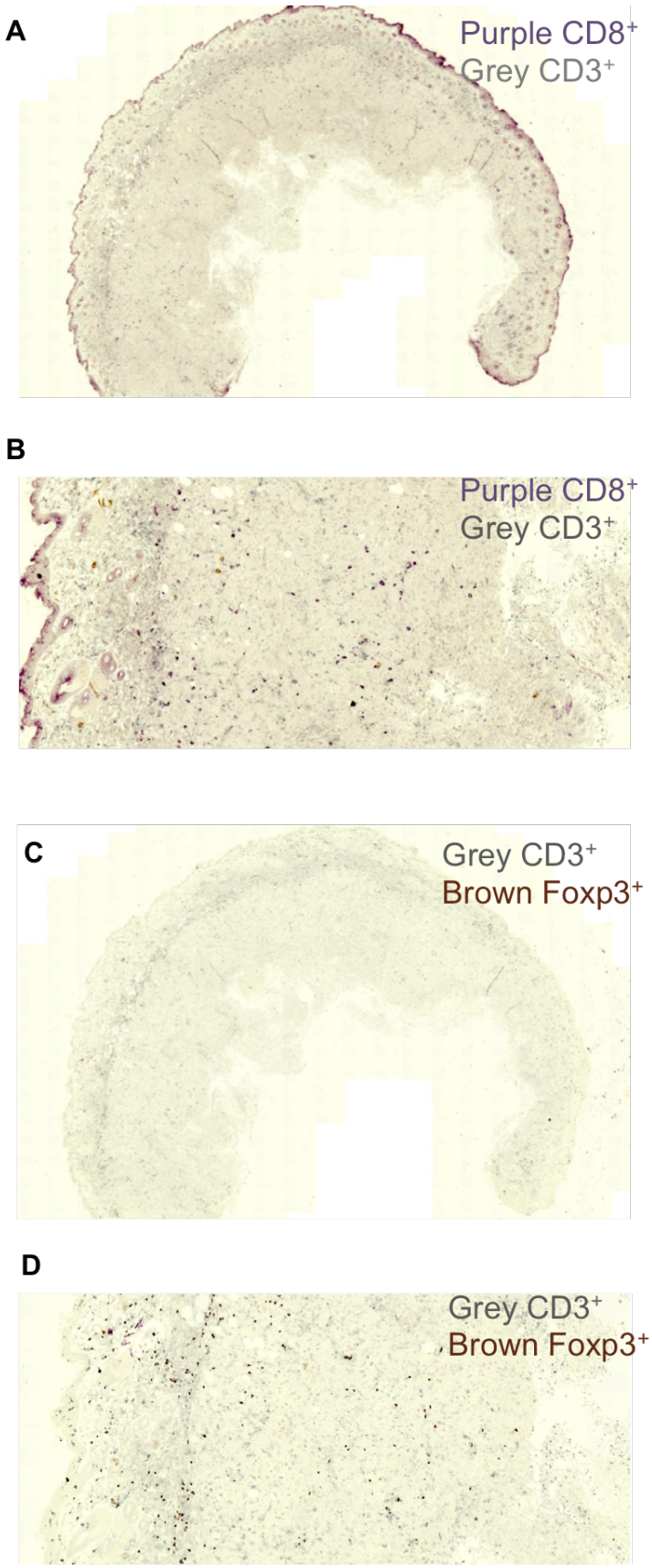

Figure 5.4| Immune cell infiltration in Treg-replete tumours. Immunohistochemistry images of an example primary tumour from a Treg-replete metastasis-bearing mouse. (A) A low power image of a primary tumour stained for CD8 and CD3. (B) A zoomed image of the tumour in (A). (C) And (D) show the same tumour stained for Foxp3 and CD3.

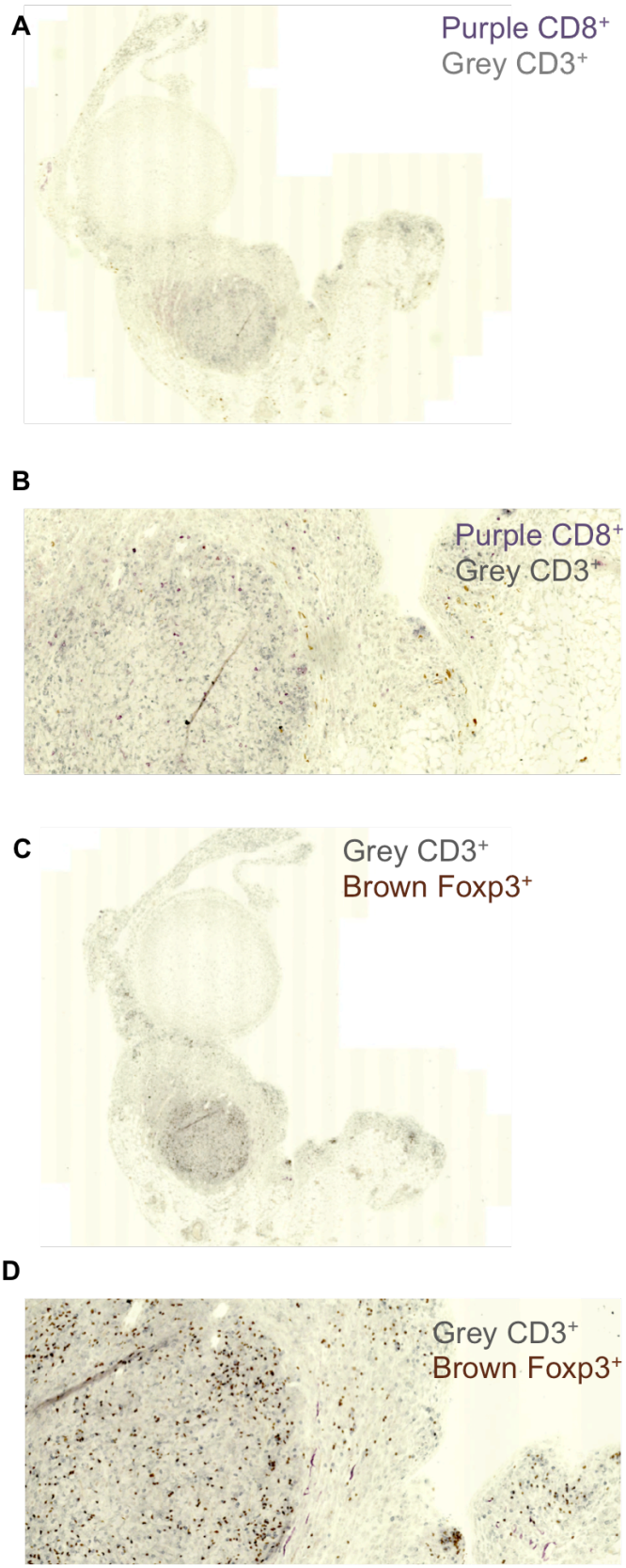

Figure 5.5| Immune cell infiltration in Treg-replete tumours. Immunohistochemistry images of an example primary tumour from a Treg-replete mouse without metastasis. (A) A low power image of a primary tumour stained for CD8 and CD3. (B) A zoomed image of the tumour in (A). (C) And (D) show the same tumour stained for Foxp3 and CD3.

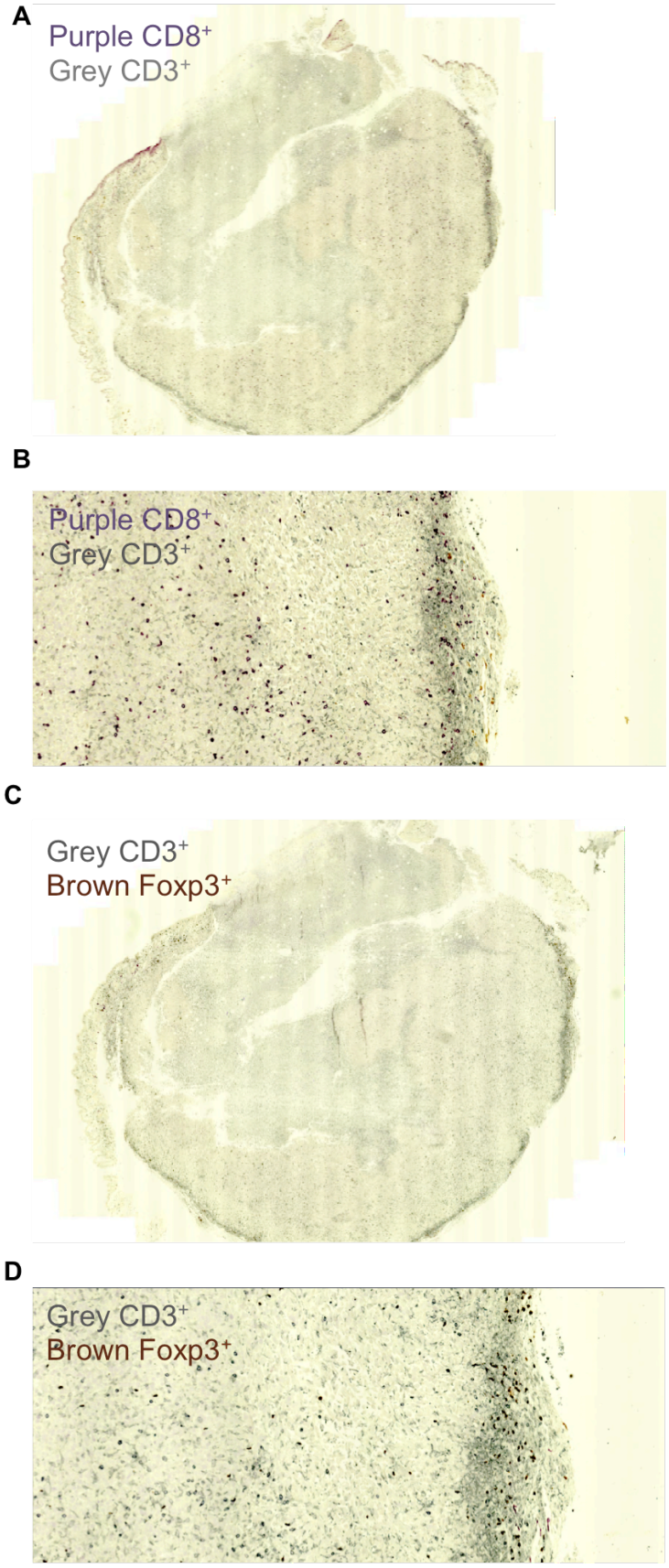

Figure 5.6| Immune cell infiltration in Treg-depleted tumours. Immunohistochemistry images of an example primary tumour from a Treg-depleted metastasis-bearing mouse. (A) A low power image of a primary tumour stained for CD8 and CD3. (B) A zoomed image of the tumour in (A). (C) And (D) show the same tumour stained for Foxp3 and CD3

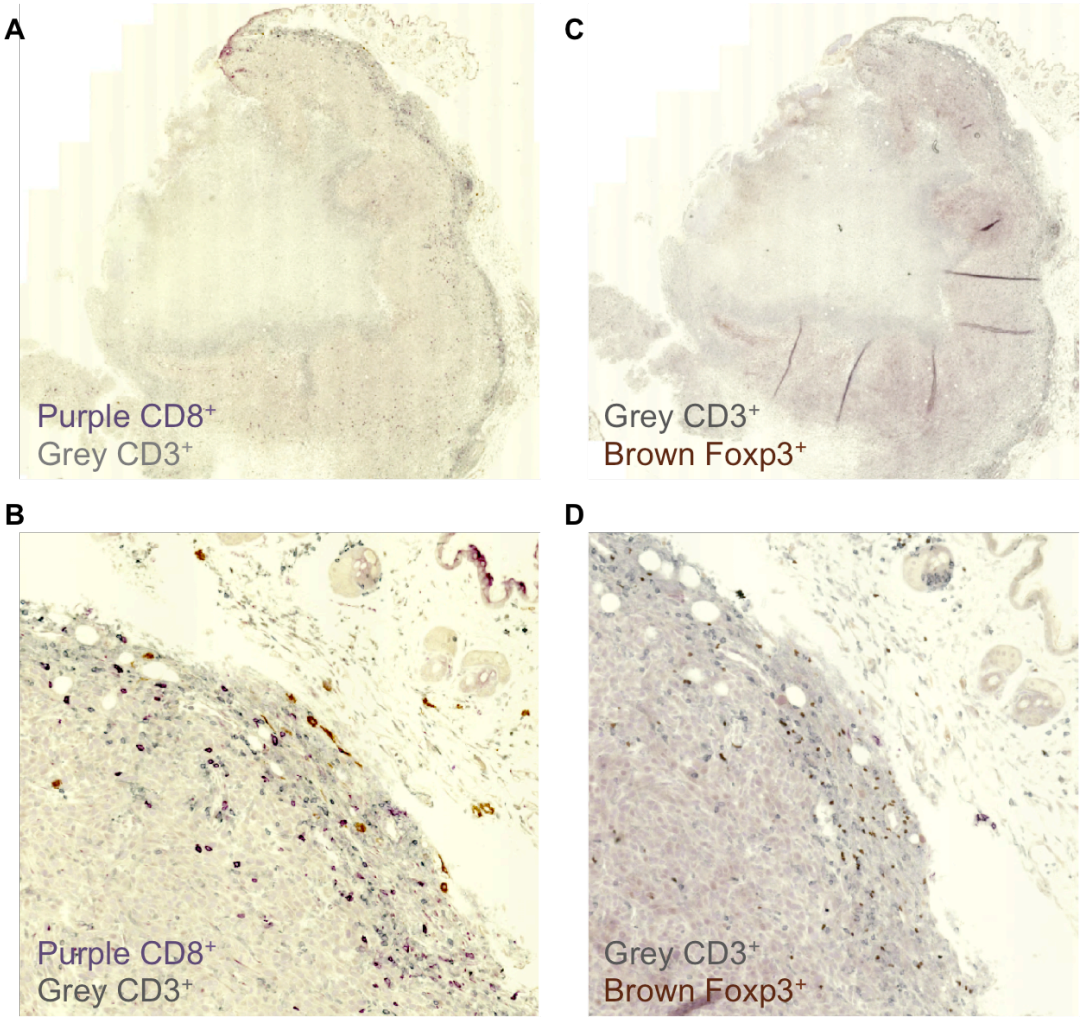

Figure 5.7| Immune cell infiltration in Treg-depleted tumours. Immunohistochemistry images of an example primary tumour from a Treg-depleted mouse without metastasis. (A) A low power image of the primary tumour stained for CD8 and CD3. (B) A zoomed image of the tumour in (A). (C) And (D) show the same tumour stained for Foxp3 and CD3.

There was no difference observed in $CD8^+$, $Foxp3^+$ or $CD8^-Foxp3^-CD3^+$ cell infiltration between Treg-depleted mice that did and did not develop metastases (Figure 5.9). However, while there is a large spread of $CD8^-Foxp3^-CD3^+$ cell infiltration in Treg-depleted mice that developed metastases, there is a trend to suggest that mice that do not develop metastases have a consistently higher infiltration of these immune cells. There was no significant difference in the immune cell infiltration between Treg-replete mice that did and did not develop metastases as shown in Figure 5.10. However, there were too few numbers of mice analysed to draw accurate conclusions from and T cell quantification in this manner is not as accurate as other methods such as flow cytometry.

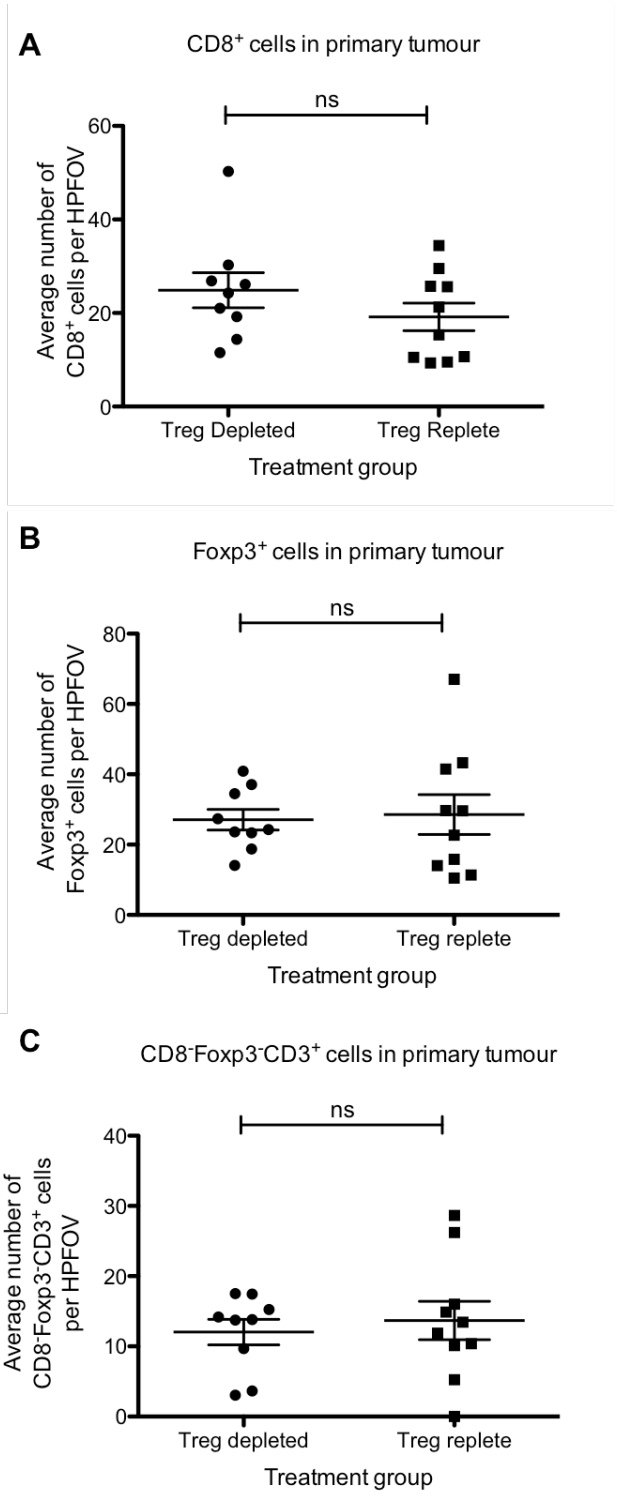

Figure 5.8| Immune cell infiltration into the primary tumour does not change after 2 rounds of DTx. Mice were injected with 4T1 cells on day 0 and treated with DTx every other day from day 10. Primary tumours were resected on day 14, embedded in paraffin and subsequently stained for CD8, CD3, and Foxp3. (A) The average number of $CD8^+$ cells per HPFOV in Treg-depleted and Treg-replete mice, where an unpaired t test gave the p value p=0.2435. (B) The average number of $Foxp3^+$ cells per HPFOV in Treg-depleted and Treg-replete, where an unpaired t test gave a p value of p=0.8314. (C) The average number of $CD8^-Foxp3^-CD3^+$ cells per HPFOV in Treg-depleted and Treg-replete mice, where an unpaired t test gave a p value of p=0.6305.

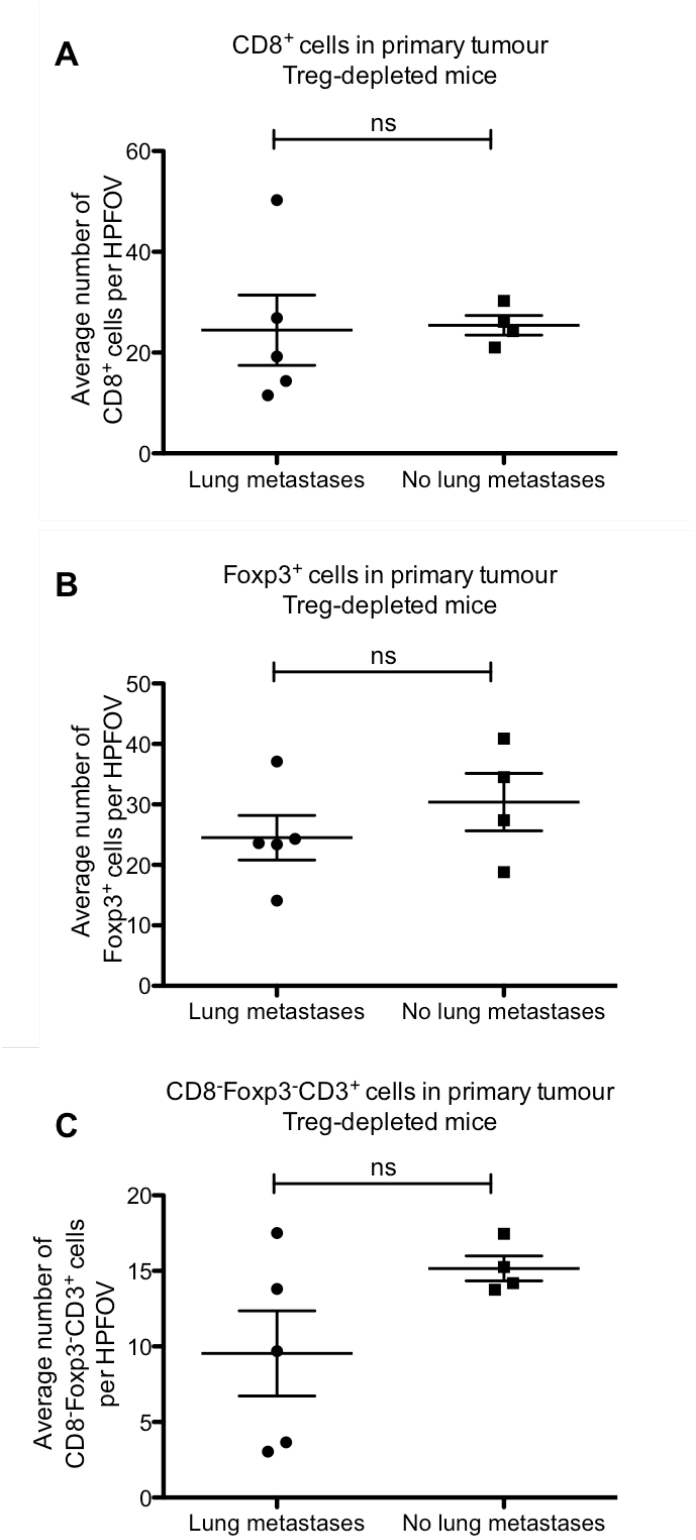

Figure 5.9| There is no difference in immune cells infiltration in Treg-depleted mice that did and did not go on to develop metastases. Data from Treg-depleted mice in Figure 5.8 was split into mice that did develop metastases and those that did not. (A) The average number of $CD8^+$ cells per HPFOV in primary tumours of Treg-depleted mice that did and did not develop metastasis, where an unpaired t test gave p=0.9083. (B) The average number of $Foxp3^+$ cells per HPFOV in primary tumours of mice in (A), where an unpaired t test gave p=0.3498. (C) The average number of $CD8^-Foxp3^-CD3^+$ cells in primary tumours of mice in (A), where an unpaired t test gave p=0.1294.

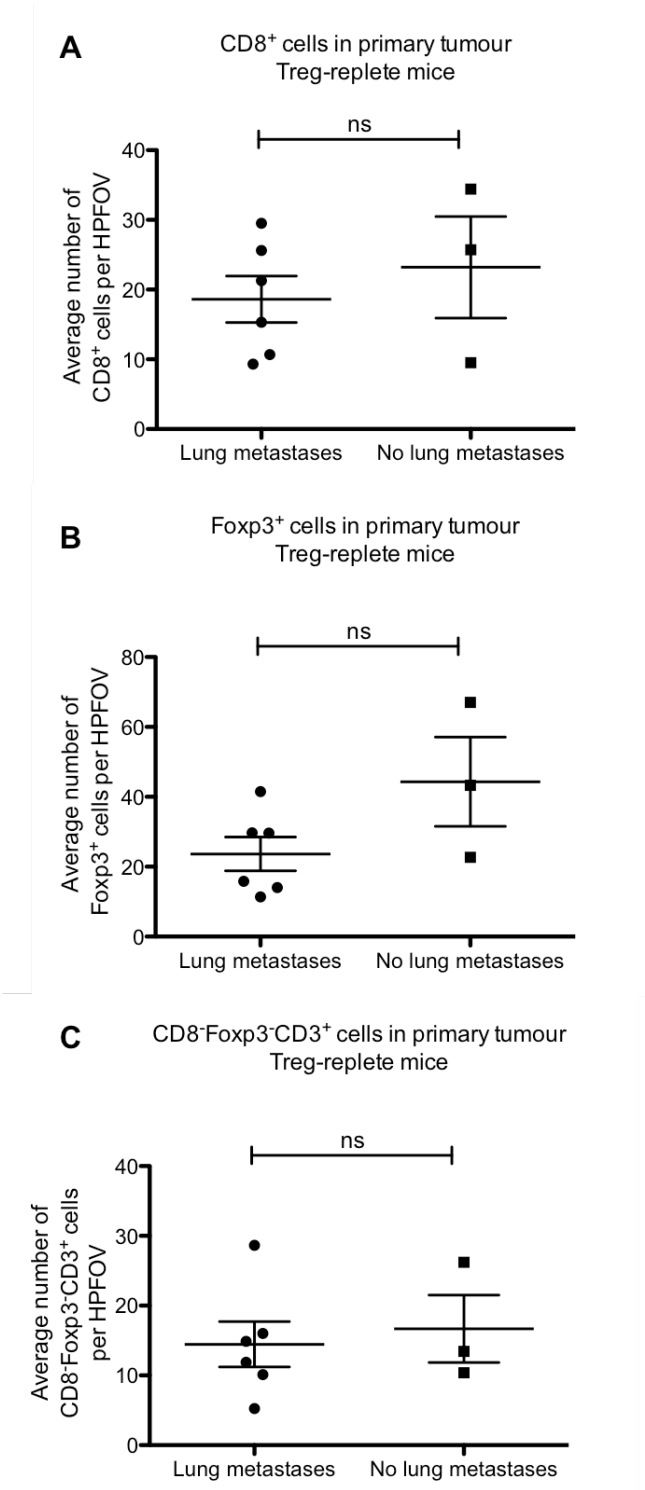

Figure 5.10| There is no difference in immune cells infiltration in Treg-replete mice that did and did not go on to develop metastases. Data from Treg-replete mice in Figure 5.8 was split into mice that did develop metastases and those that did not. (A) The average number of $CD8^+$ cells per HPFOV in primary tumours of Treg-replete mice that did and did not develop metastases, where an unpaired t test gave p=0.5241. (B) The average number of $Foxp3^+$ cells per HPFOV in primary tumours in mice from (A), where an unpaired t test gave p=0.1010. (C) The average number of $CD8^-Foxp3^-CD3^+$ cells per HPFOV in tumours of mice from (A), where an unpaired t test gave p=0.7089.

5.4 Discussion

While increased T cell infiltration into the primary tumour after prolonged Treg depletion is associated with tumour control and rejection, this does not appear to be an immediate effect as demonstrated by the data shown in this chapter. In Chapter 4, not only was it shown that Treg depletion can promote control of metastasis, but tumour growth rate was also observed to slow after 2 doses of DTx treatment. In the same experiment however, the primary tumours that demonstrate slowed tumour growth rate do not have a higher T cell infiltration than tumours with no change in tumour growth rate.

As previously discussed in Chapter 1, the ratio of Tregs:T cells is an important factor in determining tumour rejection. Tumours with a lower Treg:T cell ratio have a better outcome than those with a higher ratio, which is recapitulated in this chapter. After continued DTx treatment, Treg-depleted mice had significantly higher infiltration of CD8+ cells and CD4+ cells in comparison to their Treg-replete counterparts, while levels of Foxp3+ cell infiltration remained unchanged. Conversely, the method of quantification of immune cells used in this Chapter indicates that after two doses of DTx the ratio of Treg:T cells remains unchanged, although low numbers and limitations to the quantification mean full conclusions cannot be drawn.

Quantification of immune cells does not shed light on the functionality of the tumour-infiltrating T cells. It is possible that while an increase in T cells is not observed in primary tumours after Treg depletion, the infiltrating T cells might display increased activation in comparison to Treg-replete mice. Furthermore, in this Chapter only T cell infiltration has been quantified. It is

possible that there is an increase in NK cell, neutrophil, and macrophage infiltration into the tumour as a result of Treg depletion, all of which play a role in tumour control.

Another limitation to this method of T cell quantification is only part of the tumour is analysed. In a section, 10 HPFOV are counted and an average is taken. While the 10 sections are selected at random to avoid bias, this does not necessarily represent the whole 3D tumour. T cells appear to cluster around the edge of the tumour with very few reaching the centre, and can also appear clustered in pockets like that seen in Figure 5.5. Therefore, the infiltration in the 3D tumour might vary from the snapshot observed in a single section. The optimal way to analyse total immune cell infiltration into tumours would be through flow cytometry.

In conclusion, the experiments in this chapter demonstrate that prolonged DTx treatment to deplete Tregs alters the ratio of Tregs:T cells in a primary tumour and is associated with tumour regression. However, using the limited approach of quantification the data suggests that the initial numbers of infiltrating T cells after Treg depletion is not necessarily the limiting factor of metastasis control. Further investigation is required to determine the functional capacity of infiltrating T cells after Treg depletion as well as to determine the extent of infiltration of other immune cell subsets into the primary tumour.

Chapter Six

6 Final discussion

6.1 The role of Tregs in controlling metastasis

Foxp3+ Tregs are frequently enriched in tumours and are often associated with poor prognosis and patient outcome. The presence of Tregs within primary tumours creates a suppressive environment preventing an anti-tumour immune response (Betts et al. 2007; Nishikawa and Sakaguchi 2010; Quezada et al. 2011; Scurr et al. 2012). Presence of Tregs has also been associated with progression of metastasis in certain cancer types, and enrichment of Tregs has been observed not only at the primary tumour but also in peripheral blood of patients with metastatic disease (Huen et al. 2013).

The data displayed in this thesis has shown that in a mouse model not only does the depletion of Tregs stimulate control of the growth of a primary tumour, but neo-adjuvant Treg depletion also promotes the control of metastasis. The model of 4T1 murine breast cancer is a good representation of human stage IV breast cancer, particularly in its manner of spontaneous haematogenous metastasis. Tumours can be easily excised, and data presented in Chapter 4 demonstrated metastasis can arise from tumours >125 mm^3. Therefore, 4T1 is a good model to investigate the effect of Treg depletion on metastasis.

In the experiments performed to investigate the effect of Treg depletion on metastasis, DTx treatment commenced before primary tumour

removal (neo-adjuvant treatment). This was based on a pilot study that had low numbers but suggested a difference in metastasis control between mice receiving neo-adjuvant Treg depletion or not, when no difference was observed between adjuvant Treg depletion and Treg-replete mice. In clinical cases, treatment is usually given after primary tumour removal to promote control over metastasis disease progression. It is therefore important that the initial pilot experiment is repeated in order to investigate whether neo-adjuvant Treg depletion has a greater effect on metastasis control over adjuvant therapy, as this could have clinical implications when treating breast cancer. In order to address this issue, an experiment will be conducted in which tumours will be induced in DEREG positive and DEREG negative littermate controls on day 0 and tumours will be resected on day 14 as described in this thesis. Mice will be treated with DTx twenty-four hours after surgical resection and every other day thereafter until sacrifice on day 28. The clonogenic assay will then be used to investigate the extent of metastasis in the lungs of the mice. The hypothesis of this experiment is that the presence of a primary tumour is required to induce an anti-tumour immune response after Treg depletion and therefore there will be no difference in the number of metastatic colonies observed between the treatment groups.

Interestingly, data displayed in Chapter 4 showed some DEREG positive mice demonstrated no response after DTx treatment. Furthermore, mice that displayed slowed tumour growth after Treg depletion still went on to develop metastases in the lungs. This could be due to suppressive immune cell subsets other than Tregs acting to prevent an anti-tumour

immune response to metastasis. For example, MDSCs are enriched in 4T1 tumour-bearing mice and regulatory B cells have also been postulated to play a role in suppressing anti-tumour immune responses (duPre and Hunter Jr 2007; Olkhanud et al. 2011; Sinha et al. 2012). As the 4T1 tumour stimulates expansion of poly-morphonuclear (PMN)-MDSCs, there could be a potential to use anti-Gr1 antibodies (Sinha et al. 2012). The caveat with using this antibody is that it is not specific to PMN-MDSCs and will have off-target effects on other granulocytic myeloid cells (Sawant et al. 2012). A combination of Treg depletion and $Gr1^+$ cell depletion could have synergistic effects on metastasis control in the 4T1 model. $CD25^+$ $B220^+$ B-regs have also been identified in an intravenous model of 4T1 (Olkhanud et al. 2011). While the activity of these cells has yet to be fully determined, there is also a potential to use anti-B220 or anti-CD19 antibody to depleted B-regs numbers in the 4T1 model. Further study is needed in the Treg-depleted mice that developed metastases to ascertain whether either of these other suppressive subsets were at play.

The ability of Treg depletion to promote control of metastasis as well as a primary tumour highlights Tregs as a potential target for cancer therapies. Checkpoint blockade therapies, such as anti-CTLA4 and anti-PD-1 have been shown to not only reduce intratumoural infiltration of Tregs but also to facilitate the recruitment of anti-tumour effector cells in mice and humans (Chen et al. 2009; Curran and Allison 2009; Liakou et al. 2008; Quezada et al. 2006). Similarly, anti-CD25 antibodies and tyrosine kinase inhibitors have also been shown to reduce numbers of Tregs, although the

off-target effects of these therapies prove difficult to overcome (Byrne et al. 2011; von Boehmer and Daniel 2013).

Cyclophosphamide (CY) is a nitrogen mustard alkylating agent that is often used in high doses in chemotherapy (Martin-Suarez et al. 1997). However, low dose CY treatment has been shown to have immune-modulating effects specific to Tregs (Ghiringhelli et al. 2004; Lutsiak et al. 2005). A study by Zhao *et al* postulated that the Treg-specific effect observed with low dose CY treatment is due to low levels of intracellular ATP (Zhao et al. 2012). CY as a pro-drug is administered and subsequently catalysed and converted into its cytotoxic form aldophosphamide in the liver before being transported via the circulation (Gamcsik et al. 1999; Rooney et al. 2004). Cells detoxify aldophosphamide and other CY derivatives through conjugation with glutathione, the production of which is ATP dependent (Dirven et al. 1994; Gamcsik et al. 1999). Tregs have notably low levels of the microRNA miR-142-3p resulting in high levels of adenylyl cyclase 9, and enzyme that converts ATP to AMP (Bopp et al. 2007; Huang et al. 2009). This reduction of intratumoural ATP results in lower levels of glutathione thereby leaving Tregs susceptible to the toxic effects of CY (Zhao et al. 2012). A phase II clinical trial has utilized the capacity of low-dose CY to specifically deplete Tregs in order to boost anti-tumour immune responses induced by vaccination, resulting in increased overall survival of CCRCC patients (Walter et al. 2012). While initial studies of Treg depletion in cancer patients are promising, further investigation is needed to understand and overcome off-target effects from current Treg-targeted therapies (Halvorsen et al. 2014).

6.2 T cell infiltration

After prolonged Treg depletion, the data presented in Chapter 5 shows an increase in T cell infiltration in the primary tumour in comparison to Treg-replete mice. This is consistent with data shown in Chapter 4 where depletion of Tregs led to regression of primary tumours.

The method of analysis used in Chapter 5 for investigation of T cell infiltration is not necessarily representative of the whole tumour. However, the data is suggestive that two doses of DTx do not lead to an increase in T cell infiltration into the primary tumour even though metastasis is controlled. Immunohistochemistry does not give any information about the function of the infiltrating immune cells, which could give a better indication of anti-tumour responses. Furthermore, infiltration of other immune cell subsets has not been quantified in this model, such as NK cell, neutrophils, and macrophages, which could better our understanding of the mechanisms of metastasis-control after the depletion of Tregs. Tumours were originally analysed in this manner in order to preserve their structure to identify HEVs, although the data suggests that these blood vessels do not play as a big a role in tumour control in this model as the MCA model investigated in our lab (Colbeck et al. 2015; Hindley et al. 2012).

Further investigation is required to fully understand the infiltration of immune cells into the primary tumour and the effect on metastasis. This could be done through flow cytometry analysis not only to identify subsets of immune cells present within the tumour but also to also sort and isolate T cells for further functional analysis.

6.3 Using PET/CT imaging to monitor metastasis development

In this thesis I have successfully optimized PET/CT imaging for visualizing solid primary tumours and large metastatic nodules. While the PET component of the imaging system was not able to detect micrometastases, the use of HUs to measure the tissue density within the lungs showed promise in identifying areas of occlusion due to development of metastases. However, while over 80% of increased HU was due to metastasis in Treg-replete mice, only 50% was metastasis related in Treg-depleted mice. The remaining 50% Treg-depleted mice that displayed an increase in HU could be due to inflammation in the lungs induced by Treg depletion. In order to distinguish between lung occlusion occurring as a result of inflammation or metastases, it would be beneficial to perform an absolute baseline scan of each mouse to determine individual lung capacity and to continue scans past week 3. In this case, occlusion due to inflammation would remain constant while occlusion by metastases would continue to increase.

FDG PET/CT allows identification of cancers due to their increase in metabolic activity compared to surrounding tissue. However, this is not specific to cancers as demonstrated in Chapter 4. Studies in both humans and in mice have radiolabelled different tracers to measure the progression of different diseases. In humans, F^{18} as part of Fluoromethylcholine has been used to detect lymph node malignancies and bone metastases, and Ga^{68} labeled DOTATATE has been used to image thyroid cancers (Goel et al. 2014; Nockel et al. 2016; Poulsen et al. 2012; Sadowski et al. 2016). In preclinical studies, amino acid based radiotracers have been used to monitor

cell proliferation, while others such as F^{18} P3BZA have been used to monitor cell migration in Parkinson's disease in rats (Bu et al. 2014; Rendon et al. 2016). More recently, human HER2 antibodies have been radiolabelled for use in imaging human breast cancer xenografts in mice (Denis-Bacelar et al. 2016). While there are currently no specific antibodies available for 4T1 tumours, the above studies show promise in developing a specific radiotracer for 4T1 PET/CT imaging. This would allow the metastasis of 4T1 cells to be imaged over time and could therefore be accurately measured on a PET/CT image. Currently, there are no preclinical PET/CT studies that use FDG or other specific tracers to image metastasis or the effect of metastasis-treatment, therefore it is important to develop a mechanism by which it is possible.

6.4 Final conclusions

In this thesis I have demonstrated that PET/CT imaging can be used to visualise solid tumours and large metastatic nodules and also has the potential to be used to measure the development of micrometastases in preclinical models. I have also shown that neo-adjuvant Treg depletion promotes the control of a murine mammary carcinoma growth and metastasis. The prolonged depletion of Tregs allows expansion and infiltration of effector T cells into the primary tumour leading to primary tumour regression even after levels of Foxp3+ cells return to normal. The method of quantification used suggests that the number of T cells in the primary tumour at the point of resection does not increase in Treg-depleted mice in comparison to Treg-replete, even though better control of metastasis

was demonstrated. Therefore, further investigation is required into the function of the T cell present in the primary tumour at the point of resection, as well as the identification of other effector immune cell subsets present.

Appendix

Fluorescence Minus One (FMOs) for detecting levels of Treg depletion

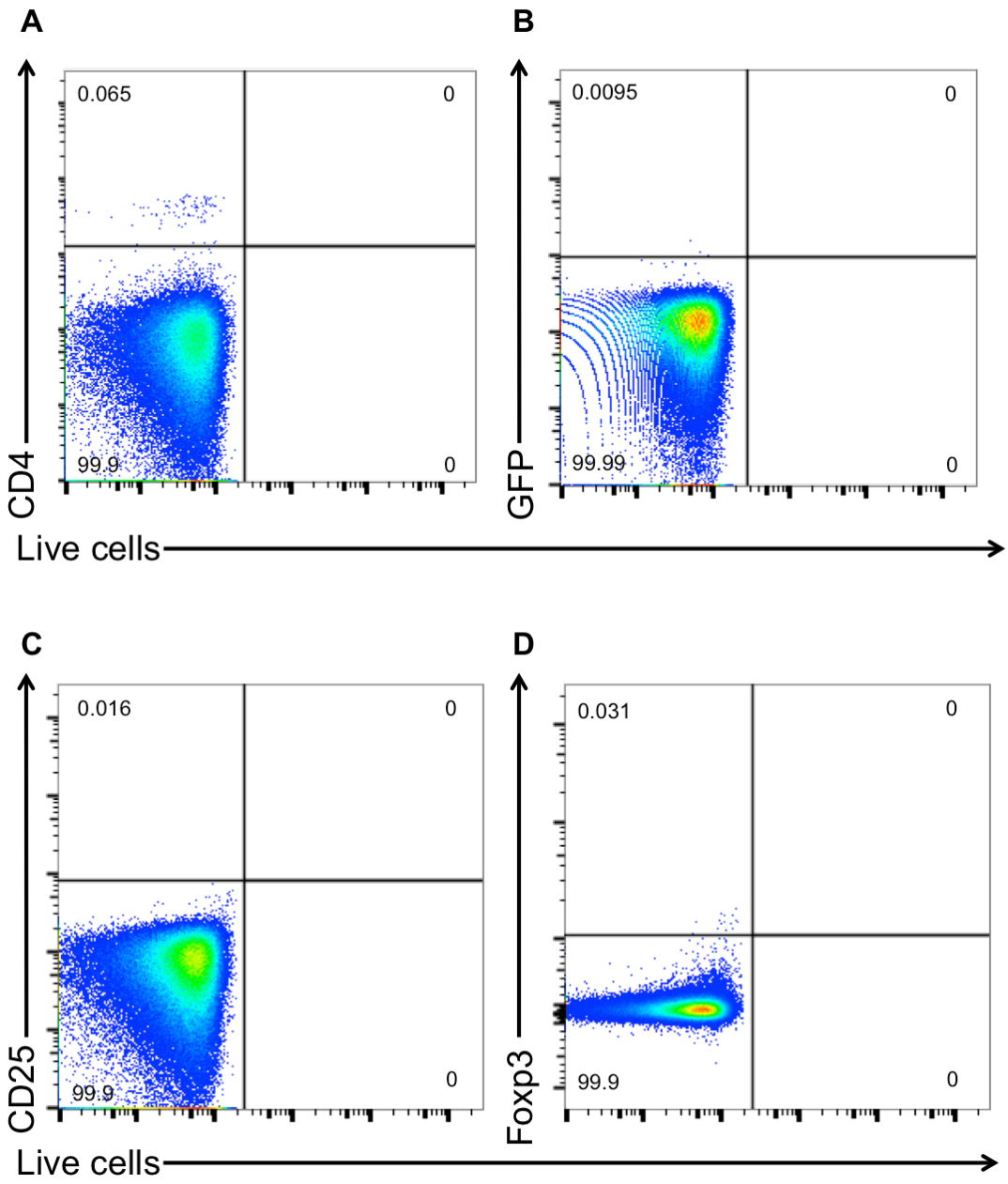

Figure A| Flow cytometry plots showing Fluorescence Minus One (FMOs) for Treg depletion detection. FMOs were prepared on spleen single cell suspensions from Treg-replete DEREG negative mice. Cells are gated on the lymphocyte population as shown in Chapter 2. Numbers represent the proportion of cells in each quadrant.

Isotype controls for Chapter 5

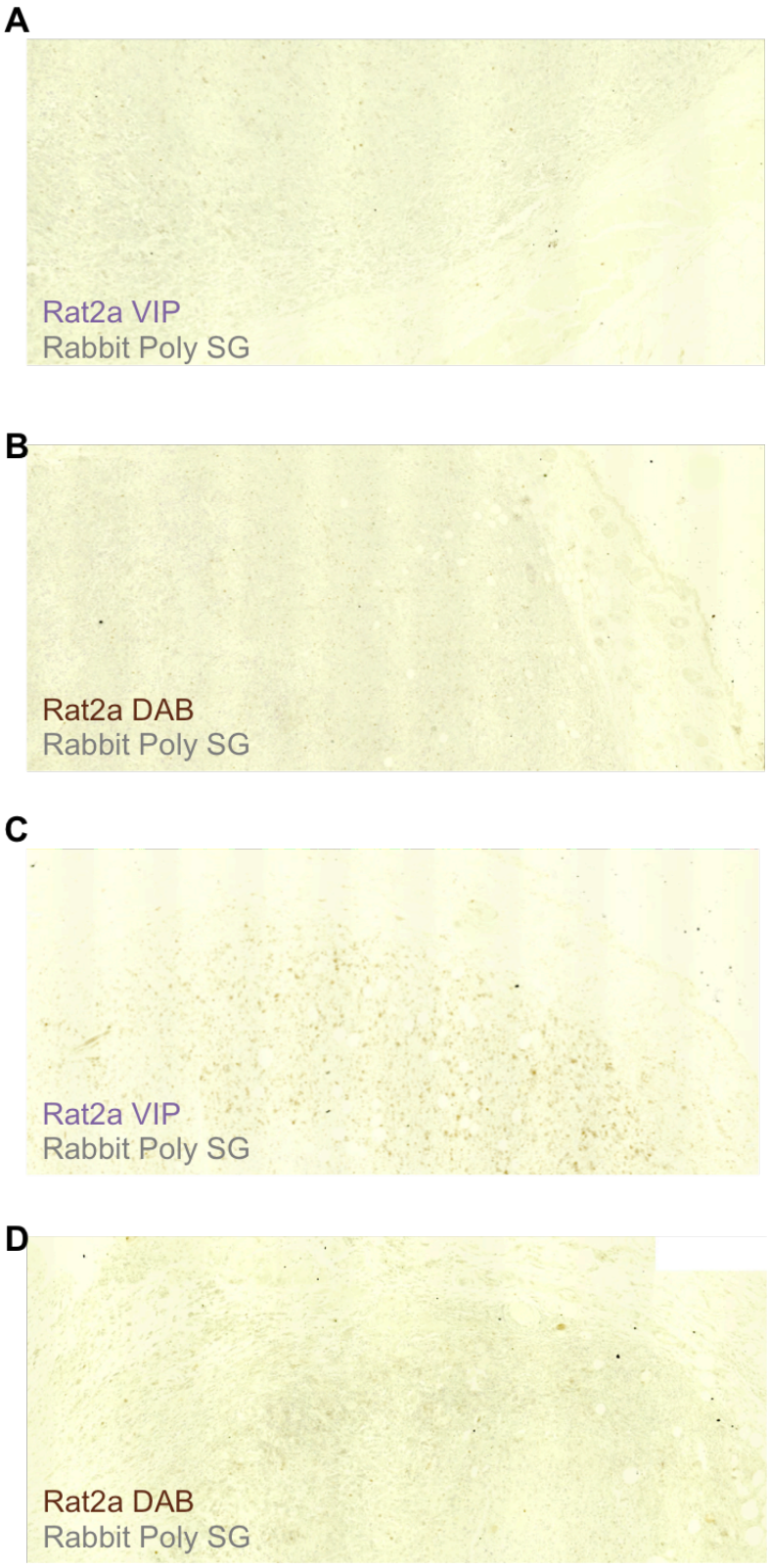

Figure B| Isotype controls for CD8 (Rat IgG2a VIP), Foxp3 (Rat IgG2a DAB), and CD3 (Rabbit polyclonal SG) in Treg-replete (A and B) and Treg-depleted (C and D) tumours. Scale bars represent 200 μm.

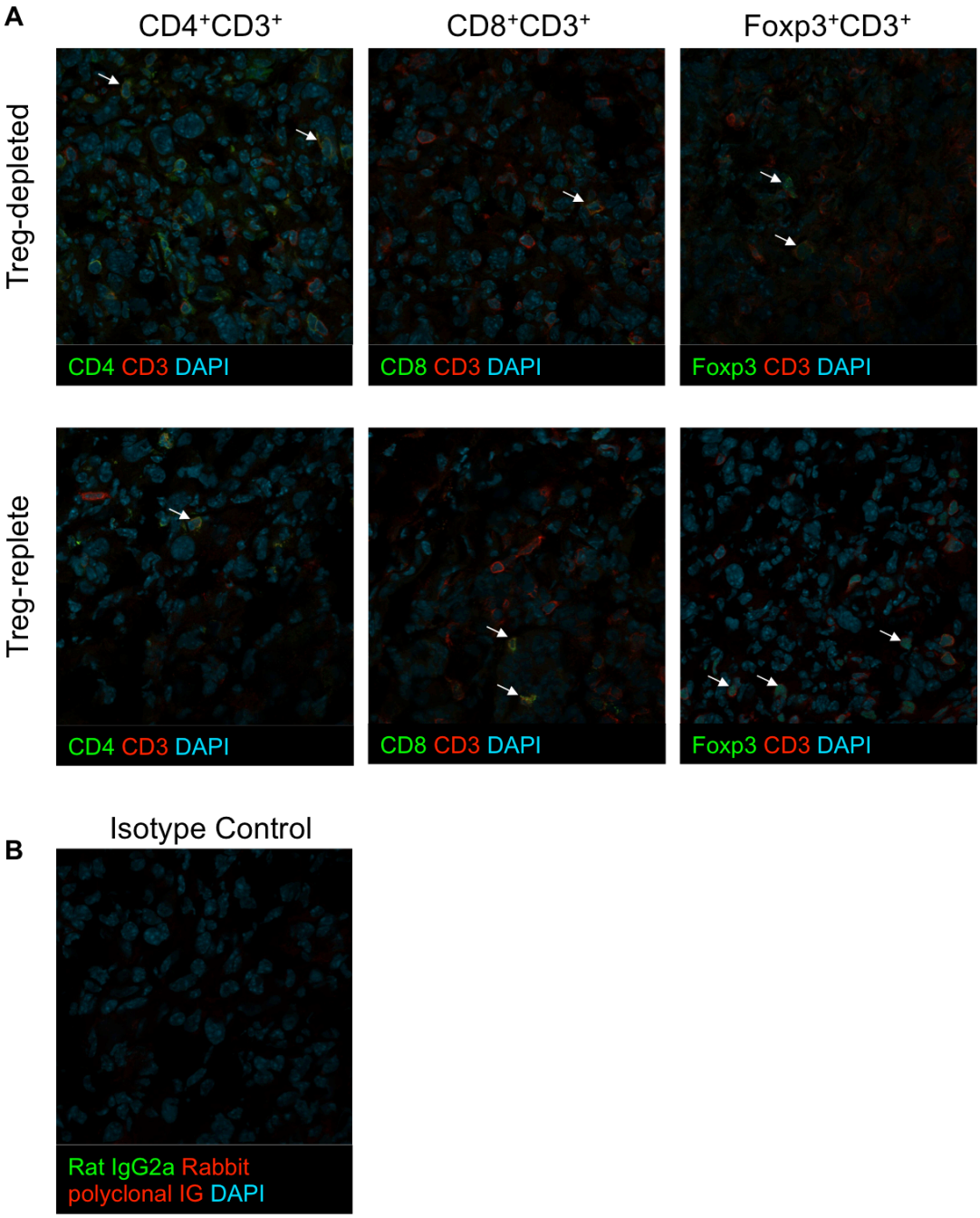

Figure C| Examples of immunofluorescence staining on Treg-depleted and Treg-replete tumours that were frozen after surgical resection. Tumour samples were sectioned as describe in Chapter 2 and serial sections were stained with CD4 CD3, CD8 CD3, and Foxp3 CD3 before subsequent staining with the nuclear stain DAPI. White arrows indicate double positive cells in each circumstance, which were quantified as number of double positive cells per high power field of view.

References

Abadi, Y. M. et al. 2013. Host B7x promotes pulmonary metastasis of breast cancer. *Journal of immunology (Baltimore, Md. : 1950)* 190(7), pp. 3806-3814.

Abel, S. et al. 2012. Strong Impact of CD4+Foxp3+ Regulatory T Cells and Limited Effect of T Cell-Derived IL-10 on Pathogen Clearance during Plasmodium yoelii Infection. *The Journal of Immunology* 188(11), p. 5467.

Acharyya, S. et al. 2012. A CXCL1 paracrine network links cancer chemoresistance and metastasis. *Cell* 150(1), pp. 165-178.

Álvaro, T. et al. 2005. Outcome in Hodgkin's Lymphoma Can Be Predicted from the Presence of Accompanying Cytotoxic and Regulatory T Cells. *Clinical Cancer Research* 11(4), p. 1467.

Amer, M. H. 1982. Chemotherapy and pattern of metastases in breast cancer patients. *J Surg Oncol.* 19(2), pp. 101-105.

Aslakson, C. J. and Miller, F. R. 1992. Selective Events in the Metastatic Process Defined by Analysis of the Sequential Dissemination of Subpopulations of a Mouse Mammary Tumor. *Cancer Research* 52(6), p. 1399.

Atsumi, T. et al. 2014. Inflammation Amplifier, a New Paradigm in Cancer Biology. *Cancer Research* 74(1), p. 8.

Avizienyte, E. et al. 2002. Src-induced de-regulation of E-cadherin in colon cancer cells requires integrin signalling. *Nat Cell Biol* 4(8), pp. 632-638.

Awwad, M. and North, R. 1988. Cyclophosphamide (Cy)_facilitated adoptive immunotherapy of a Cy-resistant tumor. Evidence that Cy permits the expression of adoptive T-cell mediated immunity by removing suppressor Y cells rather than by reducing tumour burden. *Immunology* 65, pp. 87-92.

Ayez, N. et al. 2015. The use of neo-adjuvant chemotherapy in patients with resectable colorectal liver metastases: Clinical risk score as possible discriminator. *European Journal of Surgical Oncology (EJSO)* 41(7), pp. 859-867.

Bacac, M. and Stamenkovic, I. 2008. Metastatic Cancer Cell. *Annual Review of Pathology: Mechanisms of Disease* 3(1), pp. 221-247.

Bachmann, M. F. et al. 1999. Cutting Edge: Lymphoproliferative Disease in the Absence of CTLA-4 Is Not T Cell Autonomous. *The Journal of Immunology* 163(3), p. 1128.

Bagci, U. et al. 2013. A computational pipeline for quantification of pulmonary infections in small animal models using serial PET-CT imaging. *EJNMMI Res* 3(1), p. 55.

Bald, T. et al. 2014. Ultraviolet-radiation-induced inflammation promotes angiotropism and metastasis in melanoma. *Nature* 507(7490), pp. 109-113.

Balkwill, F. et al. 2005. Smoldering and polarized inflammation in the initiation and promotion of malignant disease. *Cancer Cell* 7(3), pp. 211-217.

Baru, A. M. et al. 2012. Absence of Foxp3(+) Regulatory T Cells during Allergen Provocation Does Not Exacerbate Murine Allergic Airway Inflammation. *PLoS ONE* 7(10), p. e47102.

Bates, G. J. et al. 2006. Quantification of Regulatory T Cells Enables the Identification of High-Risk Breast Cancer Patients and Those at Risk of Late Relapse. *Journal of Clinical Oncology* 24(34), pp. 5373-5380.

Bayne, L. J. et al. 2012. Tumor-derived granulocyte-macrophage colony stimulating factor regulates myeloid inflammation and T cell immunity in pancreatic cancer. *Cancer cell* 21(6), pp. 822-835.

Bennett, C. L. et al. 2001. The immune dysregulation, polyendocrinopathy, enteropathy, X-linked syndrome (IPEX) is caused by mutations of FOXP3. *Nat Genet* 27(1), pp. 20-21.

Berod, L. et al. 2014. Rapid Rebound of the Treg Compartment in DEREG Mice Limits the Impact of Treg Depletion on Mycobacterial Burden, but Prevents Autoimmunity. *PLoS ONE* 9(7), p. e102804.

Berry, C. R. 2002. Physical Principles of Computed Tomography and Magentic Resonance Imaging.*Textbook of Veterinary Diagnostic Radiology*. Philadelphia W.B Saunders Company, pp. 28-35.

Betts, G. et al. 2007. The impact of regulatory T cells on carcinogen-induced sarcogenesis. *Br J Cancer* 96, pp. 1849-1854.

Bindea, G. et al. 2010. Natural immunity to cancer in humans. *Current Opinion in Immunology* 22(2), pp. 215-222.

Biragyn, A. et al. 2013. Inhibition of lung metastasis by chemokine CCL17-mediated in vivo silencing of genes in CCR4(+) Tregs. *Journal of immunotherapy (Hagerstown, Md. : 1997)* 36(4), pp. 258-267.

Birkeland, S. A. et al. 1995. Cancer risk after renal transplantation in the Nordic countries, 1964-1986. *Int J Cancer* 60(2), pp. 183-189.

Boissonnas, A. et al. 2010. Foxp3+ T Cells Induce Perforin-Dependent Dendritic Cell Death in Tumor-Draining Lymph Nodes. *Immunity* 32(2), pp. 266-278.

Bonertz, A. et al. 2009. Antigen-specific Tregs control T cell responses against a limited repertoire of tumor antigens in patients with colorectal carcinoma. *The Journal of Clinical Investigation* 119(11), pp. 3311-3321.

Bopp, T. et al. 2007. Cyclic Adenosine Monophosphate is a key component of regulatory T-cell mediated suppression. *Journal of Experimental Medicine* 204(6), pp. 1303-1310.

Borsellino, G. et al. 2007. Expression of ectonucleotidase CD39 by Foxp3⁺ Treg cells: hydrolysis of extracellular ATP and immune suppression. *Blood* 110(4), p. 1225.

Bos, P. D. et al. 2013. Transient regulatory T cell ablation deters oncogene-driven breast cancer and enhances radiotherapy. *The Journal of Experimental Medicine* 210(11), pp. 2435-2466.

Brien, G. et al. 2007. Downregulation of Bfl-1 protein expression sensitizes malignant B cells to apoptosis. *Oncogene* 26(39), pp. 5828-5832.

Brudvik, K. W. et al. 2012. Regulatory T-cell-mediated inhibition of antitumor immune responses is associated with clinical outcome in patients with liver metastasis from colorectal cancer. *Cancer Immunology, Immunotherapy* 61(7), pp. 1045-1053.

Brunkow, M. et al. 2001. Disruption of a new forkhead/winged-helix protein, scurfin, results in the fatal lymphoproliferative disorder of the scurfy mouse. *Nature Genetics* 27, pp. 68-73.

Bu, L. et al. 2014. Intrastriatal transplantation of retinal pigment epithelial cells for the treatment of Parkinson disease: in vivo longitudinal molecular imaging with 18F-P3BZA PET/CT. *Radiology* 272(1), pp. 174-183.

Bui, J. D. et al. 2006. Comparative Analysis of Regulatory and Effector T Cells in Progressively Growing versus Rejecting Tumors of Similar Origins. *Cancer Research* 66(14), p. 7301.

Burnet, M. 1957. Cancer—A Biological Approach: I. The Processes Of Control. II. The Significance of Somatic Mutation. *British Medical Journal* 1(5022), pp. 779-786.

Byrne, W. L. et al. 2011. Targeting Regulatory T cells in Cancer. *Cancer research* 71(22), pp. 6915-6920.

Cacayorin, E. D. et al. 1983. Intravenous digital subtraction angiography with iohexol. *AJNR Am J Neuroradiol* 4(3), pp. 329-332.

Calle, E. E. and Kaaks, R. 2004. Overweight, obesity and cancer: epidemiological evidence and proposed mechanisms. *Nat Rev Cancer* 4(8), pp. 579-591.

Carbonell, W. S. et al. 2009. The Vascular Basement Membrane as “Soil” in Brain Metastasis. *PLoS ONE* 4(6), p. e5857.

Chaffer, C. L. and Weinberg, R. A. 2011. A perspective on cancer cell metastasis. *Science* 331(6024), pp. 1559-1564.

Chambers, A. F. et al. 2002. Metastasis: Dissemination and growth of cancer cells in metastatic sites. *Nat Rev Cancer* 2(8), pp. 563-572.

Chambers, A. F. et al. 1998-1999. Preclinical assessment of anti-cancer therapeutic strategies using in vivo videomicroscopy. *Cancer Metastasis Reviews* 17(3), pp. 263-269.

Charron, M. et al. 2000. Image analysis in patients with cancer studied with a combined PET and CT scanner. *Clin Nucl Med.* 25(11), pp. 905-910.

Chaturvedi, M. M. et al. 2011. NF-κB addiction and its role in cancer: ‘one size does not fit all’. *Oncogene* 30(14), pp. 1615-1630.

Chen, H. et al. 2009. Anti-CTLA-4 therapy results in higher CD4(+)ICOS(hi) T cell frequency and IFN-γ levels in both nonmalignant and malignant prostate tissues. *Proceedings of the National Academy of Sciences of the United States of America* 106(8), pp. 2729-2734.

Chen, J. et al. 2011. CCL18 from Tumor-Associated Macrophages Promotes Breast Cancer Metastasis via PITPNM3. *Cancer cell* 19(4), pp. 541-555.

Cheng, H. et al. 2016. The combination of systemic inflammation-based marker NLR and circulating regulatory T cells predicts the prognosis of resectable pancreatic cancer patients. *Pancreatology* 16(6), pp. 1080-1084
.

Chiang, S. P. H. et al. 2016. Tumor cell intravasation. *American Journal of Physiology - Cell Physiology* 311(1), p. C1.

Chiarugi, P. and Giannoni, E. 2008. Anoikis: A necessary death program for anchorage-dependent cells. *Biochemical Pharmacology* 76(11), pp. 1352-1364.

Chopra, M. et al. 2013. Tumor necrosis factor receptor 2-dependent homeostasis of regulatory T cells as a player in TNF-induced experimental metastasis. *Carcinogenesis* 34(6), pp. 1296-1303.

Christensen, C. R. L. et al. 1998. Transcription of a Novel Mouse Semaphorin Gene, M-semaH, Correlates with the Metastatic Ability of Mouse Tumor Cell Lines. *Cancer Research* 58(6), p. 1238.

Cicchini, C. et al. 2008. TGFβ-induced EMT requires focal adhesion kinase (FAK) signaling. *Experimental Cell Research* 314(1), pp. 143-152.

Clark, E. A. et al. 2000. Genomic analysis of metastasis reveals an essential role for RhoC. *Nature* 406(6795), pp. 532-535.

Clark, G. J. and Der, C. J. 1995. Aberrant function of the Ras signal transduction pathway in human breast cancer. *Breast Cancer Res Treat* 35(1), pp. 133-144.

Clayton, A. et al. 2011. Cancer Exosomes Express CD39 and CD73, Which Suppress T Cells through Adenosine Production. *The Journal of Immunology* 187(2), p. 676.

Cohen, A. J. and Pope, C. A. 1995. Lung cancer and air pollution. *Environmental Health Perspectives* 103(Suppl 8), pp. 219-224.

Colbeck, E. J. et al. 2015. Eliminating roles for T-bet and IL-2 but revealing superior activation and proliferation as mechanisms underpinning dominance of regulatory T cells in tumors. *Oncotarget* 6(28), pp. 24649-24659.

Collison, L. W. et al. 2007. The inhibitory cytokine IL-35 contributes to regulatory T-cell function. *Nature* 450(7169), pp. 566-569.

Cook, J. and Hagemann, T. 2013. Tumour-associated macrophages and cancer. *Current Opinion in Pharmacology* 13(4), pp. 595-601.

Coussens, L. M. and Werb, Z. 2002. Inflammation and cancer. *Nature* 420(6917), pp. 860-867.

Curiel, T. J. et al. 2004. Specific recruitment of regulatory T cells in ovarian carcinoma fosters immune privilege and predicts reduced survival. *Nat Med* 10(9), pp. 942-949.

Curran, M. A. and Allison, J. P. 2009. Tumor Vaccines Expressing Flt3-Ligand Synergize with CTLA-4 Blockade to Reject Pre-Implanted Tumors. *Cancer research* 69(19), pp. 7747-7755.

Curran, M. A. et al. 2010. PD-1 and CTLA-4 combination blockade expands infiltrating T cells and reduces regulatory T and myeloid cells within B16 melanoma tumors. *Proceedings of the National Academy of Sciences of the United States of America* 107(9), pp. 4275-4280.

D'Cruz, L. M. and Klein, L. 2005. Development and function of agonist-induced CD25+Foxp3+ regulatory T cells in the absence of interleukin 2 signaling. *Nat Immunol* 6(11), pp. 1152-1159.

Dallas, S. L. et al. 2002. Proteolysis of Latent Transforming Growth Factor-β (TGF-β)-binding Protein-1 by Osteoclasts: A CELLULAR MECHANISM FOR RELEASE OF TGF-β FROM BONE MATRIX. *Journal of Biological Chemistry* 277(24), pp. 21352-21360.

Dalotto-Moreno, T. et al. 2013. Targeting Galectin-1 Overcomes Breast Cancer-Associated Immunosuppression and Prevents Metastatic Disease. *Cancer Research* 73(3), p. 1107.

Dannenberg, A. J. and Subbaramaiah, K. 2003. Targeting cyclooxygenase-2 in human neoplasia: Rationale and promise. *Cancer Cell* 4(6), pp. 431-436.

Darin, P. C. et al. 2013. In vivo characterization of tumor vasculature using iodine and gold nanoparticles and dual energy micro-CT. *Physics in Medicine and Biology* 58(6), p. 1683.

Das, K. C. and White, C. W. 1997. Activation of NF-κB by Antineoplastic Agents: ROLE OF PROTEIN KINASE C. *Journal of Biological Chemistry* 272(23), pp. 14914-14920.

De Falco, M. et al. 2015. Molecular Mechanisms of Helicobacter pylori Pathogenesis. *Journal of Cellular Physiology* 230(8), pp. 1702-1707.

de la Rosa, M. et al. 2004. Interleukin-2 is essential for CD4+CD25+ regulatory T cell function. *European Journal of Immunology* 34(9), pp. 2480-2488.

Deaglio, S. et al. 2007. Adenosine generation catalyzed by CD39 and CD73 expressed on regulatory T cells mediates immune suppression. *The Journal of Experimental Medicine* 204(6), pp. 1257-1265.

Decker, T. et al. 2012. Increased number of regulatory T cells (T-regs) in the peripheral blood of patients with Her-2/neu-positive early breast cancer. *Journal of Cancer Research and Clinical Oncology* 138(11), pp. 1945-1950.

Delgoffe, G. M. et al. 2013. Regulatory T cell stability is maintained by a neuropilin-1:semaphorin-4a axis. *Nature* 501(7466), pp. 252-256.

DeNardo, D. G. et al. 2009. CD4(+) T Cells Regulate Pulmonary Metastasis of Mammary Carcinomas by Enhancing Protumor Properties of Macrophages. *Cancer cell* 16(2), pp. 91-102.

Denis-Bacelar, A. M. et al. 2016. Pre-clinical quantitative imaging and mouse-specific dosimetry for 111In-labelled radiotracers. *EJNMMI Res* 6(1), p. 85.

Descot, A. and Oskarsson, T. 2013. The molecular composition of the metastatic niche. *Experimental Cell Research* 319(11), pp. 1679-1686.

Dexter Dl Fau - Kowalski, H. M. et al. 1978. Heterogeneity of tumor cells from a single mouse mammary tumor. *Cancer Res.* 38(10), pp. 3174-3181.

Dirven, H. A. A. M. et al. 1994. Involvement of Human Glutathione S-Transferase Isoenzymes in the Conjugation of Cyclophosphamide Metabolites with Glutathione. *Cancer Research* 54(23), p. 6215.

Dong, H. et al. 2002. Tumor-associated B7-H1 promotes T-cell apoptosis: A potential mechanism of immune evasion. *Nat Med* 8(8), pp. 793-800.

Dreesen, O. and Brivanlou, A. H. 2007. Signaling pathways in cancer and embryonic stem cells. *Stem Cell Rev* 3(1), pp. 7-17.

Du, R. et al. 2008. HIF1α Induces the Recruitment of Bone Marrow-Derived Vascular Modulatory Cells to Regulate Tumor Angiogenesis and Invasion. *Cancer cell* 13(3), pp. 206-220.

Duffy, M. J. et al. 2008. Cancer invasion and metastasis: changing views. *The Journal of Pathology* 214(3), pp. 283-293.

Dunn, G. P. et al. 2002. Cancer immunoediting: from immunosurveillance to tumor escape. *Nat Immunol* 3(11), pp. 991-998.

duPre, S. and Hunter Jr, K. 2007. Murine mammary carcinoma 4T1 induces a leukemoid reaction with splenomegaly: association with tumor-derived growth factors. *Experimental and Molecular Pathology* 82, pp. 12-24.

Duthoit, C. T. et al. 2004. Uncoupling of IL-2 Signaling from Cell Cycle Progression in Naive CD4⁺ T Cells by Regulatory CD4⁺CD25⁺ T Lymphocytes. *The Journal of Immunology* 174(1), p. 155.

Ehrlich, P. 1909. Ueber den jetzigen stand der Karzinomforschung. *Ned. Tijdschr Geneeskd* 5, pp. 273-290.

Erler, J. T. et al. 2006. Lysyl oxidase is essential for hypoxia-induced metastasis. *Nature* 440(7088), pp. 1222-1226.

Escarcega, R. O. et al. 2007. The transcription factor nuclear factor-kappa B and cancer. *Clin Oncol (R Coll Radiol)* 19(2), pp. 154-161.

Eyles, J. et al. 2010. Tumor cells disseminate early, but immunosurveillance limits metastatic outgrowth, in a mouse model of melanoma. *The Journal of Clinical Investigation* 120(6), pp. 2030-2039.

Facciabene, A. et al. 2011. Tumour hypoxia promotes tolerance and angiogenesis via CCL28 and Treg cells. *Nature* 475(7355), pp. 226-230.

Faghih, Z. et al. 2014. Immune profiles of CD4+ lymphocyte subsets in breast cancer tumor draining lymph nodes. *Immunology Letters* 158(1–2), pp. 57-65.

Fallarino, F. et al. 2003. Modulation of tryptophan catabolism by regulatory T cells. *Nat Immunol* 4(12), pp. 1206-1212.

Ferrone, C. and Dranoff, G. 2010. Dual Roles for Immunity in Gastrointestinal Cancers. *Journal of Clinical Oncology* 28(26), pp. 4045-4051.

Fife, B. T. et al. 2009. Interactions between programmed death-1 and programmed death ligand-1 promote tolerance by blocking the T cell receptor-induced stop signal. *Nature immunology* 10(11), pp. 1185-1192.

Fonager, R. F. et al. 2016. (18)F-fluoride positron emission tomography/computed tomography and bone scintigraphy for diagnosis of bone metastases in newly diagnosed, high-risk prostate cancer patients: study protocol for a multicentre, diagnostic test accuracy study. *BMC Cancer* 16, p. 10.

Fontenot, J. D. et al. 2003. Foxp3 programs the development and function of CD4+CD25+ regulatory T cells. *Nat Immunol* 4(4), pp. 330-336.

Fontenot, J. D. et al. 2005a. A function for interleukin 2 in Foxp3-expressing regulatory T cells. *Nat Immunol* 6(11), pp. 1142-1151.

Fontenot, J. D. et al. 2005b. Regulatory T Cell Lineage Specification by the Forkhead Transcription Factor Foxp3. *Immunity* 22(3), pp. 329-341.

Francescone, R. et al. 2015. Cytokines, IBD and colitis-associated cancer. *Inflammatory bowel diseases* 21(2), pp. 409-418.

Freeman, G. J. et al. 2000. Engagement of the Pd-1 Immunoinhibitory Receptor by a Novel B7 Family Member Leads to Negative Regulation of Lymphocyte Activation. *The Journal of Experimental Medicine* 192(7), pp. 1027-1034.

French, J. D. et al. 2012. Programmed Death-1(+) T Cells and Regulatory T Cells Are Enriched in Tumor-Involved Lymph Nodes and Associated with Aggressive Features in Papillary Thyroid Cancer. *The Journal of Clinical Endocrinology and Metabolism* 97(6), pp. E934-E943.

Friedl, P. et al. 2012. Classifying collective cancer cell invasion. *Nat Cell Biol* 14(8), pp. 777-783.

Fu, H.-y. et al. 2013. FOXP3 and TLR4 protein expression are correlated in non-small cell lung cancer: Implications for tumor progression and escape. *Acta Histochemica* 115(2), pp. 151-157.

Fueger, B. et al. 2006. Impact of Animal Handling on the Results of 18F-FDG PET Studies in Mice. *The Journal of Nuclear Medicine* 47(6), pp. 999-1006.

Fujino, H. et al. 2011. Prostaglandin E2 regulates cellular migration via induction of vascular endothelial growth factor receptor-1 in HCA-7 human colon cancer cells. *Biochemical Pharmacology* 81(3), pp. 379-387.

Gallimore, A. and Godkin, A. 2008. Regulatory T cell and tumor immunity - observations in mice and men. *Immunology* 123, pp. 157-163.

Gallimore, A. and Sakaguchi, S. 2002. Regulation of Tumour Immunity by CD25+ T cells. *Immunology* 107, pp. 5-9.

Gamcsik, M. P. et al. 1999. Mechanisms of resistance to the toxicity of cyclophosphamide. *Curr Pharm Des* 5(8), pp. 587-605.

Gavin, M. A. et al. 2006. Single-cell analysis of normal and FOXP3-mutant human T cells: FOXP3 expression without regulatory T cell development. *Proceedings of the National Academy of Sciences of the United States of America* 103(17), pp. 6659-6664.

Gerd, M. and Joel, S. K. 2006. Positron emission tomography. *Physics in Medicine and Biology* 51(13), p. R117.

Germain, R. N. 2002. T-cell development and the CD4-CD8 lineage decision. *Nat Rev Immunol* 2(5), pp. 309-322.

Ghiringhelli, F. et al. 2004. CD4+CD25+ Regulatory T cells suppress tumor immunity but are sensitive to cyclophosphamide which allows immunotherapy of established tumors to be curative. *European Journal of Immunology* 34, pp. 336-344.

Ghiringhelli, F. et al. 2005. Tumor cells convert immature myeloid dendritic cells into TGF-β–secreting cells inducing CD4(+)CD25(+) regulatory T cell proliferation. *The Journal of Experimental Medicine* 202(7), pp. 919-929.

Ghochikyan, A. et al. 2014. Primary 4T1 tumor resection provides critical "window of opportunity" for immunotherapy. *Clinical & experimental metastasis* 31(2), pp. 185-198.

Gocheva, V. et al. 2010. IL-4 induces cathepsin protease activity in tumor-associated macrophages to promote cancer growth and invasion. *Genes & Development* 24(3), pp. 241-255.

Goel, R. et al. 2014. (68)Ga-DOTATATE positron emission tomography/computed tomography scan in the detection of bone metastases in pediatric neuroendocrine tumors. *Indian Journal of Nuclear Medicine : IJNM : The Official Journal of the Society of Nuclear Medicine, India* 29(1), pp. 13-17.

Gondek, D. C. et al. 2005. Cutting Edge: Contact-Mediated Suppression by CD4⁺CD25⁺ Regulatory Cells Involves a Granzyme B-Dependent, Perforin-Independent Mechanism. *The Journal of Immunology* 174(4), p. 1783.

Grange, C. et al. 2011. Microvesicles Released from Human Renal Cancer Stem Cells Stimulate Angiogenesis and Formation of Lung Premetastatic Niche. *Cancer Research* 71(15), p. 5346.

Granot, Z. et al. 2011. Tumor entrained neutrophils inhibit seeding in the premetastatic lung. *Cancer cell* 20(3), pp. 300-314.

Green, E. A. et al. 2003. CD4(+)CD25(+) T regulatory cells control anti-islet CD8(+) T cells through TGF-β–TGF-β receptor interactions in type 1 diabetes. *Proceedings of the National Academy of Sciences of the United States of America* 100(19), pp. 10878-10883.

Greenwald, R. J. et al. 2004. THE B7 FAMILY REVISITED. *Annual Review of Immunology* 23(1), pp. 515-548.

Grossman, W. J. et al. 2004. Human T Regulatory Cells Can Use the Perforin Pathway to Cause Autologous Target Cell Death. *Immunity* 21(4), pp. 589-601.

Gu, X. et al. 2015. Efficacy of neo-adjuvant chemotherapy with TEC regimen on breast cancer. *Cancer Chemotherapy and Pharmacology* 75(2), pp. 301-308.

H Heppner, G. et al. 2000. Nontransgenic models of breast cancer. *Breast Cancer Research : BCR* 2(5), pp. 331-334.

Hainfeld, J. F. et al. 2006. Gold nanoparticles: a new X-ray contrast agent. (79), pp. 248-253
.

Hall, M. A. et al. 2012. Comparison of mAbs targeting epithelial cell adhesion molecule for the detection of prostate cancer lymph node metastases with multimodal contrast agents: quantitative small-animal PET/CT and NIRF. *J Nucl Med.* 53(9), pp. 1427-1437.

Halvorsen, E. C. et al. 2014. Emerging roles of regulatory T cells in tumour progression and metastasis. *Cancer and Metastasis Reviews* 33(4), pp. 1025-1041.

Hamid, O. et al. 2013. Safety and Tumor Responses with Lambrolizumab (Anti–PD-1) in Melanoma. *The New England journal of medicine* 369(2), pp. 134-144.

Hanagiri, T. et al. 2013. Clinical significance of the frequency of regulatory T cells in regional lymph node lymphocytes as a prognostic factor for non-small-cell lung cancer. *Lung Cancer* 81(3), pp. 475-479
.

Hanahan, D. and Weinberg, R. A. 2000. The Hallmarks of Cancer. *Cell* 100(1), pp. 57-70.

Hanahan, D. and Weinberg, Robert A. 2011. Hallmarks of Cancer: The Next Generation. *Cell* 144(5), pp. 646-674.

Hansen, W. et al. 2012. Neuropilin 1 deficiency on CD4(+)Foxp3(+) regulatory T cells impairs mouse melanoma growth. *The Journal of Experimental Medicine* 209(11), pp. 2001-2016.

Higano, C. S. et al. 2009. Integrated data from 2 randomized, double-blind, placebo-controlled, phase 3 trials of active cellular immunotherapy with sipuleucel-T in advanced prostate cancer. *Cancer* 115(16), pp. 3670-3679.

Hindley, J. P. et al. 2012. T Cell Trafficking Facilitated by High Endothelial Venules is Required for Tumor Control after Regulatory T Cell Depletion. *Cancer research* 72(21), pp. 5473-5482.

Hinrichs, C. S. and Rosenberg, S. A. 2014. Exploiting the curative potential of adoptive T-cell therapy for cancer. *Immunological reviews* 257(1), pp. 56-71.

Hiratsuka, S. et al. 2006. Tumour-mediated upregulation of chemoattractants and recruitment of myeloid cells predetermines lung metastasis. *Nat Cell Biol* 8(12), pp. 1369-1375.

Hiratsuka, S. et al. 2008. The S100A8-serum amyloid A3-TLR4 paracrine cascade establishes a pre-metastatic phase. *Nat Cell Biol* 10(11), pp. 1349-1355.

Hiscott, J. et al. 2001. Hostile takeovers: viral appropriation of the NF-kB pathway. *Journal of Clinical Investigation* 107(2), pp. 143-151.

Hodi, F. S. et al. 2010. Improved Survival with Ipilimumab in Patients with Metastatic Melanoma. *The New England journal of medicine* 363(8), pp. 711-723.

Hoesel, B. and Schmid, J. A. 2013. The complexity of NF-κB signaling in inflammation and cancer. *Molecular Cancer* 12, pp. 86-86.

Hori, S. et al. 2003. Control of Regulatory T Cell Development by the Transcription Factor <em>Foxp3</em&gt. *Science* 299(5609), p. 1057.

Hounsfield, G. N. 1973. Computerized transverse axial scanning (tomography). 1. Description of system. *Br J Radiol* 46(552), pp. 1016-1022.

Hoves, S. et al. 2010. The battlefield of perforin/granzyme cell death pathways. *Journal of Leukocyte Biology* 87(2), pp. 237-243.

Hsiao, Y.-W. et al. 2008. Interactions of host IL-6 and IFN-γ and cancer-derived TGF-β1 on MHC molecule expression during tumor spontaneous regression. *Cancer Immunology, Immunotherapy* 57(7), pp. 1091-1104.

Hu, H. H. et al. 2010. Identification of Brown Adipose Tissue in Mice with Fat-Water IDEAL-MRI. *Journal of magnetic resonance imaging : JMRI* 31(5), pp. 1195-1202.

Hu, Y.-Y. et al. 2015. Cervical lymph node hyperplasia on [¹⁸F]-fluorodeoxyglucose positron emission tomography/computed tomography scan after treatment of children and adolescents with malignant lymphoma. *European Journal of Radiology* 84(7), pp. 1378-1382.

Huang, B. et al. 2009. miR-142-3p restricts cAMP production in CD4+CD25- T cells and CD4+ CD25+ TREG cells by targetting AC9 mRNA. *EMBO rep* 10, pp. 180-185.

Huang, C.-T. et al. 2004. Role of LAG-3 in Regulatory T Cells. *Immunity* 21(4), pp. 503-513.

Huen, N.-Y. et al. 2013. Up-regulation of proliferative and migratory genes in regulatory T cells from patients with metastatic castration-resistant prostate cancer. *International journal of cancer. Journal international du cancer* 133(2), pp. 373-382.

Hulikal, N. et al. 2015. Utility of [18F] Fluorodeoxyglucose Positron Emission Tomography/Computed Tomography (FDG PET/CT) in the Initial Staging and Response Assessment of Locally Advanced Breast Cancer Patients Receiving Neoadjuvant Chemotherapy. *Indian Journal of Surgical Oncology* 6(4), pp. 330-336.

Iellem, A. et al. 2001. Unique Chemotactic Response Profile and Specific Expression of Chemokine Receptors Ccr4 and Ccr8 by Cd4(+)Cd25(+) Regulatory T Cells. *The Journal of Experimental Medicine* 194(6), pp. 847-854.

Ishida, T. et al. 2006. Specific Recruitment of CC Chemokine Receptor 4–Positive Regulatory T Cells in Hodgkin Lymphoma Fosters Immune Privilege. *Cancer Research* 66(11), p. 5716.

Iwai, Y. et al. 2002. Involvement of PD-L1 on tumor cells in the escape from host immune system and tumor immunotherapy by PD-L1 blockade. *Proceedings of the National Academy of Sciences of the United States of America* 99(19), pp. 12293-12297.

Izcue, A. et al. 2009. Regulatory Lymphocytes and Intestinal Inflammation. *Annual Review of Immunology* 27(1), pp. 313-338.

Janda, E. et al. 2002. Ras and TGFβ cooperatively regulate epithelial cell plasticity and metastasis: dissection of Ras signaling pathways. *The Journal of Cell Biology* 156(2), pp. 299-314.

Johnson, L. A. et al. 2009. Gene therapy with human and mouse T-cell receptors mediates cancer regression and targets normal tissues expressing cognate antigen. *Blood* 114(3), pp. 535-546.

Jones, E. et al. 2002. Depletion of CD25+ regulatory cells results in suppression of melanoma growth and induction of autoreactivity in mice. *Cancer Immun* 2, p. 1.

Josefowicz, S. Z. et al. 2012. Extrathymically generated regulatory T cells control mucosal Th2 inflammation. *Nature* 482(7385), pp. 395-399.

Joshi, P. et al. 2013. Stomach metastasis of breast carcinoma mimicking primary gastric neoplasm on fluorodeoxy glucose–positron emission tomography–computed tomography. *Indian Journal of Medical and Paediatric Oncology : Official Journal of Indian Society of Medical & Paediatric Oncology* 34(2), pp. 128-129.

Jung, T. et al. 2009. CD44v6 Dependence of Premetastatic Niche Preparation by Exosomes. *Neoplasia (New York, N.Y.)* 11(10), pp. 1093-1105.

Kalendar, W. A. 2005. *Computed Tomography - Fundamentals, System Technology, Image Quality, Applications.* Second ed. Erlangen: Publicis Corporate Publishing.

Kamby, C. et al. 1987. Incidence and methodologic aspects of the occurrence of liver metastases in recurrent breast cancer. *Cancer* 59(8), pp. 1524-1529.

Kang, M. J. et al. 2013. Tumor-infiltrating PD1-Positive Lymphocytes and FoxP3-Positive Regulatory T Cells Predict Distant Metastatic Relapse and Survival of Clear Cell Renal Cell Carcinoma. *Translational Oncology* 6(3), pp. 282-289.

Kang, Y. et al. 2003. A multigenic program mediating breast cancer metastasis to bone. *Cancer Cell* 3(6), pp. 537-549.

Kantoff, P. W. et al. 2010. Sipuleucel-T Immunotherapy for Castration-Resistant Prostate Cancer. *New England Journal of Medicine* 363(5), pp. 411-422.

Kaplan, R. N. et al. 2005. VEGFR1-positive haematopoietic bone marrow progenitors initiate the pre-metastatic niche. *Nature* 438(7069), pp. 820-827.

Karavitis, J. et al. 2012. Regulation of COX2 Expression in Mouse Mammary Tumor Cells Controls Bone Metastasis and PGE2-Induction of Regulatory T Cell Migration. *PLoS ONE* 7(9), p. e46342.

Karin, M. 2006. Nuclear factor-[kappa]B in cancer development and progression. *Nature* 441(7092), pp. 431-436.

Karin, M. 2008. The IkappaB kinase - a bridge between inflammation and cancer. *Cell Res* 18(3), pp. 334-342.

Kashimura, S. et al. 2012. CD83+ dendritic cells and Foxp3+ regulatory T cells in primary lesions and regional lymph nodes are inversely correlated with prognosis of gastric cancer. *Gastric Cancer* 15(2), pp. 144-153.

Khattri, R. et al. 2003. An essential role for Scurfin in CD4+CD25+ T regulatory cells. *Nat Immunol* 4(4), pp. 337-342.

Kienast, Y. et al. 2010. Real-time imaging reveals the single steps of brain metastasis formation. *Nat Med* 16(1), pp. 116-122.

Kii, I. et al. 2010. Incorporation of Tenascin-C into the Extracellular Matrix by Periostin Underlies an Extracellular Meshwork Architecture. *The Journal of Biological Chemistry* 285(3), pp. 2028-2039.

Kim, G. et al. 2015. SOCS3-mediated regulation of inflammatory cytokines in PTEN and p53 inactivated triple negative breast cancer model. *Oncogene* 34(6), pp. 671-680.

Kim, J. et al. 2009a. Cutting Edge: Depletion of Foxp3⁺ Cells Leads to Induction of Autoimmunity by Specific Ablation of Regulatory T Cells in Genetically Targeted Mice. *The Journal of Immunology* 183(12), p. 7631.

Kim, J. et al. 2007. Regulatory T cells prevent catastrophic autoimmunity throughout the lifespan of mice. *Nature Immunology* 8, pp. 191-197.

Kim, M. S. et al. 2009b. Prognostic nomogram for predicting the 5-year probability of developing metastasis after neo-adjuvant chemotherapy and definitive surgery for AJCC stage II extremity osteosarcoma. *Ann Oncol* 20(5), pp. 955-960.

Kim, P. S. et al. 2014. Pan-Bcl-2 Inhibitor, GX15-070 (Obatoclax), Decreases Human T Regulatory Lymphocytes While Preserving Effector T Lymphocytes: a Rationale for Its Use in Combination Immunotherapy. *Journal of immunology (Baltimore, Md. : 1950)* 192(6), pp. 2622-2633.

Kinahan, P. E. et al. 1998. Attenuation correction for a combined 3D PET/CT scanner. *Med Phys.* 25(10), pp. 2046-2053.

Kissick, H. T. and Sanda, M. G. 2015. The role of active vaccination in cancer immunotherapy: lessons from clinical trials. *Current Opinion in Immunology* 35, pp. 15-22.

Kitagawa, Y. et al. 2017. Guidance of regulatory T cell development by Satb1-dependent super-enhancer establishment. *Nat Immunol* 18(2), pp. 173-183.

Kitamura, T. et al. 2015. Immune cell promotion of metastasis. *Nature reviews. Immunology* 15(2), pp. 73-86.

Klages, K. et al. 2010. Selective Depletion of Foxp3⁺ Regulatory T Cells Improves Effective Therapeutic Vaccination against Established Melanoma. *Cancer Research* 70(20), p. 7788.

Klimp, A. H. et al. 2001. Expression of Cyclooxygenase-2 and Inducible Nitric Oxide Synthase in Human Ovarian Tumors and Tumor-associated Macrophages. *Cancer Research* 61(19), p. 7305.

Kluetz, P. G. et al. 2000. Combined PET/CT Imaging in Oncology. Impact on Patient Management. *Clin Positron Imaging* 3(6), pp. 223-230.

Knutson, K. L. et al. 2015. Regulatory T cells, inherited variation, and clinical outcome in epithelial ovarian cancer. *Cancer immunology, immunotherapy : CII* 64(12), pp. 1495-1504.

Kobie, J. J. et al. 2006. T Regulatory and Primed Uncommitted CD4 T Cells Express CD73, Which Suppresses Effector CD4 T Cells by Converting 5′ -Adenosine Monophosphate to Adenosine. *The Journal of Immunology* 177(10), p. 6780.

Kochenderfer, J. N. et al. 2010. Eradication of B-lineage cells and regression of lymphoma in a patient treated with autologous T cells genetically engineered to recognize CD19. *Blood* 116(20), pp. 4099-4102.

Koebel, C. M. et al. 2007. Adaptive immunity maintains occult cancer in an equilibrium state. *Nature* 450(7171), pp. 903-907.

Koop, S. et al. 1996. Independence of metastatic ability and extravasation: metastatic ras-transformed and control fibroblasts extravasate equally well. *Proceedings of the National Academy of Sciences of the United States of America* 93(20), pp. 11080-11084.

Kotb, A. M. et al. 2011. Replacement of E-cadherin by N-cadherin in the mammary gland leads to fibrocystic changes and tumor formation. *Breast Cancer Research : BCR* 13(5), pp. R104-R104.

Kowalski, P. J. et al. 2003. E-cadherin expression in primary carcinomas of the breast and its distant metastases. *Breast Cancer Research* 5(6), pp. R217-R222.

Krummel, M. F. and Allison, J. P. 1996. CTLA-4 engagement inhibits IL-2 accumulation and cell cycle progression upon activation of resting T cells. *The Journal of Experimental Medicine* 183(6), pp. 2533-2540.

Krummel, M. F. and Allison, J. P. 2011. Pillars Article: CD28 and CTLA-4 Have Opposing Effects on the Response of T Cells to Stimulation. The Journal of Experimental Medicine. 1995. 182: 459–465. *The Journal of Immunology* 187(7), p. 3459.

Krummel, M. F. et al. 1996. Superantigen responses and co-stimulation: CD28 and CTLA-4 have opposing effects on T cell expansion in vitro and in vivo. *Int Immunol* 8(4), pp. 519-523.

Kuang, D.-M. et al. 2009. Activated monocytes in peritumoral stroma of hepatocellular carcinoma foster immune privilege and disease progression through PD-L1. *The Journal of Experimental Medicine* 206(6), pp. 1327-1337.

Lahl, K. et al. 2007. Selective depletion of Foxp3+ regulatory T cells induces a scurfy-like disease. *Journal of Experimental Medicine* 204(1), pp. 57-63.

Lahl, K. et al. 2009. Nonfunctional Regulatory T Cells and Defective Control of Th2 Cytokine Production in Natural Scurfy Mutant Mice. *The Journal of Immunology* 183(9), p. 5662.

Lal, A. et al. 2013. FOXP3-positive regulatory T lymphocytes and epithelial FOXP3 expression in synchronous normal, ductal carcinoma in situ, and invasive cancer of the breast. *Breast Cancer Research and Treatment* 139(2), pp. 381-390.

Landsberg, J. et al. 2012. Melanomas resist T-cell therapy through inflammation-induced reversible dedifferentiation. *Nature* 490(7420), pp. 412-416.

Layland, L. E. et al. 2013. Schistosoma mansoni-Mediated Suppression of Allergic Airway Inflammation Requires Patency and Foxp3(+) Treg Cells. *PLoS Neglected Tropical Diseases* 7(8), p. e2379.

Leach, D. R. et al. 1996. Enhancement of Antitumor Immunity by CTLA-4 Blockade. *Science* 271(5256), p. 1734.

Lee, H. M. and Hsieh, C.-S. 2009. Rare Development of Foxp3(+) Thymocytes in the CD4(+)CD8(+) Subset. *Journal of immunology (Baltimore, Md. : 1950)* 183(4), pp. 2261-2266.

Lee, J. E. et al. 2012. Diagnostic value for extrahepatic metastases of hepatocellular carcinoma in positron emission tomography/computed tomography scan. *World Journal of Gastroenterology : WJG* 18(23), pp. 2979-2987.

Lee, O. et al. 2013. Multimodal evaluation of xenograft tumors in mice with an in-vivo stereo imaging system and small-animal PET/CT. *Melanoma Res* 23(5), pp. 349-359
.

Lelekakis, M. et al. 1999. A novel orthotopic model of breast cancer metastasis to bone. *Clin Exp Metastasis* 17(2), pp. 163-170.

Lepage, G. A. 1963. Basic biochemical effects and mechanisms of action of 6-thioguanine. *Cancer Res.* 23, pp. 1202-1206.

Levental, K. R. et al. 2009. Matrix Crosslinking Forces Tumor Progression by Enhancing Integrin signaling. *Cell* 139(5), pp. 891-906.

Lewis, C. and Murdoch, C. 2005. Macrophage Responses to Hypoxia : Implications for Tumor Progression and Anti-Cancer Therapies. *The American Journal of Pathology* 167(3), pp. 627-635.

Li, D.-M. and Feng, Y.-M. 2011. Signaling mechanism of cell adhesion molecules in breast cancer metastasis: potential therapeutic targets. *Breast Cancer Research and Treatment* 128(1), p. 7.

Li, J. et al. 2003. Complete Regression of Experimental Solid Tumors by Combination LEC/chTNT-3 Immunotherapy and CD25⁺ T-Cell Depletion. *Cancer Research* 63(23), p. 8384.

Li, X. et al. 2010. Efficient Treg depletion induces T-cell infiltration and rejection of large tumors. *European Journal of Immunology* 40(12), pp. 3325-3335.

Li, Y. M. et al. 2013. Diphtheria toxin-based targeted toxin therapy for brain tumors. *Journal of Neuro-Oncology* 114(2), pp. 155-164.

Liakou, C. I. et al. 2008. CTLA-4 blockade increases IFNγ-producing CD4(+)ICOS(hi) cells to shift the ratio of effector to regulatory T cells in cancer patients. *Proceedings of the National Academy of Sciences of the United States of America* 105(39), pp. 14987-14992.

Liang, B. et al. 2008. Regulatory T Cells Inhibit Dendritic Cells by Lymphocyte Activation Gene-3 Engagement of MHC Class II. *The Journal of Immunology* 180(9), p. 5916.

Lin, E. Y. et al. 2006. Macrophages Regulate the Angiogenic Switch in a Mouse Model of Breast Cancer. *Cancer Research* 66(23), p. 11238.

Lin, E. Y. et al. 2001. Colony-Stimulating Factor 1 Promotes Progression of Mammary Tumors to Malignancy. *The Journal of Experimental Medicine* 193(6), pp. 727-740.

Lin, Q. and Yun, Z. 2010. Impact of the Hypoxic Tumor Microenvironment on the Regulation of Cancer Stem Cell Characteristics. *Cancer biology & therapy* 9(12), pp. 949-956.

Lio, C.-W. J. and Hsieh, C.-S. 2008. A two-step process for thymic regulatory T cell development. *Immunity* 28(1), pp. 100-111.

Liu, V. C. et al. 2007. Tumor Evasion of the Immune System by Converting CD4⁺CD25[−] T Cells into CD4⁺CD25⁺ T Regulatory Cells: Role of Tumor-Derived TGF-β. *The Journal of Immunology* 178(5), p. 2883.

Loeser, S. et al. 2007. Spontaneous tumor rejection by cbl-b–deficient CD8(+) T cells. *The Journal of Experimental Medicine* 204(4), pp. 879-891.

Lu, J. et al. 2013. Endothelial Cells Promote the Colorectal Cancer Stem Cell Phenotype Through a Soluble Form of Jagged-1. *Cancer cell* 23(2), pp. 171-185.

Lu, X. and Kang, Y. 2010. Hypoxia and hypoxia-inducible factors (HIFs): master regulators of metastasis. *Clinical cancer research : an official journal of the American Association for Cancer Research* 16(24), pp. 5928-5935.

Lukanidin, E. and Sleeman, J. P. 2012. Building the niche: The role of the S100 proteins in metastatic growth. *Seminars in Cancer Biology* 22(3), pp. 216-225.

Lutsiak, M. et al. 2005. Inhibition of CD4+25+ T Regulatory cell function implicated in enhanced immune response by low-dose cyclophosphamide. *Blood* 105, pp. 2862-2868.

Makkouk, A. and Weiner, G. 2015. Cancer Immunotherapy and Breaking Immune Tolerance-New Approaches to an Old Challenge. *Cancer research* 75(1), pp. 5-10.

Mannori, G. et al. 1995. Differential Colon Cancer Cell Adhesion to E-, P-, and L-selectin: Role of Mucintype Glycoproteins. *Cancer Research* 55(19), p. 4425.

Mansfield, A. S. et al. 2009. Simultaneous Foxp3 and IDO expression is associated with sentinel lymph node metastases in breast cancer. *BMC Cancer* 9, pp. 231-231.

Mantovani, A. et al. 2008. Cancer-related inflammation. *Nature* 454(7203), pp. 436-444.

Mantovani, A. et al. 2002. Macrophage polarization: tumor-associated macrophages as a paradigm for polarized M2 mononuclear phagocytes. *Trends in Immunology* 23(11), pp. 549-555.

Martin-Liberal, J. et al. 2015. Anti-programmed cell death-1 therapy and insulin-dependent diabetes: a case report. *Cancer Immunology, Immunotherapy* 64(6), pp. 765-767.

Martin-Suarez, I. et al. 1997. Immunosuppressive treatment in severe connective tissue diseases: effects of low dose intravenous cyclophosphamide. *Annals of the Rheumatic Diseases* 56(8), pp. 481-487.

Matsushita, H. et al. 2012. Cancer Exome Analysis Reveals a T Cell Dependent Mechanism of Cancer Immunoediting. *Nature* 482(7385), pp. 400-404.

Maude, S. L. et al. 2014. Chimeric Antigen Receptor T Cells for Sustained Remissions in Leukemia. *The New England journal of medicine* 371(16), pp. 1507-1517.

Mayer, C. T. et al. 2014a. Few Foxp3+ regulatory T cells are sufficient to protect adult mice from lethal autoimmunity. *European Journal of Immunology* 44(10), pp. 2990-3002.

Mayer, C. T. et al. 2014b. Advantages of Foxp3(+) regulatory T cell depletion using DEREG mice. *Immunity, Inflammation and Disease* 2(3), pp. 162-165.

McGinnis, G. J. et al. 2016. Neuroinflammatory and cognitive consequences of combined radiation and immunotherapy in a novel preclinical model. LID - 10.18632/oncotarget.13551 [doi]. *Oncotarget* (1949-2553 (Electronic)).

McIntire Kr Fau - Sell, S. et al. 1964. PATHOGENESIS OF THE POST-NEONATAL THYMECTOMY WASTING SYNDROME. *Nature* 204, pp. 151-155.

Mego, M. et al. 2010. Molecular mechanisms of metastasis in breast cancer[mdash]clinical applications. *Nat Rev Clin Oncol* 7(12), pp. 693-701.

Mellor, A. L. and Munn, D. H. 2004. Ido expression by dendritic cells: tolerance and tryptophan catabolism. *Nat Rev Immunol* 4(10), pp. 762-774.

Meltzer, C. C. et al. 2000. Whole-body FDG positron emission tomographic imaging for staging esophageal cancer comparison with computed tomography. *Clin Nucl Med.* 25(11), pp. 882-887.

Minn, A. J. et al. 2005. Genes that mediate breast cancer metastasis to lung. *Nature* 436(7050), pp. 518-524.

Mitchell, K. et al. 2010. Suppression of integrin α3β1 in breast cancer cells reduces COX-2 gene expression and inhibits tumorigenesis, invasion, and crosstalk to endothelial cells. *Cancer research* 70(15), pp. 6359-6367.

Mittal, D. et al. 2014. New insights into cancer immunoediting and its three component phases — elimination, equilibrium and escape. *Current opinion in immunology* 27, pp. 16-25.

Mittra, E. S. et al. 2016. Pilot Preclinical and Clinical Evaluation of (4S)-4-(3-[18F]Fluoropropyl)-L-Glutamate (18F-FSPG) for PET/CT Imaging of Intracranial Malignancies. *PLoS ONE* 11(2), p. e0148628.

Moore, F. E. and Langenau, D. M. 2012. Through the Looking Glass: Visualizing Leukemia Growth, Migration, and Engraftment Using Fluorescent Transgenic Zebrafish. *Advances in Hematology* 2012, p. 478164.

Morath, C. et al. 2004. Malignancy in Renal Transplantation. *Journal of the American Society of Nephrology* 15(6), pp. 1582-1588.

Morgan, R. A. et al. 2006. Cancer Regression in Patients After Transfer of Genetically Engineered Lymphocytes. *Science (New York, N.Y.)* 314(5796), pp. 126-129.

Muller, A. et al. 2001. Involvement of chemokine receptors in breast cancer metastasis. *Nature* 410(6824), pp. 50-56.

Myron Kauffman, H. et al. 2002. Transplant tumor registry: donor related malignancies. *Transplantation* 74(3), pp. 358-362.

Na, Y.-R. et al. 2013. Cyclooxygenase-2 Inhibition Blocks M2 Macrophage Differentiation and Suppresses Metastasis in Murine Breast Cancer Model. *PLoS ONE* 8(5), p. e63451.

Nakamura, K. et al. 2001. Cell Contact–Dependent Immunosuppression by Cd4(+)Cd25(+)Regulatory T Cells Is Mediated by Cell Surface–Bound Transforming Growth Factor β. *The Journal of Experimental Medicine* 194(5), pp. 629-644.

Nakanishi, C. and Toi, M. 2005. Nuclear factor-[kappa]B inhibitors as sensitizers to anticancer drugs. *Nat Rev Cancer* 5(4), pp. 297-309.

Nelson, B. H. 2008. The impact of T-cell immunity on ovarian cancer outcomes. *Immunological Reviews* 222(1), pp. 101-116.

Nenoi, M. et al. 2015. In vivo radioadaptive response: A review of studies relevant to radiation-induced cancer risk. *Human & Experimental Toxicology* 34(3), pp. 272-283.

Nicholaou, T. et al. 2011. Immunoediting and persistence of antigen-specific immunity in patients who have previously been vaccinated with NY-ESO-1 protein formulated in ISCOMATRIX™. *Cancer Immunology, Immunotherapy* 60(11), p. 1625.

Nishikawa, H. and Sakaguchi, S. 2010. Regulatory T cells in tumour immunity. *International Journal of Cancer* 127, pp. 759-767.

Nishizuka, Y. and Sakakura, T. 1969. Thymus and Reproduction: Sex-Linked Dysgenesia of the Gonad after Neonatal Thymectomy in Mice. *Science* 166(3906), p. 753.

Nockel, P. et al. 2016. The Rate and Clinical Significance of Incidental Thyroid Uptake as Detected by Gallium-68 DOTATATE Positron Emission Tomography/Computed Tomography. *Thyroid* 26(6), pp. 831-835.

Nogami, Y. et al. 2015. The efficacy of preoperative positron emission tomography-computed tomography (PET-CT) for detection of lymph node metastasis in cervical and endometrial cancer: clinical and pathological factors influencing it. *Japanese Journal of Clinical Oncology* 45(1), pp. 26-34.

North, R. 1982. Cyclophosphamide-facilitated adoptive immunotherapy of an established tumor depends on elimination of tumor-induced suppressor T Cells. *Journal of Experimental Medicine* 55, pp. 1063-1074.

North, R. and Awwad, M. 1990. Elimination of cycling CD4+ suppressor T cells with an anti-mitotic drug releases non-cycling CD8+ Tcells to cause regression of an advanced lymphoma. *Immunology* 71, pp. 90-95.

North, R. and Bursuker, I. 1984. Generation and decay of the immune response to a progressive fibrosarcoma. I. Ly-1+2- suppressor T cells down-regulate the generation of Ly-1-2+ effector T cells. *The Journal of Experimental Medicine* 159(5), pp. 1295-1311.

Novitskiy, S. V. et al. 2011. TGF-β Receptor II Loss Promotes Mammary Carcinoma Progression by Th17 Dependent Mechanisms. *Cancer discovery* 1(5), pp. 430-441.

Oberle, N. et al. 2007. Rapid Suppression of Cytokine Transcription in Human CD4⁺CD25[−] T Cells by CD4⁺Foxp3⁺ Regulatory T Cells: Independence of IL-2 Consumption, TGF-β, and Various Inhibitors of TCR Signaling. *The Journal of Immunology* 179(6), p. 3578.

Oderup, C. et al. 2006. Cytotoxic T lymphocyte antigen-4-dependent down-modulation of costimulatory molecules on dendritic cells in CD4(+) CD25(+) regulatory T-cell-mediated suppression. *Immunology* 118(2), pp. 240-249.

Ohlerth, S. and Scharf, G. 2007. Computed tomography in small animals – Basic principles and state of the art applications. *The Veterinary Journal* 173(2), pp. 254-271.

Ohnishi, S. et al. 2013. DNA Damage in Inflammation-Related Carcinogenesis and Cancer Stem Cells. *Oxidative Medicine and Cellular Longevity* 2013, p. 387014.

Olkhanud, P. B. et al. 2009. Breast cancer lung metastasis requires expression of chemokine receptor CCR4 and T regulatory cells. *Cancer research* 69(14), pp. 5996-6004.

Olkhanud, P. B. et al. 2011. Tumor-evoked regulatory B cells promote breast cancer metastasis by converting resting CD4(+) T cells to T regulatory cells. *Cancer research* 71(10), pp. 3505-3515.

Ondondo, B. et al. 2015. A distinct chemokine axis does not account for enrichment of Foxp3(+) CD4(+) T cells in carcinogen-induced fibrosarcomas. *Immunology* 145(1), pp. 94-104.

Ondondo, B. et al. 2013. Home Sweet Home: The Tumor Microenvironment as a Haven for Regulatory T Cells. *Frontiers in Immunology* 4, p. 197.

Onizuka, S. et al. 1999. Tumor Rejection by in Vivo Administration of Anti-CD25 (Interleukin-2 Receptor α) Monoclonal Antibody. *Cancer Research* 59(13), p. 3128.

Oskarsson, T. et al. 2011. Breast cancer cells produce tenascin C as a metastatic niche component to colonize the lungs. *Nat Med* 17(7), pp. 867-874.

Oukka, M. 2007. Interplay between pathogenic Th17 and regulatory T cells. *Annals of the Rheumatic Diseases* 66(Suppl 3), pp. iii87-iii90.

Overgaard, N. H. et al. 2015. CD4+/CD8+ double-positive T cells: more than just a developmental stage? *Journal of Leukocyte Biology* 97(1), pp. 31-38.

ÖZtÜRk, H. and Karapolat, İ. 2015. Efficacy of (18)F-fluorodeoxyglucose-positron emission tomography/computed tomography in restaging muscle-invasive bladder cancer following radical cystectomy. *Experimental and Therapeutic Medicine* 9(3), pp. 717-724.

Pages, F. et al. 2009. Immune infiltration in human tumors: a prognostic factor that should not be ignored. *Oncogene* 29(8), pp. 1093-1102.

Paget, S. 1889. THE DISTRIBUTION OF SECONDARY GROWTHS IN CANCER OF THE BREAST. *The Lancet* 133(3421), pp. 571-573.

Pandiyan, P. et al. 2007. CD4+CD25+Foxp3+ regulatory T cells induce cytokine deprivation-mediated apoptosis of effector CD4+ T cells. *Nat Immunol* 8(12), pp. 1353-1362.

Park, J. W. et al. 2015. 18F-FDG PET/CT monitoring of beta3 agonist-stimulated brown adipocyte recruitment in white adipose tissue. *J Nucl Med.* 56(1), pp. 153-158.

Peinado, H. et al. 2012. Melanoma exosomes educate bone marrow progenitor cells toward a pro-metastatic phenotype through MET. *Nature medicine* 18(6), pp. 883-891.

Peinado, H. et al. 2011. The secreted factors responsible for pre-metastatic niche formation: Old sayings and new thoughts. *Seminars in Cancer Biology* 21(2), pp. 139-146.

Pere, H. et al. 2011. A CCR4 antagonist combined with vaccines induces antigen-specific CD8⁺ T cells and tumor immunity against self antigens. *Blood* 118(18), p. 4853.

Perrone, G. et al. 2008. Intratumoural FOXP3-positive regulatory T cells are associated with adverse prognosis in radically resected gastric cancer. *European Journal of Cancer* 44(13), pp. 1875-1882.

Pham, S. M. et al. 1995. Solid tumors after heart transplantation: Lethality of lung cancer. *The Annals of Thoracic Surgery* 60(6), pp. 1623-1626.

Plitas, G. and Rudensky, A. 2016. Regulatory T cells: Differentiation and Function. *Cancer Immunology Researcg* 4(9), pp. 721-725.

Poulsen, M. H. et al. 2012. [18F]fluoromethylcholine (FCH) positron emission tomography/computed tomography (PET/CT) for lymph node staging of prostate cancer: a prospective study of 210 patients. *BJU International* 110(11), pp. 1666-1671.

Provenzano, P. P. et al. 2008. Contact Guidance Mediated Three-Dimensional Cell Migration is Regulated by Rho/ROCK-Dependent Matrix Reorganization. *Biophysical Journal* 95(11), pp. 5374-5384.

Psaila, B. and Lyden, D. 2009. The Metastatic Niche: Adapting the Foreign Soil. *Nature reviews. Cancer* 9(4), pp. 285-293.

Pulaski, B. and Ostrand-Rosenberg, S. 2000. Mouse 4T1 breast tumor model. *Current Protocols in Immunology* 29, pp. 20.22.21-20.22.16.

Pulaski, B. A. and Ostrand-Rosenberg, S. 1998. Reduction of established spontaneous mammary carcinoma metastases following immunotherapy with major histocompatibility complex class II and B7.1 cell-based tumor vaccines. *Cancer Res.* 58(7), pp. 1486-1493.

Qian, B.-Z. et al. 2011. CCL2 recruits inflammatory monocytes to facilitate breast tumor metastasis. *Nature* 475(7355), pp. 222-225.

Quezada, S. A. and Peggs, K. S. 2013. Exploiting CTLA-4, PD-1 and PD-L1 to reactivate the host immune response against cancer. *British Journal of Cancer* 108(8), pp. 1560-1565.

Quezada, S. A. et al. 2006. CTLA4 blockade and GM-CSF combination immunotherapy alters the intratumor balance of effector and regulatory T cells. *Journal of Clinical Investigation* 116(7), pp. 1935-1945.

Quezada, S. A. et al. 2011. Shifting the equilibrium in cancer immunoediting: from tumor tolerance to eradication. *Immunological reviews* 241(1), pp. 104-118.

Quezada, S. A. et al. 2008. Limited tumor infiltration by activated T effector cells restricts the therapeutic activity of regulatory T cell depletion against established melanoma. *The Journal of Experimental Medicine* 205(9), pp. 2125-2138.

Qureshi, O. S. et al. 2011. Trans-endocytosis of CD80 and CD86: a molecular basis for the cell extrinsic function of CTLA-4. *Science (New York, N.Y.)* 332(6029), pp. 600-603.

Raposo, T. P. et al. 2015. Inflammation and cancer: Till death tears them apart. *The Veterinary Journal* 205(2), pp. 161-174.

Read, S. et al. 2006. Blockade of CTLA-4 on CD4+CD25+ Regulatory T Cells Abrogates Their Function In Vivo. *The Journal of Immunology* 177(7), p. 4376.

Read, S. et al. 2000. Cytotoxic T Lymphocyte–Associated Antigen 4 Plays an Essential Role in the Function of Cd25(+)Cd4(+) Regulatory Cells That Control Intestinal Inflammation. *The Journal of Experimental Medicine* 192(2), pp. 295-302.

Recchia, F. et al. 2013. Vascular endothelial growth factor expression and T-regulatory cells in premenopausal breast cancer. *Oncology Letters* 5(4), pp. 1117-1122.

Redjimi, N. et al. 2012. CXCR3⁺ T Regulatory Cells Selectively Accumulate in Human Ovarian Carcinomas to Limit Type I Immunity. *Cancer Research* 72(17), p. 4351.

Rendon, D. A. et al. 2016. Mapping Radiation Injury and Recovery in Bone Marrow Using 18F-FLT PET/CT and USPIO MRI in a Rat Model. *J Nucl Med.* 57(2), pp. 266-271.

Robert, C. et al. 2014a. Nivolumab in Previously Untreated Melanoma without BRAF Mutation. *New England Journal of Medicine* 372(4), pp. 320-330.

Robert, C. et al. 2014b. Anti-programmed-death-receptor-1 treatment with pembrolizumab in ipilimumab-refractory advanced melanoma: a randomised dose-comparison cohort of a phase 1 trial. *The Lancet* 384(9948), pp. 1109-1117.

Robert, C. et al. 2011. Ipilimumab plus Dacarbazine for Previously Untreated Metastatic Melanoma. *New England Journal of Medicine* 364(26), pp. 2517-2526.

Rolli, M. et al. 2003. Activated integrin αvβ3 cooperates with metalloproteinase MMP-9 in regulating migration of metastatic breast cancer cells. *Proceedings of the National Academy of Sciences of the United States of America* 100(16), pp. 9482-9487.

Rolny, C. et al. 2011. HRG Inhibits Tumor Growth and Metastasis by Inducing Macrophage Polarization and Vessel Normalization through Downregulation of PlGF. *Cancer Cell* 19(1), pp. 31-44.

Rooney, P. H. et al. 2004. The Role of Cytochrome P450 in Cytotoxic Bioactivation: Future Therapeutic Directions. *Current Cancer Drug Targets* 4(3), pp. 257-265.

Rösel, D. et al. 2008. Up-Regulation of Rho/ROCK Signaling in Sarcoma Cells Drives Invasion and Increased Generation of Protrusive Forces. *Molecular Cancer Research* 6(9), p. 1410.

Rosen, S. D. 2004. Ligands for L-Selectin: Homing, Inflammation, and Beyond. *Annual Review of Immunology* 22(1), pp. 129-156.

Rosenberg, S. A. and Restifo, N. P. 2015. Adoptive cell transfer as personalized immunotherapy for human cancer. *Science* 348(6230), p. 62.

Ruffell, B. et al. 2010. Lymphocytes in cancer development: polarization towards pro-tumor immunity. *Cytokine & growth factor reviews* 21(1), pp. 3-10.

Sackstein, R. 2005. The lymphocyte homing receptors: gatekeepers of the multistep paradigm. *Curr Opin Hematol* 12(6), pp. 444-450.

Sadowski, S. M. et al. 2016. Prospective Study of (68)Ga-DOTATATE Positron Emission Tomography/Computed Tomography for Detecting Gastro-Entero-Pancreatic Neuroendocrine Tumors and Unknown Primary Sites. *Journal of Clinical Oncology* 34(6), pp. 588-596.

Sakaguchi, S. et al. 1995. Immunological self-tolerance maintained by activated T cells expressing IL-2 receptor alpha-chains (CD25). Breakdown of a single mechanism of self-tolerance causes various autoimmune diseases. *Journal of Immunology* 155, pp. 1151-1164.

Sakaguchi, S. et al. 2008. Regulatory T Cells and Immune Tolerance. *Cell* 133(5), pp. 775-787.

Salomon, B. and Bluestone, J. A. 2001. COMPLEXITIES OF CD28/B7: CTLA-4 COSTIMULATORY PATHWAYS IN AUTOIMMUNITY AND TRANSPLANTATION. *Annual Review of Immunology* 19(1), pp. 225-252.

Samstein, R. M. et al. 2012. Extrathymic generation of regulatory T cells in placental mammals mitigates maternal-fetal conflict. *Cell* 150(1), pp. 29-38.

Sandvig, K. and Olsnes, S. 1981. Rapid entry of nicked diphtheria toxin into cells at low pH. Characterization of the entry process and effects of low pH on the toxin molecule. *Journal of Biological Chemistry* 256(17), pp. 9068-9076.

Sangaletti, S. et al. 2008. Macrophage-Derived SPARC Bridges Tumor Cell-Extracellular Matrix Interactions toward Metastasis. *Cancer Research* 68(21), p. 9050.

Sather, B. D. et al. 2007. Altering the distribution of Foxp3(+) regulatory T cells results in tissue-specific inflammatory disease. *The Journal of Experimental Medicine* 204(6), pp. 1335-1347.

Sato, E. et al. 2005. Intraepithelial CD8(+) tumor-infiltrating lymphocytes and a high CD8(+)/regulatory T cell ratio are associated with favorable prognosis in ovarian cancer. *Proceedings of the National Academy of Sciences of the United States of America* 102(51), pp. 18538-18543.

Sawant, A. et al. 2012. Depletion of plasmacytoid dendritic cells inhibits tumor growth and prevents bone metastasis of the breast cancer cells. *Journal of immunology (Baltimore, Md. : 1950)* 189(9), pp. 4258-4265.

Schadendorf, D. et al. 2015. Pooled Analysis of Long-Term Survival Data From Phase II and Phase III Trials of Ipilimumab in Unresectable or Metastatic Melanoma. *Journal of Clinical Oncology* 33(17), pp. 1889-1894.

Schenk, S. et al. 2003. Binding to EGF receptor of a laminin-5 EGF-like fragment liberated during MMP-dependent mammary gland involution. *The Journal of Cell Biology* 161(1), pp. 197-209.

Schlecker, E. et al. 2012. Tumor-Infiltrating Monocytic Myeloid-Derived Suppressor Cells Mediate CCR5-Dependent Recruitment of Regulatory T Cells Favoring Tumor Growth. *The Journal of Immunology* 189(12), p. 5602.

Schmidt, A. et al. 2012. Molecular Mechanisms of Treg-Mediated T Cell Suppression. *Frontiers in Immunology* 3, p. 51.

Schmidt, E. M. et al. 2008. CTLA-4 Controls Regulatory T Cell Peripheral Homeostasis and Is Required for Suppression of Pancreatic Islet Autoimmunity. *The Journal of Immunology* 182(1), p. 274.

Schreiber, R. D. et al. 2011. Cancer immunoediting: integrating immunity's roles in cancer suppression and promotion. *Science* 331(6024), pp. 1565-1570.

Schulze, B. et al. 2014. CD4+FoxP3+ regulatory T cells suppress fatal T helper 2 cell immunity during pulmonary fungal infection. *European Journal of Immunology* 44(12), pp. 3596-3604.

Schumacher, T. N. and Schreiber, R. D. 2015. Neoantigens in cancer immunotherapy. *Science* 348(6230), p. 69.

Scully, O. J. et al. 2012. Breast cancer metastasis. *Cancer Genomics Proteomics* 9(5), pp. 311-320.

Scurr, M. et al. 2012. T Cell subsets and colorectal cancer: Discerning the good from the bad. *Cellular Immunology* 279, pp. 21-24.

Serra, P. et al. 2003. CD40 Ligation Releases Immature Dendritic Cells from the Control of Regulatory CD4+CD25+ T Cells. *Immunity* 19(6), pp. 877-889.

Sethi, N. et al. 2011. Tumor-derived Jagged1 Promotes Osteolytic Bone Metastasis of Breast Cancer by Engaging Notch Signaling in Bone Cells. *Cancer cell* 19(2), pp. 192-205.

Seyfried, T. N. and Huysentruyt, L. C. 2013. On the Origin of Cancer Metastasis. *Critical reviews in oncogenesis* 18(1-2), pp. 43-73.

Sharma, P. and Allison, J. P. 2015. The future of immune checkpoint therapy. *Science* 348(6230), p. 56.

Shevach, E. M. 2009. Mechanisms of Foxp3+ T Regulatory Cell-Mediated Suppression. *Immunity* 30(5), pp. 636-645.

Shimizu, J. et al. 1999. Induction of Tumor Immunity by Removing CD25⁺CD4⁺ T Cells: A Common Basis Between Tumor Immunity and Autoimmunity. *The Journal of Immunology* 163(10), p. 5211.

Shiozawa, Y. et al. 2011. Human prostate cancer metastases target the hematopoietic stem cell niche to establish footholds in mouse bone marrow. *The Journal of Clinical Investigation* 121(4), pp. 1298-1312.

Shrikant, P. et al. 1999. CTLA-4 Blockade Reverses CD8⁺ T Cell Tolerance to Tumor by a CD4⁺ T Cell– and IL-2-Dependent Mechanism. *Immunity* 11(4), pp. 483-493.

Sica, A. et al. 2006. Tumour-associated macrophages are a distinct M2 polarised population promoting tumour progression: Potential targets of anti-cancer therapy. *European Journal of Cancer* 42(6), pp. 717-727.

Simpson, T. R. et al. 2013. Fc-dependent depletion of tumor-infiltrating regulatory T cells co-defines the efficacy of anti–CTLA-4 therapy against melanoma. *The Journal of Experimental Medicine* 210(9), pp. 1695-1710.

Sinha, P. et al. 2012. Tumor-Induced Myeloid-derived Suppressor Cell Function is Independent of IFNγ and IL-4Rα. *European journal of immunology* 42(8), pp. 2052-2059.

Sleeman, J. P. 2012. The metastatic niche and stromal progression. *Cancer Metastasis Reviews* 31(3-4), pp. 429-440.

Small, E. J. et al. 2006. Placebo-Controlled Phase III Trial of Immunologic Therapy with Sipuleucel-T (APC8015) in Patients with Metastatic,

Asymptomatic Hormone Refractory Prostate Cancer. *Journal of Clinical Oncology* 24(19), pp. 3089-3094.

Smyth, M. J. et al. 2006a. Cancer Immunosurveillance and Immunoediting: The Roles of Immunity in Suppressing Tumor Development and Shaping Tumor Immunogenicity.*Advances in Immunology*. Vol. Volume 90. Academic Press, pp. 1-50.

Smyth, M. J. et al. 2006b. CD4⁺CD25⁺ T Regulatory Cells Suppress NK Cell-Mediated Immunotherapy of Cancer. *The Journal of Immunology* 176(3), p. 1582.

Smyth, M. J. et al. 2000a. Differential Tumor Surveillance by Natural Killer (Nk) and Nkt Cells. *The Journal of Experimental Medicine* 191(4), pp. 661-668.

Smyth, M. J. et al. 2000b. Perforin-Mediated Cytotoxicity Is Critical for Surveillance of Spontaneous Lymphoma. *The Journal of Experimental Medicine* 192(5), pp. 755-760.

Song, W. et al. 2012. Successful treatment of gallbladder mixed adenoneuroendocrine carcinoma with neo-adjuvant chemotherapy. *Diagnostic Pathology* 7, pp. 163-163.

Sparwasser, T. and Eberl, G. 2007. BAC to immunology - bacterial artificial chromosome-mediated transgenesis for targeting of immune cells. *Immunology* 121, pp. 308-313.

Srivastava, M. K. et al. 2012. Myeloid Suppressor Cell Depletion Augments Antitumor Activity in Lung Cancer. *PLoS ONE* 7(7), p. e40677.

Strauss, D. C. and Thomas, J. M. 2010. Transmission of donor melanoma by organ transplantation. *The Lancet Oncology* 11(8), pp. 790-796.

Street, S. E. A. et al. 2001. Perforin and interferon-γ activities independently control tumor initiation, growth, and metastasis. *Blood* 97(1), p. 192.

Street, S. E. A. et al. 2002. Suppression of Lymphoma and Epithelial Malignancies Effected by Interferon γ. *The Journal of Experimental Medicine* 196(1), pp. 129-134.

Su, S. et al. 2014. A Positive Feedback Loop between Mesenchymal-like Cancer Cells and Macrophages Is Essential to Breast Cancer Metastasis. *Cancer Cell* 25(5), pp. 605-620.

Sugarbaker, E. V. 1979. Cancer metastasis: A product of tumor-host interactions. *Current Problems in Cancer* 3(7), pp. 1-59.

Sunderkötter, C. et al. 1991. Macrophage-derived angiogenesis factors. *Pharmacology & Therapeutics* 51(2), pp. 195-216.

Sutmuller, R. P. M. et al. 2001. Synergism of Cytotoxic T Lymphocyte–Associated Antigen 4 Blockade and Depletion of Cd25(+) Regulatory T Cells in Antitumor Therapy Reveals Alternative Pathways for Suppression of Autoreactive Cytotoxic T Lymphocyte Responses. *The Journal of Experimental Medicine* 194(6), pp. 823-832.

Taichman, D. B. et al. 1991. Tumor cell surface alpha 4 beta 1 integrin mediates adhesion to vascular endothelium: demonstration of an interaction with the N-terminal domains of INCAM-110/VCAM-1. *Cell Regulation* 2(5), pp. 347-355.

Taipale, J. and Keski-Oja, J. 1997. Growth factors in the extracellular matrix. *The FASEB Journal* 11(1), pp. 51-59.

Takahashi, T. et al. 1998. Immunologic self-tolerance maintained by CD25+CD4+ naturally anergic and suppressive T cells: induction of autoimmune disease by breaking their anergic/suppressive state. *Int Immunol* 10(12), pp. 1969-1980.

Takahashi, T. et al. 2000. Immunologic Self-Tolerance Maintained by Cd25(+)Cd4(+)Regulatory T Cells Constitutively Expressing Cytotoxic T Lymphocyte–Associated Antigen 4. *The Journal of Experimental Medicine* 192(2), pp. 303-310.

Takenaka, M. et al. 2013. FOXP3 expression in tumor cells and tumor-infiltrating lymphocytes is associated with breast cancer prognosis. *Molecular and Clinical Oncology* 1(4), pp. 625-632.

Tan, M. C. B. et al. 2009. Disruption of CCR5-dependent homing of regulatory T cells inhibits tumor growth in a murine model of pancreatic cancer. *Journal of immunology (Baltimore, Md. : 1950)* 182(3), pp. 1746-1755.

Tan, W. et al. 2011. Fibroblast-recruited, tumor-infiltrating CD4(+) T cells stimulate mammary cancer metastasis through RANKL-RANK signaling. *Nature* 470(7335), pp. 548-553.

Tang, Q. et al. 2004. Distinct roles of CTLA-4 and TGF-β in CD4+CD25+ regulatory T cell function. *European Journal of Immunology* 34(11), pp. 2996-3005.

Ten Hagen, T. L. M. et al. 2008. Tumor necrosis factor-mediated interactions between inflammatory response and tumor vascular bed. *Immunological Reviews* 222(1), pp. 299-315.

Teng, M. W. L. et al. 2010. Conditional Regulatory T-Cell Depletion Releases Adaptive Immunity Preventing Carcinogenesis and Suppressing Established Tumor Growth. *Cancer Research* 70(20), p. 7800.

Teng, M. W. L. et al. 2012. Opposing roles for IL-23 and IL-12 in maintaining occult cancer in an equilibrium state. *Cancer research* 72(16), pp. 3987-3996.

Thiery, J. P. et al. 2009. Epithelial-Mesenchymal Transitions in Development and Disease. *Cell* 139(5), pp. 871-890.

Thornton, A. M. and Shevach, E. M. 1998. CD4(+)CD25(+) Immunoregulatory T Cells Suppress Polyclonal T Cell Activation In Vitro by Inhibiting Interleukin 2 Production. *The Journal of Experimental Medicine* 188(2), pp. 287-296.

Topalian, S. L. et al. 2012. Safety, Activity, and Immune Correlates of Anti–PD-1 Antibody in Cancer. *The New England journal of medicine* 366(26), pp. 2443-2454.

Topalian, S. L. et al. 2014. Survival, Durable Tumor Remission, and Long-Term Safety in Patients With Advanced Melanoma Receiving Nivolumab. *Journal of Clinical Oncology* 32(10), pp. 1020-1030.

Townsend, D. W. et al. 1993. A rotating PET scanner using BGO block detectors: design, performance and applications. *J Nucl Med.* 34(8), pp. 1367-1376.

Tsiatas, M. L. et al. 2009. Study of T lymphocytes infiltrating peritoneal metastases in advanced ovarian cancer: associations with vascular endothelial growth factor levels and prognosis in patients receiving platinum-based chemotherapy. *Int J Gynecol Cancer* 19(8), pp. 1329-1334.

Turk, M. J. et al. 2004. Concomitant Tumor Immunity to a Poorly Immunogenic Melanoma Is Prevented by Regulatory T Cells. *The Journal of Experimental Medicine* 200(6), pp. 771-782.

Vajdic, C. M. and van Leeuwen, M. T. 2009. Cancer incidence and risk factors after solid organ transplantation. *International Journal of Cancer* 125(8), pp. 1747-1754.

Valenti, R. et al. 2007. Tumor-Released Microvesicles as Vehicles of Immunosuppression. *Cancer Research* 67(7), p. 2912.

Valzasina, B. et al. 2006. Tumor-Induced Expansion of Regulatory T Cells by Conversion of CD4⁺CD25[−] Lymphocytes Is Thymus and Proliferation Independent. *Cancer Research* 66(8), p. 4488.

Van Aelst, L. and D'Souza-Schorey, C. 1997. Rho GTPases and signaling networks. *Genes & Development* 11(18), pp. 2295-2322.

van den Broek, M. E. et al. 1996. Decreased tumor surveillance in perforin-deficient mice. *The Journal of Experimental Medicine* 184(5), p. 1781.

van der Bruggen, P. et al. 1991. A gene encoding an antigen recognized by cytolytic T lymphocytes on a human melanoma. *Science* 254(5038), p. 1643.

Vaquero, J. J. and Kinahan, P. 2015. Positron Emission Tomography: Current Challenges and Opportunities for Technological Advances in Clinical and Preclinical Imaging Systems. *Annual review of biomedical engineering* 17, pp. 385-414.

Varghese, H. J. et al. 2002. Activated Ras Regulates the Proliferation/Apoptosis Balance and Early Survival of Developing Micrometastases. *Cancer Research* 62(3), p. 887.

Vaupel, P. et al. 2001. Oxygen status of malignant tumors: pathogenesis of hypoxia and significance for tumor therapy. *Semin Oncol* 28(Suppl. 8), pp. 29-35.

Vermeulen, L. et al. 2010. Wnt activity defines colon cancer stem cells and is regulated by the microenvironment. *Nat Cell Biol* 12(5), pp. 468-476.

Vignali, D. A. A. et al. 2008. How regulatory T cells work. *Nature reviews. Immunology* 8(7), pp. 523-532.

Vigneron, N. et al. 2013. Database of T cell-defined human tumor antigens: the 2013 update. *Cancer Immunity* 13, p. 15.

Vleminckx, K. et al. 1991. Genetic manipulation of E-cadherin expression by epithelial tumor cells reveals an invasion suppressor role. *Cell* 66(1), pp. 107-119.

Vogelstein, B. et al. 2013. Cancer Genome Landscapes. *Science (New York, N.Y.)* 339(6127), pp. 1546-1558.

von Boehmer, H. and Daniel, C. 2013. Therapeutic opportunities for manipulating TReg cells in autoimmunity and cancer. *Nat Rev Drug Discov* 12(1), pp. 51-63.

von Boehmer, L. et al. 2013. NY-ESO-1–specific immunological pressure and escape in a patient with metastatic melanoma. *Cancer Immunity* 13, p. 12.

Wainwright, D. A. et al. 2011. Thymus-derived rather than tumor-induced regulatory T cells predominate in brain tumors. *Neuro-Oncology* 13(12), pp. 1308-1323.

Waitz, R. et al. 2012. CTLA-4 blockade synergizes with cryoablation to mediate tumor rejection. *Oncoimmunology* 1(4), pp. 544-546.

Walter, S. et al. 2012. Multipeptide immune response to cancer vaccine IMA901 after single-dose cyclophosphamide associates with longer patient survival. *Nat Med* 18(8), pp. 1254-1261.

Walunas, T. L. et al. 1994. CTLA-4 can function as a negative regulator of T cell activation. *Immunity* 1(5), pp. 405-413.

Wang, D. and DuBois, R. N. 2010. Eicosanoids and cancer. *Nature reviews. Cancer* 10(3), pp. 181-193.

Wang, J. et al. 2016. Repeated Long-Term DT Application in the DEREG Mouse Induces a Neutralizing Anti-DT Antibody Response. *Journal of Immunology Research* 2016, p. 1450398.

Wang, X. et al. 2012. Functional Imaging of Brown Fat in Mice with (18)F-FDG micro-PET/CT. *Journal of Visualized Experiments : JoVE* (69), p. 4060.

Warburg, O. 1956. On the origin of cancer cells. *Science* 123(0036-8075 (Print)).

Warburg, O. et al. 1924. Uber den stoffwechsel der tumoren. *Biochem Z* 152, pp. 319-344.

Waris, G. and Ahsan, H. 2006. Reactive oxygen species: role in the development of cancer and various chronic conditions. *Journal of Carcinogenesis* 5, pp. 14-14.

Weathington, N. M. et al. 2006. A novel peptide CXCR ligand derived from extracellular matrix degradation during airway inflammation. *Nat Med* 12(3), pp. 317-323.

Wegener, O. H. 1993. *Whole Body Computed Tomography*. Second ed. Boston: Blackwell Scientific.

Weiss, L. 2000. Metastasis of cancer: a conceptual history from antiquity to the 1990s. *Cancer Metastasis Reviews* 19(3-4), pp. 193-383.

Wendt, M. K. et al. 2011. Down-regulation of epithelial cadherin is required to initiate metastatic outgrowth of breast cancer. *Molecular Biology of the Cell* 22(14), pp. 2423-2435.

Wheelock, M. and Johnson, K. 2003. Cadherins as Modulators of Cellular Phenotype. *Annual Review of Cell and Developmental Biology* 19(1), pp. 207-235.

Wiklund, L. M. et al. 1994. Nonionic contrast media in pediatric CT. A comparative study of intravenous use of iopentol and iohexol. *Acta Radiol.* 35(2), pp. 186-190.

Wildin, R. S. et al. 2001. X-linked neonatal diabetes mellitus, enteropathy and endocrinopathy syndrome is the human equivalent of mouse scurfy. *Nat Genet* 27(1), pp. 18-20.

Wilke, C. M. et al. 2010. Prognostic significance of regulatory T cells in tumor. *International Journal of Cancer* 127(4), pp. 748-758.

Wing, K. et al. 2008. CTLA-4 control over Foxp3+ regulatory T cell function. *Science* 322, pp. 271-275.

Wolchok, J. D. et al. 2013. Nivolumab plus Ipilimumab in Advanced Melanoma. *New England Journal of Medicine* 369(2), pp. 122-133.

Workman, C. et al. 2009. The Development and Function of Regulatory T Cells. *Cell Mol Life Sci* 66(16), pp. 2603-2622.

Workman, C. J. and Vignali, D. A. A. 2005. Negative Regulation of T Cell Homeostasis by Lymphocyte Activation Gene-3 (CD223). *The Journal of Immunology* 174(2), p. 688.

Wu, X. et al. 2013. Immune microenvironment profiles of tumor immune equilibrium and immune escape states of mouse sarcoma. *Cancer Letters* 340(1), pp. 124-133.

Wyckoff, J. et al. 2004. A Paracrine Loop between Tumor Cells and Macrophages Is Required for Tumor Cell Migration in Mammary Tumors. *Cancer Research* 64(19), p. 7022.

Wyckoff, J. B. et al. 2000. A Critical Step in Metastasis: In Vivo Analysis of Intravasation at the Primary Tumor. *Cancer Research* 60(9), p. 2504.

Wyckoff, J. B. et al. 2007. Direct Visualization of Macrophage-Assisted Tumor Cell Intravasation in Mammary Tumors. *Cancer Research* 67(6), p. 2649.

Xu, L. et al. 2010. Enrichment of CCR6+Foxp3+ regulatory T cells in the tumor mass correlates with impaired CD8+ T cell function and poor prognosis of breast cancer. *Clin Immunol* 135(3), pp. 466-475.

Yang, L. et al. 2008. Abrogation of TGFβ signaling in mammary carcinomas recruits Gr-1+CD11b+ myeloid cells that promote metastasis. *Cancer cell* 13(1), pp. 23-35.

Yang, P. et al. 2012. TGF-β-miR-34a-CCL22 Signaling-Induced Treg Cell Recruitment Promotes Venous Metastases of HBV-Positive Hepatocellular Carcinoma. *Cancer cell* 22(3), pp. 291-303.

Yang, S. et al. 2011. Foxp3+IL-17+ T cells promote development of cancer-initiating cells in colorectal cancer. *Journal of Leukocyte Biology* 89(1), pp. 85-91.

Yao, X. et al. 2014. Targeting interleukin-6 in inflammatory autoimmune diseases and cancers. *Pharmacology & Therapeutics* 141(2), pp. 125-139.

Yaqub, S. et al. 2008. Regulatory T cells in colorectal cancer patients suppress anti-tumor immune activity in a COX-2 dependent manner. *Cancer Immunology, Immunotherapy* 57(6), pp. 813-821.

Yu, P. et al. 2005. Intratumor depletion of CD4(+) cells unmasks tumor immunogenicity leading to the rejection of late-stage tumors. *The Journal of Experimental Medicine* 201(5), pp. 779-791.

Yu, Q. and Stamenkovic, I. 2000. Cell surface-localized matrix metalloproteinase-9 proteolytically activates TGF-β and promotes tumor invasion and angiogenesis. *Genes & Development* 14(2), pp. 163-176.

Zabuawala, T. et al. 2010. An Ets2-Specific Transcriptional Program in Tumor Associated Macrophages Promotes Tumor Metastasis. *Cancer research* 70(4), p. 1323.

Zarek, P. E. et al. 2008. A(2A) receptor signaling promotes peripheral tolerance by inducing T-cell anergy and the generation of adaptive regulatory T cells. *Blood* 111(1), pp. 251-259.

Zelenay, S. et al. 2015. Cyclooxygenase-Dependent Tumor Growth through Evasion of Immunity. *Cell* 162(6), pp. 1257-1270.

Zhang, X. H. F. et al. 2009. Latent bone metastasis in breast cancer tied to Src-dependent survival signals. *Cancer cell* 16(1), pp. 67-78.

Zhao, J. et al. 2012. Selective depletion of CD4+CD25+Foxp3+ Regulatory T Cells by Low-Dose Cyclophosphamide is Explained by Reduced Intracellular ATP levels. *Cancer Research* 70, pp. 4850-4858.

Zhong, H. et al. 2014. Origin and pharmacological modulation of tumor-associated regulatory dendritic cells. *International journal of cancer. Journal international du cancer* 134(11), pp. 2633-2645.

Zhou, S. et al. 2013. CCR7 Expression and Intratumoral FOXP3(+) Regulatory T Cells are Correlated with Overall Survival and Lymph Node Metastasis in Gastric Cancer. *PLoS ONE* 8(9), p. e74430.

Zhou, Z. N. et al. 2014. Autocrine HBEGF expression promotes breast cancer intravasation, metastasis and macrophage-independent invasion in vivo. *Oncogene* 33(29), pp. 3784-3793.

Zou, W. and Chen, L. 2008. Inhibitory B7-family molecules in the tumour microenvironment. *Nat Rev Immunol* 8(6), pp. 467-477.

Zou, W. and Restifo, N. P. 2010. T(H)17 cells in tumour immunity and immunotherapy. *Nature reviews. Immunology* 10(4), pp. 248-256.

Zovickian, J. et al. 1987. Potent and specific killing of human malignant brain tumor cells by an anti-transferrin receptor antibody-ricin immunotoxin. *Journal of Neurosurgery* 66(6), pp. 850-861.